

**The Characteristics of Mesoscale Convective Complexes
(MCCs) over the Indonesian Maritime Continent and their
Relationships with Rainfall and the Large-scale
Environment**

A Dissertation in
Earth and Environmental Sciences
Faculty of Science and Technology
Hirosaki University

By
Trismidianto

Submitted to the Graduate School of Science and Technology
in Partial Fulfillment of the Requirements
for the Degree of Doctor of Philosophy
in the School of Science and Technology

HIROSAKI UNIVERSITY

2017

ABSTRACT

This study comprises an analysis of the climatology of mesoscale convective complexes (MCCs) over the Indonesian Maritime Continent (IMC), identified by infrared satellite imagery using an algorithm that combined information about cloud coverage, eccentricity, and the cloud lifetimes of MCCs, for the 15-year period from 2001 to 2015. A case study and composite analysis were used to examine the environmental conditions during MCC events. The contribution of MCCs to the total rainfall was determined from the ratio of total rainfall accumulated during the MCC events to the total rainfall accumulated at each grid point over the 15-year period. The contribution of MCCs to the extreme rainfall was determined from the ratio of extreme rainfall accumulated during the MCC events to the extreme rainfall accumulated at each grid point over the 15-year period. Brightness temperature (T_{BB}) is obtained from the Himawari generation satellite data for the period from 2001 to 2015 which consist of Geostationary Meteorological Satellite (GMS-5), Multi-functional Satellite imagery Transport SATellite (MTSAT 1R and MTSAT 2), Himawari 8 and Geostationary Operational Environmental Satellites (GOES-9). Rainfall data from TRMM (Tropical Rainfall Measuring Mission) Multi-satellite Precipitation Analyses (TMPA-RT) 3B41RT v7 for the period from 2001 to 2015. Wind data from the *Cross-Calibrated Multi-Platform* (CCMP) for the period from 2001 to 2015. The environmental parameter data is obtained from The European Center for Medium-Range Weather Forecasts (ECMWF) ERA-Interim Reanalysis for the period from 2001 to 2015. A total of 1028 MCCs were identified and tracked during the 15-year period from 2001 to 2015. Most of these MCCs were over the continental area, mainly near the mountains and the high elevation areas. The oceanic MCCs, which lasted for more than 12 hours, were longer-lived than the continental and coastal MCCs. Small-sized and large-sized MCCs most frequently occurred over the continental area and the ocean, respectively. The MCCs over the IMC had an average cloud shield area of around 315,000 km². MCCs developed when several small clouds or orographic clouds merged and grew larger because of interactions between the convergent surface wind flows and the land-sea breeze. Those observed in this study were usually nocturnal and reached a maximum at midnight. Convergent wind flows allowed the clouds to grow to a maximum size, and land-sea breezes became stronger during the mature stage. The MCCs decayed and dissipated because of divergent outflows from the cold pool, in conjunction with the land-sea breezes that generated and propagated new convective systems. These new convective systems migrated to areas

surrounding the MCCs, helped by land-sea breezes and interactions between the cold pool outflow and the westerly/southerly/easterly/northerly winds. During propagation, the new convective systems induced convective clouds in the areas surrounding them, which also followed the propagation of advection and convergence fields. It triggered new growth of either convective systems or continuous heavy rainfall systems induced by the new convective systems. The results from this study showed that, in general, the initial stage of the MCC was characterized by strong low-level convergence and vertical convection and was largely driven by the convergence of the moisture flux in the lower troposphere. The mature stage of the MCC was characterized by weak surface convergence, strong upper-level divergence, and a shortwave ridge in the mid- and upper-levels. Where there was strong surface divergence, the decay and dissipation stages were very similar, and surface convergence left the system. Movement of most MCCs resulted from the combined contributions of advection and the propagation of surface convergence. Results from this research show that these large convective systems tended to form in the vicinity of the terminus of a low-level jet that transported moist and warm air to the originating regions of the MCCs. Shortwave troughs and baroclinic zones were associated with MCC development. Results from the composite analysis were consistent with the case study, which indicates that MCCs in the same area as the case study shared the characteristics of the case study. The MCCs that occurred over the western coastal of Sumatra influenced the convective activity over the island of Sumatra; those that occurred over the northern coastal area of Kalimantan triggered a diurnal cycle over the South China Sea, and those that occurred in the coastal region of Papua near Merauke were related to cloud development over the Arafura Sea. Over the 15-year period, MCCs accounted for up to 20% of the total rainfall. Seasonal and monthly increases meant that MCCs accounted for up to 24% and 30%, respectively, of the total rainfall and, except July, the increases in the seasonal and monthly contributions were greater over the continental area than over the oceans. MCCs contributed to rainfall in both MCC areas and the surrounding areas. They contributed to extreme rainfall events over the IMC, mainly when they had reached their maximum extent. Almost all of the MCCs over the IMC produced extreme rainfall because the contributions from the MCCs were up to 45% greater for type 3 extreme events than for the other types. In future studies, this information about the development of MCCs should be integrated into regional weather models to allow precise prediction of MCCs. For further long-term predictions, however, the effects of large-scale

environments, i.e. the Madden-Julian Oscillation (MJO), El Niño-Southern Oscillation (ENSO), and Indian Ocean Dipole (IOD), on MCCs in the IMC need to be considered.

ACKNOWLEDGEMENTS

First and foremost, I wish to give thanks to the Allah SWT (God) that has given me strength and ability with the throughout my life, and in the process completed this study. I'm grateful to the National Institute of Aeronautics and Space (LAPAN), as institutions where I work that has to give me permission to continuing the study. I would also like to acknowledge to the Ministry of Research and Technology of the Government of Indonesia which had provided a full scholarship to my study. I wish to sincerely thank my first advisor, Professor Y. Kodama, for taking me on as a doctoral student in Hirosaki University, who is currently experiencing a serious health problem. I really hope he is quickly cured. I would like to express my gratitude to Prof. Kosuga and Prof. Nagase as supervisor too who has provided support and advised in the process complete my dissertation. I would like to express my sincere gratitude to Dr. Ishida who have helped me during a studying process in Hirosaki University, including administrative issues on campus. I would also like to thank the members of my dissertation committee; Prof. Iikura, Prof. Kataoka, and Prof. Ariga. I appreciate the time you took to understand my research and the eagerness with which you encouraged it.

Special thanks are offered to Dr. Moteki (Japan Agency for Marine-Earth Science and Technology, Yokosuka, Japan), Dr. Manda (Mie University), Dr. Iizuka (Monitoring and Forecast Research Department, National Research Institute for Earth Science and Disaster Prevention, Tsukuba, Japan) who have contributed at the same guiding so I could finish my first international paper. From them, I get the knowledge of how to make a good international paper. Special too thanks are offered to Prof. Yoshihiro Tachibana (Mie University, Japan), Prof. Hiroyuki Yamada (University of the Ryukyus, Japan), and Dr. Masaki Katsumata (Japan Agency for Marine–Earth Science and Technology, Japan), who have all offered critical comments and suggestions for the improvement of this paper. I am also very grateful to Dr. Kim Whitehall (Howard University) and Prof. Joshua D Durkee (Western Kentucky University) who has been willing to be consulted and responded all of my questions, even though just via email, about the identification methods of the MCCs (Dr. Kim) and the method of determining the contribution of MCCs to total rainfall (Prof. Durkee) that is very important in this research. Also thank for institution or official that provided the data of Himawari, CCMP, TRMM, OGIMET, and ECMWF, where these data are very important to complete this research. I must also acknowledge and thank the administrative staffs of the

Hirosaki University for their guidance throughout around the three half years while I'm studying in this university.

Finally, I wish to sincerely thank and dedicate this research to my lovely family (my wife and my daughters) that give happiness and support that is enough to keep me smiling. Happiness that can make me strong during this studying process. Special thank to my parents and my families in Indonesia, who pray for me and give support to success completed this study. Also thank for my Muslim brothers in Hirosaki (Ibnu, Ijlal, Taqi, Fahri, Amar, Amir, Babul, Sakur, Zubair, Waris and the others) and my Japanese friend (Keisuke San and his family), and acknowledge them for their support, friendships, and encouragement through it all.

TABLE OF CONTENT

ABSTRACT	i
ACKNOWLEDGEMENT	iv
TABLE OF CONTENT	vi
LIST OF TABLES	x
LIST OF FIGURES	xi
LIST OF ABBREVIATIONS AND SYMBOLS	xxi
1. INTRODUCTION	1
1.1. Background studies	1
1.2. Problem statement and motivation	2
1.2.1. Global distribution of MCSs over IMC	2
1.2.2. Climatology and characteristics of MCCs in several region.....	3
1.2.3. Review of the development and movement of MCCs over IMC	8
1.2.4. Review of the environmental conditions during MCC events	13
1.2.5. Review of the contribution of MCCs to rainfall	15
1.3. Research objectives and scopes	17
1.3.1. Research objectives	17
1.3.2. Research scopes	18
1.4. Research data	19
1.4.1. Satellite data for brightness temperature	19
1.4.2. Rainfall data from TRMM and OGIMET	20
1.4.3. Surface wind from CCMP data	21
1.4.4. ECMWF ERA-Interim data for environmental parameters	22
1.5. Research methods	23
1.5.1. Identification of MCCs and analyze of climatology of MCCs	23
1.5.2. Analyses of the evolution and propagation of the MCCs	24
1.5.3. Analyses of the environmental during MCC events	27
1.5.4. Determining the contribution of MCCs to rainfall.....	28
1.6. Research contribution and new finding report	30
1.7. Dissertation organization.....	31

2. LITERATURE REVIEW	32
2.1. Climate system in Indonesian Maritime Continent	32
2.1.1. IMC is one of the equatorial heat source regions.....	32
2.1.2. Atmospheric scale interaction over IMC	36
2.2. Atmospheric phenomena over IMC	38
2.2.1. Madden-Julian Oscillation (MJO)	39
2.2.2. El Niño Southern Oscillation (ENSO)	40
2.2.3. Indian Ocean Dipole (IOD).....	41
2.2.4. The Inter-Tropical Convergence Zone (ITCZ)	42
2.2.5. Monsoon.....	43
2.2.6. Land-sea breeze circulation	45
2.2.7. Mountain and valley breeze	46
2.3. Convective activity and rainfall system over IMC.....	46
2.3.1. Diurnal variation of convective activity.....	46
2.3.2. Rainfall system over IMC	51
2.4. The environmental parameters	55
2.4.1. Troposphere layer	55
2.4.2. Wind component	56
2.4.3. Temperature and geopotential height.....	57
2.4.4. Humidity and divergence field.....	60
2.4.5. Potential temperature and equivalent potential temperature.....	62
2.4.6. Moisture flux convergence and advection	63
2.5. MCS and MCC	64
2.5.1. Definition and types	64
2.5.2. The importance of MCS/MCC.....	65
 3. THE CLIMATOLOGY OF MESOSCALE CONVECTIVE COMPLEXES (MCCs)	
 IN INDONESIAN MARITIME CONTINENT DURING 15-YEARS PERIOD	68
3.1. Distribution of MCC occurrences	68
3.1.1. Global distribution of MCC occurrences	68
3.1.2. Seasonal distribution of MCC occurrences.....	74
3.1.3. Monthly distribution of MCC occurrences	76
3.1.4. Diurnal distribution of MCC occurrences.....	80

3.2. Morphological Characteristics of MCC	82
3.2.1. MCC maximum-extent distribution	82
3.2.2. MCC eccentricity at the time of maximum extent	83
3.3. Duration and life-cycle of MCC	84
3.3.1. MCC duration	84
3.3.2. MCC life-cycle.....	86
 4. THE EVOLUTION AND PROPAGATION OF THE MESOSCALE CONVECTIVE COMPLEXES (MCCs) OVER INDONESIAN MARITIME CONTINENT	 89
4.1. Evolution of the development of the MCC	89
4.1.1. MCC composite region	89
4.1.2. The oceanic MCC	92
4.1.3. The continental MCC.....	96
4.1.4. The coastal MCC	99
4.1.5. MCC composite region 1, region 4 and region 6.....	101
4.2. The development of new convective systems	103
4.2.1. The oceanic MCC	103
4.2.2. The continental MCC.....	107
4.2.3. The coastal MCC	111
4.2.4. MCC composite region 1, region 4 and region 6.....	113
4.3. Structure of the propagation of the MCC	117
4.4. Rainfall system during MCC events.....	119
4.4.1. Horizontal distribution of rainfall from TRMM	120
4.4.2. Comparison with observation data from OGIMET	123
 5. THE LARGE-SCALE ENVIRONMENTAL CONDITION DURING THE CRITICAL STAGE OF MESOSCALE CONVECTIVE COMPLEXES (MCCs) OVER THE INDONESIAN MARITIME CONTINENT	 126
5.1. Condition over the initial region.....	127
5.2. Condition over the mature region.....	137
5.3. Condition over the decay region.....	143
5.4. Condition over the dissipation or post-MCC region	149
5.5. Vertical cross section analysis.....	151

5.5.1. Divergence and vertical velocity field	151
5.5.2. Temperature advection and vorticity advection field	158
5.5.3. Equivalent potential temperature and relative humidity field.....	164
 6. THE CONTRIBUTION OF MESOSCALE CONVECTIVE COMPLEXES TO TOTAL RAINFALL AND EXTREME RAINFALL OVER INDONESIAN MARITIME CONTINENT	 168
6.1. The contribution of MCC to total rainfall	168
6.1.1. Global analysis	168
6.1.2. Seasonal analysis.....	170
6.1.3. Monthly analysis	172
6.2. The contribution of MCC to extreme rainfall.....	175
6.2.1. Spatial analysis of MRV and STD	175
6.2.2. Extreme threshold analysis	177
6.2.3. Accumulated rainfall produced by extreme rainfall	179
6.2.4. Seasonal contribution of MCCs to extreme rainfall.....	181
 7. CONCLUSION AND FUTURE WORK.....	 186
7.1. Conclusion.....	186
7.2. Future work	204
 REFERENCE	 206

LIST OF TABLES

Table 1.1.	Physical characteristics of MCCs (Maddox 1980)	4
Table 1.2.	Channel for Himawari 5 until Himawari 8.....	20
Table 7.1.	The comparison of the environmental condition of the continental, coastal and oceanic MCC during the initial stage.....	199
Table 7.2.	The comparison of the environmental condition of the continental, coastal and oceanic MCC during the mature stage.....	200
Table 7.3.	The comparison of the environmental condition of the continental, coastal and oceanic MCC during the decay and dissipation stage.....	201

LIST OF FIGURES

Figure 1.1. Annual climatology of MCS anvil clouds for calendar year 2007. Color shows percentage of area covered by anvil clouds associated with all.....	2
Figure 1.2. (a) Density of (top) CMCSs and (bottom) SMCSs for the years 2007–2010, expressed as number of systems per $1^\circ \times 1^\circ$ grid box per year (Virtz and Houze 2015). (b) (top) Jan 1993 (Mohr and Zipser 1996) and	3
Figure 1.3. Global distribution of mesoscale convective complexes and regions of widespread frequent deep convection as inferred by outgoing long-wave radiation (OLR) minima. Light shading indicates OLR minima.	5
Figure 1.4. (a) Relative frequency distribution of the duration of MCCs in Africa, South America (S. Amer), the United States (U.S), the western Pacific region (WPR). and the Indian subcontinent (ISC) on two-year population.....	6
Figure 1.5. (a) The locations of the cloud shields overlaid centroid locations from the 330 MCCs over South America observed between the warm season months of October–May during 1998–2007. Durkee and Mote (2009).....	7
Figure 1.6. Classification of meso- α -scale, convectively driven weather systems according to physical characteristics, organization, and location. Capital letters indicate types of systems that have been frequently considered in the literature.....	8
Figure 1.7. Schematic of the development of diurnally generated mesoscale precipitation feature of the coast of Kalimantan	10
Figure 1.8. Schematic diagram for the hierarchy of the intraseasonal variations (ISV)	11
Figure 1.9. Distribution of all very cold (<208 K) cloud clusters $1000\text{--}3000 \text{ km}^2$ in area observed in images at (a) 2300 UTC (0900 LT) and (b) 0800 UTC (1800 LT) for period of 1 November 1986 - 28 February 1987.....	11
Figure 1.10. Schematic illustration of a westward-propagating meso- α -scale over Sumatera and precipitation systems within an orographic cloud system over the mountain range in western Sumatera	12
Figure 1.11 Schematic illustration of northward propagating MCSs based on satellite images at (a) 2100 LT on 14 June 2005 and at (b) 0300 LT, (c) 0900 LT, and (d) 1500 LT on 15 June 2005. LE denotes the low-pressure.....	13
Figure 1.12. (a) MCS fractional contribution to rainfall and (b) MCS contribution to monthly rainfall (mm/month).....	16
Figure 1.13 IMC map	18

Figure 1.14. (a) Average track of 122-cases composite MCC. S, X, and E denote centroid area at the Start, Maximum and End. McAnelly and Cotton (1988). (b) Stratification of 12-cases of MCC using composite analysis.....	25
Figure 1.15. Horizontal distribution of rainfall accumulation during MCC event at 14 - 15 April 2012 that shows the example of what is the meaning of the MCC rainfall in storm area or MCC area (red circle) and MCC rainfall as affected area by MCC (red dotted circle). Unit for rainfall is mm/hr	28
Figure 2.1. The map show that IMC as equatorial region is in located between two continents (Asia and Australia) and between two oceans (Indian and Pacific Ocean)	32
Figure 2.2. Schematics of the global Walker Circulation for Winter (DJF) based on computations of upper and lower tropospheric divergent winds.	33
Figure 2.3. a) Three cells on each side of the equator control vertical and horizontal air flows. b) A schematic diagram of the Hadley circulation and its associated zonal flows and surface circulation	34
Figure 2.4. Global annual radiation budget (W m^{-2})	35
Figure 2.5. Average kinetic energy spectra (spectral density) of the free-atmospheric zonal wind as a function of frequency. Numbers show maximum kinetic energy at particular periods.....	36
Figure 2.6. Scale interaction for the climate system over IMC	39
Figure 2.7. Equatorial vertical cross section of the MJO as it propagates from the Indian Ocean to the western Pacific	40
Figure 2.8. Normal, El Niño and La Niña conditions across the Pacific Ocean. The Maritime Continent lies at the left hand edge of the schematics	41
Figure 2.9. Schematic of a positive and negativ IOD event. SST anomalies are shaded (red color is for warm anomalies and blue is for cold).....	42
Figure 2.10 As the Intertropical Convergence Zone (ITCZ) changes location through the year, the winds, rains, and the location of wet monsoon weather changes, too. In this example from Asia and Australia.....	43
Figure 2.11 Schematic of monsoon wind for the boreal summer (June- September) (left) and the boreal winter (December-February) (right)	44
Figure 2.12 Schematic of sea-breeze (top) and land-breeze (bottom).....	45
Figure 2.13 Valley breezes blow uphill during the day; mountain breezes blow downhill at night. (The L's and H's represent pressure, whereas the purple lines represent surfaces of constant pressure.	46

Figure 2.14 Schematic of convection process; a) The process of rising air mass / parcels due to the thermal force, b) mechanical process due to sea breeze forcing the air parcel of rising because of the effect of orographic	47
Figure 2.15. NOAA Interpolated Outgoing Longwave Radiation (OLR)- a proxy for deep convective activity, highlighting the majortropical convective centres.....	48
Figure 2.16. Schematic pictures of diurnal land–sea rainfall peak migration and circulations related to the migration	49
Figure 2.17. (a) Daily mean precipitation rate for northern winter 2008–2009	51
Figure 2.18. Rainfall patterns in IMC. Yellow is for monsoon pattern, green is for equatorial pattern and red is for local pattern	52
Figure 2.19 The averaged (2003-2006) CMORPH seasonal rainfall (mm/day) (shahed).....	53
Figure 2.20. Monthly and longitudinal variations in the total rainfall (TRMM- 3B42) over 15°S–15°N	53
Figure 2.21 Climatological diurnal cycle of precipitation rate from TRMM 3B42HQ for November to April, 1998/99 to 2011/12. Time of day is given in local solar time for all longitudes	54
Figure 2.22. The layer of the Earth's atmosphere	55
Figure 2.23. Illustration of wind direction (a) and zonal-meridional wind flow (b)	57
Figure 2.24. Illustration of the trough and ridges in the middle level of the troposphere.	59
Figure 2.25. Example of two shortwave troughs embedded in a longwave system.....	59
Figure 2.26. Illustrating of; (a) the baroclinic boundary/zone and (b) low-level jet	60
Figure 2.27. Horizontal convergence, divergence and vertical motion of air	61
Figure 2.28. A squall line, (b) Bow echo over Springdale, Arkansas, 21 May 2013	65
Figure 3.1. Geographical distribution of MCCs in Indonesian Maritime Continent during 15-years (2001-2015). Locations are for the MCC at the time of maximum extent of the interior cloud size area when the mature stage. The circles representing the interior cloud size area (10^3 km^2)	69
Figure 3.2. Percentage of MCC occurrences over the IMC during 15-years (2001-2015) in ocean, coastal and continent.....	70
Figure 3.3. A total of MCC occurrences over the IMC during 15-years (2001-2015) for each year.....	73

Figure 3.4. Percentage of MCC occurrences over the IMC during 15-years (2001-2015); (a) for each season. (b) for each season in coastal, continent and ocean	74
Figure 3.5. Geographical distribution of MCCs in Indonesian Maritime Continent during 15-years (2001-2015) for each season; (a) DJF, (b) MAM, (c) JJA and (d) SON.....	75
Figure 3.6. A total of MCC occurrences over the IMC during 15-years (2001-2015); (a) for each month, (b) for each season in coastal, continent and ocean.....	77
Figure 3.7. Geographical distribution of MCCs in Indonesian Maritime Continent during 15-years (2001-2015) for each month; (a) January, (b) February, (c) March, (d) April, (e) May and (f) June	78
Figure 3.8. Same with Figure 3.7 but for; (a) July, (b) August, (c) September, (d) October, (e) November and (f) December.....	79
Figure 3.9. Diurnal distribution of MCCs in Indonesian Maritime Continent during 15-years (2001-2015); (a) 0000 - 0300 LT, (b) 0400 - 0700 LT, (c) 0800 - 1100 LT, (d) 1200 - 1500 LT, (e) 1600 - 1900 LT and (f) 2000 - 2300 LT	80
Figure 3.10. Frequency distribution of; a) MCC cloud shield maximum area and b) MCC interior cloud maximum area during 15-years.....	82
Figure 3.11. (a) Box and Whisker plot of interior cloud size area of MCC frequency by month during 15-years	83
Figure 3.12. Number of MCC eccentricity at the time of maximum extent during 15-years (2001-2015).....	84
Figure 3.13. (a) Frequency distribution of duration of MCCs over the IMC during 15-years. (b) Box and Whisker plot of duration of MCC frequency during 15-years.....	85
Figure 3.14. Frequency distribution of duration of MCCs over the coastal region, ocean, and continent during 15-years.....	85
Figure 3.15. Scatter plots showing relationship; (a) between latitude and duration, (b) between duration and interior cloud size and.....	86
Figure 3.16. Frequency distribution of all MCCs during critical stage (initial, mature, decay and dissipation or post-MCC stage).....	87
Figure 3.17. Frequency distribution of coastal, continent and oceanic MCCs during critical stage (initial, mature, decay and dissipation or post-MCC stage)	88
Figure 4.1. (a) same with Figure 3.1 but the red box show the MCC composite region with number label 1, 2, 3, 4, 5 and 6 as region 1, region 2, region 3, region 4, region 5 and region 6, respectively	90

Figure 4.2. Frequency distribution of the initiation, mature, decay, and dissipation or post-MCC time of the MCC in each region. where; (a) region 1, (b) region 2, (c) region 3, (d) region 4, (e) region 5, (f) region 6.....	92
Figure 4.3. Horizontal distribution of black body temperature (T_{BB}) for Mesoscale Convective Complex (MCC) criteria from infrared data obtained by MTSAT-1R over the Indian Ocean near Sumatra on 27–28 October 2007, showing the eight stages of MCC evolution.....	93
Figure 4.4. Horizontal distribution of composite of the T_{BB} for 29-case of MCC composite region 2 over the nearly same area with the case study 1	94
Figure 4.5. Horizontal distribution of T_{BB} for MCC criteria from infrared data obtained by MTSAT-1R over Kalimantan Island on 14-15 April 2012.....	96
Figure 4.6. Horizontal distribution of composite of the T_{BB} for 45-case of the MCC composite region 3: (a), (b) Initial stage (around 1800 LT and 2000 LT)), (c),(d) mature stage (around 2300 LT to 0100 LT), (e),(f) decay stage (around 0400 LT and 0700 LT), (g),(h) dissipation stage (around 1000 LT and 1100 LT)	98
Figure 4.7. Horizontal distribution of T_{BB} for MCC criteria from infrared data obtained by MTSAT-1R over Kalimantan Island on 22 - 23 October 2011	100
Figure 4.8. Horizontal distribution of composite of the T_{BB} for 11-case of MCC composite region 5 over the nearly same area with the case study 1	101
Figure 4.9. Same with Figure 4.8 but for 38-case of MCC composite region 1.....	102
Figure 4.10. Same with Figure 4.8 but for 42-case MCC composite region 4.....	102
Figure 4.11. Same with Figure 4.8 but for 42-case of MCC composite region 6	103
Figure 4.12. Horizontal distribution of convective index (C_I) (shaded) from infrared data of MTSAT-1R, wind surface vector anomaly (vector) from Cross-Calibrated Multi-Platform (CCMP) data, and surface potential temperature (contour) from the European Centre for Medium-Range Weather Forecasts (ECMWF) ERA-Interim data during the occurrence of the Mesoscale Convective Complex (MCC)	104
Figure. 4.13. Horizontal distribution of the composite analysis of the average rainfall (shaded), wind surface vector anomaly (vector) data, and surface θ (contour) for several cases of the MCC that occur in the region 2 on the hours of initiation, mature, decay and dissipation or post-MCC.	106
Figure 4.14. Horizontal distribution of convective index (C_I) (shaded) from infrared data of MTSAT-1R, wind surface vector anomaly (vector) from CCMP data, and surface θ (contour) from the ECMWF ERA-Interim data during the occurrence of the MCC over the Central Kalimantan	108

Figure 4.15. Horizontal distribution of the composite analysis of the average rainfall (shaded), wind surface vector anomaly (vector) data, and surface θ (contour) for several cases of the MCC that occur in region 3.....	110
Figure 4.16. Horizontal distribution of convective index (C_1) (shaded) from infrared data of MTSAT-1R, wind surface vector anomaly (vector) from CCMP data, and surface θ (contour) from the ECMWF ERA-Interim data during the occurrence of the MCC over the western coastal of Sulawesi	111
Figure 4.17. Horizontal distribution of the composite analysis of the average rainfall (shaded), wind surface vector anomaly (vector) data, and surface θ (contour) for several cases of the MCC that occur in region 5.....	112
Figure 4.18. Horizontal distribution of the composite analysis of the average rainfall (shaded), wind surface vector anomaly (vector) data, and surface θ (contour) for several cases of the MCC that occur in region 1.....	114
Figure 4.19. Horizontal distribution of the composite analysis of the average rainfall (shaded), wind surface vector anomaly (vector) data, and surface θ (contour) for several cases of the MCC that occur in region 4.....	115
Figure 4.20. Horizontal distribution of the composite analysis of the average rainfall (shaded), wind surface vector anomaly (vector) data, and surface θ (contour) for several cases of the MCC that occur in region 6.....	117
Figure 4.21. Time-longitude cross-sections (averaged for latitude $6^{\circ}\text{S} - 0^{\circ}\text{N}$) during the oceanic MCC in case study 1	118
Figure 4.22. Latitude-time cross-sections (averaged for longitude $102-116^{\circ}\text{E}$) during the continental MCC in case study 2	119
Figure. 4.23. Time-longitude cross-sections (averaged for latitude $5^{\circ}\text{S} - 2^{\circ}\text{N}$) during the coastal MCC in case study 3	119
Figure 4.24. Horizontal distribution of rainfall from TRMM TMPA 3B41RT data during the occurrence of the MCC in case study 1	120
Figure 4.25. Horizontal distribution of rainfall from TRMM TMPA 3B41RT data during the occurrence of the MCC in case study 2	121
Figure 4.26. Horizontal distribution of rainfall from TRMM TMPA 3B41RT data during the occurrence of the MCC in case study 3	122
Figure. 4.27 Horizontal distribution of rainfall accumulated from the Pre-MCC stage until 6 hours after the post-MCC stage. Rainfall data obtained from TRMM TMPA 3B41RT (a) Case study 1; (b) case study 2 that.....	123
Figure 4.28. Rainfall observational data during the occurrence of oceanic MCC in the case study 1 over the Indian Ocean near Sumatra on 28 October 2007 (1300–2400 LT).....	124

Figure 4.29. (a) Surface θ and surface pressure at Palangkaraya and Pangkalan Bun, (b) Relative humidity and surface temperature, and (c) Rainrate at Palngkaraya and Pangkalan Bun from OGIMET	125
Figure 4.30. (left) Surface θ and surface pressure at Samarinda and Balikpapan, (middle) Relative humidity and surface temperature at Samarinda and Balikpapan and (right) Rainrate at Samarinda and Balikpapan	125
Figure 5.1. Environmental conditions during initial stage of the oceanic MCC in case study 1 using ECMWF ERA-Interim data, showing; (a). 1000-hPa θ (potential temperature in K, shaded), 1000-hPa geopotential height (m, contour) and 1000-hPa wind vector (ms^{-1} , vector). Red circle refers to the MCC location. (b).	128
Figure 5.2. Same with Figure 5.1, but for the environmental conditions during the initial stage of the continental MCC in case study 2. The red circle in figure (a) refers to the MCC location.....	131
Figure 5.3. Same with Figure 5.1, but for the environmental conditions during the initial stage of the coastal MCC in case study 3. The red circle in figure (a) refers to the MCC location.....	133
Figure 5.4. Composite analysis of the environmental conditions during initial stage using ECMWF ERA-Interim data, showing; in MCC composite region 2; (a).	134
Figure 5.5. Same with Figure 5.4 but (a), (b), (c) and (d) for MCC composite region 1. (e), (f), (g), (h) for MCC composite region 4. While (i), (j), (k) and (l) for MCC composite region 6.	136
Figure 5.6. Same with Figure 5.1, but for the environmental condition during mature stage of the oceanic MCC in case study 1	137
Figure 5.7. Same with Figure 5.1, but for the environmental conditions during mature stage of the continental MCC in case study 2	138
Figure 5.8. Same with Figure 5.1, but for the environmental conditions during mature stage of the coastal MCC in case study 3.....	139
Figure 5.9. Same with Figure 5.4 but for mature stage	141
Figure 5.10. Same with Figure 5.4 but for mature stage; (a), (b), (c) and (d) for MCC composite region 1; (e), (f), (g), (h) for MCC composite region 4; and (i), (j), (k) and (l) for MCC composite region 6	142
Figure 5.11. Same with Figure 5.1, but for the environmental conditions during decay stage of the oceanic MCC in case study 1	144
Figure 5.12. Same with Figure 5.1, but for the environmental conditions during decay stage of the continental MCC in case study 2	145

Figure 5.13. Same with Figure 5.1, but for the environmental condition during decay stage of the coastal MCC in case study 3	146
Figure 5.14. Same with Figure 5.4 but for decay stage	147
Figure 5.15. Same with Figure 5.4 but for decay stage; (a), (b), (c) and (d) for MCC composite region 1; (e), (f), (g), (h) for MCC composite region 4; and (i), (j), (k) and (l) for MCC composite region 6.	148
Figure 5.16. Same with Figure 5.1, but for the environmental conditions during dissipation or post-MCC stage of the oceanic MCC in case study 1.....	149
Figure 5.17. Same with Figure 5.1, but for the environmental conditions during dissipation stage or post-MCC of the continental MCC in case study 2.....	150
Figure 5.18. Same with Figure 5.4 but for dissipation stage.	151
Figure 5.19. Pressure-longitude cross section (averaged for latitude $6^{\circ}\text{S} - 0^{\circ}\text{N}$) of divergence (10^{-5} s^{-1} , shaded), vertical velocity ($10^{-2} \text{ Pa s}^{-1}$, contour) and horizontal wind (vector; ms^{-1} ; upward represents northward) for MCC case study 1	152
Figure 5.20. Pressure-latitude cross section (averaged for longitude $110^{\circ} - 116^{\circ}\text{E}$) of divergence (10^{-5} s^{-1} , shaded), vertical velocity ($10^{-2} \text{ Pa s}^{-1}$, contour) and horizontal wind (vector; ms^{-1} ; upward represents northward) for MCC case study 2	154
Figure 5.21. Pressure-longitude cross section (averaged for latitude $5^{\circ}\text{S} - 2^{\circ}\text{N}$) of divergence (10^{-5} s^{-1} , shaded), vertical velocity ($10^{-2} \text{ Pa s}^{-1}$, contour) and horizontal wind (vector; ms^{-1} ; upward represents northward) for MCC in case study 3	155
Figure 5.22. Same with Figure 5.19 but for MCC composite region 2	156
Figure 5.23. Same with Figure 5.20 but for MCC composite region 3	157
Figure 5.24. Same with Figure 5.21 but for MCC composite region 5	158
Figure 5.25. Pressure-longitude cross section (averaged for latitude $6^{\circ}\text{S} - 0^{\circ}\text{N}$) of vorticity advection (contour; 10^{-8} s^{-1}) and temperature advection (shaded; 10^{-5} K s^{-1}) for MCC case study 1	160
Figure 5.26. Same with Figure 5.25 but for composite analysis of MCC composite region 2	161
Figure 5.27. Pressure-latitude cross section (averaged for longitude $110^{\circ} - 116^{\circ}\text{E}$) of vorticity advection (contour; 10^{-6} s^{-1}) and temperature advection (shaded; 10^{-5} K s^{-1}) for MCC case study 2	162
Figure 5.28. Same with Figure 5.27 but for composite analysis of MCC composite region 3	163

Figure 5.29. Pressure-longitude cross section (averaged for latitude 5°S - 2°N) of vorticity advection (contour; 10^{-8} s^{-1}) and temperature advection (shaded; 10^{-5} K s^{-1}) for MCC case study 3	164
Figure 5.30. Same with Figure 5.28 but for MCC composite region 5	164
Figure 5.31. Pressure-longitude cross section (averaged for latitude 6°S - 0°N) of θ_E (contour; K) and relative humidity (shaded; %) and horizontal wind (vector; ms^{-1} ; upward represents northward) for MCC in case study 1	165
Figure 5.32. Pressure-latitude cross section (averaged for longitude 110° - 116°E) of θ_E (contour; K) and relative humidity (shaded; %) and horizontal wind (vector; ms^{-1} ; upward represents northward) for MCC in case study 2	166
Figure 5.33. Pressure-longitude cross section (averaged for latitude 5°S - 2°N) of θ_E (contour; K) and relative humidity (shaded; %) and horizontal wind (vector; ms^{-1} ; upward represents northward) for MCC in case study 3	167
Figure 6.1. The frequency distribution of MCC contribution to total rainfall during 2001-2015. The legend is representing the percentage of MCC contribution	170
Figure 6.2. Spatial distribution of percentage for the MCC contribution to total rainfall during 2001-2015 in each season; (a) DJF, (b) MAM, (c) JJA, and (d) SON.	171
Figure 6.3. Frequency distribution of percentage for the MCC contribution to monthly rainfall during 2001-2015 (shaded), the legend representing the percentage of MCC contribution..	173
Figure 6.4. Same with Figure 6.3 but for July, August, September, October, November, and December	174
Figure 6.5. Horizontal distribution of climatology of the maximum rainfall during 15-years on 2001-2015 period for each season; a) DJF, b) MAM, c) JJA, d) SON.....	175
Figure 6.6. Horizontal distribution of standard deviation from mean of maximum rainfall during 15-years on 2001-2015 period for every season.....	176
Figure 6.7. Extreme threshold (a) DJF (left) and (b) MAM (right) during 15-years on 2001-2015 period for all type	178
Figure 6.8. Same with Figure 6.7 but for (a) JJA and (b) SON.....	179
Figure 6.9. The climatology of accumulated rainfall of (a) DJF (lef) and (b) MAM (right) during 15-years on 2001-2015 period for all type	180
Figure 6.10. Same with Figure 6.9 but for (a) JJA and (b) SON.....	181
Figure 6.11. The contribution of MCC for extreme rainfall at (a) DJF and (b) MAM during 15-years (2001-2015).....	182

Figure 6.12. Same with Figure. 6.11 but for (a) JJA	184
Figure 7.1. Schematic representations of the evolution and propagation of the MCC over region 1	190
Figure 7.2. Schematic representations of the evolution and propagation of the MCC over region 2	191
Figure 7.3. Schematic representations of the evolution and propagation of the MCC over region 3	192
Figure 7.4. Schematic representations of the evolution and propagation of the MCC over region 4	193
Figure 7.5. Schematic representations of the evolution and propagation of the MCC over region 5	194
Figure 7.6. Schematic representations of the evolution and propagation of the MCC over region 6	195
Figure 7.7. Vertical schematic representations of the development of the MCC over region 2 related in the Indian Ocean	198

LIST OF ABBREVIATIONS AND SYMBOLS

Abbreviation:

AMSR-E	Advanced Microwave Scanning Radiometer for Earth Observing System
CAPE	Convective Available Potential Energy
CC	Cloud Clusters
CCMP	Cross-Calibrated Multi-Platform
CIT	Convectively induced turbulence
CMCS	Connected MCSs
DJF	December, January and February (wet seasons)
EET	Extreme Event Type
ECMWF	European Center for Medium-Range Weather Forecasts
ENSO	El Niño Southern Oscillation
EOF	Empirical Orthogonal Function
EUMETSAT	European Organization for the Exploitation of Meteorological Satellites
GMS	Geostationary Meteorological Satellite
GMS-IR	Geostationary Meteorological Satellite Infrared
GOES	Geostationary Operational Environmental Satellites
hPa	hectoPascals
IMC	Indonesian Maritime Continent
IOD	Indian Ocean Dipole
IR	Infrared
ISC	The Indian Subcontinent
ISCCP	International Satellite Cloud Climatology Project
ISO	Intraseasonal Oscillation
ISV	Intraseasonal Variation
ITCZ	Intertropical Convergence Zone
JAXA	Japan Aerospace Exploration Agency
JJA	June, July and August (dry seasons)
JMA	Japan Meteorological Agency
LLJ	Low Level Jet
LT	Local Time

MAM	March, April and May (transition seasons from dry to wet)
MASCOTTE	Maximum Spatial Correlation Tracking Technique
MB	Milibars
MCC	Mesoscale Convective Complexes
MCS	Mesoscale Convective Systems
MFC	Moisture Flux Convergence
MJO	Madden Julian Oscillation
MODIS	Modulate Resolution Imaging Spectroradiometer
MRV	Maximum Rainfall Value
MTSAT	Multi-functional satellite imagery Transport SATellite
NCT	Near-cloud Turbulence
NOAA	National Oceanic and Atmosphere Administration
NVA	Negative Vorticity Advection
OLR	Outgoing Longwave Radiation
PCT	Polarized Corrected Temperature
PGM	Portable Grey Map
PVA	Positive Vorticity Advection
RSS	Remote Sensing Systems
SC	Superclusters
SMCS	Separated MCSs
SON	September, October and November (transition season from wet to dry)
STD	Standard Deviation
TMPA	TRMM Multi-satellite Precipitation Analyses
TRMM	Tropical Rainfall Measuring Mission
U.S	United States
VAM	Variational Analyses Method
W-MONEX	the International Winter Monsoon Experiment
WPR	The Western Pacific Region

Symbols:

C_i	Convective Index
EET-1	Extreme Event Type 1
EET-2	Extreme Event Type 2

EET-3	Extreme Event Type 3
θ	Potential Temperature
θ_E	Equivalent Potential Temperature
T_{BB}	Brightness Temperature or Black Body Temperature

CHAPTER ONE

INTRODUCTION

1.1 Background studies

This research was a continuation of the research conducted by Trismidianto (2012) as part of his final master's thesis submitted to Bandung Institute of Technology entitled "A study of mesoscale convective complexes (MCCs) activities in the western Indian Ocean and their effects on convection over Sumatra Island". Mesoscale convective complexes (hereafter MCCs) are a special case of mesoscale convective systems (hereafter MCSs), where MCS was portrayed as an organized ensemble of convective elements, whose lifecycle is longer than that of the individual convective elements, and the largest of the convective storms. They form, when clouds occurring in response to convective instability amalgamate and organize upscale into a single cloud system with a very large upper cirriform cloud structure and rainfall covering large contiguous rain areas (Houze 2004).

Trismidianto (2012) have reported that MCC in the Indian Ocean near of Sumatra Island influencing weather pattern in several regions over Sumatra Island. His result has been posited that there is the role of cold pools during MCC in influencing the rainfall, but he only analyzed the present of new convective systems using convective index by spatial analysis, not only over the Indian Ocean but also over Indonesian Maritime Continent (hereafter IMC). Such that, the enthusiasm to give a deep understanding of the mechanism of MCC that relates to the land-sea breeze influencing the rainfall. For 10-years (i.e, 2000 - 2009), Trismidianto (2012) also realized the greatest frequency of MCC occurrence in the transition season March, April, and May, and duration of the life cycle of MCC in the Indian Ocean about 12 to 15 hours.

The existence and characteristic of MCCs over IMC have been studied using infrared (hereafter IR) satellite imagery from geostationary meteorological satellite (GMS) observations of 5-years (i.e., 2001-2005) periods cited by Ismanto (2011). He has reported that 36% of MCC found in the Eastern Indian Ocean (including Sumatra Island), 15 % in Papua Island, 13% in Northern Papua, 13% in Kalimantan Island, 9.5% in Northern Australian and 13.5% in the widespread area except those regions. He found that MCCs appearances are predominantly nocturnal with an average lifetime of 12.2 hours, but, Ismanto (2011) only used short data to explain the characteristics of the MCC over the IMC.

1.2 Problem statement and motivation

1.2.1 Global distribution of MCSs over IMC

Yuan and Houze (2010) have identified MCSs using three A-train satellite instruments; Moderate Resolution Imaging Spectroradiometer (MODIS) for cloud-top size and coldness, Advanced Microwave Scanning Radiometer for Earth Observing System (AMSRE) for rain area size and intensity, and CloudSat for horizontal and vertical dimensions of anvils. They distinguished two types of MCSs, namely, separated MCSs (SMCS) and connected MCSs (CMCS), where all of those MCS types in the tropics produce extensive anvil clouds, which significantly affect the transfer of radiation. They also show that the anvil clouds from active MCSs concentrate in tropical deep convective regions and that the greatest fractional coverage of them relatively found over the Indian Ocean, Kalimantan Island, and Papua Island as shown in Figure 1.1. Yuan and Houze (2010) also noted that SMCSs frequently observed over the Maritime Continent region. CMCSs are not frequent over the Maritime Continent nevertheless, account for about 30% of all MCSs in the Indian Ocean ITCZ (Inter-Tropical Convergence Zone) extending westward from Sumatra south of the equator; the western Pacific Ocean ITCZ centered around 5° – 7° N, and the southeast of New Guinea or Papua Island. Briefly, they stated that IMC is one of the most frequently found of MCS.

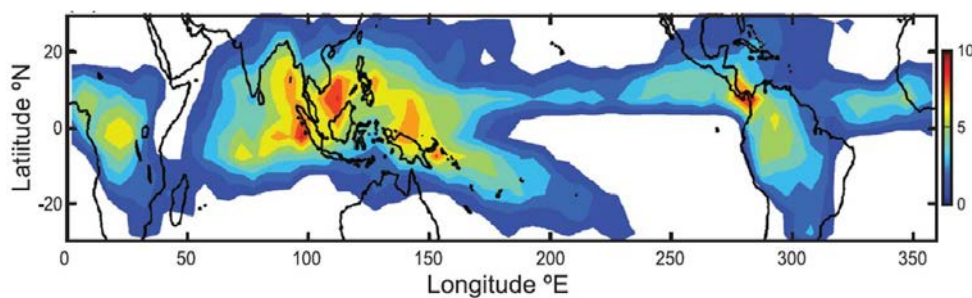


Figure 1.1. Annual climatology of MCS anvil clouds for the calendar year 2007. Color shows the percentage of area covered by anvil clouds associated with all of the MCSs for each $5^{\circ} \times 5^{\circ}$ grid (Yuan and Houze 2010).

Virts and Houze (2015) have reported the characteristics of MCSs in regions affected by the Madden–Julian oscillation (hereafter MJO) using a similar method with Yuan and Houze (2010). They found 33,548 number of MCSs over Maritime Continent and 20,760 over the Indian Ocean for four years (i.e., 2007 - 2010) as shown in Figure 1.2 (a). Mohr and Zipser (1996) have reported that IMC is one of the frequently occurred areas for MCS

development as shown in Figure 1.2 (b). They have identified MCS using the physical basis for the PCT (polarized corrected temperature) that calculated from the 85-GHz horizontally and vertically polarized brightness temperature by comparing SSM/I satellite imagery with radar reflectivity. The greatest number of large MCSs found over North America and the North Atlantic, subtropical South America, and the South Pacific and Tropics (include IMC). The most intense MCSs were found over land or very near the coasts. This finding, is supported by the studies of LeMone and Zipser (1980), Zipser and LeMone (1980), Jorgensen and LeMone (1989), and Lucas et al. (1994).

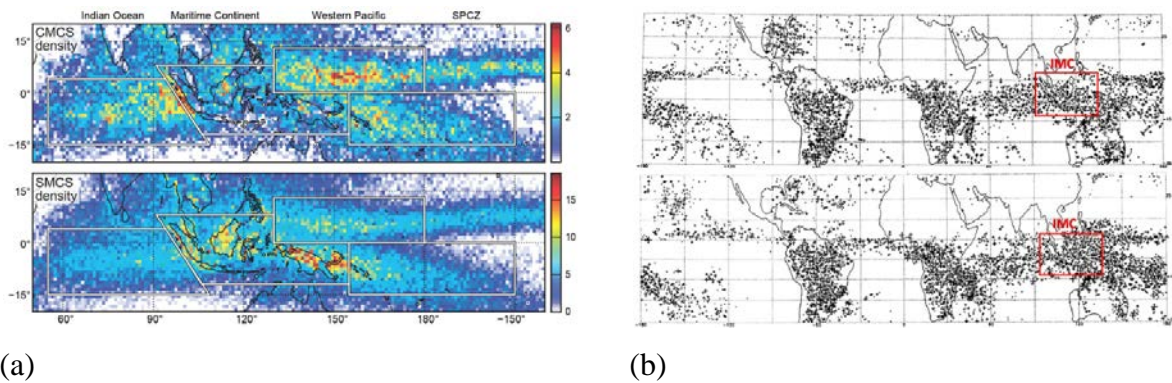


Figure 1.2. (a) The density of (top) CMCSs and (bottom) SMCSs for the years 2007–2010, expressed as some systems per $1^\circ \times 1^\circ$ grid box per year (Virtz and Houze 2015). (b) (top) Jan 1993 (Mohr and Zipser 1996) and (bottom) Jan 1996 MCSs by PCT (polarization-corrected temperature) class (Mohr and Zipser 1996).

Zolman et al. (2000) share a similar method with Mohr and Zipser (1996) and they found 9151 number of MCSs from 1993 - 1995 over IMC, where around 2810 exists in winter seasons and around 2019 also exist in summer. Similar to Toracinta and Zipser 2001, they have found 9965 from June 1995 to May 1996 in IMC. On average, almost all the previous researches about MCS over IMC which were explained earlier have stated IMC is one of the frequently concentrated areas for MCS development. In lieu of that, it is possible the existence of MCC from their result since MCC is one of the types of MCS. The climatology and characteristics of MCS or MCC over IMC was not categorically been explained by them.

1.2.2 Climatology and characteristics of MCCs in several region

Before 1980, the study of convective activity at the mesoscale level was limited to tropical phenomena such as cloud clusters (hereafter CCs), squalls and hurricanes, midlatitude

squall lines and land-sea breeze systems. In 1980, Robert A. Maddox introduced the concept of the MCC after a careful study of satellite IR images over the central United States during 1978. The MCC was contrasted with the midlatitude squall line and found to be a unique entity, forming under different synoptic conditions and having completely different characteristics. With these differences in mind, he created an admittedly arbitrary and somewhat artificial definition to promote further research. Characteristics of MCC was first reported by Maddox (1980). He stated that MCC have cloud shield with continuously brightness temperature or black body temperature (hereafter T_{BB}) $\leq -32^{\circ}\text{C}$ (in this study converted to 241 K) and must have an area $\geq 100,000 \text{ km}^2$. The interior cold cloud has $T_{BB} \leq -52^{\circ}\text{C}$ (in this study converted to 221 K) and must have an area $\geq 50,000 \text{ km}^2$ for over six hours, although the cloud shield does not have to maintain an eccentricity of ≥ 0.7 for its entire life cycle. The eccentricity is also important to distinguish MCC from the other MCS type, for example; squall line, bow echo, CC and the others. The areal extent and eccentricity values used to determine the duration and life cycle of the MCCs, while the centroid position indicated the path of propagation of the systems. The explanation of MCC based on Maddox (1980) criteria over IMC is still rarely found, so it became interesting to explore MCC over IMC based on Maddox (1980). The physical characteristics of MCC by Maddox (1980) as noted in Table 1.1.

Table 1.1. Physical characteristics of MCCs (Maddox 1980)

Size:	A-Cloud shield with continuously low $T_{BB} \leq -32^{\circ}\text{C}$ (241 K) must have an area $\geq 100,000 \text{ km}^2$ B-Interior cold cloud region with $T_{BB} \leq -52^{\circ}\text{C}$ (221 K) must have an area $\geq 50,000 \text{ km}^2$
Initiate:	Size definitions A and B are first satisfied
Duration:	Size definition A and B must be met for period of ≥ 6 hours
Maximum extent:	Contiguous cold cloud shield ($T_{BB} \leq -32^{\circ}\text{C}$ (241 K)) reaches a maximum size
Shape:	Eccentricity (minor axis/major axis) ≥ 0.7 at time of maximum extent
Terminate:	Size definitions A and B no longer satisfied

Several groups of scientists all over the world have used satellites to study MCC, for example; MCC in Africa (Laing and Fritsch 1993b; Laing 1999), Tropical African (e.g. Arnaud et al. 1992; Machado et al. 1992; Mathon and Laurent 2001), India (Laing and Fritsch 1993a), Australia (James 1992), Europe (Laing and Fritsch 1997), South America (Laing and

Fritsch 2000; Vera et al. 2006; Salio et al. 2007), most extensively in North America (Maddox 1980; Rodgers et al. 1983; Merritt and Fritsch 1984; Kane et al. 1987; Tollerud et al. 1987; Cotton et al. 1989; McAnelly and Cotton 1989; Tollerud and Rogers 1991; Tollerud and Collander 1993; Anderson and Arritt 1998; Ashley et al. 2003, among others), most notably the central plains of the United States (e.g., Maddox 1980; Rodgers et al. 1983), Central and South America (Velasco and Fritsch 1987), China, Australia, and the Western Pacific Region (Miller and Fritsch 1991). In general, they came to a conclusion that, MCCs are mainly nocturnal MCSs which last about 10 hours and MCCs principally occur over land or close to the coast. However, the climatology of MCCs has not been given attention in detail over IMC.

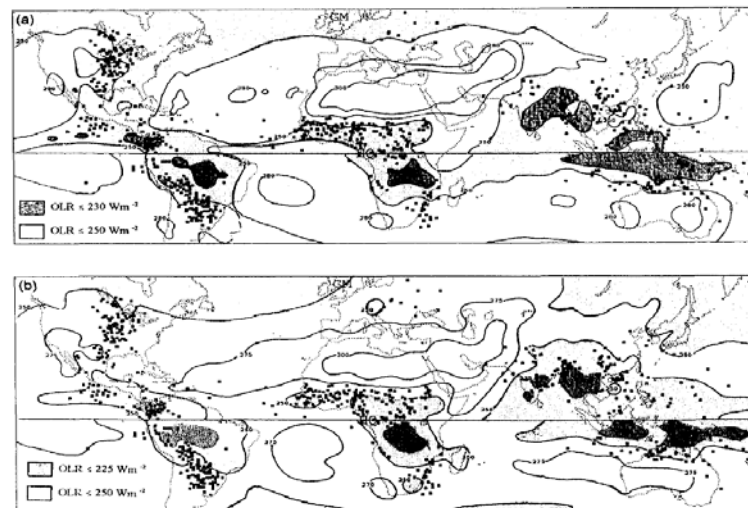


Figure 1.3. Global distribution of MCC and regions of widespread, frequent deep convection as inferred by outgoing long-wave radiation (OLR) minima. Light shading indicates OLR minima. OLR measurements in W m^{-2} obtained from (a). Earth Radiation Budget Experiment for July (above the line) and January (below the line) 1985-86, and (b). Earth-Atmosphere Radiation Budget analyses, for June-August (above the line) and December-February (below the line), 1974-78.

Laing and Fritsch (1997) have studied the characteristics of MCCs globally. They are of the view that, more than 400 MCCs occur at various locations around the globe each year, but mostly in tropical and mid-latitude locations, with approximately 66 percent of the occurrences in the Northern Hemisphere. They also found that, 91% over continents even though they can occur over oceans as shown in Figure 1.3. The average duration of these systems is 10 hours with a cloud shield size of $354,000 \text{ km}^2$ at the time of maximum extent,

but this varies according to location. In general, the systems are long lasting in the Southern Hemisphere than in the Northern Hemisphere, and MCCs which are originating over the oceans are long lasting than those originating over land. The typical MCC developed in the late afternoon, the maximum cloud-shield reached its maximum size in the early morning hours of the following day, and the system dissipates just after sunrise. MCCs also identified primarily as a warm-season phenomenon, which indicates their connection to the seasonal radiative cycle.

Laing and Fritsch (1993b) have documented the MCC over Africa, South America (S. Amer), the United States (U.S), the Western Pacific Region (WPR), and the Indian Subcontinent (ISC) on two-year population. Most MCC systems reached their maximum extent around 0100 LT (Local Time), and dissipation usually occurred between 0600 and 1100 LT. The frequency distribution of the duration of African systems is shown in Figure 1.4 (a). The modal duration was 9 hours, and the average duration was 11.5 hours. Similar distributions of duration found in the Americas, the Indian subcontinent, China, Australia, and the Western Pacific Region. Figure 1.4 (b) illustrates the similarity of the size distributions of the other MCC populations around the world. All of the major populations exhibit a maximum frequency of cold cloud shield area between 2×10^5 and $3 \times 10^5 \text{ km}^2$.

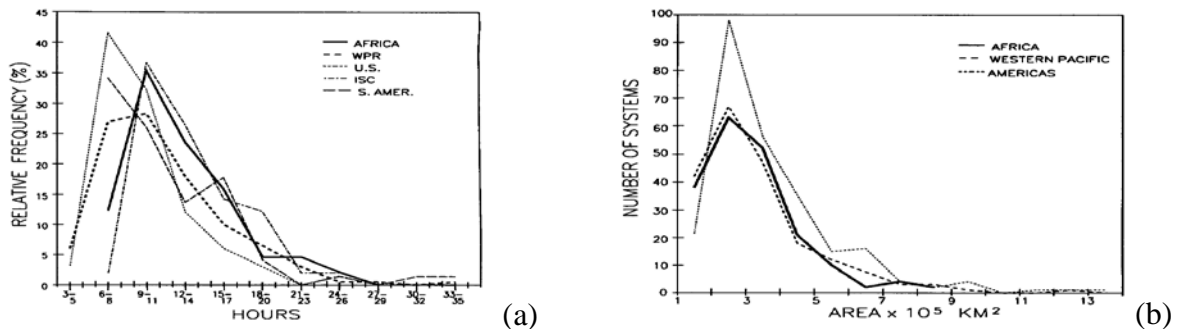


Figure 1.4. (a) Relative frequency distribution of the duration of MCCs in Africa, South America (S. Amer), the United States (U.S), the Western Pacific Region (WPR), and the Indian Subcontinent (ISC) on two-year population. (b) frequency distribution of the two-year population of MCC cold cloud shield maximum area for African, American, and Western Pacific Region MCCs.

The other previous research about the climatology of MCCs, such as; Durkee and Mote (2009) examined climatology and physical characteristics of MCCs during the austral warm season (October–May) for 1998–2007 in subtropical South America. Within the nine warm seasons, 330 events have been documented. An average of 37 MCCs occurred each

warm season and reached a maximum cloud-shield size of 256,500 km² as shown in Figure 1.5 (a), and longer lasting 14 hours on average than North America. Although 85% of the MCC population occurred over the South American continent, the remaining systems that occurred over the adjacent Atlantic Ocean were significantly larger by nearly 30%. These findings show MCCs in SSA are larger and longer-lived than shown in previous work. They also noted that relationships between latitude, and MCC maximum extent or duration are weak or non-existent, respectively.

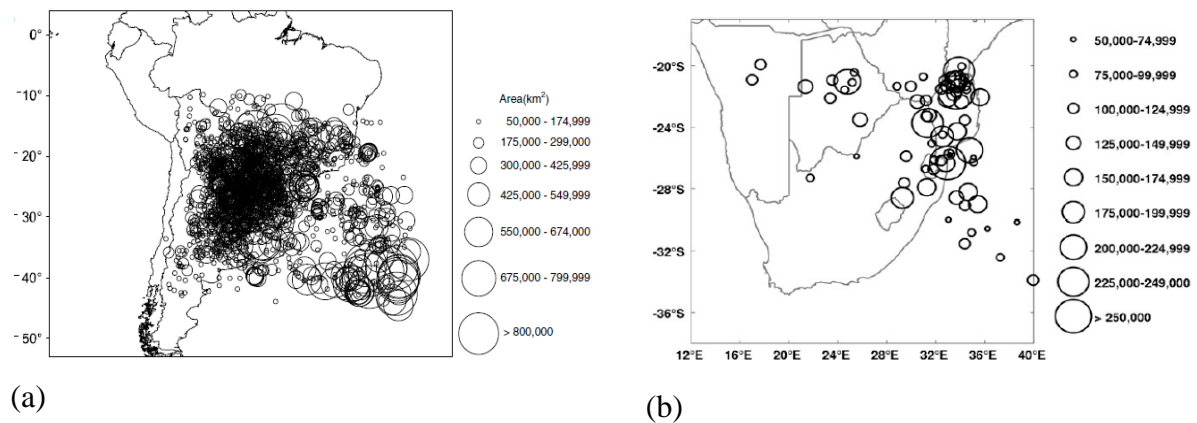


Figure 1.5. (a) The locations of the cloud shields overlaid centroid locations from the 330 MCCs over South America observed during the warm season months of October–May during 1998–2007 (Durkee and Mote 2009). (b) The distribution of MCCs over Southern Africa during September 1998 until April 2006 at maximum extent (Blamey and Reason 2012). The circles representing the cloud shield size (km²).

Blamey and Reason (2012) have reported the climatology of 70 MCCs that occurred during the austral summer months over southern Africa during the 1998–2006. Most of MCCs clustered along the eastern regions of southern Africa as shown in Figure 1.5 (b). The systems found to predominantly occur during the months of November–February, with maximum activity occurring in November and December. The transition from a more midlatitude dominated circulation to a tropical circulation over the region during the late summer leads to an uncharacteristic equatorward migration of the MCC distribution then. The analyses also suggest that there is variability in MCC frequency on monthly and seasonal time scales. Although fewer in number (about nine per season) compared to MCC populations in other regions, the systems do tend to follow the nocturnal life cycle as documented elsewhere.

This subchapter already shows the various characteristics of MCCs over several regions in the world. Some of the regions have similar characteristics, but there is also region

have different characteristics. It is interesting and important to document the climatology of MCCs with analyze the characteristics of MCC over IMC and compare it with previous research and the global characteristics of MCCs in the other region. Based on literature review, the climatology of MCC with long-period data over IMC not yet reported, so that the characteristics of MCCs over IMC is not yet well understood.

1.2.3 Review of the development and movement of MCCs over IMC

According to Maddox (1980), MCC included in the type of meso- α -scale as MCS, where he classified the meso- α -scale as convectively driven weather systems based on their physical characteristics, organization, and location of occurrence as shown in Figure 1.6. Meso- α -scale defined in his paper as the length of scales of 250 – 2500 km with duration ≥ 6 hours. He has divided MCS into two types as linear and circular type, and MCC include as the circular type that found in midlatitude and tropics region. So that this figure also show that MCC can occur over IMC due to IMC is one of the regions in tropics and MCC is different with CCs, where they have a horizontal scale that nearly similar but different in their shape. MCC have time scale less than from CC is around 6-12 hours while CC has time scale around 2 - 3 day. The CCs is an MCS with a scale of 100-500 km and containing both deep convective cells and stratiform precipitation (Houze and Betts 1981).

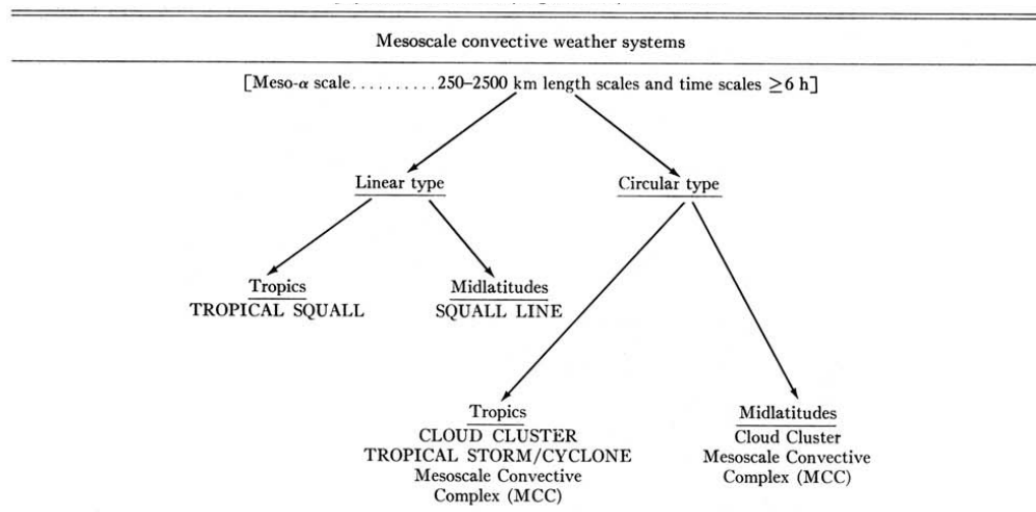


Figure 1.6. Classification of meso- α -scale, convectively driven weather systems according to physical characteristics, organization, and location. Capital letters indicate types of systems that have frequently considered in the literature (Maddox 1980).

William and Houze (1987) developed an objective technique to identify and track connected areas of cloudiness with T_{BB} less than a specified threshold of CCs. Houze et al. (1981) have presented the diurnal cycle of CCs in the vicinity of northern Kalimantan Island or Kalimantan Island during December 1978, the intensive observation period of the International Winter Monsoon Experiment (W-MONEX). They identify CCs using satellite data by analyzing the Cirrus canopies of the cloud, which have a horizontal dimension of a few hundred to a thousand kilometers based on the method by Frank (1970). They stated that the diurnal land–sea circulation “controlled the atmosphere’s convective response near North Kalimantan.

In general, when the offshore wind component (generated diurnally) begins near midnight, these result in an immediate commencement of convection over the sea. The large-scale convergence is then locally concentrated where the diurnal land breeze meets the low-level monsoon flow. The cycle of convection over South China Sea has been well documented as shown in Figure 1.7. It was typically initiated at about midnight when a low-level offshore wind began. After midnight, the convection continued to develop, and at morning it had evolved into an organized mesoscale system with a precipitation area often continuous over a horizontal distance of 200 km. The mesoscale systems typically began dissipating at midday, when the offshore wind reverted to onshore wind, and low-level convergence became concentrated over land.

Williams and Houze (1987) using a similar method, study area and period data with Houze et al. (1981) have reported the characteristics of CCs over Kalimantan Island. A pronounced diurnal cycle characterized by a preference for the very large CCs to reach the middle of their lifetime over the sea during the morning. Monsoon surge conditions over the South China Sea also strongly favored the occurrence of large clusters over the water north of Kalimantan. The convection over Kalimantan-related to sea breeze convergence can aggregate into MCSs later in the day, which moves offshore to give the greatest precipitation during the local morning time over the oceans (Williams and Houze 1987). The diurnal cycle that generated offshore CCs north of Kalimantan with the other type of MCS like MCC in other parts of the IMC maybe indicates their structural might also be similar. it is interesting to investigated especially using long-period data. They also stated that the cloud system that forms diurnally off the northern coast of Kalimantan behaves as a CC that contains one such

mesoscale rainfall area. However, they have not explained in detail the mechanism of CC in influencing rainfall.

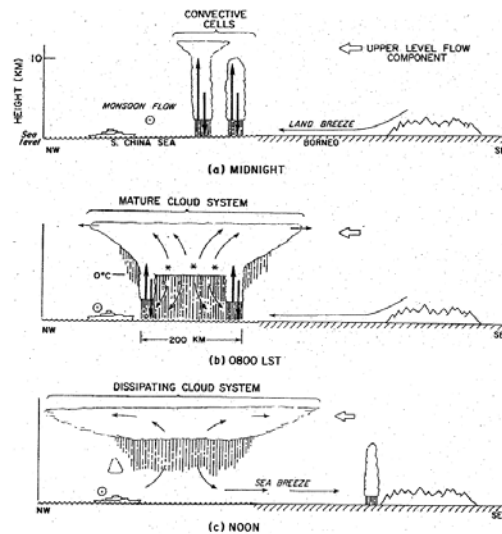


Figure 1.7. Schematic of the development of diurnally generated mesoscale precipitation feature of the coast of Kalimantan (Houze et al. 1981).

Nakazawa (1988) have examined the development and movement of the supercluster (hereafter SC) that consist CCs with analyzing the convective index using 3-hourly Geostationary Meteorological Satellite Infrared (GMS-IR) data during the active phase of the intraseasonal variation (hereafter ISV) at a case study on May-July 1980. The schematic figure that is illustrating the hierarchical structure within the ISVs is shown in Figure 1.8. The left portion of the figure shows that there exist several eastward-moving super clusters during the active phase of the ISV. The right portion exhibits the fine structure of the SC. He defines an SC as an ensemble of CCs having different life stages with an observed horizontal scale of several thousand kilometers found near the equator during the active phase of ISVs.

There are several SCs observed with a horizontal scale of several thousand kilometers. An SC consists of two or three CCs several hundred kilometers wide which have a 1-2 day life scale. An SC moves eastward, while each CC moves westward. A new CC generated 1000-2000 km east of the mature-stage CC. The composite analyses of SCs show that the origin of a new CC generated east of an old CC appears to be the low-level convergence found $10-20^\circ$ east of the convective center along the equator. He recognized as eastward-propagating envelopes of convection, composed of westward-propagating CCs in mesoscale. The generation mechanism and the phase propagation of the SCs and why do the CCs within

the SCs move westward is not well explained. The climatology and characteristics of CC, and how about relationship CCs with rainfall, is not yet explained in detail in his paper. Such synoptic-scale convective systems termed SCCs. Based on the time scale and characteristics, MCC is different with CC, but there is a relationship with each other.

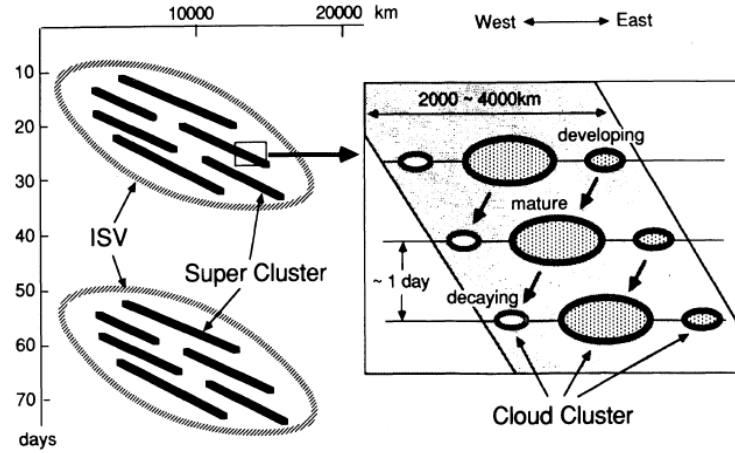


Figure 1.8. Schematic diagram of the hierarchy of the intraseasonal variations (ISV)

Mapes and Houze (1993); Chen and Houze (1997) have examined the size distributions of CCs, and the temperature distribution, as functions of location, year, phase of the ISV, and time of day over IMC. Almost similar with Nakazawa (1988), they stated that the ISV modulates CCs of all size, but larger clusters proportionately more affected than smaller clusters, and there are many of MCC occur over IMC. The small, short-lived convective clouds shown in Figure 1.9 occur over the large island of the maritime continent during the afternoon, and over the surrounding seas during the night and morning.

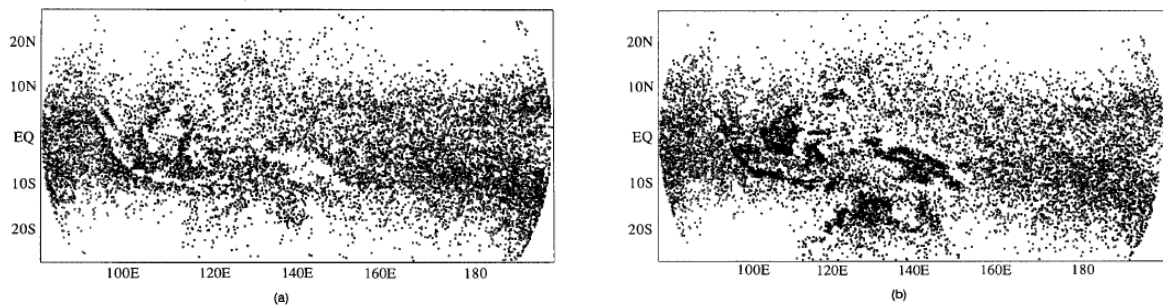


Figure 1.9. Distribution of all very cold (<208 K) CCs $1000-3000 \text{ km}^2$ in the area observed in images at (a) 2300 UTC (0900 LT) and (b) 0800 UTC (1800 LT) for 1 November 1986 - 28 February 1987.

Shibagaki et al. (2006) show that the cloud systems characterized by westward-propagating meso- β -scale CCs which developed in eastern Sumatra, and an orographic cloud system formed over a mountain range in western Sumatra during the active phase of intraseasonal oscillation (ISO) in a case study of November 2012. Meso- β -scale defined as length scales of 25-250 km with duration <6 hours. The cloud systems characterized by westward-propagating meso- β -scale CCs that developed over eastern Sumatra, and an orographic cloud system that formed over the mountain range in western Sumatra. The Meso- α -scale CCs crosses over Sumatra, its structure changes from an organized cloud system consisting of meso- β -scale CCs into a developing orographic cloud system over the mountain range as shown in Figure 1.10. Shibagaki et al. (2006) just explain the formation of Meso- α -scale CC that related with SC from several meso- γ -scale convective precipitation systems (horizontal scale of <10 km). The mechanism of meso- α -scale in influencing the rainfall not explained in his paper. Therefore, this research will give a deeper insight into the mechanism of propagation of MCC in several case and region that possibly related to their result.

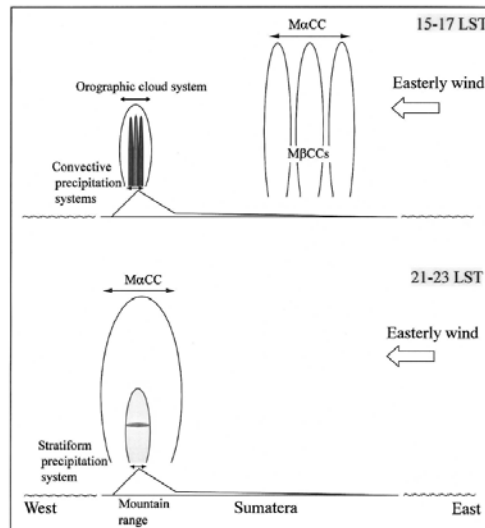


Figure 1.10. Schematic illustration of a westward-propagating meso- α -scale over Sumatra Island and precipitation systems within an orographic cloud system over the mountain range in western Sumatra (Shibagaki et al. 2006).

Moteki et al. (2008) in their paper have been described the structure and evolution of northward propagating MCSs observed over the tropical western Pacific near Papua Island on 15 June 2005 as shown in Figure 1.11. The cold air mass initially formed by cold advection

from the south and maintained by cooling with the MCSs. Their result stated that the easterly wave helped locally promote northward MCSs during the initial MCSs generated along the land-breeze front, an easterly wave, which accompanied by low-level southerly wind and a low-pressure area, was located near Palau. The cold air mass associated with the land breeze between 132° and 137° E locally extended toward the center of the low-pressure area. The results suggest that the easterly wave located around Palau helped locally promote northward cold advection from New Guinea, inducing the long-distance northward propagation of MCSs generated along the land-breeze front. They analyze of MCS using buoy data and satellite data in horizontal analyses. They did not examine the relationships between the propagation of the land-sea breeze circulation and various synoptic-scale disturbances or large-scale environment condition.

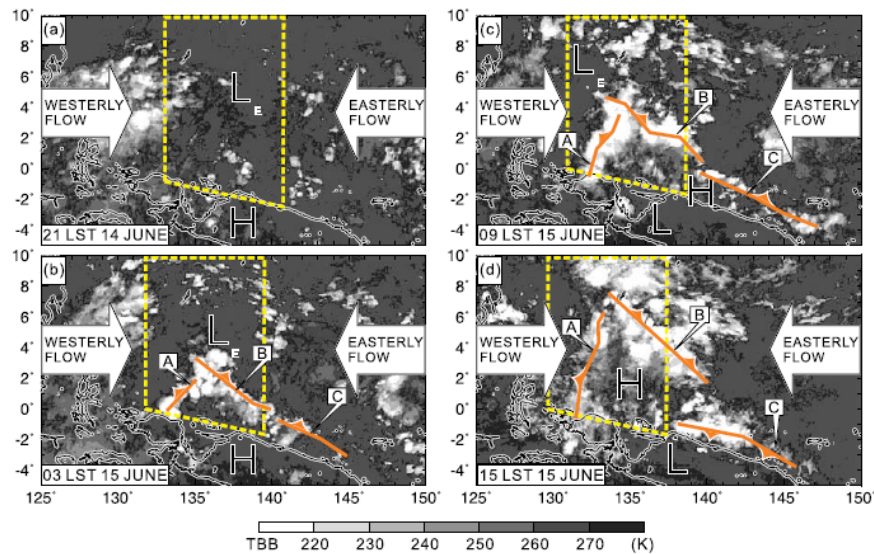


Figure 1.11. Schematic illustration of northward propagating MCSs based on satellite images at (a) 2100 LT on 14 June 2005 and at (b) 0300 LT, (c) 0900 LT, and (d) 1500 LT on 15 June 2005. LE denotes the low-pressure area associated with the easterly wave. H and L denote the relatively high- and low-pressure areas around and over New Guinea (Papua Island), respectively. The yellow dashed line surrounds the area of the 3- to 6-d southerly wind associated with the easterly wave. The symbol of the cold front represents the front that originated from a land (sea) breeze on the island of New Guinea. Arrows indicate the westerly and easterly flow regions (Moteki et al. 2008).

1.2.4 Review of the environmental conditions during MCC events

The mean genesis environment has constructed for each of five MCCs population centers around the world (Africa, Australia, China, South America, and the United States)

have reported by Laing and Fritsch (2000). In particular, MCCs initiate within prominent baroclinic zones characterized by locally large values of lower-tropospheric vertical wind shear and convective available potential energy (CAPE). Typically, a low-level jet of air with low static stability, high equivalent potential temperature, oriented nearly perpendicular to the baroclinic zone, intrudes into the genesis region and is forced to ascend over a relatively shallow, surface-based layer of relatively cool air. Pronounced warm advection accompanied by strong lower-tropospheric veering overlays the surface-based cool layer. A local maximum in absolute humidity and a local minimum in static stability mark the favored region for formation of the convective system. Low-level convergence, upper-level divergence, and an approaching mid-level vorticity maximum associated with a weak short-wave trough are also typical of the mean genesis environment.

The large-scale environment very effects to the development of MCCs. Laing and Fritsch (2000) also found that MCCs around the globe typically form near a maximum in low-level shear, lending support to the idea that low-level shear may be important for the development of long-lived MCSs. In generally, MCCs tend to initiate in locations where there is: (1) a low-level jet (LLJ); (2) a low-level convergence; (3) upper-level divergence; (4) an approaching mid-level vorticity maximum (associated with a weak short wave trough). The early stage of the MCC life cycle is characterized by convergence, vertical motion, and heating being centered in the lower troposphere. The systems achieve and maintain its maximum divergence, upward motion, and anticyclonic vorticity in the upper troposphere during the latter half of the life cycle (Cotton et al. 1989).

Velasco and Fritsch (1987) used IR satellite data and surface data to study MCCs in Central and South America. They found that MCCs tend to occur over land and at night. Miller and Fritsch (1991) found similar characteristics in their study of the western Pacific, as did Laing and Fritsch in their studies of African (1993b), Indian (1993a), and global MCCs (1996). MCCs are important because they produce a large fraction of warm season rainfall (Fritsch et al. 1986) and often are associated with severe weather (Maddox et al. 1982; Wetzel et al. 1983; Rodgers et al. 1983, 1985). They commonly occur over land in the lee of major mountain ranges and association with LLJs, and likely make significant contributions to local and global hydrologic budgets (Laing and Fritsch 1997). The MCC typically forms in association with a weak mid-tropospheric shortwave trough and a weak surface front or outflow boundary. Its environment often exhibits pronounced low-level temperature and

moisture advection in association with a well-defined LLJ (Maddox 1983; Cotton et al. 1989; Augustine and Howard 1991). The critical importance of early explosive growth has been noted previously by Zhang and Fritsch (1988) and Tollerud et al. (1992). Thus, strong early growth may be the distinguishing factor in the longevity and size distributions of MCCs. It is not readily apparent, however, why strong early growth is more effective at producing long-lasting systems in the summer than in the spring or fall.

MCC nocturnal organization associated with differential radiative heating between the convective system that is warm core, and the environment that is cooler. In mid-latitude locations, this configuration is a result of cloud-clear radiative processes whereby such temperature gradients lead to subsidence in the ambient atmosphere and low-level convergence into the system (Gray and Jacobson 1977). Additionally, radiative cooling at the cloud top and warming at the cloud base enhance the convective instability in mature convective systems (Webster and Stephens 1980). In tropical locations, the convective systems are modulated via large-scale atmospheric destabilization (Miller and Frank 1993). In general, large-scale factors such as the position of long waves such as Rossby waves, and gradient zones between maxima and minima OLR influence MCC formation (Augustine and Howard 1991; Laing and Fritsch 1997). MCC formation also correlates with a location on the globe. Regional factors influencing MCC formation are the position of the LLJ, and low-level frictional effects associated with elevation as MCCs tend to form on the lee-side about the prevailing mid-level flow of elevated terrain (Laing and Fritsch 1993b).

In general, the previous researcher found that some areas have environments that are very similar and exhibit many of the same dynamic and thermodynamic structures that are present with systems, but several areas have different environmental conditions during MCC events. It is interesting to analyze the environmental conditions during MCCs that occur over IMC and compare its results with the previous work in several regions to give a deep understanding of the conditions of the environment during MCC occurrences.

1.2.5 Review of the contribution of MCCs to rainfall

MCSs represent the largest of the convective storms in spatial dimensions and lifetime as well as a significant source of rainfall. MCSs have been broadly defined as an ensemble of multiple intense convective cells accompanied by a stratiform region that quickly evolves into organized clusters forming a single mesoscale cloud. They are mostly concentrated in the

tropics and mid-latitudes where they account for a large proportion of rainfall (Desbois et al. 1988; Carvalho and Jones 2001; Houze 2004; Wallace and Hobbs 2006). Nesbitt et al. (2006) have reported that MCSs (5-years data) produce as much as 90% of rainfall in certain land areas. For the global tropics, they produce more than 50% of the rainfall in heavily raining areas as shown in Figure 1.12.

Nesbitt et al. (2006) also documented that MCSs produce more than 70% of the rainfall in western equatorial Africa. MCSs also contribute around 50%–90%, for heavy rain regions of the global tropics, including the Sahel, the south-central United States, and the west coast of Central America. MCSs contribute greater than 70% of the rainfall in the Tropics but make up a much smaller fraction of the cloud cover (Mohr et al. 1999), and MCSs also play a major role in the rainfall regimes of the tropics include IMC (Houze 1977; Chong et al. 1987). Yuan and Houze (2010) showed that the active MCSs to be associated with 56% of tropical precipitation and Mohr et al. (1999) concluded that MCS over ten different tropical regions of the world accounted for at least 70 % of the wet season rain.

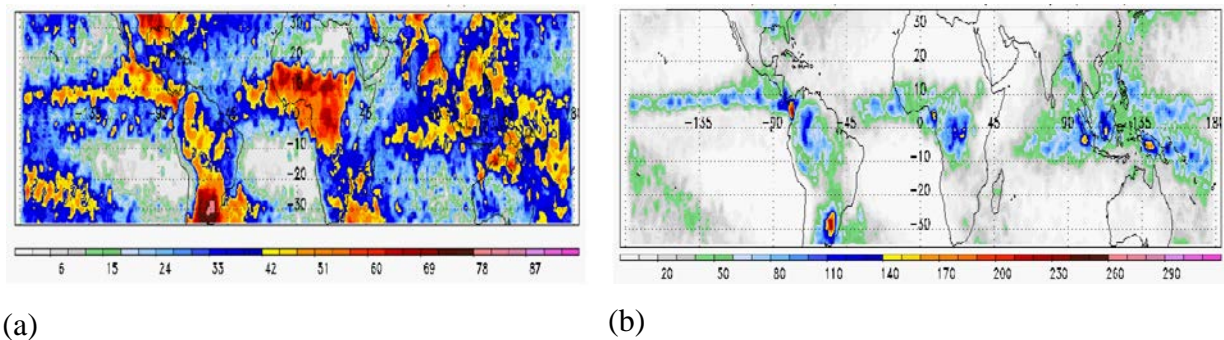


Figure 1.12. (a) MCS fractional contribution to rainfall and (b) MCS contribution to monthly rainfall (mm/month) (Nesbitt et al. 2006).

Some papers (e.g., Maddox, 1980; McAnelly and Cotton, 1989) reported that the MCCs produce the heavy rainfall that caused of several of the hazards (flooding, localized flash floods, mudslides, and property and crop damage). MCCs are also important because they produce a large fraction of warm season rainfall (Fritsch et al. 1986). An enormous amount of rain can fall from MCCs; the average system produces between 3 and 9 km³ of rainfall (Kane et al. 1987; McAnelly and Cotton 1989; Tollerud and Collander 1993). Fritsch et al. (1986) and McAnelly and Cotton (1989) were able to determine that most of the summer rainfall over the great US central plains produced by these MCCs. MCCs also play a major

role in the rainfall regimes of the tropics (Houze 1977; Chong et al. 1987). The convection related to sea breeze convergence can aggregate into MCCs later in the day, which moves off land to give the greatest precipitation during the local morning time over the oceans (Williams and Houze 1987).

D'Amato and Lebel (1998) showed from a rain gauge network validated against IR satellite imagery that MCCs contribute to more than 70% of the seasonal rainfall in Niger. They found that the mean storm rainfall in their study area was climatologically stationary, thus making it a stable parameter for characterizing rainfall in the Sahel, as it indicates the interannual rainfall variability is dependent on the number of rainfall events. Durkee et al. (2009) examined the contributions that MCCs make to rainfall totals across subtropical South America for 1998-2007. They determined that MCCs account for a considerable portion of total warm season precipitation in subtropical South America, with 11%-20% of the total rainfall in most warm seasons provided by MCCs in much of the study domain, on smaller temporal and spatial scales, MCCs often had a greater impact. For example, MCCs accounted for 30%-50% of December precipitation in northern Argentina and portions of Paraguay, while provinces in west-central Argentina received up to 66% of their November rainfall from MCCs contributed ~22% of the rainfall. However, the contribution of MCC over IMC to total rainfalls, even to extreme rainfall not yet documented.

1.3 Research objectives and scopes

1.3.1 Research objectives

Based on the explanation of problem statement and motivation in subchapter 1.2 have appeared some of the research questions, i.e., (1). How about the climatology of MCC over IMC?, (2). How the mechanism of the development and the movement of MCC over IMC?, (3). How the mechanism of MCC in influencing rainfall over IMC?, (4). How the environmental condition during MCC event?, (5). How much the contribution of MCC to total rainfall over IMC?, (6). Is there a relationship of MCC to extreme rainfall over IMC?. Therefore, this research will explain in detail about MCC over IMC to give an answer that research questions. In detail, the objective of this research, i.e.,

Objective 1: Identify MCCs over IMC during 15-years for the 2001-2015 period, and investigate the climatology of MCCs over IMC which include characteristics (distribution of

MCCs, life-cycle of MCC, area size of MCCs, and evolution characteristics) of MCCs over IMC, and comparison the MCCs with rainfall and convective activity.

Objective 2: Explaining the structure and mechanism of the development and the movement of MCC in IMC that discuss the type of the cloud as a trigger of MCC and the propagation of MCC after dissipated.

Objective 3: Explaining the mechanism of MCC in influencing rainfall over IMC related the land-sea breeze and cold pool as a trigger of the new convective system.

Objective 4: Examining the condition of the environmental during MCC events over IMC.

Objective 5: Determining of MCCs contribution to total rainfall and extreme rainfall over IMC.

1.3.2 Research scopes

The scope of this research explains about the MCC based on the physical characteristics of MCC by Maddox (1980) as described in Table 1.1. This research describes the climatology of MCC over IMC, the development of MCC over IMC based on case study and composite analyses, the environmental condition during MCC event over IMC, and the contribution of MCC to rainfall total and extreme rainfall over IMC. This research takes the region study in IMC as shown in Figure 1.13. However, we just take area in the latitude of 10°S - 8°N and longitude of 90°E - 140°E .



Figure 1.13. IMC map

1.4 Research data

1.4.1 Satellite data for brightness temperature

The identification of MCCs depends on IR satellite imagery, and sometimes visible, satellite data. The IR satellite data provides information about the extinction of the emitted IR radiation by a medium (the surface), assuming a non-scattering environment in local thermal equilibrium. The satellite sensor detects within the thermal band (10-12 μ m) of the electromagnetic spectrum, and observes downwards to the surface (or as far as possible) in a narrow cone, with the tip of the cone originating at the local vertical of the instrument. The IR sensor observes a particular location continuous in space and time, irrespective of the time of the day.

The previous study, such as Maddox (1980), Anderson and Arritt (1998), Durkee et al. (2009) and the others have utilized IR satellite image from Geostationary Operational Environmental Satellites (GOES). Laing and Fritsch (1993a and 1993b), Morel and Senesi (2002) and several others, have utilized the METEOSAT IR images from the International Satellite Cloud Climatology Project (ISCCP) B3 stage radiance data. The METEOSAT is a geostationary meteorological satellite, operated by the European Organization for the Exploitation of Meteorological Satellites (EUMETSAT), with multiple series. IR data provides the variable T_{BB} that gives information about the cloud temperature and altitude, where, as a general rule, the colder the object, the larger the altitude. T_{BB} uniquely related to the (sensed) wavelength.

This research utilized T_{BB} from the Himawari geostationary satellites, provided by the Japan Meteorological Agency (JMA), which support weather forecasting, tropical cyclone tracking, and meteorology research. Himawari carries a camera called an imagery that captures visible and IR light coming from the earth. These images provide information on clouds, atmospheric water vapor, and land/sea surfaces. Analysis of the images produces a wide range of weather-related information on considerations such as cloud type, cloud height, and the position and scale of typhoons, depressions, and fronts. Environmental information on influences such as the distribution of yellow sand, volcanic ash, and sea ice also acquired.

Since the launch of GMS-1 (Himawari-1) in 1977, there have been three generations, including GMS (Geostationary Meteorological Satellite), MTSAT (Multi-functional Satellite imagery Transport SATellite), and Himawari 8/9. However, this research utilizing data from Himawari-5 until Himawari-8 and add the data GOES-9 because from May 2003 to June

2005, JMA rented the GOES-9 satellite from the National Oceanic and Atmospheric Administration (NOAA) for observation of the western Pacific region to fill the gap between the operational periods of Himawari-5 and Himawari-6. In detail, the data consists of Himawari-5/GMS-5 for data from January 2001-April 2003, Pacific GOES/GOES-9 for data from May 2003- June 2005, Himawari-6/MTSAT-1R for data from July 2005 - June 2010, Himawari-7/MTSAT-2 for data from July 2010 - June 2015, and Himawari-8 for data from July 2015 - December 2015.

In general, Himawari satellite data has five channels as shown in Table 1.2, however, this research utilizing IR1 channel with a wavelength around 10.8 μm . This satellite data also has spatial and time resolutions $0.05^\circ \times 0.05^\circ$ and one hour, respectively. This satellite data could be downloaded from <http://weather.is.kochiu.ac.jp/sat/GAME> with format file in Portable Grey Map (PGM) with compression Gzip. T_{BB} data obtained with convert of PGM file with its calibration value by using the computer program in Unix.

Table 1.2. Channels for Himawari 5 until Himawari 8

	Himawari-5 (GMS-5)	GOES-9	Himawari-6 (MTSAT-1R) / Himawari-7 (MTSAT-2)	Himawari-8 / Himawari-9
Visible (VIS)	0.55-0.90 μm @ (1.25km / 6bits)	0.55-0.75 μm @ (1km / 10bits)	0.55-0.90 μm @ (1km / 10bits)	0.47, 0.51, 0.64* μm @ (0.5*-1km / bits)
Infrared 1 (IR1)	10.5-11.5 μm @ (5km / 8bits)	10.2-11.2 μm @ (4km / 10bits)	10.3-11.3 μm @ (4km / 10bits)	10.4, 11.2 μm @ (2km / bits)
Infrared 2 (IR2)	11.5-12.5 μm @ (5km / 8bits)	11.5-12.5 μm @ (4km / 10bits)	11.5-12.5 μm @ (4km / 10bits)	12.4, 13.3 μm @ (2km / bits)
Infrared 3 (IR3)	6.5-7.0 μm @ (5km / 8bits)	6.50-7.00 μm @ (8km / 10bits)	6.5-7.0 μm @ (4km / 10bits)	6.2, 6.9, 7.3, 8.6, 9.6 μm @ (2km / bits)
Infrared 4 (IR4)	Not Available	3.80-4.00 μm @ (4km / 10bits)	3.5-4.0 μm @ (4km / 10bits)	3.9 μm @ (2km / bits)
Near Infrared (NIR)	Not Available	Not Available	Not Available	0.86*, 1.6, 2.3 μm @ (1*-2km / bits)
Frequency	1 hour	1 hour	1 hour (two observations in one hour for the northern and the southern hemisphere)	10 minutes
Position (Equator / 35,800km above)	140 E	155 E	140 E (MTSAT-2 in standby at 145 E)	140.7 E

1.4.2 Rainfall data from TRMM and OGIMET

Satellite data from the Tropical Rainfall Measuring Mission (TRMM), - a mission between NASA and the Japan Aerospace Exploration Agency (JAXA), provide the distribution of rainfall within the tropics through combining data from various instruments³ and is used in this study. TRMM launched in 1997 into an equatorial orbit, staying between 35 degrees north and south of the equator. TRMM Multi-satellite Precipitation Analyses (TMPA) provides a calibration-based sequential scheme for combining precipitation estimates

from multiple satellites. TMPA is available both after and in real time, based on calibration by the TRMM Combined Instrument and TRMM Microwave Imager precipitation products, respectively. Only the after-real-time product incorporates gauge data at present. The dataset covers the latitude band 50°N–S for the period from 1998 to the delayed present.

The estimated rainfall data, corresponding to the MCCs in this research, were obtained from the Real-Time TRMM TMPA (TMPA-RT) 3B41RT v7 dataset, which has hourly temporal resolution and $0.25^\circ \times 0.25^\circ$ spatial resolution. (Huffman, J.G. 2013). These data could be downloaded from <ftp://disc2.nascom.nasa.gov/data/TRMM/Gridded/3B41RT/>. To comparing the satellite data, this research using rainfall observation from synoptic data that obtained from the OGIMET meteorological database (Valor and López 2014). These data could be downloaded from <http://www.ogimet.com/synopsc.phtml.en>.

1.4.3 Surface wind from CCMP data

The Cross-Calibrated Multi-Platform (CCMP) data set combines cross-calibrated satellite microwave winds and instrument observations using a Variational Analyses Method (VAM) to produce high-resolution (0.25 degree) gridded analyses. Satellite wind retrievals derived by Remote Sensing Systems (RSS) from some satellite-borne passive and active microwave instruments used. RSS inter-calibrates radiometers at the brightness temperature level to within 0.2 degree Celsius, applying a refined sea surface emissivity model and radiative transfer function to derive surface winds. The resulting wind retrievals are highly consistent between microwave radiometer instrument platforms, including SSM/I, SSMIS, AMSR, TMI, WindSat, and GMI. RSS has also developed a geophysical model function for deriving wind speeds and directions from microwave scatterometers, including QuikSCAT and ASCAT. Both radiometer and scatterometer data validated against ocean moored buoys, which confirm the measurements are in agreement (to within 0.8 m/s) despite the difference in wind measurement and retrieval methodologies.

The VAM combines RSS instrument data with moored buoy measurements and a starting estimate (first-guess) of the wind field. The European Center for Medium-Range Weather Forecasts (ECMWF) ERA-Interim Reanalyses winds used in the CCMP V2.0 processing as the first-guess wind field. This 0.25-degree model wind field is consistently processed, as opposed to that of the ECMWF operational model for which the model changes over time. All wind observations (satellite and buoy) and model analyses field referenced to a

height of 10 meters. The VAM analyses are used to assign directions to the microwave radiometer wind speed datasets. Pentad and monthly average data sets are also available. The impact of satellite sampling induced by the effect of rain on the microwave instruments can be a substantial disadvantage and must be considered in any analyses based on “satellite-only” data. For most purposes, the VAM analyses should be used because these fit the microwave surface wind data very closely where such data are available and can improve upon the ECMWF analyses of cyclonic winds.

This research utilizing the CCMP V2.0 Level-3 (L3) winds that available as netCDF-4 data files which cover the global ocean for the period of 20-years with 6-hourly temporal resolution and 25-km spatial resolution. Each daily data file contains three arrays of size 1440 (longitude) by 628 (latitude for the range -78.375 to 78.375) by 4 (time of 00 UTC (Universal Time Coordinated), 06 UTC, 12 UTC, 18 UTC). Two of the arrays are the zonal (U) and meridional (V) wind components in meters/second (m/s). Standard U and V coordinates apply, meaning the positive U is to the right and positive V is above the axis. Winds in the CCMP product are of the oceanographic convention, meaning a wind blowing toward the Northeast has a positive U component and a positive V component. The third array in the file is the number of observations used to derive the wind components. Some abs value of 0.0 means that the wind vector for that grid cell is obtained from the background field only as no satellite or moored buoy wind data were available (Atlas et al. 2011). These data can be downloaded at <http://www.remss.com/measurements/ccmp>.

1.4.4 ECMWF ERA-Interim data for environmental parameters

The environmental parameter data is obtained from ECMWF ERA-Interim. ERA-interim is a reanalysis of the global atmosphere covering the data-rich period since 1979 (originally, ERA-Interim ran from 1989, but the 10-year extension for 1979-1988 produced in 2011). ERA-Interim is the latest global atmospheric reanalysis produced by the ECMWF. This data has a time resolution of 6-hourly, a horizontal resolution of $1^{\circ} \times 1^{\circ}$ in latitude and longitude in 27 pressure level that include 1000, 975, 950, 925, 900, 875, 850, 825, 800, 775, 750, 700, 650, 600, 550, 500, 450, 400, 350, 300, 250, 225, 200, 175, 150, 125 and 100 hPa. The environmental parameters that used in this study are the wind, relative humidity, temperature, specific humidity, divergence, vertical velocity, vorticity and geopotential height. However, there are some parameters should be derived by using equation from some

variable of ECMWF ERA-Interim data due to is not available. The environmental parameters described in detail in Chapter 2. These data can be downloaded at <http://www.ecmwf.int/>.

1.5 Research methods

1.5.1 Identification of MCCs and analyze of climatology of MCCs

MCC identified by input the temperature, latitude, and longitude values for each cloud shield pixel that obtained from IR to a modified version of a computerized MCC program using MATLAB based on characteristics of MCCs (Maddox 1980). This method adapts the method from Ismanto (2011) and Trismidianto (2012) that based on the maximum spatial correlation tracking technique (MASCOTTE) method by Carvalho and Jones (2001). In detail, the procedure to identify of MCC;

1. Change the satellite data to become binary data with replacing the each grid value that has T_{BB} less than 241 K as cloud shield and less than 221 K as interior cloud become a value of "1" and the other value replaced by a value of "0".
2. The binary data then searched the size of the area eligible temperatures (procedure 1, pixel which has a value of "1") by counting the number of pixels that connected to the four surrounding grid connection.
3. Select the area that only has area size of cloud shields $\geq 100,000 \text{ km}^2$ that equivalent around 3246 pixels, and interior cloud $\geq 50,000 \text{ km}^2$ that equivalent around 1623 pixels.
4. Find the center point of the selected area; the focal point is the center of mass of interconnected areas. To find a center point can be made by formula (Carvalho and Jones 2001).

$$X_0 = \frac{\sum_i^N X_i}{N}; \text{ and } Y_0 = \frac{\sum_i^N Y_i}{N} \dots \dots \dots (1.1)$$

Where X_i =pixel position of "i" on X axis; Y_i = pixel position of "i" on Y axis; X_0 and Y_0 = centroid; N = area size / total of pixel.

5. Calculate the eccentricity. There are three methods for calculating the eccentricity level can be done include Method Machado (Least Square), Ellip fittings, Empirical Orthogonal Function (EOF) Methods. This research using EOF methods following the methods by Ismanto (2011). In basically, EOF method to determine the variability of a single variable (scalar) that can describe the variability of each point cloud system, describes the

distribution of positions and variations of pixels cloud system. With EOF cloud system was studied variations in longitude and taken two modes/biggest eigenvalue, then each mode before normalization, and the results to calculate the level of eccentricity $| \text{EOF2} | / | \text{EOF1} |$. Eccentricity is one tool to determine the shape of an image eccentricity (cloud system). This eccentricity has a value between 0 and 1, to methods of EOF value of "0" indicates that the object is more elliptical and otherwise the value "1" of the object is round/circle.

6. Manual tracking to get the time of MCC stage that adapts Fiolleau and Roca (2013). We define the "initiation" of the MCC as when the contiguous area within the -52°C IR isotherm first exceeds $50,000 \text{ km}^2$. An MCC is considered to have reached its "maturity" when this area attains its largest size. The "decay" stage is mid-point between mature and dissipation sub-period, and it "ends" or "dissipates" when this area again becomes less than $50,000 \text{ km}^2$ like Cotton et al. (1989).
7. Final result the program give the MCC information which includes MCC location (longitude, latitude, and centroid), time of the MCC occurrence at each stage (date, month and year), the size of cloud shield and interior cloud, eccentricity, and duration time of the MCC life-cycle.

That MCC information used to explain the climatology of MCC over IMC with analyzing the distribution of MCCs in globally, seasonal, manually and diurnal, analyze of a number of the MCC occurrences, the duration time of MCC life-cycle, the area size of cloud and eccentricity and analyze the evolution characteristics of MCC.

1.5.2 Analyses of the evolution and propagation of the MCCs

To understanding the role that MCCs in influencing of rainfall, in this research, the evolution, and propagation of the MCCs is analyzed by spatial analyses with taking some of the case study of MCCs in ocean, coastal and continent. The evolution process of MCCs is analyzed each stage based on MCC stage definition by Cotton et al. (1989) using spatial analyses of T_{BB} . The relationship MCC to rainfall system and convective activity is also analyzed using spatial analyses with seen the evolution of rainfall system and convective index during MCC event.

The convective activity is analyzed by using convective index (hereafter C_I) that determined by taking the temperature below the threshold. The purpose of determining the

threshold value is to separate between surface temperature with high convective clouds. This research utilized the threshold of 253 K corresponding research of Adler and Negri (1988) because the threshold of 253 K as the warmest of T_{BB} to determine the clouds which allegedly resulted in the rain. The value of convective index indicates the strength of convective activity that occurs, the greater the value, the stronger the convective activity occurs, and otherwise. If T_{BB} is smaller than the threshold value ($C_I = \text{threshold} - T_{BB}$, for $T_{BB} < \text{threshold}$) and a convective index equal to zero for the T_{BB} greater than or equal to the threshold value, ($C_I = 0$, for $T_{BB} \geq \text{threshold}$). As shown in equation 1.6;

$$C_I = 253 - T_{BB}; \text{ to } T_{BB} < 253 K$$

$$C_I = 0; \text{ to } T_{BB} \geq 253 K \dots \dots \dots (1.2)$$

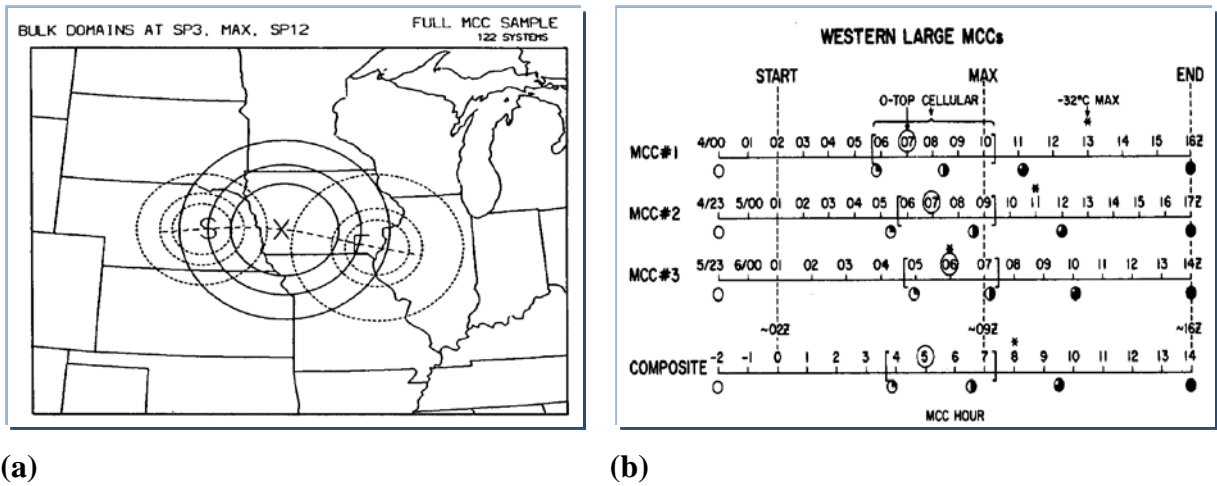


Figure 1.14. (a) Average track of 122-cases composite MCC. S, X, and E denote centroid area at the Start, Maximum and End. McAnelly and Cotton (1989). (b) Stratification of 12-cases of MCC using composite analysis illustrated by McAnelly and Cotton (1986).

To explain the similarities and consistency of the evolution and propagation of the MCCs in the case study and the other several regions over IMC in this research is utilized composite analysis that adapted from McAnelly and Cotton 1986 and 1989. We create a composite region with taking 6 (six) region that most frequently concentrated of MCCs, include the case study region. The region was chosen also has the grid locations of the MCC center and the duration of time of life cycle almost same by taking the point of the life cycle

of the nearest hour. The characteristics of region chosen explained in detail in chapter four. The example of MCC region for composite analysis is illustrated by McAnelly and Cotton, 1989 as shown in Figure 1.14 (a). The example composite analysis approach to the evolution of the MCC development illustrated by McAnelly and Cotton, 1986 in Figure 1.14 (b), where the timing of the T_{BB} -defined life cycle characteristics are indicated along an hourly time axis for each MCC.

In the composite category, the composite for initiation, mature, decay and dissipation determined by the average the hour of initiation, mature, decay and dissipation for each MCC, around to the nearest hour. In this study, in the composite category, the all cases of MCCs in each region considered to have common composite times of initiation, mature, decay and dissipation. Besides the similarities in genesis region, maximum area and mature duration, the MCCs in each category were reasonably consistent in term of other T_{BB} characteristics. These include; the duration of initiation to mature stage, mature to decay and decay to dissipation or post-MCC stage. The composite for initiation, mature, decay and dissipation determined by the average the hour of initiation, mature, decay and dissipation for each MCC, or around to the nearest hour. In the first, we determined the average the hour of the initiation of all case in each region, and then plus 1, 2 or 3 hours to reaches the average the hour of mature, the same way to reaches the average the hours of dissipation or post-MCC. So that, the average from *initial-to-maximum*, *maximum-to-dissipation* with 1, 2, or 3 duration time.

The surface wind from CCMP data which available at 6-hourly is utilized to analyzing the propagation of MCC. The composite analysis for the propagation of MCC determined by the average of surface wind data in the critical stage just for the time at 0000 UTC, 0600 UTC, 1200 UTC, and 1800 UTC due to the data available in 6-hourly. However, in this study, we consider the data on time in 2300, 0000 and 0100 UTC as the time on 0000 UTC, and the data on time in 0500, 0600 and 0700 UTC as the time on 0600 UTC. We also consider the data on time in 1100, 1200 and 1300 UTC as the time on 1200 UTC, and the data on time in 1700, 1800 and 1900 UTC as the time on 1800 UTC. So that, we did composite analyses just for the hours of initiation, mature, decay and dissipation or post-MCC at the time as mentioned above in each region. For example, from 45-case of MCC composite region 3, we just take 24-case during the initial stage, 28-case during the mature stage, 34-case during the decay stage and 22-case during the dissipation or post-MCC stage.

1.5.3 Analyses of the environmental during MCC events

In the present study, analyses of the environments of MCCs in the United States (Maddox 1983; Cotton et al. 1989) and comparison of several regions (Laing and Fritsch 2000) were used as a baseline to check the validity of using the ECMWF data for defining the environments of the global MCC populations. Similar to their methods, in this research, the environmental condition of MCCs just analyzed during the critical stage of MCCs. i.e., initial, mature, decay and dissipation or post-MCC stage. To analyses, the condition of the environment during MCC event is utilized several data from the ECMWF ERA-Interim analysis fields, which are available at 6-hourly intervals with $1^\circ \times 1^\circ$ horizontal resolution (Dee et al. 2011). We also calculate some equation if the data is not available from the ECMWF as already explained in subchapter 1.4.1.4. We start to explain the environmental condition during the MCC in the case study that described in subsection 1.4.2.2.

To explain the similarities and differences of the large-scale environments of MCCs in the case study, this research presents the kinematic structure, dynamics, and thermodynamics of MCC evolution obtained via the composite analysis for each composite MCC region. The composite MCC region is described in the subsection 1.4.2.2. Maddox 1983 presents a summary of environmental conditions for MCC generation and development in the USA using a composite of the wind and thermodynamic fields. Cotton et al. (1989) also reported the environmental condition during MCC over the USA using composite model. This study adapts the method like them to analysis the MCC development. Similar with case overview, the environmental condition of MCCs just analyzed during the critical stage of MCCs. i.e., initial, mature, decay and dissipation or post-MCC stage.

To analyses, the condition of the environment during MCC event is utilized several data from the ECMWF ERA-Interim analysis fields, which are available at 6-hourly intervals with $1^\circ \times 1^\circ$ horizontal resolution (Dee et al. 2011). We also calculate some equation if the data is not available from the ECMWF as already explained in subchapter 1.4.1.4. The composite analysis for the environmental conditions during MCC determined by the average of environmental parameters just for the critical stages that occurred at 0000 UTC, 0600 UTC, 1200 UTC, and 1800 UTC due to the data is available in 6-hourly. However, in this study, we consider the data on time in 2300, 0000 and 0100 UTC as the time on 0000 UTC, and the data on time in 0500, 0600 and 0700 UTC as the time on 0600 UTC. We also consider the data on time in 1100, 1200 and 1300 UTC as the time on 1200 UTC, and the data on time in 1700,

1800 and 1900 UTC as the time on 1800 UTC. So that, we did a composite analysis of environmental parameters just for the critical stages that occurred at the time as mentioned above in each region. For example, from 45-case of MCC composite region three, but we just take 24-case during the initial stage that occurs in the time available data, 28-case during the mature stage, 34-case during the decay stage and 22-case during the dissipation or post-MCC stage.

1.5.4 Determining the contribution of MCCs to rainfall

The contribution of MCC to total rainfall determined from the ratio of rainfall accumulated during the MCC event from initial stage until post-MCC stage at each grid point to the total rainfall accumulated at each grid point during 15-years over IMC. The contribution of MCC rainfall in seasonal is expressed as the ratio of MCC rainfall in each season to the total rainfall in each season at each grid point.

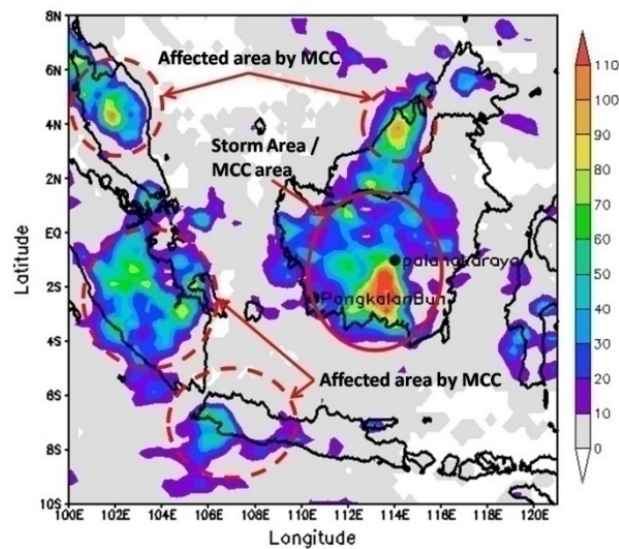


Figure 1.15. Horizontal distribution of rainfall accumulation during MCC event at 14 - 15 April 2012 that shows the example of what is the meaning of the MCC rainfall in storm area or MCC area (red circle) and MCC rainfall as affected area by MCC (red dotted circle). Unit for rainfall is mmhr^{-1} .

The contribution of MCC rainfall in monthly is expressed as the ratio of MCC rainfall in every month to the total rainfall in every month at each grid point. This method is nearly similar with the methods from papers of Laing (1999), Durkee et al. (2009), and Blamey and Reason (2012) but we do not determine the storm area for MCC rainfall use the convex hull

method like them. The MCC rainfall determined from rainfall accumulated during the MCC event from initial stage until post-MCC stage at each grid point that occurred from 2001 - 2015 over IMC and the total rainfall is accumulated rainfall over IMC during 2001 - 2015. The MCC over IMC is not only contributing to rainfall in the MCC area, but the MCC give a contribution to its surrounding area as shown in Figure 1.15.

Total rainfall values for each MCC were tabulated for each year and compared with the overall rainfall for that year and each season. MCC rainfall values were also aggregated by each month for the entire period. Additionally, the percentages of precipitation due to MCCs for several temporal periods are calculated. These percentages were obtained by summing the total amount of MCC rainfall during the period and dividing that total by the sum of all rainfall. We adapt the method from Frich et al. (2002), Gao and Giorgi (2006), Supari (2012) and Brito (2014) to determined the extreme rainfall. The extreme rainfall events as a function of the average of the maximum rainfall value (MRV) with indices of extreme rainfall Rx1d, maximum rainfall daily (WMO, 2009). Thereafter, the MRV is calculated according to the following equation:

$$MRV = \frac{\sum Xi_{max}}{n} \dots\dots\dots (1.3)$$

Where Xi_{max} denotes the maximum rainfall in each selected grid point, and n is the number of time-series data. A comparison between the MRV and the observed rainfall value determines the existence of an extreme rainfall event as follows: if the rainfall value is equal to or larger than the MRV it is considered to be an extreme rainfall event; otherwise, the rainfall value considered as a normal event. In this case, we have a rainfall day that could be considered either normal or extreme; however, this tells us nothing about the intensity or strength of the rainfall event. To select different kinds of extreme rainfall events we need to consider a threshold value from the MRV. This threshold value can be achieved by calculating the standard deviation (STD) of the maximum rainfall occurrences in one-day intervals. The advantage of this threshold is that it is not fixed but space-dependent, which makes the selection of rainfall extremes more robust. The STD is calculated from the following equation:

$$STD = \sqrt{\frac{(Xi_{max} - \overline{X_{max}})^2}{n-1}} \dots\dots\dots(1.4)$$

Where $\overline{X_{max}}$ denotes the average of maximum rainfall. Thus, different kinds of extreme rainfall are classified as follows: if the value of the rain recorded at the gridpoint either equals or exceeds the value of the MRV but is less than the MRV plus one STD, the event is considered an extreme event type I (named as EET-I, meaning Extreme Event Type-I). In the same way a rainfall event is considered to be an EET-II (Extreme Event Type-II) if the amount of rainfall recorded at the grid point lies between $MRV + (1 \times STD)$ and $MRV + (2 \times STD)$. An amount of rainfall exceeding $MRV + (3 \times STD)$ is classified as EET-III (Extreme Event Type-III).

1.6 Research contribution and new finding report

The results of this study can be expected to recommended in the making of daily weather prediction, especially related to extreme weather or extreme rainfall due to the predictability of rainfall should consider all scales that it occurs included in mesoscale. A new report from this research indicates an understanding of the climatology of MCCs over IMC that important for several climate-related studies based on predictions of rainfall, such as hydrological studies, agriculture planning, and disaster management. This study will enhance understanding about MCCs over IMC and became a reference to the next research. An environmental condition during MCCs is also very important to know about how the MCC developed over IMC and where the MCC migration that can predict rainfall due to MCCs. This research will give contribute in the development of regional modeling system and satellite disaster early warning system over Indonesia which is a project in my institution.

The climatology of MCCs based on Maddox (1980) over IMC during 15-years using Himawari-generation satellite data is a new report due to not yet detail documented by previous research. The mechanism of MCC in influencing rainfall in some area over IMC is maybe a new report due to still not yet clearly understood about that. The analysis about large-scale environmental condition during MCC over IMC will give a new knowledge about how the MCC development and movement over IMC. The contribution of MCCs to rainfall total and extreme rainfall is new finding due to there is not yet previous research that accounts about that.

1.7 Dissertation organization

Chapter 1: This chapter describes the background study from the author, problem statement, and motivation why we do this research, research objective and scope, research data and method. And this chapter is also written the research contribution and organization.

Chapter 2: This chapter explain the literature review that contains about how the climate system over IMC and diurnal variability in IMC. This chapter also explains what MCS and MCC is.

Chapter 3: This chapter describe the climatology of MCC over IMC during 15-years in a period of 2001 - 2015, the globally, seasonally, monthly and diurnal analysis for climatology of MCC have been reported in this chapter. The life cycle, duration and size of MCC over IMC also documented. This chapter to given the answer the number 1 of research objective.

Chapter 4: This chapter explains the structure and mechanism of the evolution and the propagation of the MCC in the IMC with taking some of the case study of MCCs in ocean, coastal and continent. This chapter also explains the similarities and consistency of the evolution and propagation of the MCCs in the case study and the other several regions over IMC by using composite analysis. The point of this chapter is to explain the research objective in number 2 and 3.

Chapter 5: This chapter explains the environmental condition during a critical stage of the MCC by using case study analyses and composite analyses. This chapter is to strengthen the analyses in Chapter 4 in explaining the research objective in number 2 and 3. However, the point of this chapter to explained the research objective number 4.

Chapter 6: This chapter to explain the research objective in number 5 and 6, that contains about determination for the contribution of MCCs to total rainfall and extreme rainfall.

CHAPTER TWO

LITERATURE REVIEW

2.1 Climate system in Indonesian Maritime Continent

2.1.1 IMC is one of the equatorial heat source regions

IMC lies at the heart of tropical region's warm pool. It is one of the world's most convectively active areas and thereby affects the global climate system. It is located between two continents (Asia and Australia) and between two oceans (Indian and the Pacific Ocean) as shown in Figure 2.1. The IMC is unique geographical region due to composed of a complex system of mountainous islands and consists of five large (Papua, Kalimantan, Sumatera, Sulawesi, and Jawa) and more than 13,000 smaller islands, and has about 5000 km or 1/8 of the equatorial circumference in longitude. In this latitude–longitude region of about 10,000,000 km² the land area (including territories of Indonesia, Malaysia, Papua New Guinea, and East Timor) is about 2,720,000 km², of which the land–sea ratio (2.7:7.3) is close to that of the whole Earth (3:7) (Yamanaka 2016).

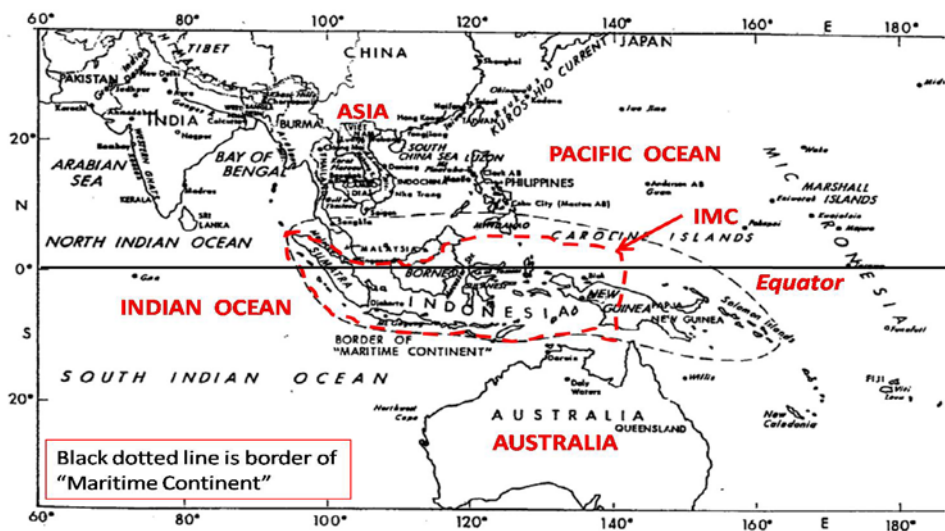


Figure 2.1. The map shows that IMC as the equatorial region is located between two continents (Asia and Australia) and between two oceans (Indian and the Pacific Ocean).

Original figure source: http://www.meteo.physik.uni-muenchen.de/lehre/roger/Tropical_Meteorology/Tropics_Ch01.pdf

This unique IMC situation results in an air mass character of a maritime continent and the fundamental role played by the maritime continent, the region of multiple islands of

Southeast Asia making up the largest archipelago in the world, such that the Indonesian Archipelago is also named the "Maritime Continent" (Ramage, 1968), the area of maritime continent is shown in Figure 2.1. Ramage (1968) recognized the major importance of this region of heating as one of the primary energy sources for the entire global circulation system. As it is, the air is mostly humid, and the enhanced cloudiness indicates massive exchanges of energy that are fundamentally important in the general circulation of the global atmosphere. Of this region, none is more important in global climate dynamics than the maritime continent region, because of its role in providing energy for the operation of the north-south tropical Hadley cell and the east-west Walker circulation, both important components of the global circulation (Sturman and Tapper 1996). McBride (1999) and recently Slingo et al. (2003) have shown that the IMC heat source is a major driver of the global circulation.

The major large-scale zonal circulation of importance to the IMC region is the Walker circulation. This equatorial atmospheric circulation is associated with zonal pressure and temperature gradients across the Pacific Ocean (Bjerknes 1969). The Walker Circulation features low-level winds blowing from east to west across the central Pacific, rising motion over the warm water of the western Pacific, returning flow from west to east in the upper troposphere, and sinking motion over the cold water of the eastern Pacific as shown in Figure 2.2.

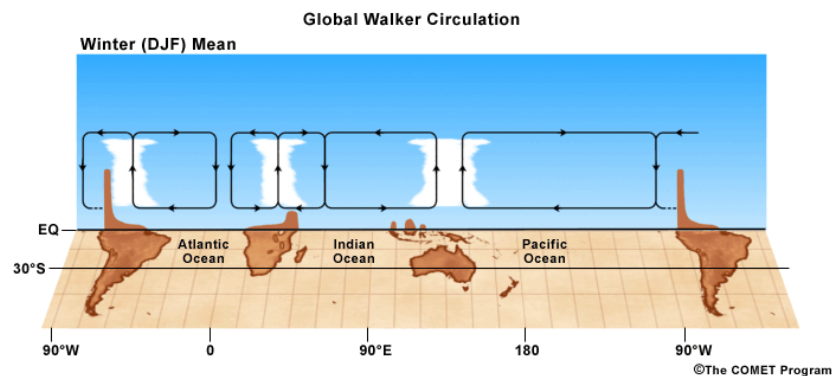


Figure 2.2. Schematics of the global Walker Circulation for Winter (DJF) based on computations of upper and lower tropospheric divergent winds.

The Walker circulation is primarily driven by heating on the western flanks of the equatorial circulations. This heating is both atmospheric and oceanic in nature. Atmospheric heating is driven by the sensible heating of the equatorial land masses of Indonesia, Africa, and South America and the latent heat release associated with deep, moist convection that forms in the moist, unstable environment resulting from a combination of such heating and an abundant supply of lower tropospheric moisture. Weak to modest contributions to the

development of deep, moist convection are provided by upslope flow on the eastern side of the mountain ranges of Africa and South America. Oceanic heating reflects sensible heating associated with the zonal variability in sea surface temperatures and oceanic heat storage as driven by the easterly trades. In addition to motions in the zonal and vertical direction, the tropical atmosphere also has considerable motion in the meridional direction as part of, for example, the Hadley circulation.

The Hadley circulation is a tropical atmospheric circulation that features air rising near the equator and air sinking at roughly 30° latitude, flowing poleward at 10–15 kilometers above the surface, descending in the subtropics and then flowing equatorward near the surface as shown in Figure 2.3 (a). The Hadley circulation is strongest over southeast Asia and the western Pacific in the winter hemisphere as a response to a stronger meridional temperature gradient. Equatorward low-level winds, making up the lower branch of the Hadley circulation, are driven by the resulting major pressure gradient from the subtropical high-pressure belt to the equatorial low-pressure regions. The easterly trade winds flowing across the equatorial Pacific into the East Maritime Continent, an important component of the low-level convergence into the region, are the product of equatorward winds of the Hadley circulation being deflected westwards by the Coriolis force.

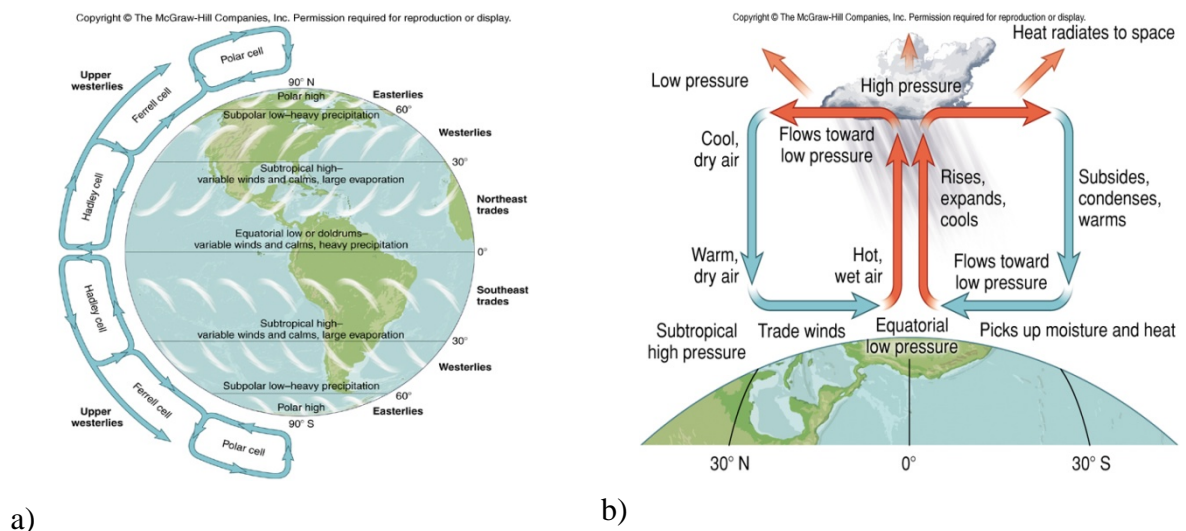


Figure 2.3. (a) Three cells on each side of the equator control vertical and horizontal air flows. (b) A schematic diagram of the Hadley circulation and its associated zonal flows and surface circulation. Source: Kaufmann, Robert K., and Cleveland, Cutler J. 2007. Environmental Science (McGraw-Hill, Dubuque, IA)

This circulation creates the trade winds, tropical rain belts and hurricanes, subtropical deserts and the jet streams. The energy associated with the equatorial maximum in solar

radiation released through vigorous atmospheric convection is the ultimate driver of the mean position of the Hadley circulation (Lindzen and Hou 1988). Atmospheric convection cell warm air rises at the equator. As it rises, it cools and generates large amounts of precipitation. The air cools as it moves away from the equator. At about 30° north or south the dense air falls toward Earth's surface. As it does, it warms and tends to reduce precipitation. Once this air reaches the surface, pressure differences cause air to move along the surface toward the equator as shown in Figure 2.3 (b).

Almost all of the energy that drives atmospheric and oceanic circulation comes from the sun. The radiation balance of the earth-atmosphere system must, therefore, be taken into account when analyzing atmospheric circulation, and hence atmospheric activity over the IMC region. Figure 2.4 shows the distribution of mean incoming and outgoing radiation at the edge of the atmosphere averaged zonally and over a year. If the earth-atmosphere system is in thermal equilibrium, these two streams of energy must balance.

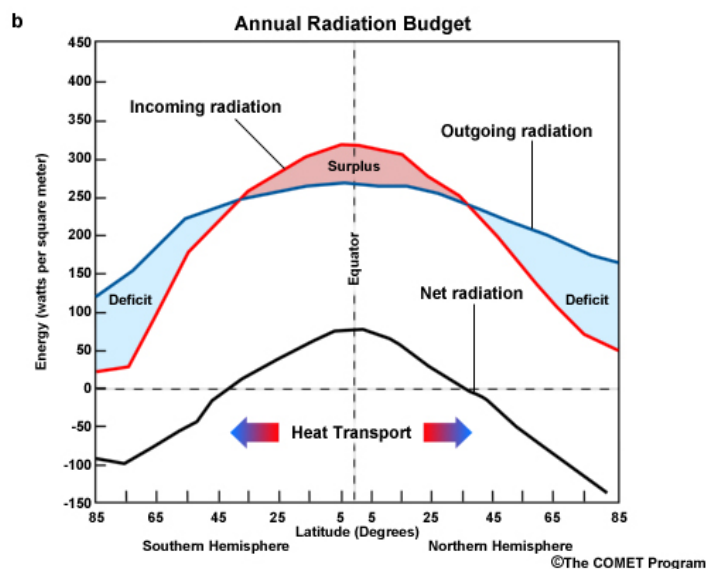


Figure 2.4. Global annual radiation budget (W m^{-2}) (Source: the COMET program).

It is evident that there is a surplus of radiative energy in the tropics and a net deficit in middle and in high latitudes, requiring on average a poleward transport of energy by the atmospheric circulation. Despite the surplus of radiative energy in the tropics, the tropical atmosphere is a region of net radiative cooling (Newell et al. 1974). The fact is that this surplus energy heats the ocean and land surfaces and evaporates moisture. In turn, some of this heat lands its way into the atmosphere in the form of sensible and latent heat, and it is the energy of this type that is transported polewards by the atmospheric circulation. Cloud

systems directly affect the surface energy budget through their modification of the net radiative fluxes. Clouds are also a key factor in the coupling between the atmosphere and the ocean through their influence in the surface radiative, heat, and momentum fluxes (Strachan 2007).

2.1.2 Atmospheric scale interaction over IMC

The term "scale" has an accurate definition in fluid mechanics but is often used qualitatively in meteorology that describes space scale and time scales in term of wavelength and periods, respectively. Due to different force balances, atmospheric motions behave differently for fluid systems with different time and spatial scales. To understand the dynamical and physical processes, different approximations have been taken to resolve the problems. Therefore, a proper scaling will facilitate the choice of appropriate approximations of the governing equations. Scaling of atmospheric motions normally based on observational and theoretical approaches. From observational approach, the atmospheric processes categorized through direct empirical observations and the utilities used. Since observational data recorded in discrete time intervals and the record of these data in a weather map reveals a discrete set of phenomena, which then classified into discrete scales. For example, sea breezes occur on the timescale of one day and spatial scale of 10 to 100 km, while the cumulus convection occurs on the time scale of 30 minutes and spatial scale of several km.

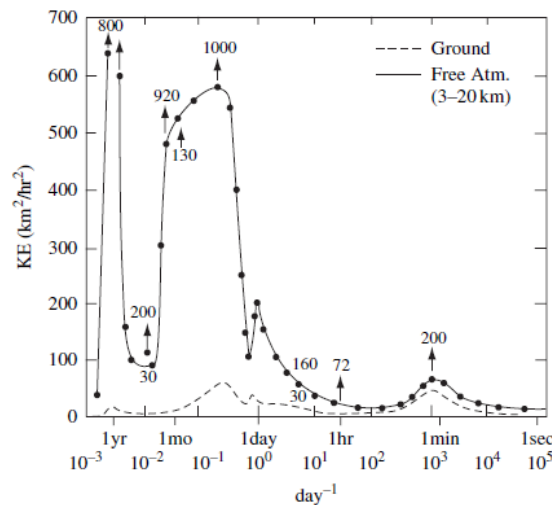


Figure 2.5. Average kinetic energy spectra (spectral density) of the free atmospheric zonal wind as a function of frequency. Numbers show maximum kinetic energy at particular periods.

Consideration the atmospheric measurements represented in Figure 2.5 that show a kinetic energy spectrum for various time scales where the kinetic energy of the atmosphere is not spread uniformly over all wavelengths but has certain preferred scales, with gaps in between. Although the spectrum is continuous, it does exhibit some distinct peaks. There are strong peaks at frequencies ranging from a few days (the synoptic scale) to a few weeks (the planetary scale). There are also peaks at one year and one day and a smaller peak at a few minutes, though the latter may be an artifact of the analysis. The spectral analysis technique used to generate Figure 2.5 involved a transformation of the temporal distribution of zonal kinetic energy to a distribution regarding frequency space. A similar technique can be used to transform the spatial distribution of some variable to its distribution in wavenumber space. It may suggest a division into three scales: macroscale, mesoscale, and microscale. From the kinetic energy spectrum (Figure 2.5), the mesoscale may serve as a scale for allowing the energy to transfer from the large scale to small scale and vice versa. Energy transfer from small scales to the mesoscale also serve as a primary energy source for mesoscale convective systems. For example, mesoscale convective systems may start as individual convective cells, which grow and combine to form thunderstorms and convective systems, such as squall lines, mesocyclones, mesoscale convective complexes and hurricanes. On the other hand, energy transfer from the macroscale to mesoscale also serves as an energy source to induce mesoscale circulations or weather systems.

The different scales for atmospheric motions can be defined: (a) Macroscale is the largest scale, and includes two important sub-scales. i.e., planetary scale and synoptic scale. The planetary scale is circulations last for weeks or months, and extend in size from 5000 to 40,000 km that its examples are the Asian monsoon, El Nino, and La Nina. The synoptic scale in meteorology (also known as large-scale or cyclonic scale) is a horizontal length scale of the order of 100 to 5000 km and time scale around days to weeks. It corresponds to a horizontal scale typical of mid-latitude depressions (e.g. extratropical cyclones). Most high and low-pressure areas seen on weather maps such as surface weather analyses are synoptic-scale systems, driven by the location of Rossby waves in their respective hemisphere. Low-pressure areas and their related frontal zones occur on the leading edge of a trough within the Rossby wave pattern, while surface highs form on the back edge of the trough. Most precipitation areas occur near frontal zones. Examples are the high- and low-pressure systems we see on weather maps. Also, hurricanes are synoptic scale phenomena.

(b) Mesoscale meteorology is the study of weather systems smaller than synoptic scale systems but larger than microscale and storm-scale cumulus systems. Horizontal dimensions range from around 5 kilometers to several hundred kilometers and time scale around minutes to hours. Examples of mesoscale weather systems are sea breezes, squall lines, and mesoscale convective complexes. Vertical velocity often equals or exceeds horizontal velocities in mesoscale meteorological systems due to non-hydrostatic processes such as buoyant acceleration of a rising thermal or acceleration through a narrow mountain pass. Mesoscale Meteorology divided into these subclasses: Meso- α is 200–2000 km scale of phenomena like fronts, squall lines, MCS, tropical cyclones at the edge of the synoptic scale. Meso- β is 20–200 km scale of phenomena like sea breezes, lake effect snow storms. And Meso- γ is 2–20 km scale of phenomena like thunderstorm convection, complex terrain flows (at the edge to microscale, also known as storm-scale). As a note, tropical and subtropical cyclones are classified by National Hurricane Center as a synoptic scale rather than mesoscale.

(c) Microscale meteorology is the study of short-lived atmospheric phenomena smaller than mesoscale, about 1 km or less. These two branches of meteorology are sometimes grouped together as "mesoscale and microscale meteorology" (MMM) and together study all phenomena smaller than synoptic scale; that is they study features too small to be depicted on a weather map. These include small and fleeting cloud "puffs" and other small cloud features. Microscale meteorology controls the most important mixing and dilution processes in the atmosphere. Important topics in microscale meteorology include heat transfer and gas exchange between soil, vegetation, and surface water and the atmosphere caused by near-ground turbulence. Measuring these transport processes involves the use of micrometeorological (or flux) towers. Variables often measured or derived include net radiation, sensible heat flux, latent heat flux, ground heat storage, and fluxes of trace gasses important to the atmosphere, biosphere, and hydrosphere.

2.2 Atmospheric phenomena over IMC

Based on the scale interaction, the mean climate of the IMC is made up of contributions from various weather systems occurring on a range of temporal and spatial scales, from individual cumulus clouds, through cloud SC and tropical storms, right up to planetary scale interannual variations which constitute the El Niño Southern Oscillation (ENSO) as shown in Figure 2.6. It is the multi-modal variability of this convective activity, on both spatial and temporal scales, which makes this such a fascinating region of study. An

understanding of the climate of the IMC and its importance to the global climate system implies gaining an understanding of the constituent tropical weather systems and in general the large-scale dynamics of the tropics (Strachan 2007).

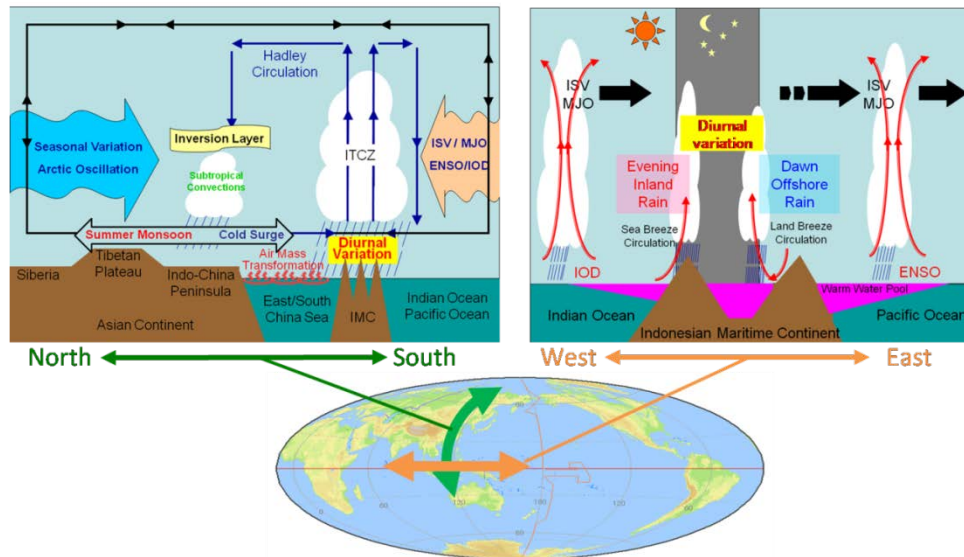


Figure 2.6. Scale interaction for the climate system over IMC (Yamanaka 2016).

Figure 2.6 shows the variability which influencing the climate of the IMC occurs on timescales ranging from intra-diurnal (e.g. sea-breezes) to interannual (e.g. the El Niño Southern Oscillation) and on spatial scales ranging from a few kilometres (e.g. individual cloud cells), to thousands of kilometres (e.g. the Madden-Julian Oscillation), to planetary scale ENSO oscillations. Each of these modes of variability will be considered, focusing on their general characteristics and the role they play over the Maritime Continent. However, it must be kept in mind that the various modes of variability are highly interlinked- focusing on individual phenomena does not allow a comprehensive summary of the climate of the region to be constructed. It is impossible to consider how a single phenomenon will affect the Maritime Continent without taking into account how it interacts with the other phenomena occurring over the region. The atmosphere phenomena that are influencing the climate of IMC, among others, are;

2.2.1 Madden-Julian Oscillation (MJO)

MJO is an intraseasonal fluctuation or “wave” occurring in the global tropics. The MJO is responsible for the majority of weather variability in these regions and results in variations in several important atmospheric and oceanic parameters which include both lower-

and upper-level wind speed and direction, cloudiness, rainfall, sea surface temperature (SST), and ocean surface evaporation. The MJO is a naturally occurring component of our coupled ocean-atmosphere system, and the typical length of the MJO cycle or wave is approximately 30-60 days (Madden and Julian 1971; Madden and Julian 1994; Zhang 2005). The MJO is characterized by eastward propagation of regions of enhanced and suppressed tropical rainfall, primarily over the Indian and Pacific Oceans. Figure 2.7 illustrates an equatorial vertical cross section of the MJO showing the changes in cloudiness, rainfall, wind speed and direction, and SST as the MJO propagates eastward around the global tropics (Adapted from Madden and Julian, 1971; 1972).

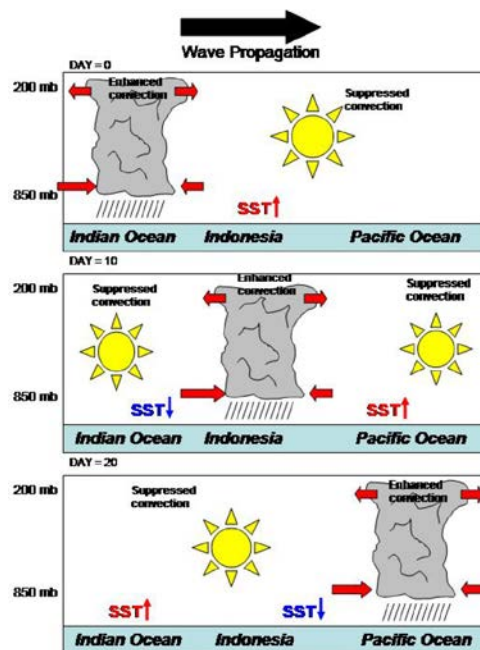


Figure 2.7. Equatorial vertical cross section of the MJO as it propagates from the Indian Ocean to the western Pacific. Red arrows indicate the direction of the wind and red (blue) SST labels indicate positive (negative) SST anomalies respectively. Figure adapted from Madden and Julian, 1971; 1972.

2.2.2 El Niño Southern Oscillation (ENSO)

ENSO is an irregularly periodical variation in winds and sea surface temperatures over the tropical Eastern Pacific Ocean, affecting much of the tropics and subtropics. The warming phase is known as El Niño and the cooling phase as La Niña. Southern Oscillation is the accompanying atmospheric component, coupled with the sea temperature change: El Niño accompanied with high, and La Niña with low air surface pressure in the tropical western Pacific. ENSO contributes significantly to the rainfall pattern in the IMC region, and many studies have analyzed the relationship between ENSO and IMC rainfall variability (e.g.

Hendon, 2003). It has been suggested (Haylock and McBride, 2001) that convective activity over the Maritime Continent region varies coherently on an interannual timescale associated with ENSO variability. During ENSO-neutral conditions, surface trade winds blow westward across the equatorial Pacific Ocean. Blowing against the ocean's surface, these winds result in a westward current. During El Niño conditions, the usually present east to west winds weaken, and an anomalous west to east flow develops. The west to east flow drives warm equatorial waters from the western Pacific towards the eastern Pacific and northern South America. The SSTs surrounding IMC are cooler than average, following a movement of the warmest SSTs into the central Pacific. The shift in warmest SSTs typically leads to 'drought conditions' (reduced convective rainfall) over IMC during winter and an anomalous flow of easterly winds across the region. During La Niña conditions, The opposite tends to occur during the cool La Niña phase of ENSO. The Walker circulation is much stronger, with a strong rising branch over IMC, bringing increased rainfall over the region, and a westward sinking branch over the equatorial central and western Indian Ocean. The east to west flow present during neutral conditions intensified. The Normal, El Niño and La Niña of ENSO are shown in Figure 2. 8.

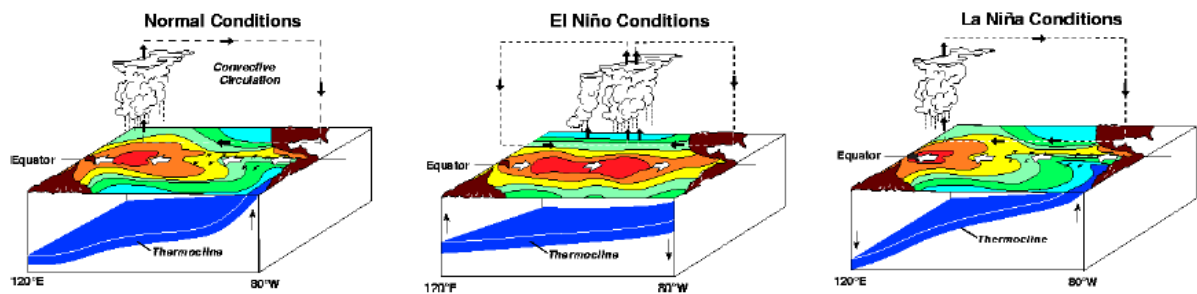


Figure 2.8. Normal, El Niño and La Niña conditions across the Pacific Ocean. The Maritime Continent lies at the left-hand edge of the schematics. *Source: in Strachan (2007) from www.pmel.noaa.gov/tao/elnino/nino-home.html.*

2.2.3 Indian Ocean Dipole (IOD)

The Indian Ocean Dipole (IOD), also known as the Indian Niño, is an irregular oscillation of sea-surface temperatures in which the western Indian Ocean becomes alternately warmer and then colder than the eastern part of the ocean. It is normally characterized by an anomalous cooling of SST in the southeastern equatorial the Indian Ocean and anomalous warming of SST in the western equatorial Indian Ocean. Associated with these changes the normal convection situated over the eastern Indian Ocean warm pool shifts to the west and

brings heavy rainfall over the east Africa and severe droughts/forest fires over the IMC region. Like ENSO, the change in temperature gradients across the Indian Ocean results in changes in the preferred regions of rising and descending moisture and air. Positive IOD events are often associated with El Niño and negative events with La Niña as shown in Figure 2.9. If the sea surface temperature of the western end rises above normal (0.4°C) and becomes warmer than the eastern end, it leads to a positive IOD. This condition is favorable for the Indian Monsoon as it causes a kind of barrier in the eastern Indian Ocean and all the southwesterly winds blow towards the Indian sub-continent. Accordingly, the waters in the eastern Indian Ocean cools down, which tends to cause droughts in adjacent land areas of Indonesia and Australia. Conversely, during a negative IOD period, the waters of the tropical eastern Indian Ocean is warmer than water in the tropical western Indian Ocean. This results in increased rainfall over parts of southern Australia.

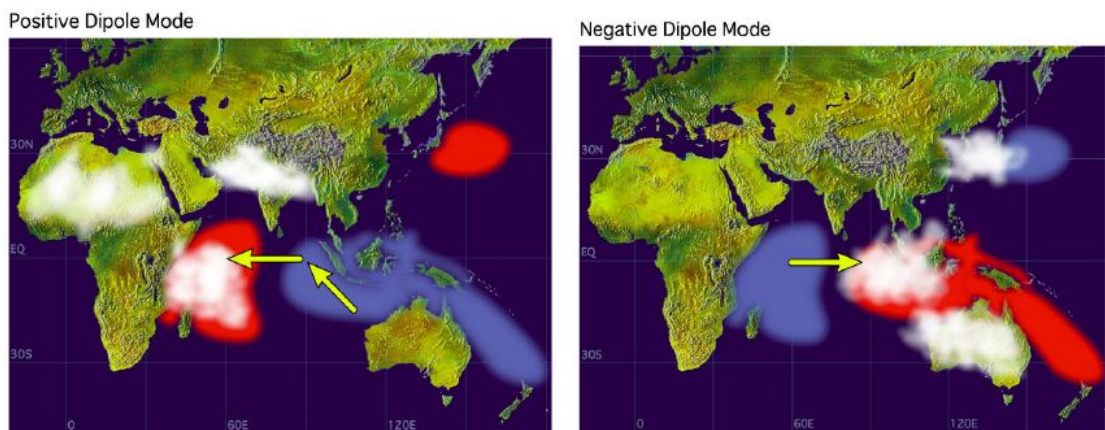


Figure 2.9. Schematic of a positive and negative IOD event. SST anomalies are shaded (red color is for warm anomalies, and blue is for cold). White patches indicate increased convective activities and arrows indicate anomalous wind directions during IOD events. Figure source: http://www.jamstec.go.jp/frcgc/research/d1/iod/e/iod/about_iod.html

2.2.4 The Inter-Tropical Convergence Zone (ITCZ)

The ITCZ was known by sailors as the doldrums, is a belt of low pressure which circles the Earth generally near the equator where the trade winds of the Northern and Southern Hemispheres come together. It is characterized by convective activity which often generates vigorous thunderstorms over large areas. It is most active over continental land masses by day and relatively less active over the oceans. During December and January, the Southern Hemisphere is heated more strongly by the sun than the Northern Hemisphere, so the hottest air – the air that rises in the ITCZ – is found a little south of the equator. Winds

from the Northern Hemisphere blow across the equator towards the ITCZ. During June and July, the Northern Hemisphere is heated more strongly by the sun, so the ITCZ and its rising hot air lies a little north of the equator and winds blow from the Southern Hemisphere across the equator to reach the ITCZ in the Northern Hemisphere as shown in Figure 2.10. Where the trade winds are weak, the ITCZ characterized by isolated Cumulus and Cumulonimbus cells. However, where the trade winds are stronger, the ITCZ can spawn a solid line of active Cb cells embedded with other cloud types developing as a result of instability at higher levels. Variation in the location of the ITCZ drastically affects rainfall in many equatorial nations, resulting in the wet and dry seasons of the tropics rather than the cold and warm seasons of higher latitudes. Longer term changes in the intertropical convergence zone can result in severe droughts or flooding in nearby areas. In some cases, the ITCZ may become narrow, especially when it moves away from the equator; the ITCZ can then be interpreted as a front along the leading edge of the equatorial air. There appears to be a 15- to 25-day cycle in thunderstorm activity along the ITCZ, which is roughly half the wavelength of MJO.

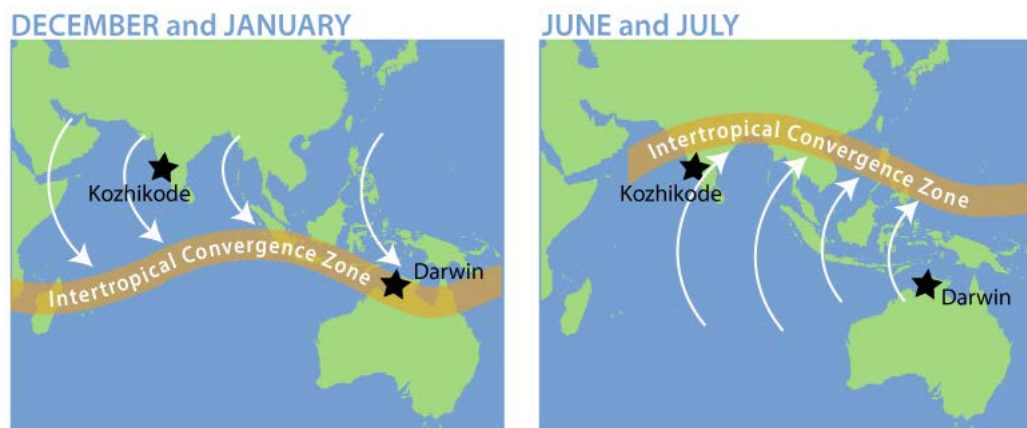


Figure 2.10. As the Intertropical Convergence Zone (ITCZ) changes location through the year, the winds, rains, and the location of wet monsoon weather changes, too. In this example from Asia and Australia, the ITCZ moves from the Southern Hemisphere (left map) to the Northern Hemisphere (right map). (Source: <http://monsoon.yale.edu/why-monsoons-happen/>)

2.2.5 Monsoon

Monsoon is traditionally defined as a seasonal reversing wind accompanied by corresponding changes in precipitation but is now used to describe seasonal changes in atmospheric circulation and precipitation associated with the asymmetric heating of land and sea. Usually, the term monsoon is used to refer to the rainy phase of a seasonally-changing pattern, although technically there is also a dry phase. The location of IMC in between two continents (Asia and Australia) and between two oceans (Indian and the Pacific Ocean) had

an impact in the form the East and South Asian monsoon and Australia monsoon which had an impact in the form of seasons, wet (rain) and dry (dry). The direction of the wind over the Indonesian region in boreal mid-winter (January) and mid-summer (July) may be seen in Figure 2.11.

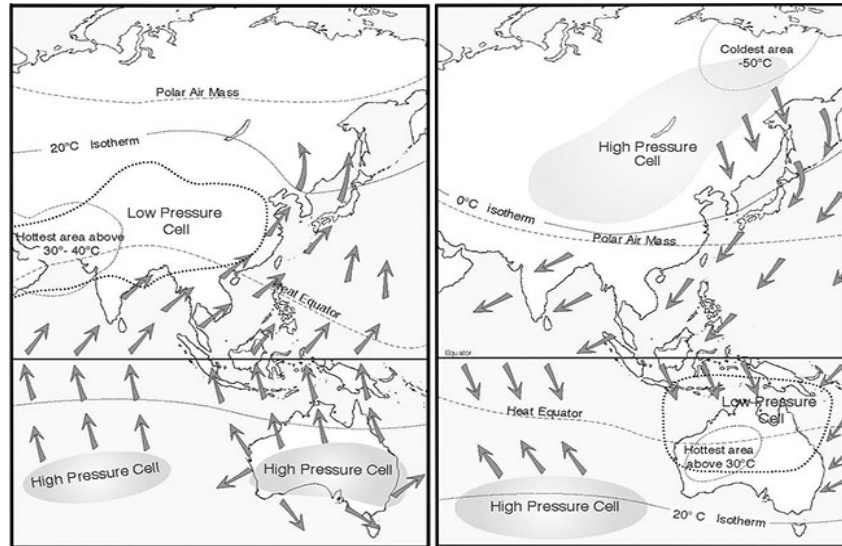


Figure 2.11. Schematic of monsoon wind for the boreal summer (June- September) (left) and the boreal winter (December-February) (right). (Source: <https://maximos62.wordpress.com/2015/09/25/forest-burning-and-haze-in-indonesia-malaysia-and-singapore/>)

In northern hemisphere winter (December, January, February), monsoon wind blows from Siberia region toward Australian continent. During this period go on west to northwest winds over southern hemisphere Indonesia, such as southern Sumatera, Java, Bali, Lombok, Nusa Tenggara up to Papua. Boreal winter monsoon is called West monsoon and the season is called west monsoon season, while over northern hemisphere Indonesia, such as northern Sumatera and West Kalimantan, monsoon wind come from northeast direction called northeast monsoon and the season is called northeast monsoon season. In boreal summer, on the contrary, the wind blows from Australian continent toward Asian continent. In the region extends from the end of southern Sumatera, Java, Bali, Lombok, Nusa Tenggara up to Papua, wind direction from east to west called east monsoon and the season is called East monsoon season, while over northern hemisphere Indonesia, the wind blows from southwest toward northeast called southwest monsoon and the season is called southwest monsoon season. Due to IMC is one of monsoon region, the seasons of IMC divided into two seasons. i.e., wet seasons on December, January and February (hereafter DJF) and dry seasons on June, July

and August (hereafter JJA), however, there are two transition seasons. i.e., March, April, and May (hereafter MAM) as transition seasons from wet to dry seasons and September, October and November (hereafter SON) as transition seasons from dry to wet seasons.

2.2.6 Land-sea breeze circulation

The diurnal cycle of land-sea breeze circulations over the islands and surrounding seas of the IMC is a major process behind the diurnal scale variability of convection over the region. Numerous studies have been undertaken to gain an understanding of these complex circulations which primarily driven by the variability in the land-sea temperature contrasts around the vast length of the coastline of the islands that constitute the IMC (Hadi et al. 2002). A land breeze or offshore breeze as shown in Figure 2.12 (bottom) is a gentle wind blowing from land to the sea that created when the land is cooler than the water such as at night, and the surface winds have to be very light.

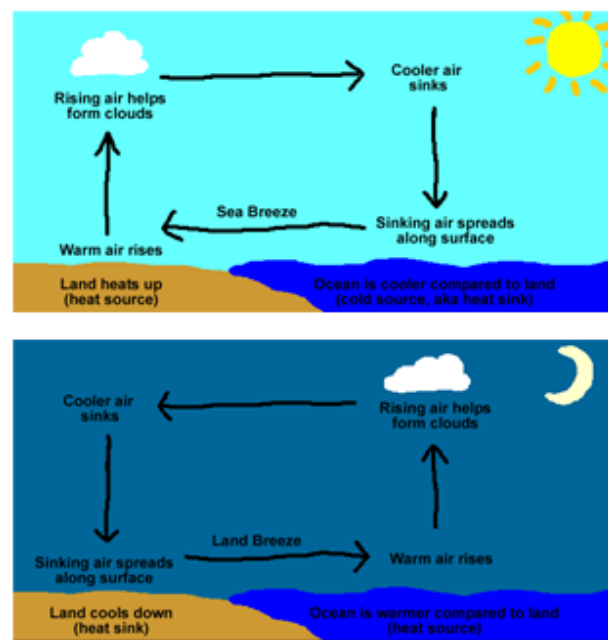


Figure 2.12. Schematic of sea-breeze (top) and land-breeze (bottom)

When this happens the air over the water slowly begins to rise, as the air begins to rise the air over the surface of the ocean has to be replaced, this is done by drawing the air from the land over the water, thus creating a sea breeze. A sea breeze or onshore breeze as shown in Figure 2.12 (top) is a gentle wind blowing from the sea toward the land that created when the surface of the land is heated sufficiently to start air rising. As air rises, it is replaced by air

from the sea; you have now created a sea breeze. Sea breezes tend to be much stronger and can produce gusty winds as the sun can heat the land to very warm temperatures, thereby creating a significant temperature contrast to the water.

2.2.7 Mountain and valley breeze

A mountain breeze and a valley breeze are two related, localized winds that occur one after the other on a daily cycle which also give a contribution to convective activity over IMC due to IMC is a unique geographical region that composed of a complex system of mountainous islands. Mountain and valley breezes as shown in Figure 2.13 form through a process similar to sea and land breezes. During the day, the sun heats up valley air rapidly. Convection causes it to rise, causing a valley breeze. At night, the process is reversed. Mountain air cools rapidly at night and "falls" downslope, causing a mountain breeze. These breezes occur mostly during calm and clear weather.

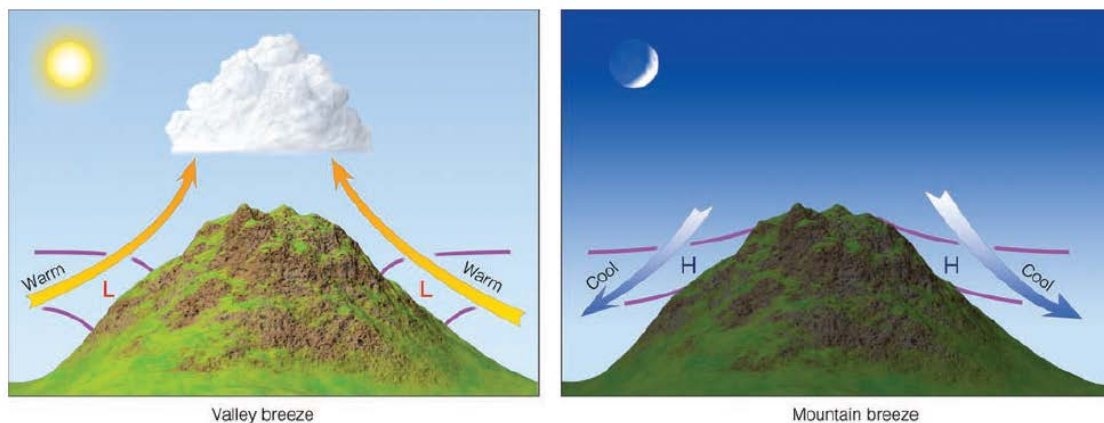


Figure 2.13. Valley breezes blow uphill during the day; mountain breezes blow downhill at night. (The L's and H's represent pressure, whereas the purple lines represent surfaces of constant pressure). (Ahrens 2001)

2.3 Convective activity and rainfall system over IMC

2.3.1 Diurnal variation of convective activity

In meteorology, convection refers primarily to atmospheric motions in the vertical direction. As the earth is heated by the sun, different surfaces absorb different amounts of energy and convection may occur where the surface heats up very rapidly. As the surface warms, it heats the overlying air, which gradually becomes less dense than the surrounding air and begins to rise. The process of convection occurs due to the relative difference between the weight of an air mass to the air mass around it, where the air masses heavier drops down

while the mass of lighter air will be pushed to the top. It will be pushed upward by force equal to the difference between the weight and the weight of liquid displaced. The upward force is also known as the buoyant force (buoyancy). This causes the buoyant force of air parcels to accelerate vertically. Thus, the presence of the buoyant force is the basis for the formation of the updraft and downdraft in a convective system.

Convection plays an important role in the movement and distribution of mass and energy in the atmosphere medium. Convection also allows the formation of clouds and rain, which is one link in the hydrological cycle, which is essential for life on earth. The process of convection are the main drivers of the circulation of the atmosphere and play a role in cloud-radiation equilibrium. Thus, it is not surprising that the process of convection affects almost all atmospheric variables. Convection major cause of weather could of thermal convection or convection mechanical, consisting of processes as shown in Figure 2.14, among others; (a) The process of rising air mass/parcels due to the thermal force, (b) mechanical process due to sea breeze forcing the air parcel of rising because of the effect of orographic, (c) the process of parcel of rising due to the convergence wind, and (d) because the front.

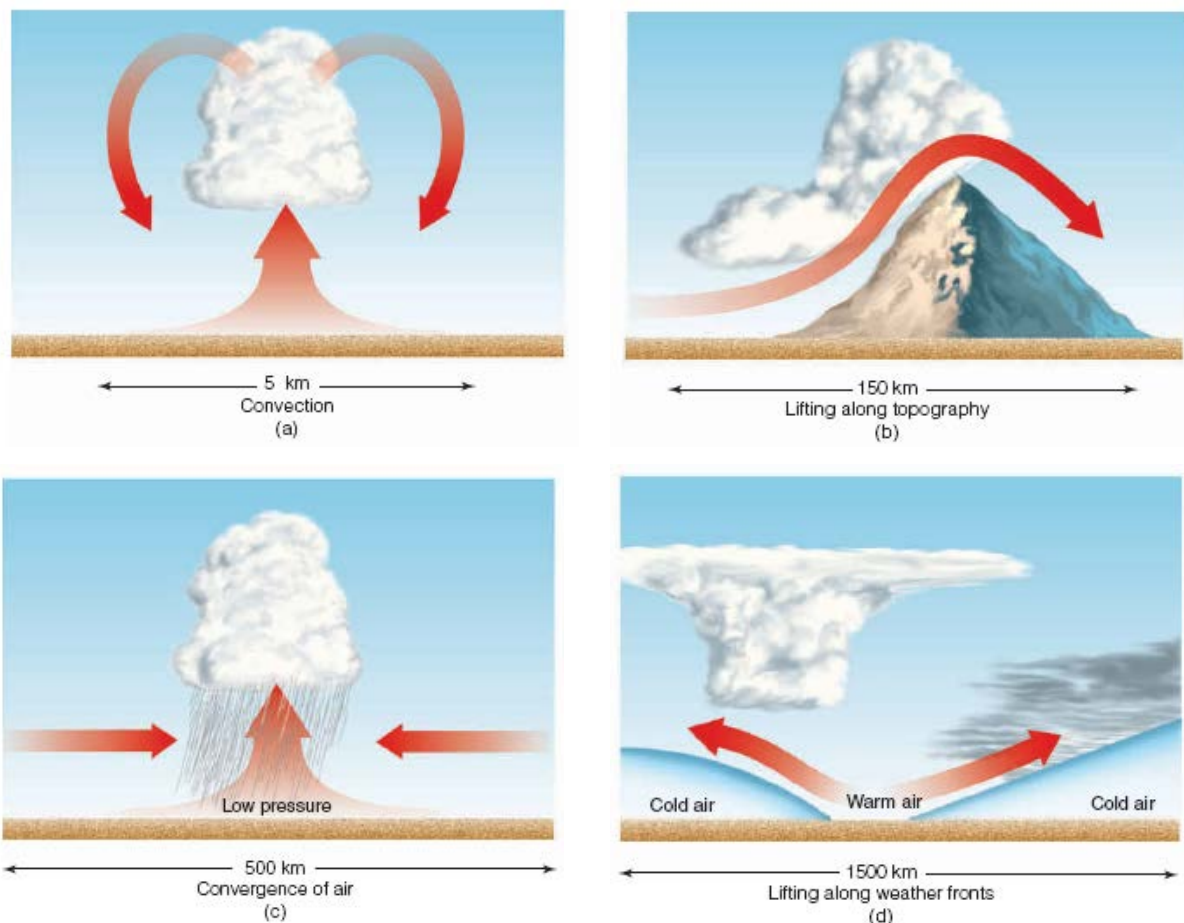


Figure 2.14. Schematic of convection process of; (a) The process of rising air mass/parcels due to the thermal force, (b) mechanical process due to sea breeze forcing the air parcel of rising because of the effect of orographic, (c) the process of parcel of rising due to the convergence wind, and (d) because the front (Ahrens 2001).

Globally there are three equatorial heat sources that are interpreted as the driving force for the global circulation, i.e., over the equatorial landmasses of central Africa, southeast Asia (included IMC), and the Amazon as shown in Figure 2.15 (Ramage 1968). IMC is one of the regions where deep cumulus convection occurs most frequently in the tropics. Convective activity over Indonesia is a powerful atmospheric wave source and heat engine affecting the upper atmosphere and global atmospheric circulation. However, the dynamical coupling processes of the equatorial atmosphere have not made clear due to the sparseness of observation data in that region. Other than convection with a period of longer than several days, the diurnal cycle of cumulus convection induced by local circulation (land-sea and mountain-valley breeze circulation) is also prominent, because IMC is composed of many islands and the surrounding sea.

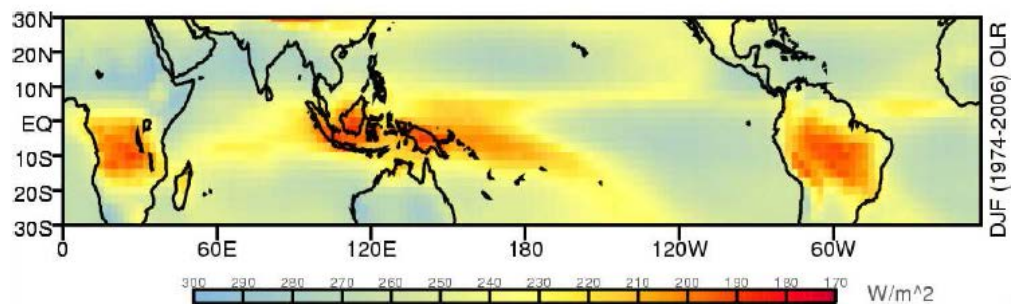


Figure 2.15. NOAA Interpolated Outgoing Longwave Radiation (OLR)- a proxy for deep convective activity, highlighting the major tropical convective centers. DJF seasonal mean (1974-2006) data from NCEP-NCAR reanalysis. Low ORL indicates cold clouds and hence deep convective activity (Strachan 2007).

One of the most important modes of atmospheric variability occurring over the IMC region is the local convective activity associated with the diurnal cycle of convection over the islands that called as a diurnal cycle or diurnal variation. It is the surface inhomogeneity of IMC, due to the complex system of islands, narrow peninsulas, and shallow seas, that gives rise to the complex localized forcing of the convective activity (Yang and Slingo 2001). Most studies have been explained the diurnal variation over IMC, especially over Sumatera using satellite, objective analysis, and daily and/or monthly rainfall data in terms of diurnal (Hamada et al. 2008; Qian 2008; Sakurai et al. 2005; Yang and Slingo 2001; and others),

intraseasonal (Hamada et al. 2008; Nitta et al. 1992; Ichikawa and Yasunari 2008; and others), seasonal (Hamada et al. 2002; Matsumoto 1992; Murakami and Matsumoto 1994; and others), and interannual variations (Hamada et al. 2002; Yasunari 1981; and others). Tropical convective systems with wide ranges of sizes have long been observed based on precipitation and cloud measurements from radars, microwave imagers, infrared and visible sensors (Lopez 1977; Houze and Cheng 1977, 1979; Williams and Houze 1987; Mapes and Houze 1993; Mohr and Zipser 1996; Chen et al. 1996; Yuan and Houze 2010; and others).

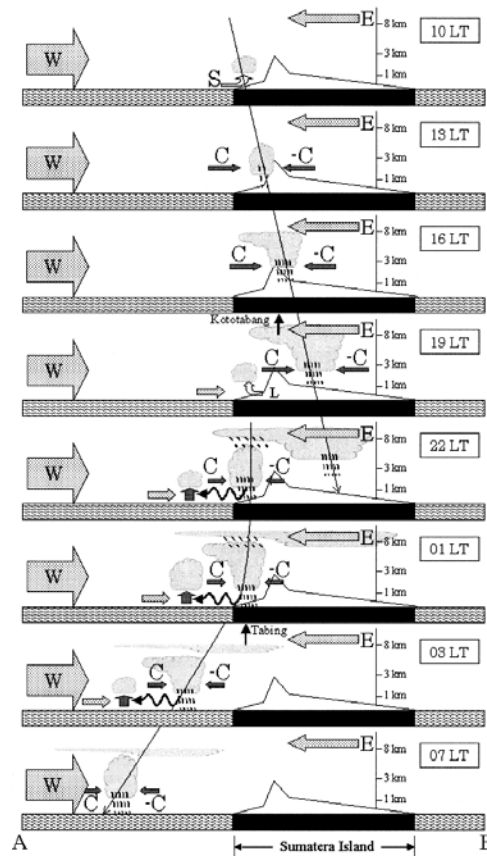


Figure 2.16. Schematic pictures of diurnal land–sea rainfall peak migration and circulations related to the migration (Mori et al. 2004).

Most of the previous studies indicated that diurnal rainfall variations in the Tropics have their peaks in the late evening over land regions and in the early morning over adjacent sea regions (e.g., Gray and Jacobson 1977; Murakami 1983; Houze et al. 1981) due to there exist a distinct difference in the timing of the maximum in convective activity between land (evening) and sea (morning) areas within the IMC (Murakami 1983; Nitta and Sekine 1994; Yang and Slingo 2001). The diurnal variation in Tropics has a close relation to the regional distribution of rainfall (e.g., Yang and Slingo 2001; Collier et al. 2004; Kikuchi and Wang

2008). The diurnal variation of convective activity occurred almost every day, and westward migrations of cloud systems were commonly observed in Central Sumatera (Mori et al. 2011). Additionally, the complex topography of the IMC leads to strong land–sea breeze circulations, with integral convection and precipitation, over the larger islands (Yang and Slingo 2001), such as; Sumatra (Mori et al. 2004), Borneo (Ichikawa and Yasunari 2006), and New Guinea (Ichikawa and Yasunari 2008).

The propagating diurnal variation also identified by Mori et al. (2004) as shown in Figure 2.16, who also described the accompanying anomalies in wind, humidity, and stability as part of a land–sea breeze circulation. Over the whole of Sumatera Island throughout a year, mainly using the GMS data which are continuous in space and time rather than TRMM. The phenomenon is that cloud systems develop in the afternoon along the mountain range of Sumatera Island and migrate toward the both (west and east) coastlines for several hundred kilometers during night. So that, the convective rainfall predominates in the afternoon to evening over the land area, the cause of the precipitation system is first generated in the evening around the southwestern mountains near the coastline of Sumatra whereas compound stratiform and convective rain is predominant in the morning over the surrounding sea region. He also suggested that the eastward migration until the late evening might be due to the background westerly wind in the lower troposphere, whereas the westward migration might arise from the generation of new convection on the windward side by self-replication and gravity wave mechanisms. They showed a clear contrast between the evening (1200–2300 LT) and morning (0000–1100 LT) rain along the coastlines of major islands of the IMC, such as Sumatra, Kalimantan, Jawa, Sulawesi, and Papua Islands.

IMC can be recognized as a major center of atmospheric activity, not only because of the mean amplitude of convective activity that occurs over the region, but because of the large range of atmospheric phenomena that affect, and are affected by, the region's climate. This review of the various spatial and temporal modes of atmospheric activity of importance to the climate of the IMC shows that activity occurs on intradural to interannual time scales, and on spatial scales from individual convective storms to global atmospheric circulations systems. Climate system in IMC is also dependent on complicated interactions among various scales of convective systems (e.g., Johnson and Kriete 1982; Janowiak et al. 1994; Nitta and Sekine 1994; Oki and Musiaka 1994; Asai et al. 1998).

Several studies have suggested that local circulation caused by topography like Sumatra topography plays an important role in the formation of convection with a diurnal

cycle (Mori et al. 2004; Wu et al. 2003). However, large-scale circulation plays an important role in the maintenance of heat and moisture supply into the region. It is also important to recognize that the mean climate of the region has an impact not only on the local and tropical atmospheric circulation but also on atmospheric conditions in the extra-tropics through perturbation of global atmospheric circulation patterns. Therefore, essential to keep in mind the importance of both local and remote climate conditions and processes regarding the impact on the IMC, and the response to the resulting atmospheric conditions over the IMC.

2.3.2 Rainfall system over IMC

Rainfall and its variability are important factors of the global hydrological cycle; they affect all living organisms on the Earth. The study of rainfall variability over short timescales is important and has a wide range of applications such as; to compare model predictions with atmospheric observations; to understand the atmospheric physics; to understand the local weather mechanisms, etc. The IMC receives a large amount of rainfall throughout the year, and the rainfall varies considerably across the region (e.g., Nakazawa 1988; Sui et al. 1992, Hirose et al. 2009) as shown in Figure 2.17 (a). In daily average, the heavy rainfall is most frequently concentrated on all large islands in Indonesia (Love et al. 2011) as shown in Figure 2.17 (b). Therefore, this region is a major atmospheric heat source that affects the circulation over the entire tropics (Ramage 1968).

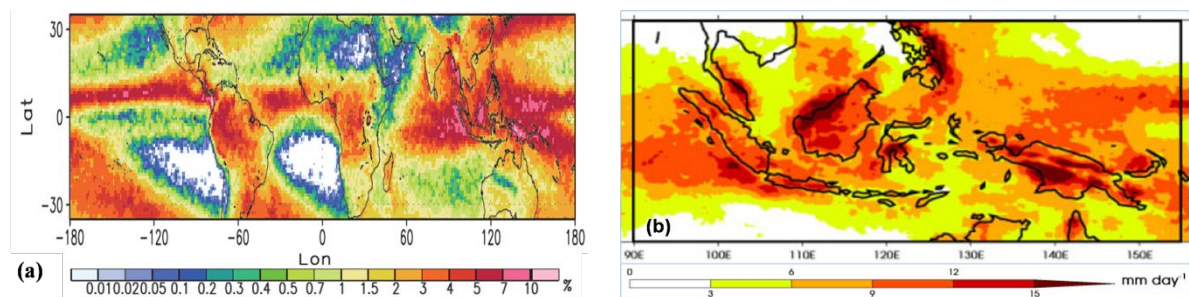


Figure 2.17. (a) Daily mean precipitation rate for northern winter 2008–2009 from TRMM (Love et al. 2011), (b) Fraction large precipitation during 1998–2007 (Hirose et al. 2009). The unit is %.

Spatial and temporal variations in rainfall affect the global circulation through latent heat release, because the IMC is composed of a large area of land-sea complex consisting of more than ten thousand islands, which are located between the Pacific and Indian Oceans and between the Asian and Australian continents and as the center of global multi-scale

interactions involving the global mean circulation and variability in a wide range of timescales including convective, diurnal, synoptic, intraseasonal, seasonal, interannual, decadal, and longer periods (McBride 1998; Chang et al. 2004). In previous studies of the convective rainfall fraction, Takayabu (2002) found 50% of the ocean and 61% of the land as a global average using TRMM.

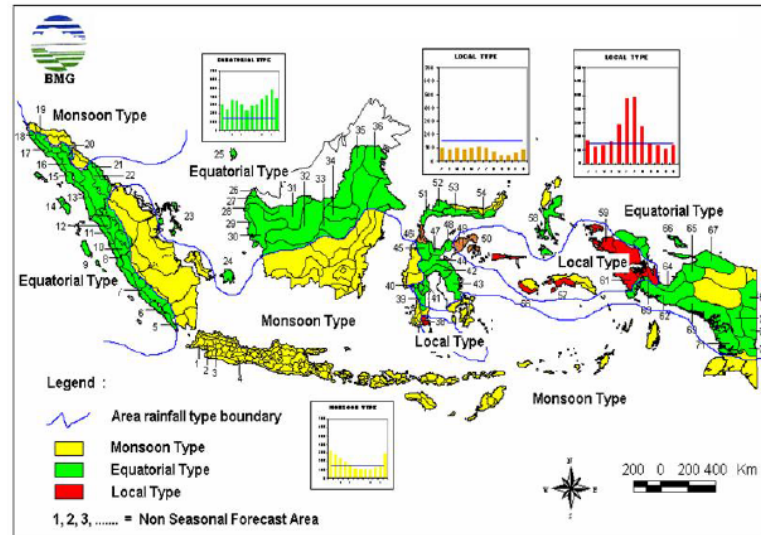


Figure 2.18. Rainfall patterns in IMC. Yellow is for monsoon pattern; green is for the equatorial pattern and red is for the local pattern (sources: Meteorology Agency (BMG), Indonesia).

There are three main types of rainfall pattern over IMC as shown in Figure 2.18, namely: (1). *Monsoonal type*, these patterns are influenced by the sea breeze and land breeze on a very large scale. It is characterized by the existence of a clear distinction between the period of the rainy season and the dry season of the year. This condition occurs in Java, Bali and Nusa Tenggara. Monsoon Asia influences the distribution of monthly rainfall. (2). *Equatorial type*, this pattern related to the movement pattern of convergence zone to the north and south following the apparent movement of the sun. It was characterized by a maximum of two times the monthly rainfall in one year. The regions which follow this pattern is largely Sumatra and Kalimantan. The distribution of monthly rainfall is affected by equinoxes, so the distribution shows double maxima. (3). *Local type*, this patterns strongly influenced by local conditions, especially rising air to the highland or mountain, and the existence of local heating that is not balanced. The condition is common in Maluku, Papua, and part of Sulawesi. This pattern is influenced by local condition, and monthly rainfall distribution is the opposite of monsoonal type.

Figure 2.19 shows the seasonal mean rainfall derived from the CMORPH dataset that shows the heavy rainfall is mostly concentrated over continent than the ocean on each season. The greatest maximum rainfall is most frequently found in Kalimantan, Southern Sumatra, and Papua Island. In contrast, the maximum rainfall was rarely found along Java Island until East Nusa Tenggara in each season except over Java in DJF. Conditions are particularly conducive to rainfall along the coasts and mountain ranges exposed to the northeast monsoon flow from the South China Sea. This wet season peaks in January. During this season, a quasi-permanent low-pressure center develops over the region.

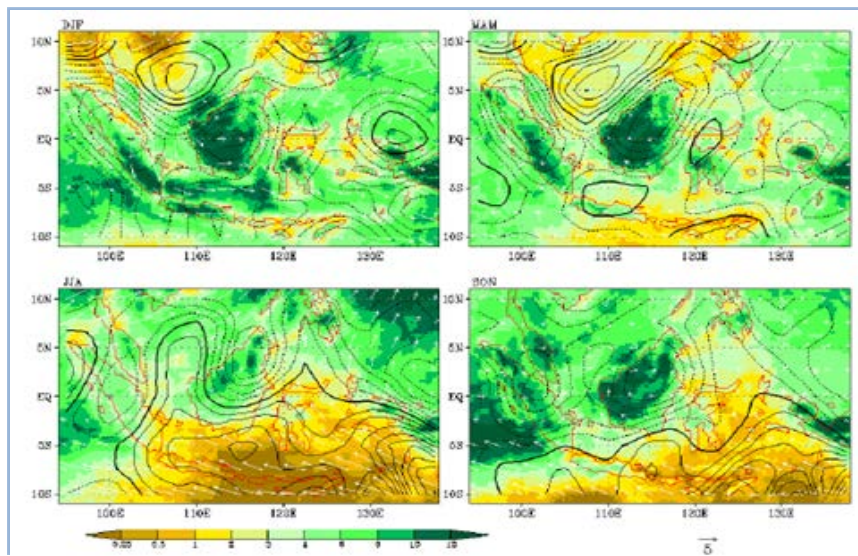


Figure 2.19. The averaged (2003-2006) CMORPH seasonal rainfall (mm/day) (shaded) Qian 2008).

Figure 2.20 shows the seasonal and monthly variations in total rainfall. The rainfall amounts are largest over the Indian Ocean and the central Pacific (around 150°E–180°E); the rainfall shows a clear seasonal progression, which starts in the Indian Ocean in boreal fall and ends in the western Pacific (around 120°E–150°E) in boreal winter. The largest rainfall over Indian ocean is most frequently occur in June until October.

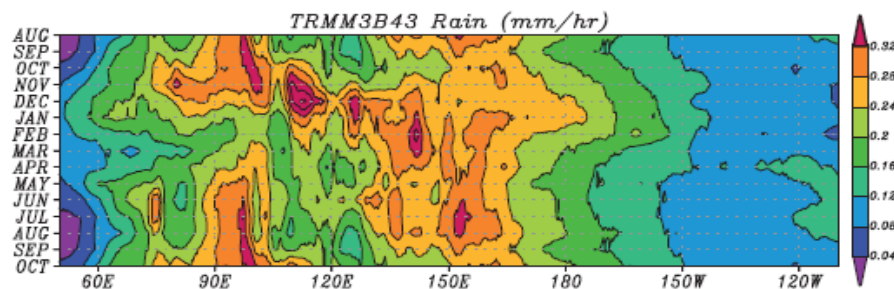


Figure 2.20. Monthly and longitudinal variations in the total rainfall (TRMM- 3B42) over 15°S–15°N.

Similar with diurnal variation, over the ocean, the diurnal cycle of rainfall is weak and peaks in the early morning (Nesbitt and Zipser 2003; Peatman et al. 2014) as shown in Figure 2.21. Overland, it is stronger and peaks in the evening. It is due to the different heat capacities of the two surfaces and related local land-sea circulations (Tao et al. 1996; Sui et al. 1998; Zhou and Wang 2006). Rainfall systems appeared mostly between afternoon and late evening over land, but rainfall associated with MCSs lingered past midnight. The number of MCSs increased over adjacent sea regions during morning hours. In addition to these large-scale features, more regional investigation of rainfall activity provided a more advanced understanding of the rainfall characteristics of this region of complex terrain.

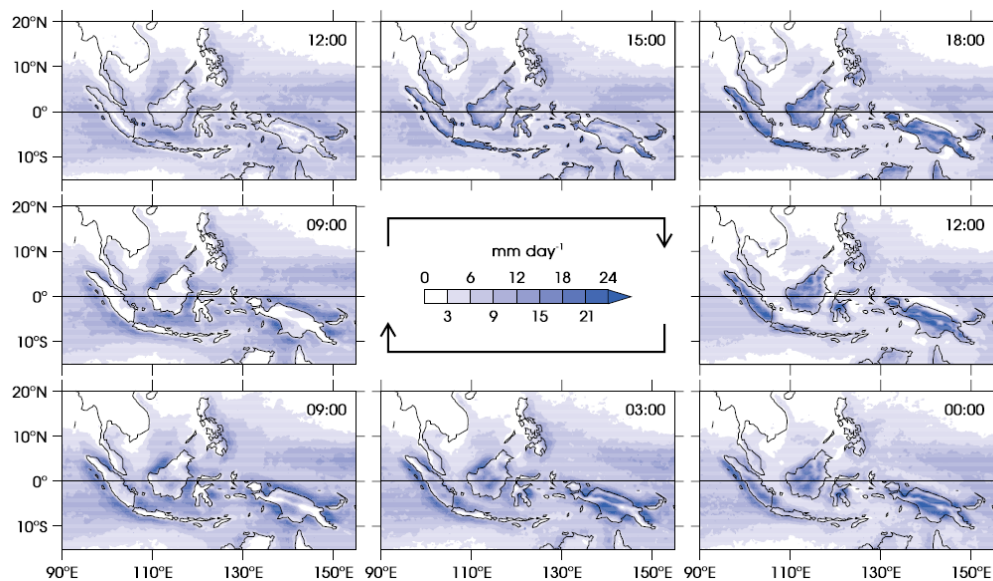


Figure 2.21. Climatological diurnal cycle of precipitation rate from TRMM 3B42HQ for November to April, 1998/99 to 2011/12. Time of day is given in LT for all longitudes and moves forward in the clockwise direction round the diagram. Peatman et al. 2014.

Nesbitt and Zipser (2003) found that the diurnal variation of rainfall over the ocean is small, but that the observed early morning maximum occurs because of an increase in the number of MCSs rather than an increase in system coverage or conditional rain rate. The diurnal variation of rainfall over land is much larger, with the afternoon maximum occurring because of an increase in convective intensities and the number of non-MCS features. The diurnal variation of rainfall associated with MCSs over land varies significantly because of their sensitivity to environmental conditions besides solar insolation.

2.4 The environmental parameters

2.4.1 Troposphere layer

Earth's atmosphere is a mixture of gasses that surrounds our home planet. Besides providing us with something to breathe, the atmosphere helps make life on Earth possible in several ways. Earth's atmosphere has a series of layers, each with its specific traits. The Earth's atmosphere can be divided into several layers. How the layers are defined can vary depending on what properties are taken into consideration. Layers defined by different types of properties can overlap. Temperature is one important property that varies in our atmosphere. Based on temperature changes, the atmosphere can be broken into exosphere and four major layers as shown in Figure 2.22. The other three small intermediate layers that serve as transition regions from one layer to the next. From highest to lowest, the five main layers are exosphere (700 to 10,000 km), thermosphere (80 to 700 km), mesosphere (50 to 80 km), the stratosphere (12 to 50 km) and troposphere (0 to 12 km).

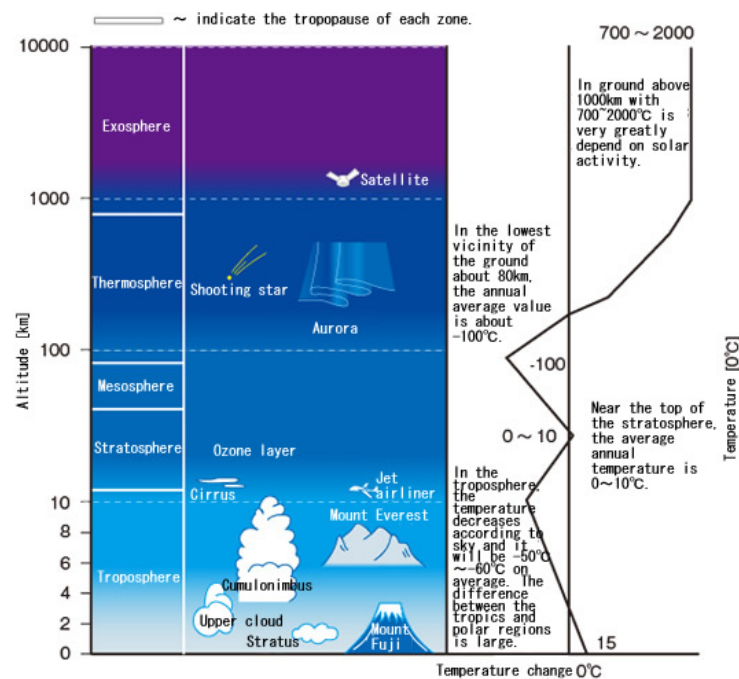


Figure 2.22. The layer of the Earth's atmosphere (source: http://www.apiste-global.com/ffu-bs/technology_pau_ffu-bs/detail/id=1215)

The troposphere is the lowest layer of Earth's atmosphere where the typical weather takes place. It extends from the Earth's surface to the tropopause (the boundary between the troposphere and the stratosphere). Most of the mass (about 75-80%) of the atmosphere is in the troposphere. Most types of clouds are found in the troposphere, and almost all weather

occurs within this layer. The troposphere is divided up into a couple of common ways when weather analysis is done. In commonly, the troposphere layers divided into three layers. The surface to 700 hPa is the low levels, 700 hPa to 500 hPa is the middle levels, and 500 hPa and above is the upper levels. In practice, the 700 hPa chart is typically classified as middle levels while the 500 hPa chart is classified as upper levels. Breaking the low levels into low and middle levels is helpful since several tropospheric processes are much different between the surface and 700 hPa than they are from 700 hPa to 500 hPa.

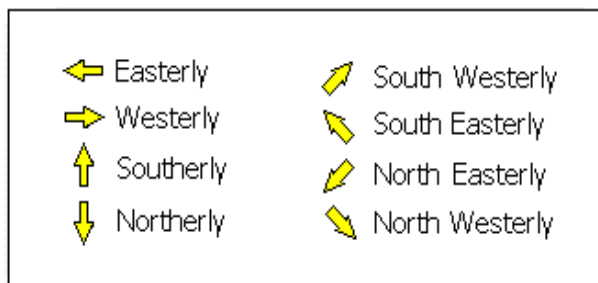
The surface layer and 850 hPa are influenced more by the ground surface, and air flow is more turbulent. Above 700 hPa, the air flow is typically smoother with less influence from the ground surface. This, of course, can change when storms occur. Using three-layer approach, the surface chart and 850 hPa chart are used for low-level analysis, the 700 hPa chart is used for middle-level analysis and the 500 hPa, and 200 hPa charts are used for upper-level analysis. In high elevation regions where the 700 hPa level is closer to the surface, then 700 hPa is used more or less as another low-level chart. The structure of an MCC can be separated into three layers. The low-levels of the MCC near the surface (1000 - 850 hPa), the mid-levels in the middle of the troposphere (800 - 400 hPa), and the upper-levels in the upper-troposphere (>200 hPa). (Maddox 1983; Houze 2004; and Cotton et.al. 1989).

2.4.2 Wind component

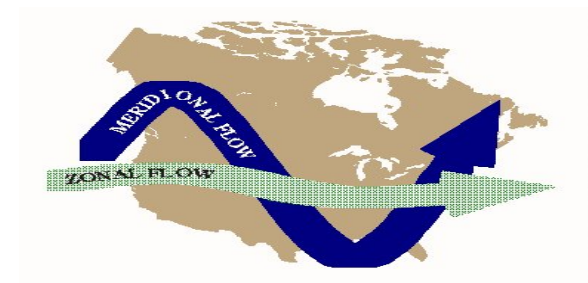
The winds are moving air and caused by differences in air pressure within our atmosphere. Air under high pressure moves toward areas of low pressure. The greater the difference in pressure, the faster the air flows. In meteorology, the wind is described as direction and speed. The direction of the wind is expressed as the direction from which the wind is blowing. For example, easterly winds blow from east to west, while westerly winds blow from west to east as shown in Figure 2.23 (a). Winds have different levels of speed, such as “breeze” and “gale,” depending on how fast they blow. Wind speeds are based on the descriptions of winds in a scale called the Beaufort Scale, which divides wind speeds into 12 different categories, from less than one mph to more than 73 mph. The wind vector represents the motion of the air mass over the ground. It is described by wind speed and the inverse of wind direction. Note that by convention wind direction is given as the direction the wind is from. The meteorological convention for winds is that U component (zonal wind) is positive for a west to east flow (eastward wind) and the V component (meridional wind) is positive for

the south to north flow (northward wind). Both of this data is used to create a wind vector. The unit of this data is m/s. The zonal and meridional wind is illustrated in Figure 2.23 (b).

To produce the wind anomaly vectors, the zonal and meridional daily wind anomalies are computed separately. Vectors show the resultant wind anomaly direction, and the vector length indicates the magnitude of the resultant wind anomaly. A vector scale in the lower-right-hand corner of the map indicates the length of the vector for a given speed, in units of m/s. Signed wind speed anomalies are calculated by subtracting the magnitude of the resultant daily climatological wind speed from the magnitude of the resultant observed wind speed, for example, wind anomaly vector at 00 UTC on 28 October 2007, calculated by subtracting the magnitude of the resultant daily wind speed on 28 October 2007 from the magnitude of the resultant wind speed at 00 UTC. The authors ever try using calculation with subtracting the magnitude of the resultant monthly climatological wind speed (2000 - 2009) from the magnitude of the resultant observed wind speed; the result almost is similar.



(a)



(b)

Figure 2.23. Illustration of wind direction (a) and zonal-meridional wind flow (b).

2.4.3 Temperature and geopotential height

A temperature is an objective comparative measurement of hot or cold. It is measured by a thermometer. Several scales and units exist for measuring temperature, the most common being Celsius (denoted °C; formerly called centigrade), Fahrenheit (denoted °F), and, especially in science, Kelvin (denoted K). Geopotential height is a vertical coordinate referenced to Earth's mean sea level, an adjustment to geometric height (elevation above mean sea level) using the variation of gravity with latitude and elevation. Thus it can be considered a "gravity-adjusted height." One usually speaks of the geopotential height of a certain pressure level, which would correspond to the geopotential height necessary to reach the given pressure. The unit is a meter (m).

Geopotential height approximates the actual height of a pressure surface above mean sea-level. Therefore, a geopotential height observation represents the height of the pressure surface on which the observation was taken. Since cold air is denser than warm air, it causes pressure surfaces to be lower in colder air masses, while less dense, warmer air allows the pressure surfaces to be higher. Thus, heights are lower in cold air masses, and higher in warm air masses. A line drawn on a weather map connecting points of equal height (in meters) is called a height contour. That means, at every point along a given contour, the values of geopotential height are the same.

At an elevation of h , the geopotential is defined as:

$$\Phi(h) = \int_0^h g(\phi, z) dz \dots\dots\dots(2.1)$$

where $g(\phi, z)$ is the acceleration due to gravity, ϕ is latitude, and z is the geometric elevation. Thus geopotential is the gravitational potential energy per unit mass at the elevation h . The geopotential height is:

$$Z_g(h) = \frac{\Phi(h)}{g_0} \dots\dots\dots(2.2)$$

A plot of geopotential height for a single pressure level shows the troughs and ridges, Highs and Lows, which are typically seen on upper air charts. The geopotential thickness between pressure levels - a difference of the 850 hPa and 1000 hPa geopotential heights, for example, is proportional to mean virtual temperature in that layer. Geopotential height contours can be used to calculate the geostrophic wind, which is faster where the contours are more closely spaced and tangential to the geopotential height contours.

The primary characteristic of a trough is that a trough is a region of lower heights. Height is a function of the average temperature of air below that height surface. A trough is a region with relatively lower heights tend to bring in cooler weather. A ridge is the opposite of a trough. A ridge is a region with relatively higher heights. A broad region of sinking air or a deep warm air mass will both lead to ridging. Since air is often sinking within a ridge, they tend to bring warmer and drier weather. Troughs and ridges are usually associated and more visible in the middle and upper levels of the atmosphere. Troughs and ridges are analyzed on pressure surfaces aloft such as 850, 700, 500 and 300 hPa. The trough and ridges are illustrated in Figure 2.24.

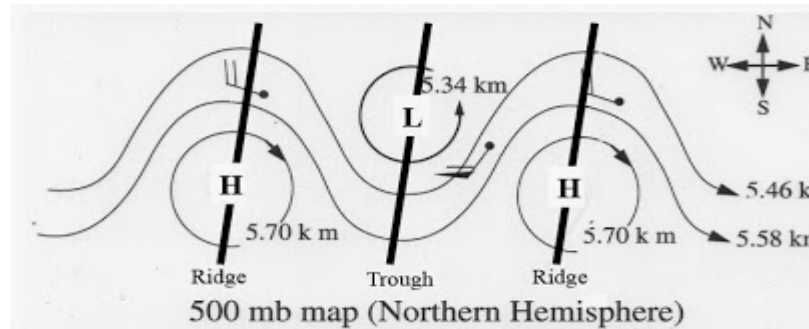


Figure 2.24. Illustration of the trough and ridges in the middle level of the troposphere. H is representing the high pressure, and L is representing the low pressure. (Source: https://charliesweatherforecasts.blogspot.jp/2013_10_01_archive.html)

A shortwave trough is an embedded kink in the trough/ridge pattern. Its length scale is much smaller than that of long waves, which are responsible for the largest scale (synoptic scale) weather systems. Shortwaves may be contained within or found ahead of long waves and range from the mesoscale to the synoptic scale. Shortwaves are most frequently caused by either a cold pool or an upper-level front. A shortwave trough is illustrated in Figure 2.25.

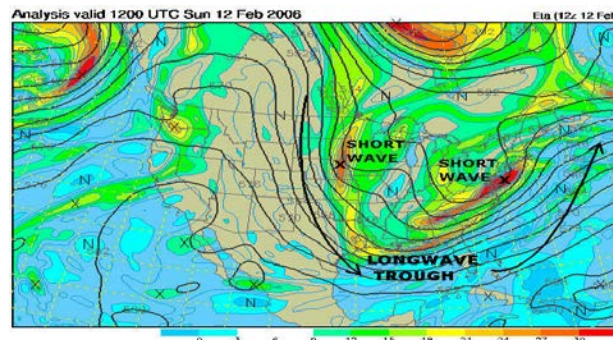


Figure 2.25. Example of two shortwave troughs embedded in a longwave system (source: <http://www.philip-lutzak.com/weather/snow%20storm%2002-11-2006%20project/snow%20storm%2002-11-2006.htm>)

Shortwaves have a counterclockwise kink to the height contours. Shortwaves are often associated with warm air advection or cold air advection, which influence temperature often represent baroclinic zone in the troposphere. The baroclinic zone is a region in which a temperature gradient exists on a constant pressure surface. Baroclinic zones are favored areas for generating the LLJ which important to the convection development, and sometimes mid-level cyclone. LLJ is a region of relatively strong winds in the lower part of the atmosphere which important for enhances convective and increases instability. Baroclinic zone and low-level jet are illustrated in Figure 2.26.

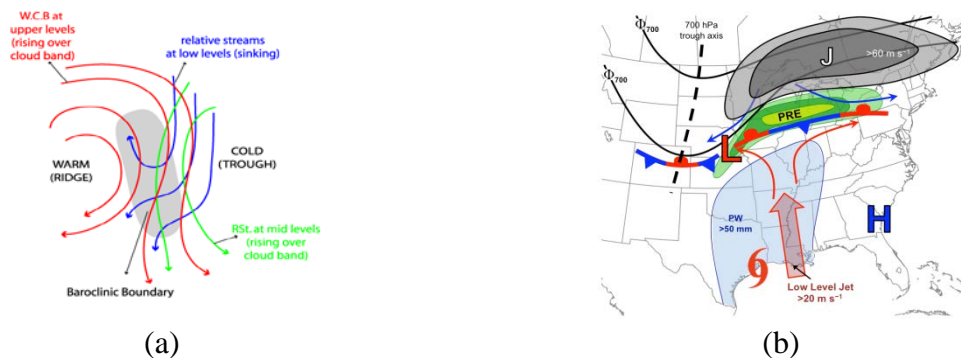


Figure 2.26. Illustrating of; (a) the baroclinic boundary/zone and (b) low-level jet (source: (a) <http://rammb.cira.colostate.edu/wmovl/VRL/Tutorials/SatManu-eumetsat/SatManu/CMs/BclB/backgr.htm> and (b) <https://hmt.noaa.gov/news/2011/PRE-map.html>).

Due to the way they move the air around them and the way air moves away from them, shortwaves generate positive curvature vorticity and positive shear vorticity, respectively. Ahead of a shortwave, there is large-scale lift due to divergence from positive vorticity advection which often causes precipitation. In a capped environment, the lift generated by a shortwave may cool the inversion layer as a result of the rapid expansion of the air (adiabatic cooling), allowing for deep, moist convection. Shortwaves are embedded within the longwave trough/ridge pattern and move faster than long waves (usually more than twice as fast).

2.4.4 Humidity and divergence field

Humidity is the amount of water vapor in the air. Water vapor is the gaseous state of water and is invisible. Humidity indicates the likelihood of precipitation, dew, or fog. The units for specific humidity and relative humidity are kg/kg and %, respectively. There are three main measurements of humidity: absolute, relative and specific. Absolute humidity is the water content of air at a given temperature expressed in gram per cubic meter. Relative humidity is the ratio of the partial pressure of water vapor to the equilibrium vapor pressure of water at a given temperature. Relative humidity depends on temperature and the pressure of the system of interest. It requires less water vapor to attain high relative humidity at low temperatures; more water vapor is required to attain high relative humidity in the warm or hot air. Relative humidity is normally expressed as a percentage; a higher percentage means that the air–water mixture is more humid, which is vital for the development of clouds and precipitation.

Specific humidity is a ratio of the water vapor content of the mixture to the total air content on a mass basis. The mixing ratio defined as the ratio of the mass of water vapor to the mass of dry air and is expressed in grams per gram or grams per kilogram. It differs from specific humidity only in that it is related to the mass of dry air instead of to the total dry air plus water vapor. The unit data is kg/kg. The equation is;

$$w = 0.622 \frac{e}{P-e} \dots\dots\dots (2.3)$$

where an actual vapor pressure (e) must be computed for values of dewpoint temperature and station pressure (P) must be converted to millibars (MB) or hectoPascals (hPa).

Convergence and divergence roughly determine where air will be sinking or rising. Rising air is associated with clouds and precipitation; sinking air is associated with clear, calm conditions and good weather. Divergence is a net outflow of air molecules from a region of the atmosphere (the opposite of convergence), where the convergence is a net inflow of air molecules into a region of the atmosphere. Weather is directly affected by the vertical motion of air which, in turn, is influenced by horizontal convergence and divergence. In the atmosphere, the distribution of horizontal convergence and divergence of air is rather complicated. Sometimes, convergence occurs at the low level, and divergence appears aloft; while the opposite may occur at other times. From Figure 2.27, we can see that convergence at the upper part of the troposphere together with divergence at the lower level will lead to a downward motion of air and bring fine weather. If the opposite occurs, upward motion of air will be developed, leading to the formation of cloud and even rain. The concept of convergence and divergence is very important in weather forecasting, and therefore forecasters often look into regions of convergence and divergence on the forecast charts.

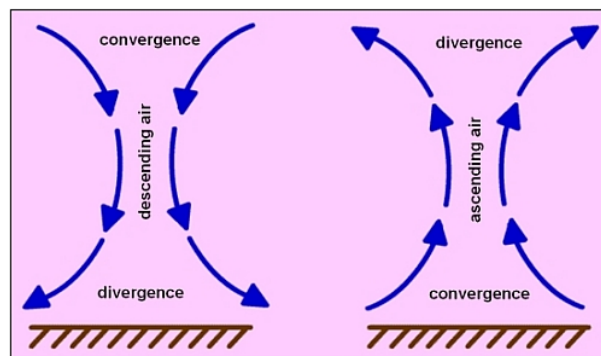


Figure. 2.27. Horizontal convergence, divergence and vertical motion of air (*source: <http://www.hko.gov.hk/education/edu01met/wxphe/ele-condiv-e.htm>*)

2.4.5 Potential temperature and equivalent potential temperature

Potential temperature (θ) is the temperature a parcel would have if it were to expand or compress adiabatically from its present pressure and temperature to a reference pressure level. $P_0 = 1000$ hPa. The unit data is K. The equation is;

$$\theta = T \left(\frac{P_0}{P} \right)^{R/c_p} \dots\dots\dots(2.4)$$

Where T is the current absolute temperature (in K) of the parcel, R is the gas constant of air, and c_p is the specific heat capacity at a constant pressure. $R/c_p=0.286$ for air (meteorology). P is pressure at the point (hPa), and P_0 is standard reference pressure (1000 hPa).

Equivalent potential temperature (θ_E) is the temperature a parcel of air would reach if all the water vapor in the parcel were to condense, releasing its latent heat, and the parcel was brought adiabatically to a standard reference pressure, usually 1000 hPa (1000 hPa) which is roughly equal to atmospheric pressure at sea level. In stable conditions, it increases with altitude. The unit data is K. The equation is;

$$\theta_E = T_e \left(\frac{P_0}{P} \right)^{R_d/c_{pd}} \dots\dots\dots(2.5)$$

where T_e is the equivalent temperature (in K) of the parcel, R_d/c_{pd} is the ratio of the specific gas constant to the specific heat of dry air at constant pressure (0.2854), P is pressure at the point (hPa), and P_0 is standard reference pressure (1000 hPa).

The θ can be used to compare temperatures at different elevations, and the trajectory air parcels will take (rising or sinking), while θ_E can be used to compare both moisture content and temperature of the air. θ_E is found by lowering an air parcel to the 1000 hPa level and releasing the latent heat in the parcel. The lifting of a parcel from its original pressure level to the upper levels of the troposphere will release the latent heat of condensation and freezing in that parcel. The more moisture the parcel contains, the more latent heat that can be released. θ_E is used operationally to map out which regions have the most unstable and thus positively buoyant air. The θ_E of an air parcel increases with increasing temperature and increasing moisture content. Therefore, in a region with adequate instability, areas of relatively high θ_E (called θ_E ridges) are often the burst points for thermodynamically induced

thunderstorms and MCS's. θ_E ridges can often be found in those areas experiencing the greatest warm air advection and moisture advection.

2.4.6 Moisture flux convergence and advection

Moisture flux convergence (MFC) is a term in the conservation of water vapor equation and was first calculated in the 1950s and 1960s as a vertically integrated quantity to predict rainfall associated with synoptic-scale systems. MFC was eventually suggested for use in forecasting convective initiation. The unit data is $10^{-4} \text{ g kg}^{-1} \text{ s}^{-1}$. The equation is;

$$MFC = -u \frac{\partial q}{\partial x} - v \frac{\partial q}{\partial y} - q \left[\frac{\partial u}{\partial x} + \frac{\partial v}{\partial y} \right] \dots \dots \dots (2.6)$$

where q is specific humidity, u is zonal wind velocity, and v is meridional wind velocity.

Temperature advection is the rate of change in temperature at a particular place due to the departure of air at one temperature and its replacement by air arriving from upwind with a different temperature. Temperature advection is the process by which the wind transfers heat energy horizontally through the atmosphere. Cold air advection involves wind carrying cooler air into an area that already contains warmer air. By contrast, warm air advection involves wind carrying warmer air into an area that already contains cooler air. Temperature advection is measured regarding the amount of temperature change that occurs in a given interval of time. The units used to express temperature advection are “degrees Fahrenheit per hour.”

Vorticity is a clockwise or counterclockwise rotation in the troposphere. 500-hPa vorticity also termed vertical vorticity (the rotation is in relation to a vertical axis). This vorticity caused by troughs and ridges and other embedded waves or height centers (speed and directional wind changes in relation to a vertical axis). A wind flow through a vorticity gradient will produce regions of PVA (Positive Vorticity Advection) and NVA (Negative Vorticity Advection). PVA (NVA in Southern Hemisphere) area is typically associated with divergence and upward motion. NVA (PVA in Southern Hemisphere) area will be associated with convergence and downward motion. The unit data in s^{-1} .

2.5 MCS and MCC

2.5.1 Definition and types

MCS is an organized group of thunderstorms that produces a contiguous precipitation area measuring 100 km or more in at least one direction. This system grows upscale from convective towers to a convective-stratiform coupled vertical circulation, ultimately meeting its demise as only a stratiform rain region. Tropical convection most often organized into mesoscale systems, with length scales of 100-1000 km and duration of several hours (Houze 2004). MCS which can evolve into tropical cyclones, form along areas such as tropical waves or easterly waves which progress westward along monsoon troughs and the ITCZ in regions of ample low-level moisture, convergent surface winds, and divergent winds aloft. This typically occurs north of the equator from Africa across the Atlantic and eastern Pacific oceans, as well as across the northwest and southwest Pacific Oceans, from Australia eastward into Oceania, the Indian Ocean, IMC, and from southeast Brazil into the southern Atlantic Ocean. MCS looks on satellite images as a circle, an oval, sometimes disorderly, but always compact. It consists of high cloud forms, to whose mostly belong cumulonimbus clouds, but also cirrostratus and (at the edge) altostratus clouds. Its size is from 20-40km (for the single thunderstorm) up to several hundred (up to ca. 200-400km), even thousand kilometers and extends its surface up to half million square kilometers. The cloud top height reaches 13-15 km, sometimes up to 16 km.

Many different types of MCSs exist and can be characterized by their environmental wind shear. Differences exist between both tropical and midlatitude MCSs as well as oceanic and terrestrial systems. In general classification, MCS can be divided into more specific classifications. The most commonly cited examples of MCSs include; Squall lines, Bow echoes and MCCs as shown in Figure 2.28. A squall line is a group of storms arranged in a line, often accompanied by “squalls” of high wind and heavy rain. Squall lines tend to pass quickly and are less prone to produce tornadoes than are supercells. They can be hundreds of miles long but are typically only 10 or 20 miles wide. A “bow echo” is a radar signature of a squall line that “bows out” as winds fall behind the line and circulations develop on either end. A strongly bowed echo may indicate high winds in the middle of the line, where the storms are moving forward most quickly. Brief tornadoes may occur on the leading edge of a bow echo. Often the north side of a bow echo becomes dominant over time, gradually evolving into a comma-shaped storm complex. A special case of MCS is the mesoscale convective complex (MCC), defined by Maddox (1980), as a very largest of MCS that are

widely observed around the globe. MCC is a particular type of MCS; an MCC is a large, circular, long-lived cluster of showers and thunderstorms identified by satellite. It often emerges out of other storm types during the late-night and early morning hours. MCCs can cover an entire state.

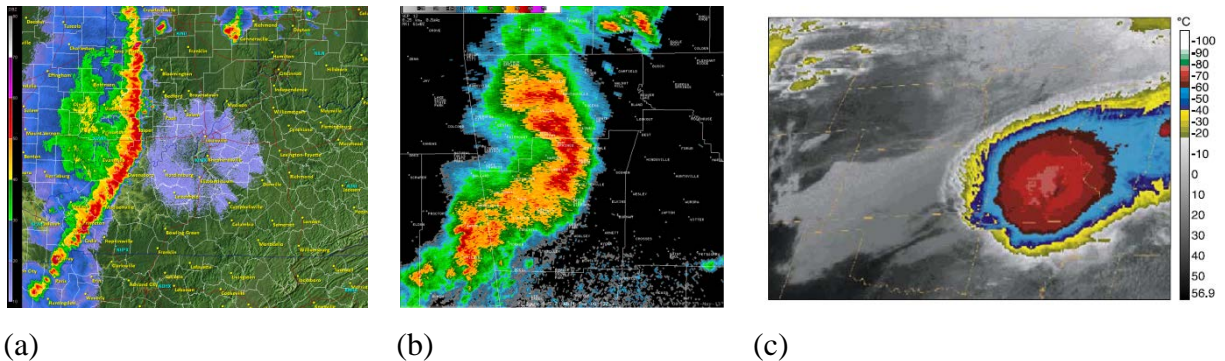


Figure 2.28. (a) A squall line, (b) Bow echo over Springdale, Arkansas, 21 May 2013, (c) Infrared satellite image of an MCC over Missouri. (Source: (a) and (b) <http://www.nssl.noaa.gov/education/svrwx101/thunderstorms/types/>, (c) Houze 2004)

2.5.2 The importance of MCS/MCC

MCC are important atmospheric phenomena. “Due to their large size and long duration, important mesoscale/large scale interactions take place, seriously impacting the accuracy of operational numerical models” (Rodgers et al. 1983). These large, long-lasting organized systems are comprised of an ensemble of thunderstorms that together, often yield intense rain rates within contiguously sizeable precipitation areas and can greatly influence the hydroclimate of a region (Durkee et al. 2009). MCCs are significant rain-producing weather systems and also produce a broad range of severe convective weather events: strong winds, hail, tornadoes, lightning, flooding and so seriously impacting the accuracy of numerical models prediction.

With any MCS, there is the possibility of strong winds, but the more low-level shear present in the environment of the system, the greater the possibility of severe surface winds (Squall Lines and especially Bow Echoes). In environments with more shear, surface winds can reach 100 kts or more. It is extremely rare in the tropics. MCCs are also one of the important sources of turbulence, namely: Convectively induced turbulence (CIT), which occurs within deep convective clouds, updrafts, downdrafts, and thunderstorm anvils and Near-cloud turbulence (NCT) in the clear air around the MCC, due to gravity waves propagating from the MCC, unstable upper-level storm outflow, and cirrus cloud bands. MCSs (including MCCs) also produce frequent lightning, small hail, occasional tornadoes,

and waterspouts. MCSs are an important link between atmospheric convection and the large-scale atmospheric circulation. For example, they are associated in various ways with large-scale wave motions (e.g., Payne and McGarry 1977; Hodges and Thorncroft 1997; Houze et al. 2000; Carbone et al. 2002), and some of the largest MCSs occur over the Pacific Ocean warm pool as a fundamental ingredient of intraseasonal and interannual climate variations (Nakazawa 1988; Chen et al. 1996).

Houze (2014), an MCS develops a mesoscale overturning circulation that is dynamically distinct from that of a convective cell, which occurs on a smaller spatial scale. While a convective cell is well described by entraining parcel concepts and consists of a buoyant plume or bubbles ~1-10 km in horizontal scale originating in the boundary layer and accelerating upward, the circulation of an MCS consists of broad layers of rising and sinking air on horizontal scales ~100 km. The mesoscale layer overturning of an MCS has been described as the gravity-wave response to the collective convective heating in a group or line of convective cells (Pandya and Durran 1996) or alternatively as a joint mesoscale response to the environmental thermal and wind stratifications (Moncrieff 1992). The layer of subsiding air in an MCS enters at middle levels (Kingsmill and Houze 1999) and is driven downward by the cooling effects of evaporation and melting of precipitation particles below a layer of upward motion and condensation heating aloft (Houze, 1982, 1993).

Fritsch et al. (1994) showed how the heating aloft and cooling below in the stratiform region generates potential vorticity, enhancing and prolonging the MCS. MCSs are of great dynamic importance for several reasons. The latent heating profile in an MCS shifts upward (becomes “top heavy”) when the stratiform component of the MCS is large. Hartmann et al. (1984) and Schumacher et al. (2004) have shown that accounting for the upward shift in the vertical distribution of heating leads to the more realistic large-scale circulation of the tropics. MCSs are also important because they account for numerous events of excessive rainfall, severe weather and floods (e.g., Hoxit et al. 1976; Bosart and Sanders 1981; Houze et al. 1990; Rasmussen and Houze 2011; Romatschke and Houze. 2013; Rasmussen et al. 2014). These facts motivate a global understanding of when and where deep convection organizes upscale into mesoscale units.

MCSs are mostly concentrated in the tropics and mid-latitudes where they account for a large proportion of rainfall (Desbois et al. 1988; Carvalho and Jones 2001; Houze 2004; Wallace and Hobbs 2006). MCS are essential for the earth equilibrium as they modify the environment on a scale many times larger than the visible cloud (Moncrieff 1992). They

regulate the transport of energy, heat, moisture and momentum in the atmosphere (Laing and Fritsch 1993b; Schröder et al. 2009) and play an important role in the input of energy to the climate system through the radiative effect of the upper tropospheric cloud and water vapour and enhanced surface fluxes (Moncrieff 1992). Accordingly, features governing MCS may be considered as triggers of local and global climate changes. For instance, as the build up of CAPE is closely related to the land surface (e.g. albedo) and surface fluxes (Mathon et al. 2002; Lauwaet et al. 2009), orography, land cover and land use changes are examples of factors that potentially modify the location of MCS and subsequent rainfall amount and pattern. Investigating the origin of changes in MCS and the impact of it on the climate requires a thorough understanding of the relations between the initiation, structure, and development of such systems with their respective rain efficiency. It is not uncommon to see new cloud clusters also forming further ahead of the leading edge (Desbois et al. 1988; Houze, 2004). Meteorologist and Climatologist assume that those new cloud clusters are induced by gravity waves (Moncrieff 1992; Houze 2004). The latter are generated by the combination of two opposing forces; on the one hand, the convective updraft which forces the stable air to rise and, on the other hand, the stable atmosphere which forces the parcel of air to sink again. Because of the momentum of the rising and sinking parcels, the gravity waves propagate further away from the MCS. The new cloud clusters created by gravity waves influence the propagation speed and direction of propagation (Desbois et al. 1988). Given suitable conditions, gravity waves generated by MCS may propagate horizontally on a scale much larger than the MCS (Moncrieff 1992; Houze 2004).

CHAPTER THREE

THE CLIMATOLOGY OF MESOSCALE CONVECTIVE COMPLEXES (MCCs) IN INDONESIAN MARITIME CONTINENT DURING 15-YEARS PERIOD

This chapter to explain the climatology of MCC over the IMC with analyzing the distribution of MCCs in globally, seasonal, manually and diurnal, analyze of some MCCs, the duration time of MCC life-cycle, the area size of cloud and eccentricity and analyze the evolution characteristics of MCC. The result of this chapter will answer clearly the research objective about the climatology of MCC over the IMC. The method to analyze the climatology of MCC over the IMC in this chapter have been described in detail in sub-section 1.4.2.1.

3.1 Distribution of MCC occurrences

A climatological study of MCCs during 2001 - 2015 over IMC has been identified using IR satellite imagery with creating an algorithm that combines criteria of cloud coverage, eccentricity, and cloud lifetime.

3.1.1 Global distribution of MCC occurrences

A total of 1028 MCCs were identified and tracked during fifteen years for the 2001 – 2015 period as shown in Figure 3.1. The MCCs developed in several concentrated areas; some of them were over the ocean and coastal areas, and others were over inland and high elevation areas. By examining the location of the interior cloud centroids for all of the MCCs, one can see that MCCs are mostly frequent occur in nine regions as shown in red dotted line in Figure 3.1. That nine regions are the Indian Ocean near Sumatra Island, along the western coastal of Sumatra Island, the South China Sea near Borneo/Kalimantan Island, the Central Kalimantan around 3°S-1°N; 111° -115°E, the East Kalimantan around 1° - 4°N; 116° - 120°E, Makassar Strait near coasts of Kalimantan Island, the Central Sulawesi around 4° - 2°S; 120° - 123°E, Merauke over Papua Island in location around of 8° - 5°S and 135.5° - 140°E, and Cendrawasih Bay near coasts of Papua Island in location around of 132.5° - 136.5°E and 4° - 1°S. From the nine regions, the oceanic MCCs only concentrated over Indian Ocean, whereas

the coastal MCCs concentrated over the Makassar Strait, Cendrawasih Bay, and the South China Sea near Kalimantan Island. The continental MCCs concentrated over the Central and East Kalimantan that is close to the mountains. MCC rarely found along the Java Island to the East Nusa Tenggara because of the low-lying region.

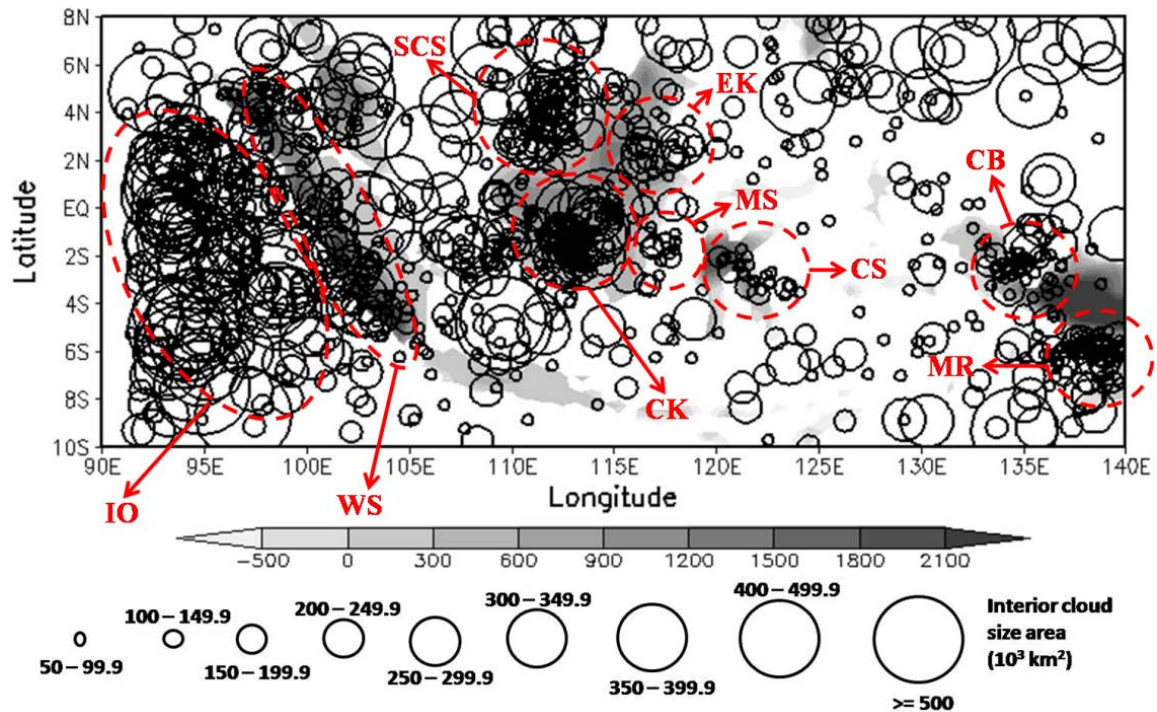


Figure 3.1. Geographical distribution of the MCCs in the IMC during 15-years (2001-2015). Locations are for the MCC at the time of maximum extent of the interior cloud size area when the mature stage. The circles representing the interior cloud size area (10^3 km^2). The red dotted line indicated the MCCs concentration region, where IO, WS, SCS, CK, EK, MS, CS, CB and MR refer to Indian Ocean, Western Sumatra, South China Sea, Central Kalimantan, East Kalimantan, Makassar Strait, Central Sulawesi, Cendrawasih Bay and Merauke, respectively. The color shaded refers to the elevation of the unit in meters (m).

Figure 3.1 shows that the MCC occurrences frequently found in the near-equatorial regions in the range of latitude 5S - 5N. It associated with the surplus of radiative energy in the tropics and a net deficit in middle and in high latitudes, requiring on average a poleward transport of energy by the atmospheric circulation, as already illustrated in Figure 2.4. The fact is that this surplus energy heats the ocean and land surfaces and evaporates moisture. In turn, some of this heat lands its way into the atmosphere in the form of sensible and latent heat, and it is the energy of this type that is transported polewards by the atmospheric circulation. Cloud systems directly affect the surface energy budget through their

modification of the net radiative fluxes. Clouds are also a key factor in the coupling between the atmosphere and the ocean through their influence in the surface radiative, heat, and momentum fluxes (Strachan 2007). The energy associated with the equatorial maximum in solar radiation released through vigorous atmospheric convection is the ultimate driver of the mean position of the Hadley circulation (Lindzen and Hou 1988), as illustrated in Figure 2.3. Atmospheric convection cell warm air rises at the equator. As it rises, it cools and generates large amounts of precipitation. The development of the MCC over near-equatorial is also possibly related with the ITCZ as a belt of low pressure which circles the Earth generally near the equator where the trade winds of the Northern and Southern Hemispheres come together. It is characterized by convective activity which often generates vigorous thunderstorms over large areas. It is most active over continental land masses by day and relatively less active over the oceans.

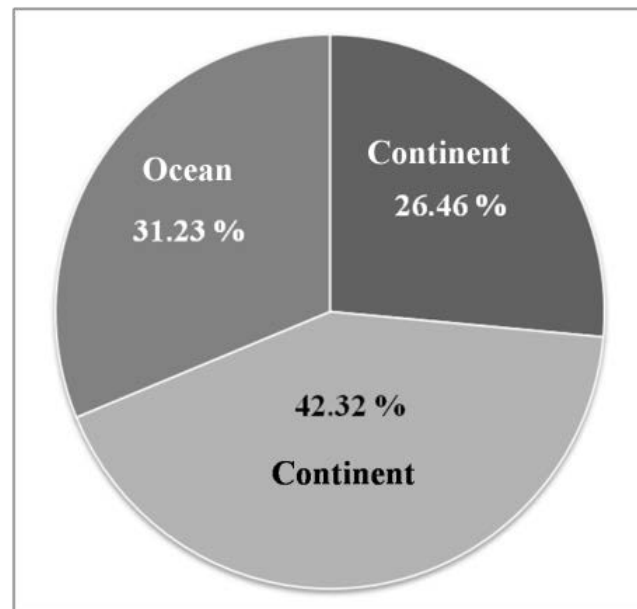


Figure 3.2. Percentage of the MCC occurrences over the IMC during 15-years (i.e., 2001-2015) over the ocean, the coastal and the continent.

Most of MCCs in the IMC occurred on the continent than at ocean where this research found 31.23% MCCs over the IMC occurred over the ocean, 26.46% occurred over the coastal and most of MCCs occurred on the continent around 42.32% as shown in Figure 3.2. In this research, we defined an oceanic (continental) MCCs as a system that reaches maximum extent while positioned over the ocean (land) as the following method by Morel

and Senesi (2002) and Blamey and Reason (2012). This research follows the method by Ogino et al. (2016) and Mori et al. (2004) to defined the coastal region. The coastal MCCs is defined the MCCs that occurred in near the coastal at between ocean and continent during MCCs reaches maximum extent or mature stage. It is similar to the characteristics of MCC globally by Laing and Fritsch (1997) that found most of the MCCs is located in continents almost of 91% though they can occur over oceans. However, MCC has a large scale are more prevalent over the oceans than on land especially over the Indian Ocean, and MCCs are originating over the oceans are longer lasting originating over land.

Most of the continental MCCs concentrated in near the mountainous and high elevation areas. This result is similar with Ashley et al. (2003) and Laing and Fritsch (2000) who reported that the mean location for the development of the MCCs in America was found on the lee side of the mountain. Morel et al. (2002) also reported that a large number of MCS over a large part of Europe using satellite infrared imagery found at mainly continental, strongly related with orography and in their majority are in phase with the diurnal radiative heating. MCC was frequently found in near mountain because the effect of topography is important for the LLJ formation. The jet appears to contribute to the formation of the MCS (including MCC) structure in the northern part of the convective system and the formation of low-level intense wind. Additionally, the effect of the convective system on the formation of the jet could also be substantial because the convective system may hydrostatically reduce the low-level pressure behind it, thereby enhancing the horizontal pressure gradient force across the mountain range (Kawashima et al. 2011). A mountain breeze and a valley breeze are two related, localized winds that occur one after the other on a daily cycle which also give a contribution to convective activity over the IMC due to IMC is a unique geographical region that composed of a complex system of mountainous islands. The interaction between the topography with the westerly wave propagation is assisted in the development of convective storm or MCC in Africa (Garstang et al. 1987).

Diurnal cycle of cumulus convection over the IMC induced by local circulation (land-sea and mountain-valley breeze circulation) because IMC is composed of many islands, mountain, and the surrounding sea. This complex topography of the IMC leads to strong land-sea breeze circulations with integral convection and precipitation over the larger islands (Yang and Slingo 2001), such as; Sumatra (Mori et al. 2004), Borneo/Kalimantan (Ichikawa and Yasunari 2006), and New Guinea/Papua (Ichikawa and Yasunari 2008). The other

previous studies using in situ rain gauge networks, limited rawinsonde observations, GMS, GOES, and Meteosat IR sensor, and atmospheric reanalysis data have gradually revealed that the diurnal variations of convective over IMC have prominent interactions with local topographical features, as well as being dependent on complicated interactions among various scales of convective systems (e.g., Johnson and Kriete 1982; Janowiak et al. 1994; Nitta and Sekine 1994; Oki and Musiak 1994; Asai et al. 1998; Ohsawa et al. 2001).

The MCC systems are longer lasting in the western Indonesian than in the central Indonesian and eastern Indonesian. Most of the oceanic MCCs concentrated over the Indian Ocean. Most of them have large interior cloud size over 300,000 km² even much going MCC which has a scale of 500,000 km² because this area is one of heat sources that interpreted as the driving force for the global circulation in the tropics (Ramage 1968). This area is also one of the regions where deep cumulus convection and heavy rainfall occurs most frequently in the tropics (Yamanaka et al. 2008). The oceanic MCCs with large size also occurs in the Pacific Ocean and the Java Sea between Kalimantan Island and Sumatra Island. Moreover, an oceanic area with the lower MCC occurrences is the Molucca Sea and the Banda Sea.

Variations in actual MCC totals per year as shown in Figure 3.3 has been observed with an obvious peak of MCC activity in 2004, 2005, 2011 and 2013 when more than 80 events occurred each year. 2001, 2007, 2010, 2012, 2014 and 2015 are all above 70 events occurred each year. A total of 53 and 62 events occurred in 2003 and 2008, respectively. The only years notably fewer events are 2002, 2006 and 2009 with 45, 45, and 44 events, respectively. Numerous studies have demonstrated that ENSO can modulate the synoptic and mesoscale environments South America, which in turn can influence convective activity and precipitation patterns across the tropical and subtropical regions (e.g., Curtis 2008; Silva and Ambrizzi 2006; Lau and Zhou 2003; Grimm et al. 2000 and Velasco and Fritsch 1987). Specifically, Velasco, and Fritsch (1987) found that the number of MCCs doubled during the 1982/83 El Nino event. However, this research showed no apparent relationship between MCC frequency and ENSO that similar with Durkee and Mote (2009) that analysis of ENSO and MCC cloud-top characteristics, longevity, and the distribution of MCC rainfall show no apparent relationship.

The MCC occurrences are most frequently occur in the region that has the high intensity and greater fraction of rainfall as shown in Figure 2.17, among other, over the Indian Ocean, Central Kalimantan, Merauke and Central Sulawesi. However, the high intensity over

Java Island not clearly related with MCCs due to only a few of MCC events found over Java Island. In detail, related to the relationship of MCCs with rainfall including over Java will be explained in the next chapter.

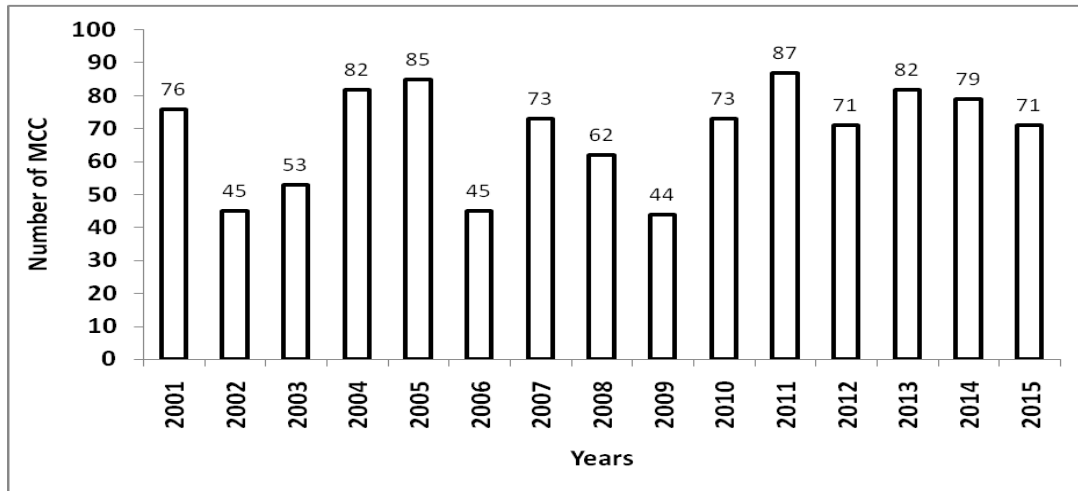


Figure 3.3. A total of MCC occurrences over the IMC during 15-years (2001-2015) for each year.

This result also supported by previous research, among other; Trismidianto (2012) that stated there are many MCC occurrences over the Indian Ocean near Sumatra and Ismanto (2011) stated that one of concentration area for oceanic MCC is the Indian Ocean. Moreover, Mori et al. 2004 stated that IMC consists of many large/small islands with very long coastlines, many narrow straits control the global (Pacific to Indian) ocean circulation and the deep convection is the major contributor to changes in tropical rainfall (Tan et al. 2015). Land-sea breeze and mountain breeze play an important role in the tropical precipitation, include IMC so that most of the precipitation in IMC concentrated over the continent than over the ocean (Qian 2008). The precipitation inside the coastal region accounts for approximately 34% of the total over the entire tropics, while that outside the coastal region accounts for 52% and 14% on the ocean and land sides, respectively (Ogino et al. 2016).

3.1.2 Seasonal distribution of MCC occurrences

As mentioned in chapter 2 that the season in Indonesia divided into four seasons, namely in December, January and February (DJF) as the wet season, March, April and May (MAM) as a transitional season from wet season to the dry season. June, July, and August (JJA) as dry season and September, October, and November (SON) is a season of transition

from dry season to the wet season. Figure 3.4 (a) shows that the peak of MCC occurrence over the IMC is during MAM with around 33.56% MCC occur in this season. This result similar with Tyson and Preston-Whyte (2000) that stated the peak of MCC activity in southern Africa is mostly occur during the early before summer months due to likely linked to the synoptic-scale environment, which is more baroclinic in nature compared to the late summer months. Velasco and Fritsch (1987) suggest that the longer MCC season maybe due to the influence of the oceans on the relatively smaller landmass. However, some of the previous paper stated that there is the effect of ENSO on MCC activity in Africa (Mason and Jury 1997) and in America (Durkee et al. 2009). 26,26 % and 25,29% MCC occurrences are found in DJF and SON, respectively. The season with fewer events is JJA, around of 14.79%.

Figure 3.4 (b) show the comparison of the coastal, oceanic and continental MCCs, where 7.59%, 10.51% and 8.17% of MCCs occurred in coastal, continent and ocean during DJF, respectively. The percentage increased in MAM around 8.46%, 16.73% and 8.37% of MCCs found in coastal, continent and ocean, respectively. It shows almost half of MCC occurrences during MAM occurred on the continent. In contrast, during JJA, most of MCCs occurrences are the oceanic MCC with 7.88% events, while the percentage of the continental and coastal MCCs are 3.31% and 3.60%, respectively. Similar with MAM, almost half of MCC in SON is the continental MCCs in the amount of 11.77% where the oceanic and coastal MCC have the same percentage around 6.81%.

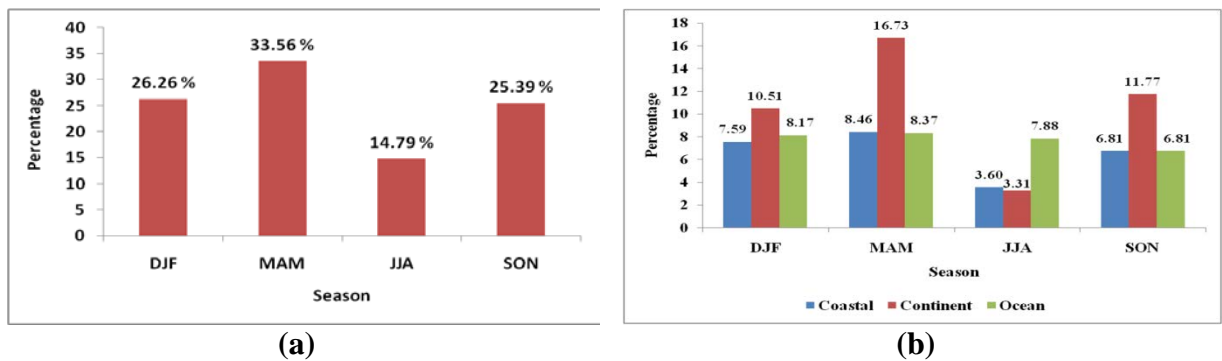


Figure 3.4. Percentage of the MCC occurrences over the IMC during 15-years (2001-2015); (a) for each season, (b) for each season in coastal, continent and ocean.

By examining the location of the interior cloud centroid for each season. In DJF, one can see MCCs are most frequent concentrated in the continent at Central Kalimantan, the South China Sea near northern Kalimantan, Central Sulawesi and Merauke as shown in

Figure 3.5 (a). However, the continental MCCs have an interior cloud in small size around 50,000 - 149,999 km². In contrast, most of the MCC with large size frequently found in the Indian Ocean near Sumatra Island. Most of them have an interior cloud in size more than 300,000 km². The MCC in medium size also concentrated in the Pacific Ocean. During MAM as shown in Figure 3.5 (b), the frequency of MCCs was almost similar with DJF, but MCCs over the Central Kalimantan became more widespread throughout to Kalimantan. Small-sized MCCs dominate MCCs that occurred over the Central Kalimantan during MAM, but several large-sized MCC also found. MCCs over Merauke also became more widespread until the Arafura Sea. Several MCCs with medium size around 200,000 - 300,000 km² found over Sumatra Island and western coastal of Sumatra. The oceanic MCC with large-sized still found in the Indian Ocean. Several MCC in small-sized also occurs over the Java Island.

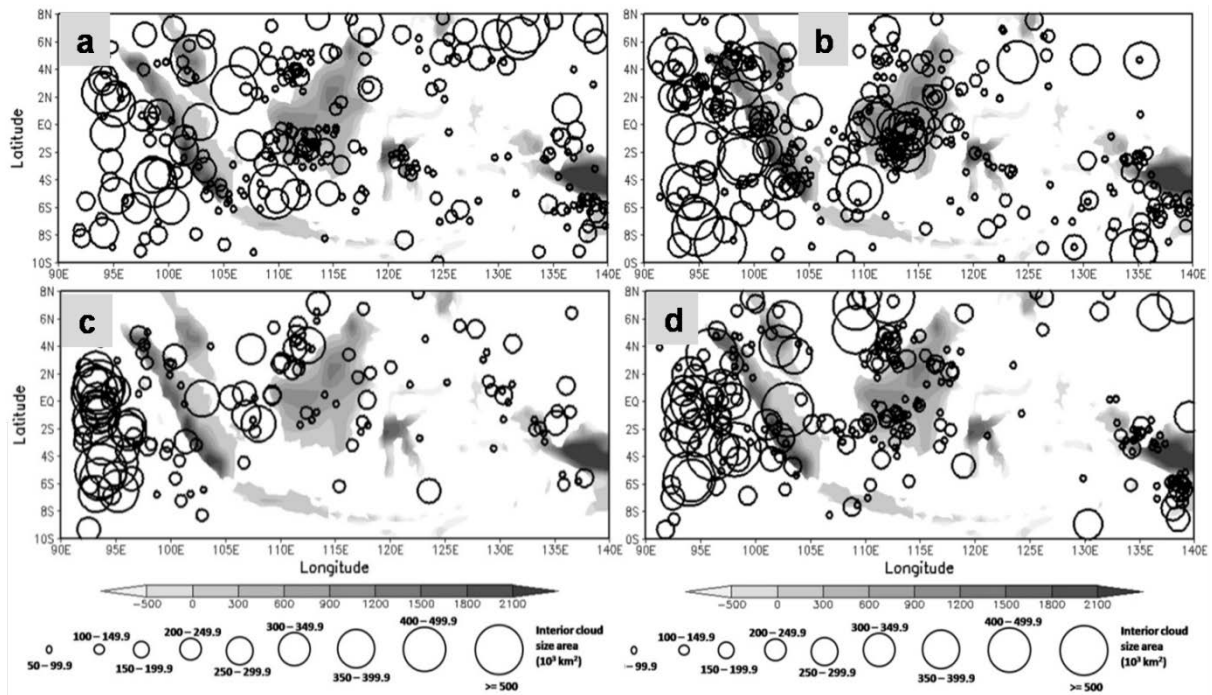


Figure 3.5. Geographical distribution of MCCs in the IMC during 15-years (2001-2015) for each season; (a) DJF, (b) MAM, (c) JJA and (d) SON. Locations are for the MCC at the time of maximum extent of the interior cloud size area when the mature stage. The circles representing the interior cloud size area (10^3 km^2). The color shaded refers to the elevation of the unit in meters (m).

During JJA as shown in Figure 3.5 (c), the continental MCCs just found in several areas, among others; Central Kalimantan and northern Sumatra in small frequency. The MCCs more concentrated over the ocean with the greatest concentration are over the Indian

Ocean. MCC is never occurred in along of the Java Island until East Nusa Tenggara during JJA. There are five concentration region of MCC events during SON as shown in Figure 3.5 (d). i.e., over the Indian Ocean, the South China Sea near northern Kalimantan, Central Kalimantan, Cendrawasih Bay and Merauke. The MCC with large size is still concentrated over the Indian Ocean, while small size concentrated over Kalimantan, especially central Kalimantan. Overall, the MCCs with large size more than 300,000 km² most frequently occurred over the Indian Ocean each season with the greatest frequency in SON season. The Central Kalimantan is one favored region for MCC occurrences each season, but most of the MCCs in this area have a small and medium size less than 300,000 km². MCCs rarely found along of the Java Island to the East Nusa Tenggara. Figure 3.4 also show the MCC most frequently occurs in region nearly equator around 2°S to 2°N. It is interesting to note that MCC possible related with ITCZ.

Comparison with Figure 2.19 about the averaged (2003-2006) CMORPH seasonal rainfall by Qian (2008), the pattern of rainfall intensity is almost similar to the pattern of MCC distribution in each season. The greatest frequency of the continental MCC is found over the Central Kalimantan in each season except in JJA, while the oceanic MCC over the Indian Ocean. It is almost similar pattern with a region that has the high intensity and greater fraction of rainfall. The boreal winter monsoon as shown in Figure 2.11 appears to influence the DJF distribution of MCC which get the impact of rainfall over northern Sumatera and West Kalimantan. It is similar with Laing and Fritsch (1993a) and Ismanto (2011) that stated MCC-related with the monsoon.

3.1.3 Monthly distribution of MCC occurrences

Variations in actual MCC totals per month as shown in Figure 3.6 (a) are reported with an obvious peak of MCC activity in April and November when more than 120 events occurred each month where the dominant of MCC that occurred in this month is the continental MCCs as shown in Figure 3.6 (b). The frequency of MCC occurrences in January, March, and May is also great with 107, 111 and 105 events, respectively. A total of 77, 66, 94 and 86 events occurred in February, June, October, and December, respectively. The fewer events found in July, August and September that has frequency 41, 45 and 40 events, respectively. Most of the fewer events are the oceanic MCCs as shown in Figure 3.6 (b).

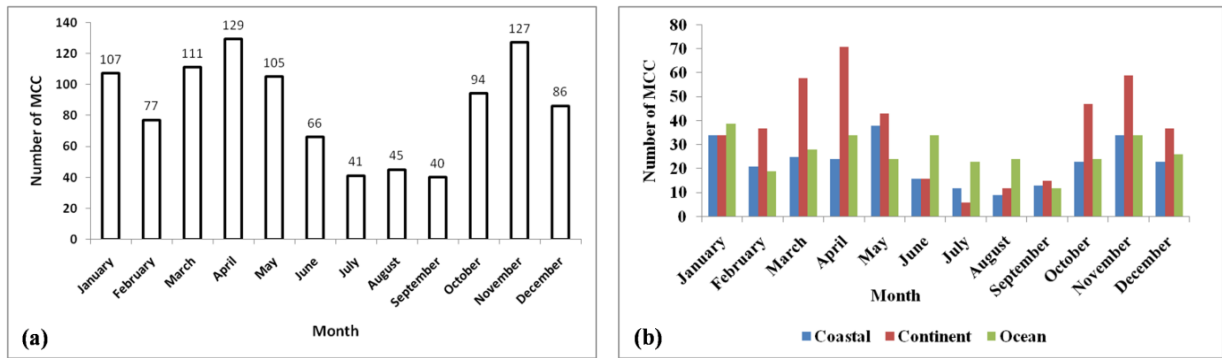


Figure 3.6. A total of MCC occurrences over the IMC during 15-years (2001-2015); (a) for each month, (b) for each season in coastal, continent and ocean.

Figure 3.7 show the monthly analysis of MCCs over the IMC during 15-years by plotting the location of the interior cloud centroid of MCCs for January until June. In January as shown in Figure 3.7 (a), the continental MCC are concentrated in the Central Kalimantan and Central Sulawesi but in small size less than 100,000 km². The MCCs with large size are predominantly the oceanic MCC that most frequently found in the Indian Ocean. The MCC with small size concentrated over the coastal of Merauke and the coastal of northern Kalimantan over the South China Sea. The frequency of MCCs over the Central Kalimantan during February as shown in Figure 3.7 (b), but MCCs became widespread until to western Kalimantan. MCCs also concentrated in Lampung, southern Sumatra, and several MCCs found in the coastal of North Sumatra. The frequency of MCC over the Indian Ocean and the other ocean decreased, just occur in a few events. During March as shown in Figure 3.7 (c), MCCs is just concentrated over the Central Kalimantan with the frequency of MCCs which greater than February, dominantly with small size. MCC also occurs in Sumatra, Sulawesi, and Papua but the small frequency. A few of large-sized MCC is found in the Indian Ocean.

The MCC with small size increased over the Central Kalimantan in April as shown in Figure 3.7 (d). Most of MCC are also located in along western of Sumatra Island. Most of them have medium size around 200,000 km². The MCC with medium size also occurs in the Indian Ocean near the coast of northern Sumatra. Several small-sized MCCs also found over Papua and Java Island. Most of the MCCs that occur in May as shown in Figure 3.7 (e) had a large size and located in the Indian Ocean. MCC rarely found over Sulawesi, Papua, and Java. In June as shown in Figure 3.7 (f), most of MCC concentrated over the ocean with the greatest frequency in the Indian Ocean. Only a few found the MCC on the continent, such as in the

Central Kalimantan and North Sumatra. Similar to May, MCC does not occur over Sulawesi, Java, and Papua.

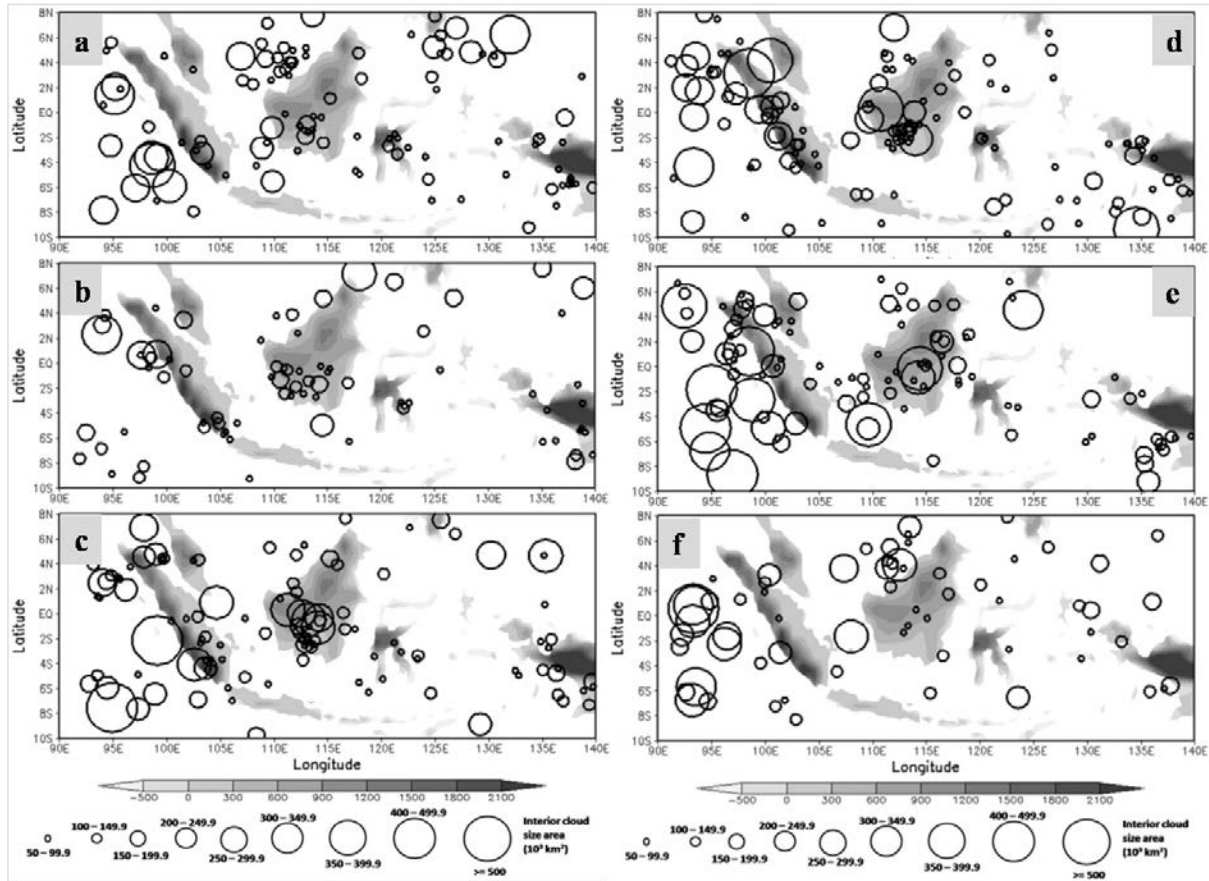


Figure 3.7. Geographical distribution of MCCs in Indonesian Maritime Continent during 15-years (2001-2015) for each month; (a) January, (b) February, (c) March, (d) April, (e) May and (f) June. Locations are for the MCC at the time of maximum extent of the interior cloud size area when the mature stage. The circles representing the interior cloud size area (10^3 km^2). The color shaded refers to the elevation of the unit in meters (m).

The frequency of MCC in July as shown in Figure 3.8 (a) was similar to June, where only found in the Indian Ocean in longitude $91^\circ - 97^\circ\text{E}$. The continental MCC is rare occur during this month. The frequency of the oceanic MCC with large size over the Indian Ocean increased in October and November as shown in Figure 3.8 (d) and (e), while in August is slightly same with July as shown in Figure 3.8 (b). However, this frequency decreased in September and December as shown in Figure 3.8 (c) and (f). In August and September, the frequency of the continental MCC is slightly same with July, only a few found in the large island of MCC. In fact, almost never occur along of the Java Island to East Nusa Tenggara. The frequency of the continental MCC over the Central Kalimantan increased in October and

November as shown in Figure 3.8 (d) and (e). However, this frequency decreased in August, September, and December as shown in Figure 3.8 (b), (c) and (f). The coastal MCC is more concentrated in coastal of Merauke from October until December. Overall, similar to seasonal, the MCCs with large size more than 300,000 km² are most frequently occurs over the Indian Ocean each month with the greatest frequency in October and November. It related with a mean of monthly rainfall as shown in Figure 2.20. Central Kalimantan is one favored region for MCC occurrences each month except June until September, but most of the MCCs in this area have a small and medium size less than 300,000 km². Along of Java Island to East Nusa Tenggara is the region that rarely found of MCC events.

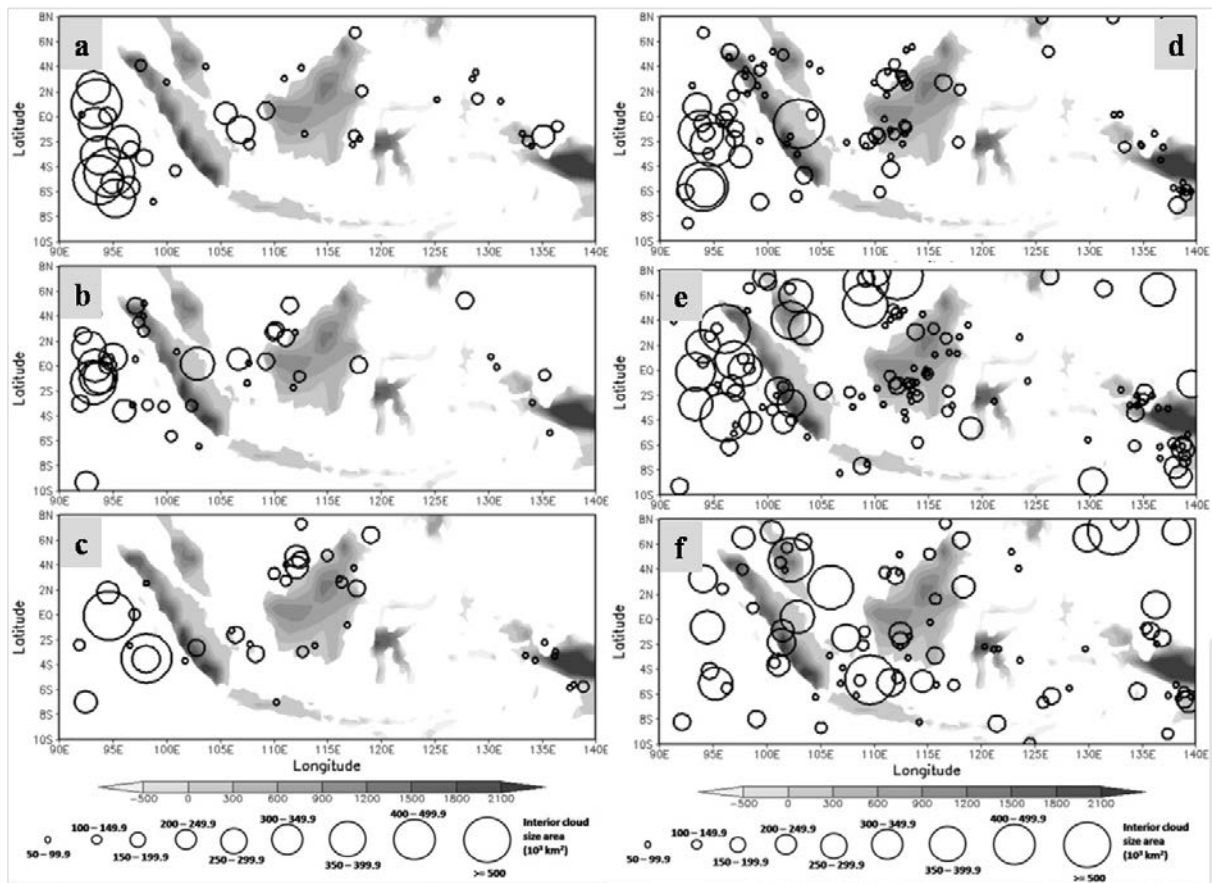


Figure 3.8. Same with Figure 3.7 but for; (a) July, (b) August, (c) September, (d) October, (e) November and (f) December. The color shaded refer to the elevation of the unit in meters (m).

3.1.4 Diurnal distribution of MCC occurrences

In the diurnal analysis, most of the continental MCCs reached maximum extent or mature stage in the midnight until morning from 20.00 - 0700 LT as shown in Figure 3.9 (f), (a) and (b). The greatest frequency of the continental MCC concentrated over the Central

Kalimantan. However, most of the continental MCC also found over western Sumatra, Merauke and near of Cendrawasih Bay. The continental MCCs are rare reached maximum extent in 0800 - 1600 LT. The oceanic MCCs are most frequent reach maximum extent in 0800 - 1100 LT as shown in Figure 3.9 (c). During the daytime at 1200 - 1500 LT and the evening at 1600 - 1900 LT, the frequency of MCC occurrences is most frequent concentrated over the Indian Ocean as shown in Figure 3.9 (d) and (e). MCCs are rare reached maximum extent at night in 2000 - 2300 LT.

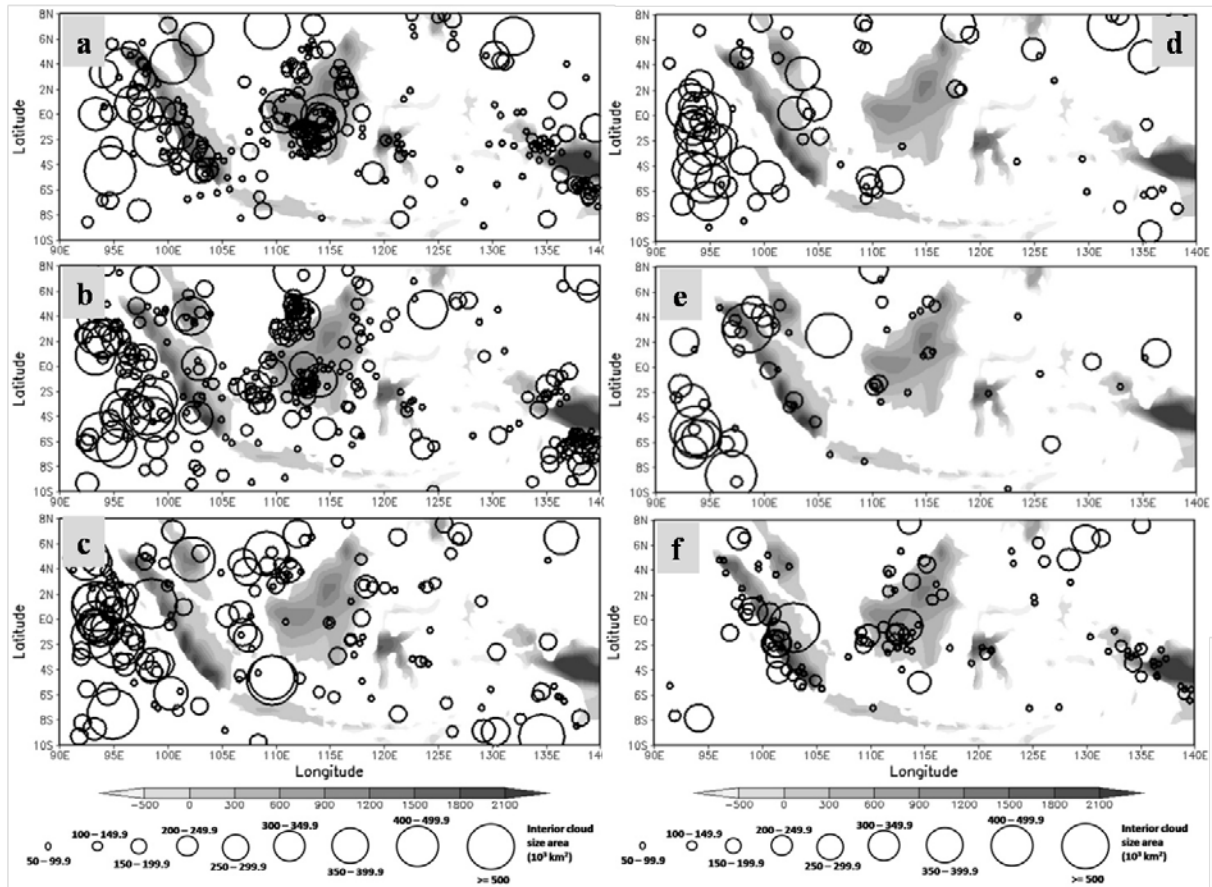


Figure 3.9. Diurnal distribution of MCCs in Indonesian Maritime Continent during 15-years (2001-2015); (a) 0000 - 0300 LT, (b) 0400 - 0700 LT, (c) 0800 - 1100 LT, (d) 1200 - 1500 LT, (e) 1600 - 1900 LT and (f) 2000 - 2300 LT. Locations are for the MCC at the time of maximum extent of the interior cloud size area when the mature stage. The circles representing the interior cloud size area (10^3 km^2).

Most of the previous study indicated that diurnal cycles of deep convection over land and sea show a distinct contrast. Convection over continents and large islands is most intense in late afternoon (around 19 LST). In contrast, convection over the seas near continents and

large islands is most intense in the morning (around 03 LST), diurnal cycle over continents and large islands are likely forced by strong surface heating during the day, whereas diurnal cycles over adjacent maritime areas arise from interactions between sea-land breeze circulations and large-scale environmental flows (Murakami 1983; Nitta and Sekine 1994). Comparison with the frequency distribution of MCC in this research, there is a gap time between oceanic MCC and diurnal variation of convective activity. The diurnal variation of convective activity over ocean reaches a maximum in the early morning around 0200 - 0500 LT, while the oceanic MCC reach a maximum around 0800 - 1100 LT. It indicated that there is a relationship between MCC with diurnal variation, possible MCCs development is triggered by diurnal variation of convective activity or otherwise. Similar with continental MCC, diurnal variation of convective activity over land reach a maximum in the late evening, while continental MCCs reach maximum extent in the midnight until early morning. It is also possible that the continental MCC development is generated by diurnal variation convective activity over land or otherwise.

The other previous researcher, Sui et al. (1997) found the average diurnal variation of rainfall from satellite infrared over an extensive tropical region that is in the central and eastern Pacific show the maximum value in the afternoon (mid-afternoon) and the second peak approaching dawn. They also stated that the strongest convection on the surface of the continent occurred towards evening or afternoon depending on the dominance of diurnal cycle of heating surface, except in areas where the difference between land and sea is very real or orographic very powerful force. On top of the ocean area that is free from the influence of the mainland, the coldest clouds and the maximum rainfall is often observed in the morning.

3.2 Morphological Characteristics of MCC

3.2.1 MCC maximum-extent distribution

The area size of cloud shield and an interior cloud of MCCs during the mature stage is shown in Figure 3.10. Most of the MCCs has cloud shield around $100 - 200 \times 10^3 \text{ km}^2$ in a total of 433 events as shown in Figure 3.10 (a) and interior cloud less than $200 \times 10^3 \text{ km}^2$ in a total of 834 systems as shown in Figure 3.10 (b). It indicated that most of the MCCs over the IMC included in the category of small-sized MCCs. However, the large-sized MCCs with cloud size area more than $600 \times 10^3 \text{ km}^2$ also occurs over the IMC. In fact, a total of 29 events

have cloud shield more than $1000 \times 10^3 \text{ km}^2$, and 20 events have interior cloud more than $500 \times 10^3 \text{ km}^2$.

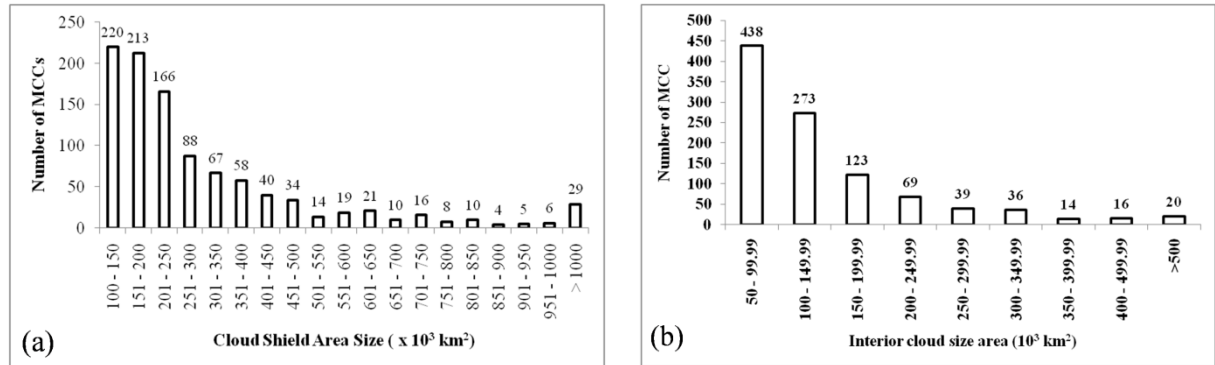


Figure 3.10. Frequency distribution of; a) MCC cloud shield maximum area and b) MCC interior cloud maximum area during 15-years.

The average of cloud shield area size of MCCs is around $315,000 \text{ km}^2$. It is slightly less than with global MCC by Laing and Fritsch (1997) that stated the mean cloud-top area for the global population is $354,000 \text{ km}^2$. However, the MCCs in IMC is more than from MCC in the western Pacific region that has the greatest frequency of MCC between $2 \times 10^5 \text{ km}^2$ until $3 \times 10^5 \text{ km}^2$ as reported by Miller and Fritsch (1991). This MCC is also more than with MCC over subtropical South America that has cloud size area $256,500 \text{ km}^2$ (Durkee and Mote 2009). Although some MCCs produce cold cloud shields that extend over a million km^2 , the size, and duration of MCSs and MCCs are positively correlated, i.e., larger systems tend to last longer (Tollerud et al. 1992, Laurent 1996, and Laing and Fritsch 1997).

Figure 3.11 (a) show the largest MCC with the greatest interior cloud more than $1000 \times 10^3 \text{ km}^2$ occurred in April. The largest MCC also occurs in March, July, September, and November with interior cloud size area more than $600 \times 10^3 \text{ km}^2$. Moreover, most of the MCC with medium size around $200 \times 10^3 \text{ km}^2$ occurred in July. The MCC with small size most frequently occurred in the continent, in contrast, the MCC with the medium and large size are most concentrated over the ocean as shown in Figure 3.11 (b). The average of cloud shield size area of MCC over ocean, continent and coastal are $387,865 \text{ km}^2$, $275,880 \text{ km}^2$ and $293,054 \text{ km}^2$, respectively. While the average of interior cloud size area of MCC over ocean, continent and coastal are $188,590 \text{ km}^2$, $122,550 \text{ km}^2$ and $135,720 \text{ km}^2$, respectively.

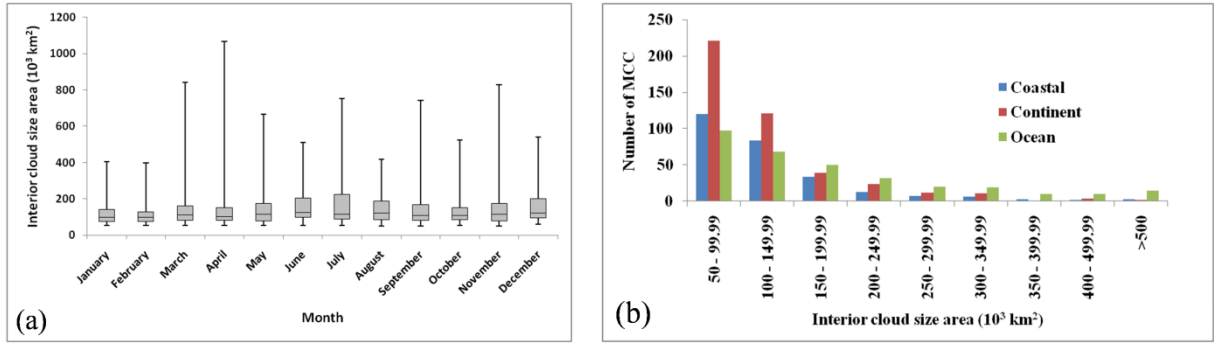


Figure 3.11. (a) Box and Whisker plot of interior cloud size area of MCC frequency by month during 15-years. (b) Frequency distribution of the MCCs interior cloud maximum area each month during 15-years.

3.2.2 MCC eccentricity at the time of maximum extent

Most climatologies of MCSs concern MCCs, and hence make use of a measure of cloud-shield shape with calculating eccentricity. The eccentricity is very important to distinguish MCC with the other type of MCS. Figure 3.12 displays the distribution of eccentricity at the time of maximum extent during mature stage. The eccentricity defined as the ratio of the minor axis to the major axis of the MCC best-fitting ellipse at the time of maximum extent.

This research found that average of eccentricity for all of the MCCs over the IMC are 0.85, with eccentricity averaged for continental, oceanic and coastal MCC are 0.84, 0.85 and 0.86, respectively. It indicated that majority of MCCs over the IMC are more circular which similar to MCCs over the USA (Augustine and Howard 1989). In general, most of the MCCs has eccentricity between 0.91 - 0.94 and between 0.76 - 0.79, most of them occurred over the ocean as shown in Figure 3.12. Most of the MCCs with large eccentricity more than 0.82 found over the ocean, while the majority of the small eccentricity occurred in the coastal region. This research just identifies MCC with eccentricity between 0.70 - 0.99, because of the eccentricity more than 1.0 tend to as a hurricane (Whitehall 2014).

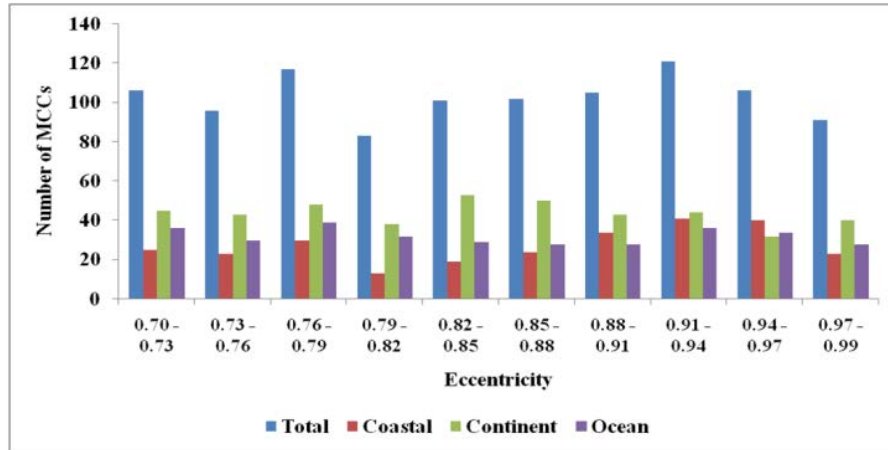


Figure 3.12. Number of MCC eccentricity at the time of maximum extent during 15-years (2001-2015).

3.3 Duration and life-cycle of MCC

3.3.1 MCC duration

In this research, we define the MCC duration as the duration between the time of initial stage and the time of dissipation stage. The frequency of distribution of the duration of all MCC systems is shown in Figure 3.13 (a). The average duration was approximate ~9.5 hours, and the maximum duration is 10 hours. The distribution and average duration are very similar to the distribution and average for MCCs in the southern Africa (~9.5 h; Blamey and Reason, 2012). However, it is slightly shorter than the global average (~10 h; Laing and Fritsch, 1997) and much less than those found in subtropical South America (14 h; Durkee and Mote, 2009). Most of the MCCs around 686 events occurred during 8 - 12 hours as shown in Figure 3.13 (a). Only 20 events are the long-lived MCCs that occurred during more than 20 hours. A total of 57 events indicated as the short-lived MCCs that has duration only 6 - 7 hours. The long-lived MCCs occurred in March, May, July, September and November as shown in Figure 3.13 (b). Most of the short-lived MCCs occurred in March-May, July, September, and December.

Figure 3.14 shows the comparison of the duration time of MCC that occurred in the continents, coastal, and the oceans. Most of the MCCs with duration around 8 - 10 hours occurred over the continent. The long-lived MCCs are most frequent concentrated in the ocean, while the short-lived MCCs are most frequent found in the continent. Most of the coastal MCCs have duration around 8 -13 hours. This result similar with the global MCCs by Laing and Fritsch (1997), where they stated that the oceanic MCCs have been found to be

slightly larger and last longer than the continental MCCs. The averaged duration of the coastal, continental and oceanic MCCs was approximate ~11.5 hours, ~10 hours and ~12.5 hours, respectively. However, this averaged duration less than average for oceanic MCCs in the southern Africa (~14 h; Blamey and Reason, 2012).

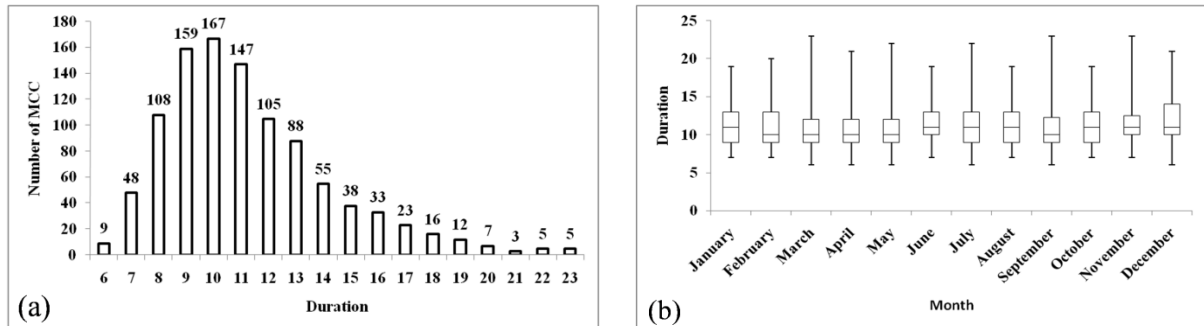


Figure 3.13. (a) Frequency distribution of duration of MCCs over the IMC during 15-years. (b) Box and Whisker plot of the duration of MCC frequency during 15-years.

Figure 3.15 (a) shows that there is not a relation between the duration with MCC locations due to the correlation is slight ($r = 0.01$). Figure 3.15 (c) show that the MCC locations are not related to a maximum area of MCCs (correlation coefficient $r = 0.06$).

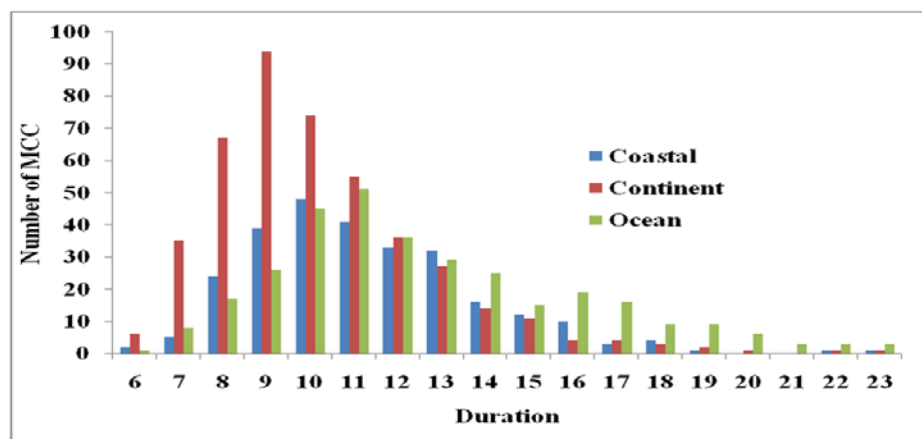


Figure 3.14. Frequency distribution of duration time of MCCs over the coastal, ocean, and continent during 15-years.

Figure 3.15 (b) indicate that there are a tendency for relation the duration and maximum area of MCCs over the IMC that has positively correlated (correlation coefficient $r = 0.58$). It indicates that systems which generated large cold-cloud shields tend to persist

longer than those which produce small shields. This result similar with global MCC population by Laing and Fritsch (1997) that stated there are relation the duration with the maximum area in the global population of MCCs that has correlation coefficient $r = 0.385$). Tollerud et al. (1992) also found a similar relationship, although the relationship is weak. This result also very similar with Durkee and Mote (2009) that stated MCC maximum size and duration of subtropical South America exhibited a significant relationship with correlation coefficient $r = 0.56$.

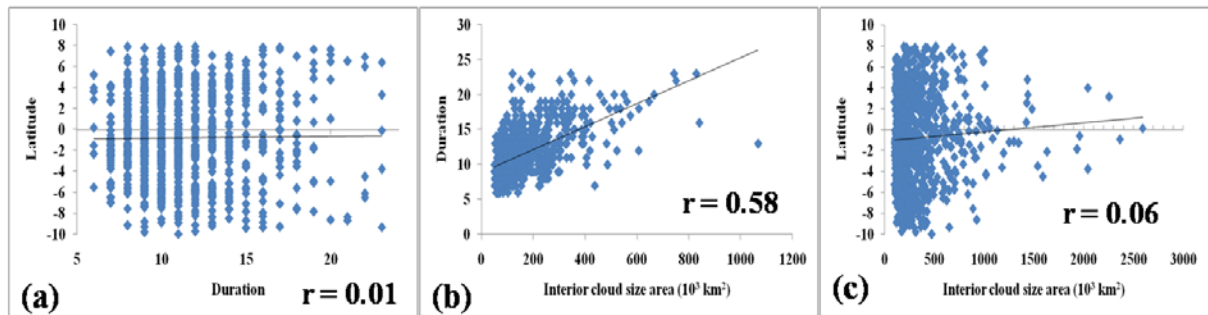


Figure 3.15. Scatter plots showing relationship; (a) between latitude and duration, (b) between duration and interior cloud size and (c) between latitude and interior cloud size. Latitude, duration and interior cloud size at the time of maximum extent or mature stage. Correlation coefficient r is shown for each case.

3.3.2 MCC life-cycle

Figure 3.16 shows that in general, the MCCs in IMC usually develops in the late afternoon and by around sunset in a few times before the initial stage. The greatest frequency of occurrences for initiation occurred between 1900 – 2200 LT. The systems reached the maximum size extent after midnight or early morning in predominantly between 0100 - 0500 LT and then MCC start to decayed in the morning a few hours after sunrise, predominantly around 0700 - 0900 LT. The systems dissipated from the daytime until the afternoon, around 1000 - 1500 LT. It indicated that characteristics of life cycle of the MCCs tends to nocturnal characteristics. This result similar with the previous studies that documented regional populations of MCCs were found to be nocturnal, among others; MCC in the Americas and the Western Pacific region, southern Africa (Maddox 1980; Velasco and Fritsch 1987; Miller and Fritsch 1991; Durkee and Mote 2009; Blamey and Reason 2012). It follows that global population is also predominantly nocturnal (Laing and Fritsch 1997).

It also strengthened by Sui et al. (1997) who stated that convective activity in the tropics has three variations. Using the results of observations COARE TOGA (Tropical Ocean Global Atmosphere Coupled Ocean- Atmosphere Response Experiment), acquired three diurnal variations of atmospheric convective activity in the tropics. The three variation, i.e., warm cumulus morning, afternoon convective showers, and nocturnal convective systems. Rainfall afternoons particularly true for convective cells, but nocturnal rainfall caused by cells deeper convective and stratiform clouds in a wide area. Further stated that convective precipitation afternoon (afternoon convective showers) are more apparent than in the period of large-scale undisturbed when the diurnal cycle of sea surface temperature occur strongly. However, the nocturnal convective system (nocturnal convective systems) and cumulus morning (warm morning cumulus) higher in the period disrupted when more moisture is available (Sui et al. 1997).

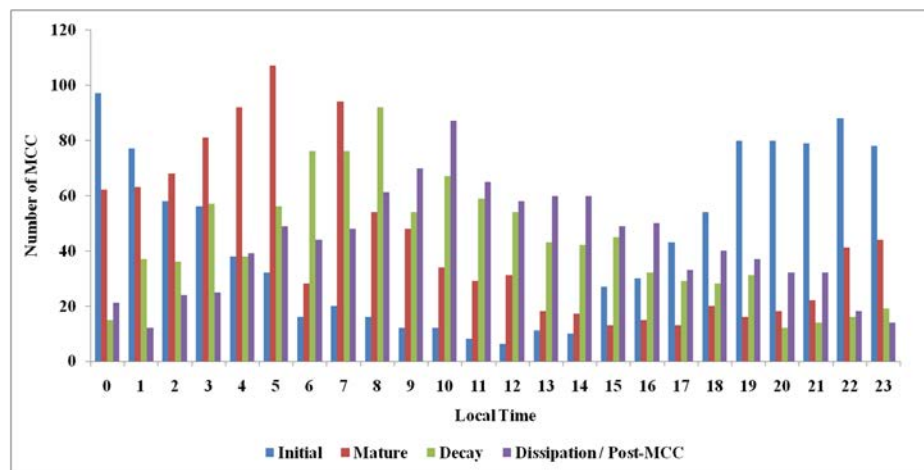


Figure 3.16. Frequency distribution of all MCCs during critical stage (initial, mature, decay and dissipation or post-MCC stage).

The comparison between the coastal, continental and oceanic MCCs is shown in Figure 3.17. The coastal MCC is usually started in the night to midnight around 1900 - 0000 LT and reached maximum size in the early morning around 0300 - 0700 LT. This system decayed in the morning, several hours after maximum extent, and then dissipated in the afternoon. Similar with the coastal MCC, the continental MCC also started in the night, but later in the afternoon. The maximum size of the continental MCCs is also predominantly in the early morning, but later than coastal around 0000 - 0400 LT. This system decayed and

dissipated in the morning and daytime, respectively. While the greatest frequency of oceanic MCC occurrences for initiation, mature, decay and dissipation/post-MCC between 0000 - 0400 LT, 0400 - 0700 LT, 1000 - 1200 LT and 1400 -1800 LT, respectively. It indicated that most of the oceanic MCCs end much later in the morning than the continental MCCs. It is similar with Blamey and Reason (2012). This result strengthens the analysis of Figure 3.9.

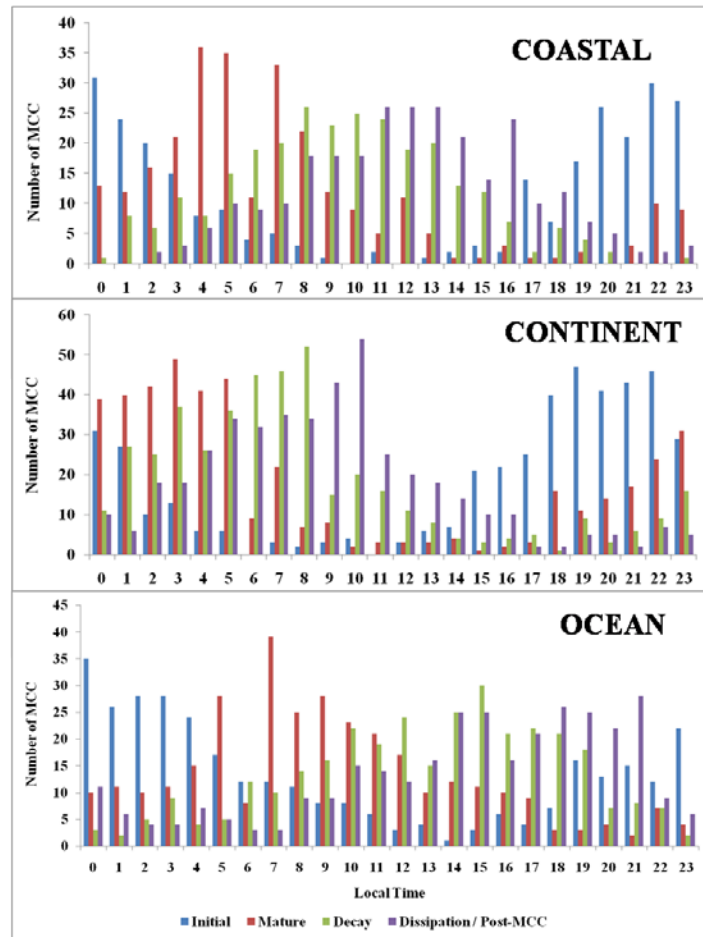


Figure 3.17. Frequency distribution of the coastal, continent and oceanic MCCs during critical stage (initial, mature, decay and dissipation or post-MCC stage).

CHAPTER FOUR

THE EVOLUTION AND PROPAGATION OF THE MESOSCALE CONVECTIVE COMPLEXES (MCCs) OVER INDONESIAN MARITIME CONTINENT

This chapter to explained the structure and mechanism of the evolution and the propagation of the MCC in the IMC with taking some of the case study of MCCs in the ocean, coastal and continent. The evolution process of MCCs is analyzed each stage based on MCC stages which defined by Cotton et al. 1989 using spatial analysis of T_{BB} . The relationship MCC to rainfall systems and convective activity is also analyzed by using spatial analysis of the evolution of rainfall system and convective index during MCC events. To explained the similarities and consistency of the evolution and propagation of the MCCs in the case study and the other several regions over IMC in this research were utilized composite analysis that adapted from the method of McAnelly and Cotton 1986 and 1989. The detailed of the method has been explained in subchapter 1.4.2.2. The result of this chapter will answer clearly the research objective about the mechanism of the development and the movement of the MCC in influencing rainfall over the IMC.

4.1 Evolution of the development of the MCC

4.1.1 MCC composite region

Chapter 3 have reported that the MCCs occurrences over the IMC during 15-years for the 2001–2015 period is a number of 1028 events. In this chapter study, six regions were selectively chosen for composite analysis based on the concentrated regions as the location of many MCC occurrences and then will be mentioned as MCC composite regions as shown in the red box (Figure 4.1 (a)). Region 1 in the coastal of the northwestern of the North Sumatra in between of longitude 93° - 100° E and latitude 1° S - 4° N. Region 2 in the Indian Ocean near of the Sumatra in between longitude 95° - 102° E and latitude 4° S - 1° N. Region 3 in the Central Kalimantan in between longitude 111° - 115° E and latitude 4° S - 1° N. Region 4 in the South China Sea near Sarawak or the northern part of the Borneo/Kalimantan Island in between longitude 109° - 115° E and latitude 2° - 6° N. Region 5 in the coastal in between Sulawesi and Kalimantan in between longitude 116° - 120° E and latitude 3° S - 0° N. Region 6 in Merauke over Papua Island in location around of 8° - 5° S and 135.5° - 140° E.

Figure 4.1 (b) illustrates the stratification of the MCC composite region 3. The timing of the T_{BB} life cycle characteristics indicated along an hourly time axis for each MCC. In the composite category, the 45-cases of MCCs in region 3 considered to have common composite times of initiation, mature, decay and dissipation. Besides the similarities in genesis region, maximum area and mature duration, the MCCs in each category were reasonably consistent in term of other T_{BB} characteristics. These include; the duration of initiation to mature stage, mature to decay and decay to dissipation or post-MCC stage. The composite for initiation, mature, decay and dissipation determined by the average the hour of initiation, mature, decay and dissipation for each MCC, or around to the nearest hour. In the first, we determined the average the hour of the initiation of all case in each region, and then plus 1, 2 or 3 hours until reaches the average the hour of mature, the same way until reaches the average the hours of dissipation or post-MCC. So that, the average from initial-to-maximum, maximum-to-dissipation with 1, 2, or 3 duration time. The resulting example of the composite time for MCC in region 3 is the initiation at 1900 LT, the mature stage at 0100 LT in the next day and MCC dissipated at 0900 LT. Nearly 110 MCC were found in the region 3 and its surrounding areas, but in this study just taken 45 cases of MCC which has a duration time for the life cycle of almost the same range and nearly same the center of the MCCs. Based on the same way, we also did this for the other region.

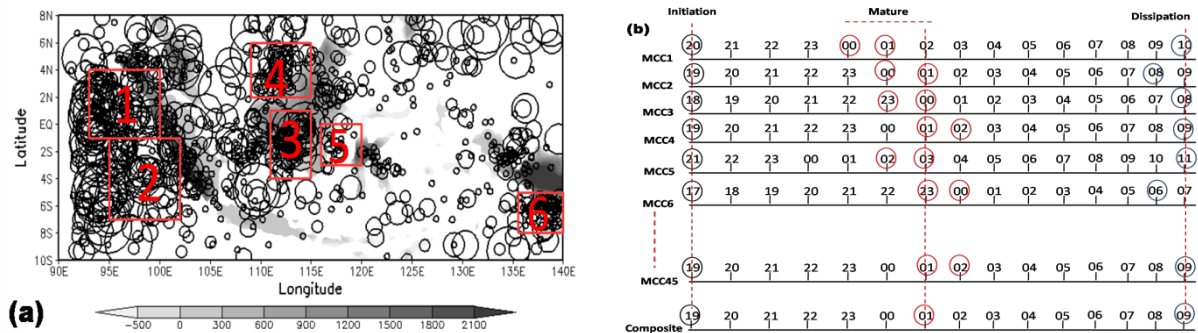
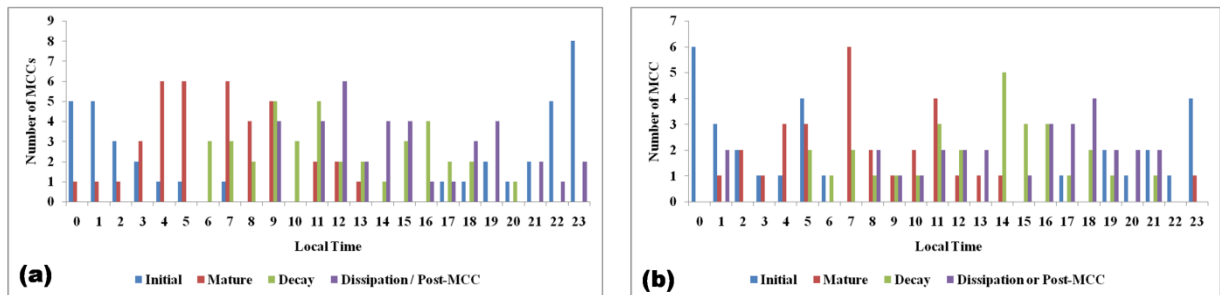


Figure 4.1. (a) same with Figure 3.1 but the red box show the MCC composite region with number label 1, 2, 3, 4, 5 and 6 as region 1, region 2, region 3, region 4, region 5 and region 6, respectively. (b) Illustrated of the stratification of the MCC composite region 3. The time shows in LT.

The surface wind from CCMP data which available at 6-hourly is utilized to analyzing the propagation of MCC. The composite analysis for the propagation of MCC determined by the average of hours the critical stage just for the time at 0000 UTC, 0600 UTC, 1200 UTC, and 1800 UTC due to the data available in 6-hourly. However, in this study, we consider the

data on time in 2300, 0000 and 0100 UTC as the time on 0000 UTC, and the data on time in 0500, 0600 and 0700 UTC as the time on 0600 UTC. We also consider the data on time in 1100, 1200 and 1300 UTC as the time on 1200 UTC, and the data on time in 1700, 1800 and 1900 UTC as the time on 1800 UTC. So that, we did composite analysis just for the hours of initiation, mature, decay and dissipation or post-MCC at the time as mentioned above in each region. For example, from 45-case of MCC composite region 3, but we just take 24-case during the initial stage that occurs in the time available data, 28-case during the mature stage, 34-case during the decay stage and 22-case during the dissipation or post-MCC stage.

The comparison of the life cycle of each composite region is shown in Figure 4.2. The MCC composite region 1 as illustrated in Figure 4.2 (a) is usually started in the night to midnight around 1900 - 0000 LT and reached maximum size in the early morning around 0400 - 0700 LT. MCC composite region 1 decayed in the morning, several hours after maximum extent, and then dissipated in the daytime until noon. Almost similar to the region 1, Figure 4.2 (b) shows the MCC composite region 2 that started in the midnight and reached maximum size in the morning. MCCs decayed and dissipated in the daytime and afternoon, respectively. Figure 4.2 (c) shows that MCC composite region 3 began to developed in the afternoon and reached a maximum extent in the midnight. The MCC composite region 3 decayed in the morning and several next hours dissipated. Most of the MCC composite region 4 as shown in Figure 4.2 (d) is usually started develops in the afternoon and reached a maximum extent in the morning, and then decayed in several hours after the mature stage. The MCC composite region 4 dissipated in the noon. The greatest frequency of the MCC composite region 5 as shown in Figure 4.2 (e) for initiation, mature, decay and dissipation/post-MCC between 1800 - 2100 LT, 0700 - 0900 LT, 1100 - 1300 LT and 1400 - 1600 LT, respectively. The MCC composite region 6 as shown in Figure 4.2 (f) is nearly similar to the MCC composite region 3.



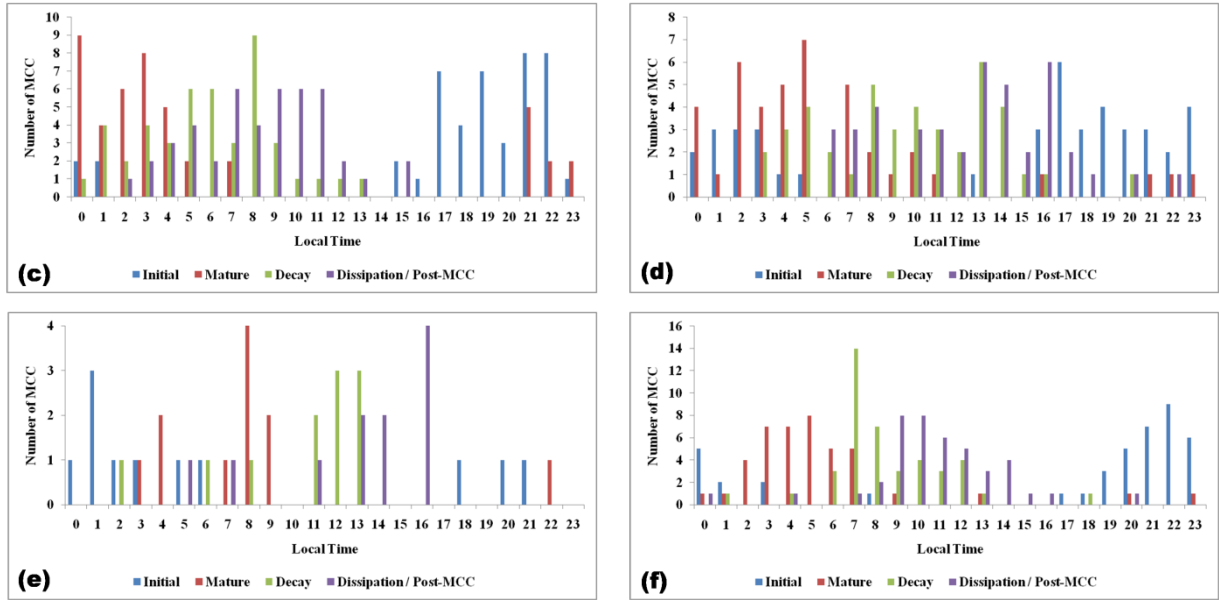


Figure 4.2. Frequency distribution of the initiation, mature, decay, and dissipation or post-MCC time of the MCC in each region. where; (a) region 1, (b) region 2, (c) region 3, (d) region 4, (e) region 5, (f) region 6.

The number of MCC occurrences in the region 1, 2, 3, 4, 5, and 6 are 38-case, 29 case, 45-case, 42-case, 11-case and 42-case, respectively. The MCC composite region 2 is largest than the other region with averaged interior cloud and cloud shield around 269,111 km² and 608,693 km², respectively. The MCC composite region 1 has averaged interior cloud and cloud shield around 220,346 km² and 496,468 km². MCCs in region 3 have averaged interior cloud and cloud shield around 138,637 km² and 324,327 km². MCCs in region 4 have averaged interior cloud and cloud shield around 133,345 km² and 243,417 km². MCCs in region 5 have averaged interior cloud and cloud shield around 91,615 km² and 168,285 km². MCCs in region 6 have averaged interior cloud and cloud shield around 117,560 km² and 212,831 km². The MCC composite region 2 is also longest than the others that have averaged duration around 15 hours. The other MCC composite region has averaged duration around 14 hours (region 1), 13 hours (region 3), 12 hours (region 4), 10 hours (region 5) and 11 hours (region 6).

4.1.2 The oceanic MCC

The first case study in this research is the oceanic MCC as shown in Figure 4.3. The MCC develops from midnight on 27 October 2007 until the early morning of 28 October 2007 over the Indian Ocean near Sumatra Island. The MCC had a cloud shield with an area of around 319,083 km², and the interior cold cloud covered an area of around 211,059 km². The

center of the MCC was around 3.21°S, 97.46°E with an eccentricity of around 0.76 and life cycle duration around 16 hours. Cotton et al. (1989) have defined eight stages in the life cycle of an MCC: MCC-12 h, pre-MCC, initial, growth, mature, decay, dissipation, and post-MCC; however, the most important period for an MCC is from the initial to the dissipation stage. The MCC-12 h stage defines the condition of the MCC around 10–15 hours before the initial stage, as shown in Figure 4.3 (a). Also, the MCC developed under a large-scale environmental situation in which the MJO index (Wheeler and Hendon 2004) was positive, but its amplitude was very weak. The MCC began to develop from the pre-MCC stage at 2200 LT on 27 October 2007. At that time, small-scale clouds were located on the western coast of Sumatra and the nearby Indian Ocean, as shown in Figure 4.3 (b).

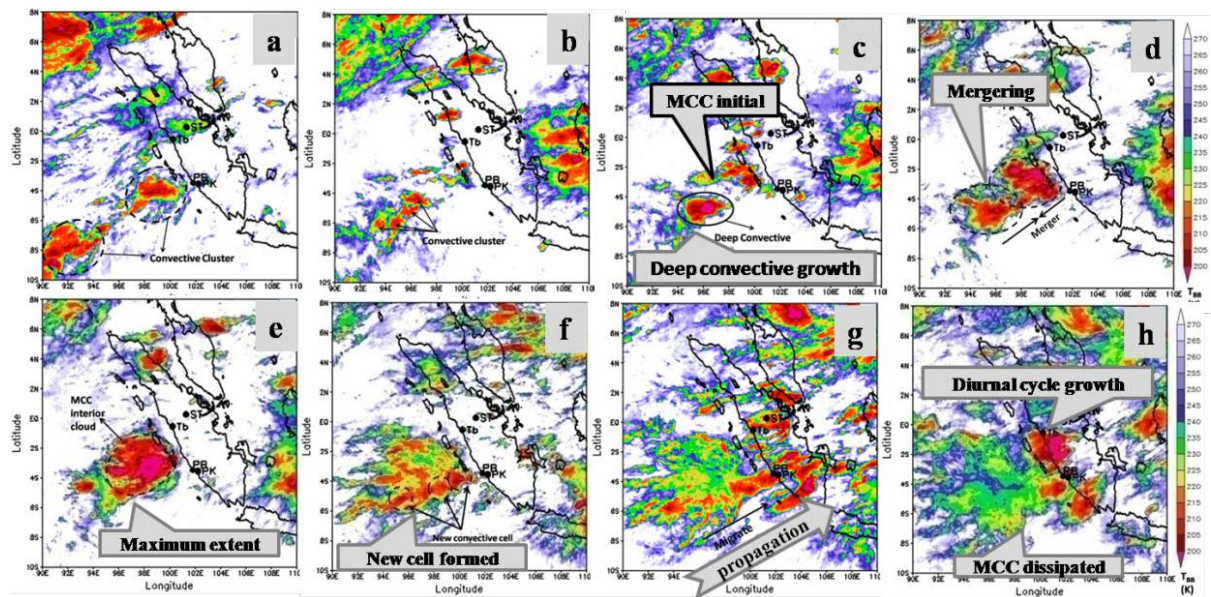


Figure 4.3. Horizontal distribution of T_{BB} for MCC criteria from infrared data obtained by MTSAT-1R over the Indian Ocean near Sumatra on 27–28 October 2007, showing the eight stages of MCC evolution: (a) MCC-12h stage (1000 local time (LT)), 27 October 2007; (b) pre-MCC stage (2200 LT), 27 October 2007; (c) initial stage (0100 LT), 28 October 2007; (d) growth stage (0400 LT), 28 October 2007; (e) mature stage (0700 LT), 28 October 2007; (f) decay stage (1300 LT), 28 October 2007; (g) dissipation stage (1600 LT), 28 October 2007; (h) post-MCC stage (1900 LT), 28 October 2007. The color indicates T_{BB} with unit Kelvin. Tb, ST, PB and PK are respectively Tabing, Simpang-tiga, Pulau Baai and Padang Kemiling shows the location of weather stations.

These groups of clouds grew rapidly until around midnight (0100 LT), which marked the onset of the initial stage (Figure 4.3 (c)). During the initial stage, deep convective seem over the Indian Ocean and several small clouds in the western coastal of Sumatra. By 0400 LT on 28 October 2007 (Figure 4.3 (d)), during the growth stage of the MCC, the sizes of the

deep convective and small clouds had increased further, and they began merging with each other, such that the maximum extent of the MCC was attained at 0700 LT (Figure 4.3 (e)). During the mature stage, the MCC had a cloud shield with an area of around 319,083 km², and the interior cold cloud covered an area of around 211,059 km². At 1300 LT, during the decay stage, the MCC began to split and dissipated (Figure 4.3 (f)). During the dissipation stage in the late afternoon (1600 LT) (Figure 4.3 (g)) and by the post-MCC stage later that evening (1900 LT) (Figure 4.3 (h)), the MCC had split into small-scale clouds that propagated eastward toward the western coast of Sumatra.

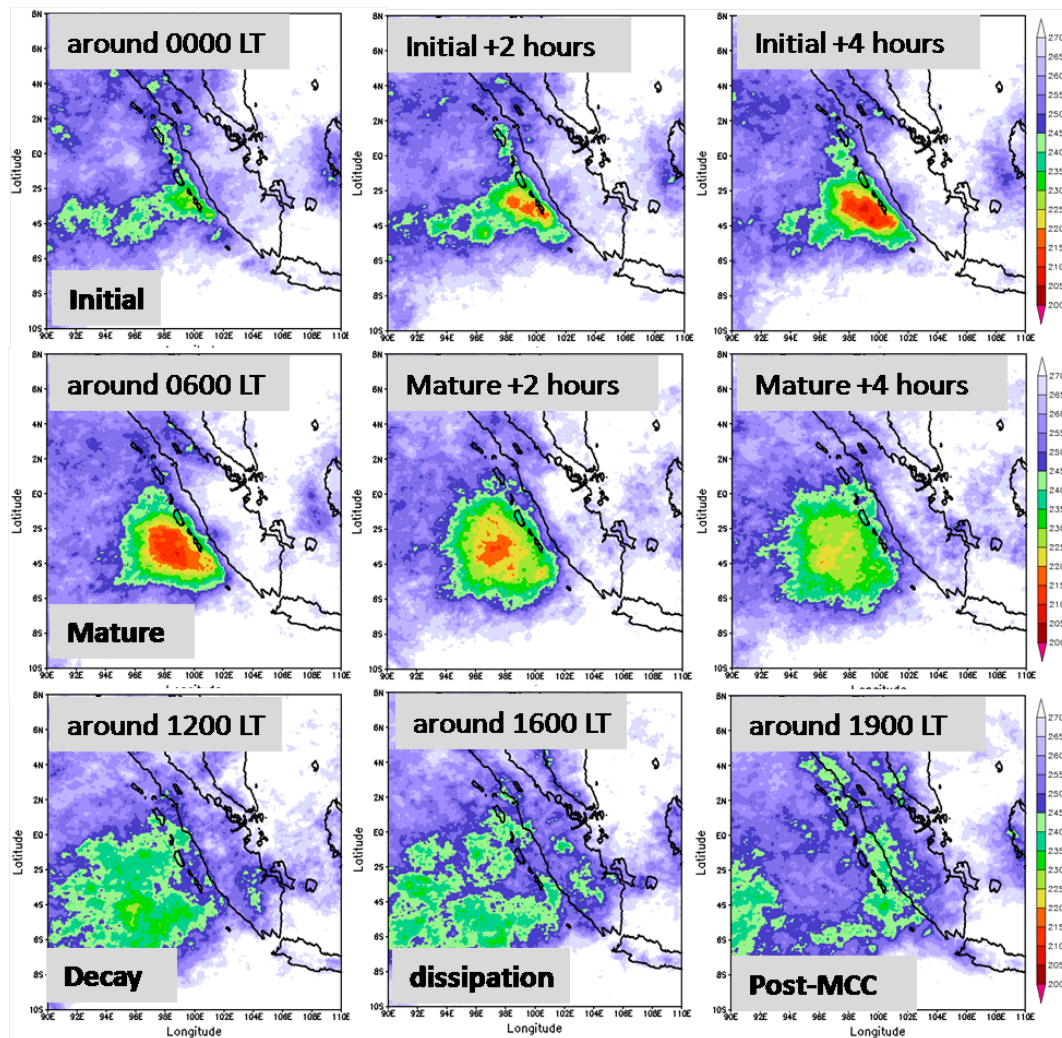


Figure 4.4. Horizontal distribution of composite of the T_{BB} for 29-case of MCC composite region 3 over the nearly same area with the case study 1. The time illustrates the average timing of the hours of initiation, mature, decay and dissipation for the 29-case composite in region 2 in term of the normalized life cycle using composite analysis. Unit for T_{BB} is Kelvin.

The MCC composite region 2 is located in nearly similar region with case study 1. The composite analysis shows that the MCC in the region 2 is triggered by the cloud from the

west and the coastal of the Sumatra in the averaged time of the initial stage around the midnight 0100 LT as shown in Figure 4.4. The sizes of the clouds had increased further, and they began merging with each other until reaches maximum size in around the morning. After around six hours from the mature stage, the MCC decayed and then dissipated in the afternoon. During the MCC dissipated, seem the cloud migrate to the west and predominantly to the east toward over the Sumatra. This evolution indicates that the 29-case of MCC composite region 2 have the similar development characteristics like the case study 1. It also strengthens the analysis of the MCC in the case study 1 where the MCC that occur over the Indian Ocean near of the Sumatra have the impact to the convective activity and rainfall over the Sumatra.

Many studies have reported the development of the convective activities over Sumatra Island. Renggono et al. (2001) showed that diurnal variations of convective activities are prominent in the mountainous area in Sumatera. They showed that convective clouds tend to develop from 1300 LT to 2100 LT and that after the decay of convective clouds, stratiform clouds develop until early morning (0600 LT). From observations by GPS-derived precipitable water, radiosondes, and surface weather station, Wu et al. (2003) showed that a rainfall events often occurs as intensive showers during a short period in the late afternoon and early evening at the mountainous area of Sumatera, and suggested that the evaporation of water from the surface by the strong solar heating and horizontal transport of water vapor by thermally induced local circulation play an important role in diurnal variations of convective activities. Mori et al. (2004) showed time and spatial variations of rainfall around the west coast of Sumatera by using data observed by TRMM satellite Precipitation Radar. They showed that the peak of rainfall in the daytime and nighttime migrate with time, starting from the southwestern coastline of Sumatera into the inland and offshore regions, respectively. They also used rawinsonde sounding data at two stations (coastline and mountainous area of Sumatera, respectively) and showed that diurnal variations of the wind, humidity, and stability in the lower troposphere agree well with the migration of rainfall peaks over both the inland and the coastal sea regions. The evolution of the MCCs over the Indian Ocean near Sumatra Island related with diurnal variation of convective activities over Sumatra. The MCCs began to develop triggered by the diurnal variation over the western Sumatra in the evening until midnight. However, the new convective system after MCCs dissipated trigger the development of the diurnal variation of convective activities over western Sumatra in the daytime until noon.

4.1.3 The continental MCC

The second case study in this research is the continental MCC as shown in Figure 4.5. The MCC occurred on 14 – 15 April 2012 in transition seasons (MAM). The center of the MCC located in latitude 2.132°S and longitude 112.425°E over the central Kalimantan. The MCC had a cloud shield with an area of around $228,201 \text{ km}^2$, and the interior cold cloud covered an area of around $133,313 \text{ km}^2$. The duration time of the life cycle of MCC around of 13 hours. The eccentricity of MCC is 0.703. This MCC reach maximum size in the midnight at 2300 LT. The phenomenon is that MCC develop in near of mountainous area in the afternoon until morning.

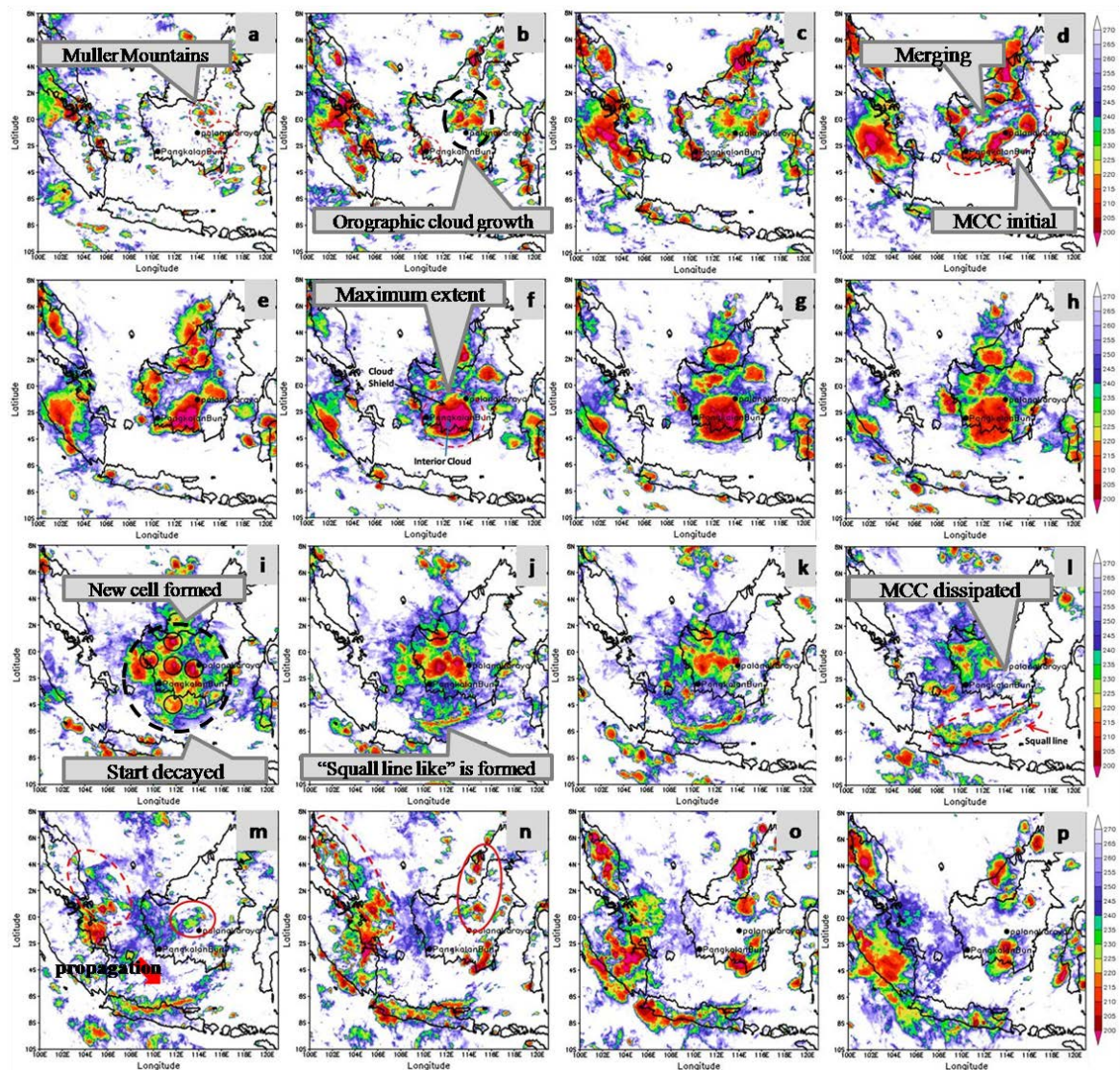


Figure 4.5. Horizontal distribution of T_{BB} for MCC criteria from infrared data obtained by MTSAT-1R over Kalimantan Island on 14-15 April 2012, showing the eight stages of MCC evolution: (a) MCC-12h or first storm stage (1300 LT), 14 April 2012; ((b),(c)) pre-MCC

stage (1500 LT to 1700 LT), 14 April 2012; (d) initial stage (1900 LT), 14 April 2012; (e) growth stage (2100 LT), 14 April 2012; ((f),(g),(h)) mature stage (2300 LT, 0000 LT, 0100 LT), 14 April 2012; ((i),(j) and (k)) decay stage (0300 LT, 0500 LT and 0700 LT), 15 April 2012; (l) dissipation stage (0900 LT), 15 April 2012; (m) post-MCC stage (1300 LT) 15 April 2012; ((n),(o) and (p)), A few hours after MCC occur (1500 LT, 1700 LT and 1900 LT), 15 April 2012. Unit for T_{BB} is Kelvin.

The MCC developments in this case generated with a diurnal cycle of the cloud system over the mountains over Muller mountains at 1300 LT as shown in Figure 4.5 (a). From 1500 - 1700 LT, this cloud continues to grow to form orographic clouds as shown in Figure 4.5 (b) and (c). Figure 4.5 (c) also show there is the other cloud development that appears in the western Kalimantan near the Central Kalimantan. At the evening (1900 LT) as shown in Figure 4.5 (d), the initial MCC was generated in the Central Kalimantan is triggered by merging of the orographic cloud that migrated southward toward to the MCC area with the other group of the cloud that grew in near the MCC area. It is different with the oceanic MCC that start develops in the midnight.

At 2100 LT, during the growth stage (Figure 4.5 (e)), this merger cloud expanded southward became grew with the larger size until reaches maximum extent or MCC mature stage in the midnight (2300 LT), as described in Figure 4.5 (f). At 0000 - 0100 LT, during the mature stage, as shown in Figure 4.5 (g) and (h), the size of the interior cloud decreased, while the size of cloud shield increased. This MCC is start decayed in the morning around 0300 - 0700 LT as shown in Figure 4.5 (i), (j) and (k). During decay stage, the new convective system was generated in the surrounding of the MCC area, especially the northern side of the MCC system as shown in the black circle in Figure 4.5 (i). In fact, the "squall line like" appear on the southern side of the MCC system as shown in Figure 4.5 (j). The MCC dissipated in the morning at 0700 - 0900 LT as shown in Figure 4.5 (l). During the dissipation stage, the new convective systems migrated to Sumatra and northern Kalimantan, while the squall line continues to grow and propagate southward to Java Island. A few hour after the MCC dissipated from daytime until afternoon (Figure 4.5 (m), (n), (o) and (p)), several cloud system appears over Java, eastern Sumatra, Malaysia and Brunei in northern Kalimantan. It indicated that the new convective systems and squall line induce the other cloud in it surrounding area during migration.

This case study is very interesting because the MCC had effect until to Java Island and Sumatra Island with inducing the other convective cloud in surrounding area so make the convective cloud developing and moving to the Java Island and Sumatra Island. The MCC in

this case also generates the squall line that is the other type of MCS. That squall line movement until to Java Island and generate some convective cloud over Java Island as shown Figure 4.5 (j) until Figure 4.5 (p). The MCC in this case study also affect to convective activity over Malaysia and Brunei as shown in Figure 4.5 (m) and (n) at red dotted circle to Malaysia and red circle to Brunei. It is indicated by the development of new convective systems from MCC that inducing the convective its surrounding area and then moves toward Malaysia and Brunei.

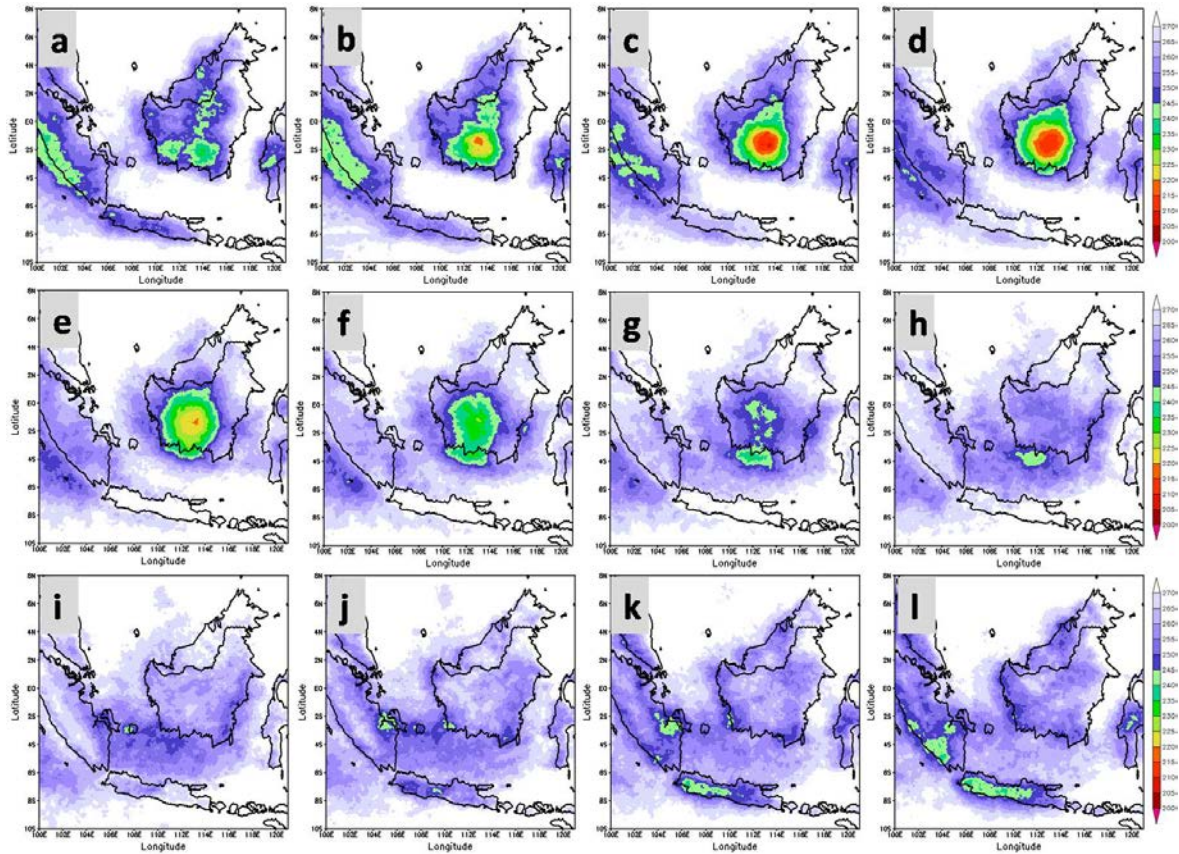


Figure 4.6. Horizontal distribution of composite of the T_{BB} for 45-case of the MCC composite region 3: (a), (b) Initial stage (around 1800 LT and 2000 LT)), (c),(d) mature stage (around 2300 LT to 0100 LT), (e),(f) decay stage (around 0400 LT and 0700 LT), (g),(h) dissipation stage (around 1000 LT and 1100 LT), (i) post-MCC stage (1400 LT) and (j), (k), (l) a few hours after post-MCC stage. The time illustrates the average timing of the hours of initiation, mature, decay and dissipation for the 45-case composite in region 3 in term of the normalized life cycle using composite analysis. Unit for T_{BB} is Kelvin.

The life cycle of the 45-cases of the MCC composite region 3 has been quantified by the composite analysis as shown in Figure 4.6. On average, the evolution of the development of the MCC composite region 3 began in the late afternoon at around 1900 LT. The MCC that

generated by the orographic clouds along the Iranian and Muller mountain is one of the contributors to the development of MCC as shown in Figure 4.6 (a) and (b). The system reaches the maximum size around four hours from the initiation. The mature stage of MCC occurs in midnight around 0100 LT as shown in Figure 4.6 (c) and (d). This system might be able to survive for four hours in maximum size, and will begin to decayed at around 0400 LT - 0700 LT as shown in Figure 4.6 (e) and (f). MCC became dissipated in the early morning at around 1000 LT - 1100 LT (Figure 4.6 (g) and (h)). However, interesting for the analyzed from this MCC development is the existence of convective clouds over the Java Island and southern Sumatra after a few hours of MCC dissipated, as shown in Figure 4.6 (i), (j), (k) and (l). The pattern of the development of the MCC composite in region 3 is similar to the case study 2. It indicates that the 45-case of MCC composite region 3 have the similar development characteristics like the case study 2. Also, it indicated the MCC that occurred in the Central Kalimantan have the impact to the convective activity and rainfall over the Java Island.

4.1.4 The coastal MCC

The third case study in this research is the coastal MCC as shown in Figure 4.7. The MCC occurred on 22 – 23 October 2011 in transition seasons (SON). The center of the MCC located in latitude 2.086°S and longitude 117.8°E in the coastal between Sulawesi and Kalimantan. The duration time of the life cycle of MCC around 13 hours and have interior cloud size around $105,807 \text{ km}^2$. The MCC in this case study is smaller and shorter than from the other case study. However, the eccentricity of MCC in this case study larger than the others is around 0.9. The MCC reached maximum size in the morning at 0600 LT. The MCC start develops from the small cloud in the western coast of Sulawesi which grew rapidly and then formed a cloud with the larger size as the initial stage of MCC from the evening to midnight as shown in Figure 4.7 (a), (b), (c) and (d). This cloud grew until reached maximum extent in the morning at 0600 LT as shown in Figure 4.7 (e) and (f). The new convective system began to appear during decay and dissipation stage at the daytime, at 1100 LT and 1300 LT, respectively as shown in Figure 4.7 (g) and (h). This case study is also interesting because of the impact of MCC until to Kalimantan Island. The bow echo like structure generated after the MCC dissipated. The bow echo induces the other cloud over the Kalimantan Island and makes the system became larger as shown in Figure 4.7 (i), (j), (k) and (l). The bow echo westward migration until to Kalimantan Island. The evolution

characteristics of this case study are almost similar with the oceanic MCC in the case study 1, but this MCC is faster dissipated than the oceanic MCC.

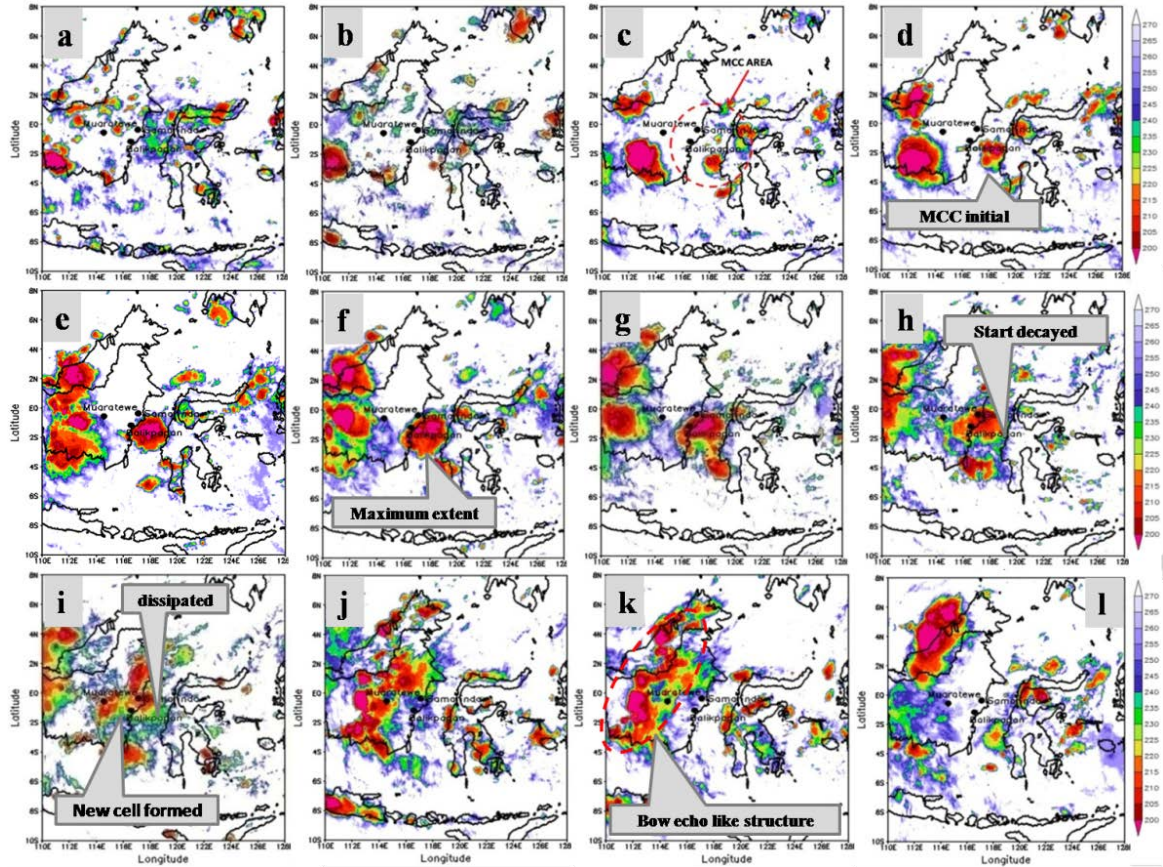


Figure 4.7. Horizontal distribution of T_{BB} for MCC criteria from infrared data obtained by MTSAT-1R over Kalimantan Island on 22 - 23 October 2011, showing the eight stages of MCC evolution: (a) MCC-12h or first storm stage (1700 LT), 22 October 2011; ((b), (c)) pre-MCC stage (1900 LT to 2200 LT), 22 October 2011; (d) initial stage (0100 LT), 23 October 2011; (e) growth stage (0500 LT), 23 October 2011; ((f), (g)) mature stage (0600 to 0800 LT), 23 October 2011; (h) decay stage (1100 LT), 23 October 2011; (i) dissipation stage (1300 LT), 23 October 2011; (j) post-MCC stage (1500 LT), 23 October 2011; (k) and (l) A few hours after MCC occur (1900 LT and 0000 LT), 23 October 2011. Unit for T_{BB} is Kelvin.

A similar analysis with the composite in the case study 1 and case study 2, the pattern of the development of the MCC composite in region 5 as shown in Figure 4.8 is similar to the case study 3. Even though, the composite time averaged in each stage is not similar to the case study 3. However, it indicated that the MCC that occur in region 5 tend to have the similar development characteristics like the case study 3. It also strengthens the analysis of the MCC in the case study 3 where the MCC development begins from the small cloud in the coastline of Sulawesi in the midnight that continue grew rapidly to reaches maximum size in the morning, decayed after several hours and then dissipated in the noon or afternoon. The MCC

that occur over the coastal of the Sulawesi tends to propagate to the Kalimantan Island after the MCC dissipated. It influenced the convective activity and rainfall over the Kalimantan.

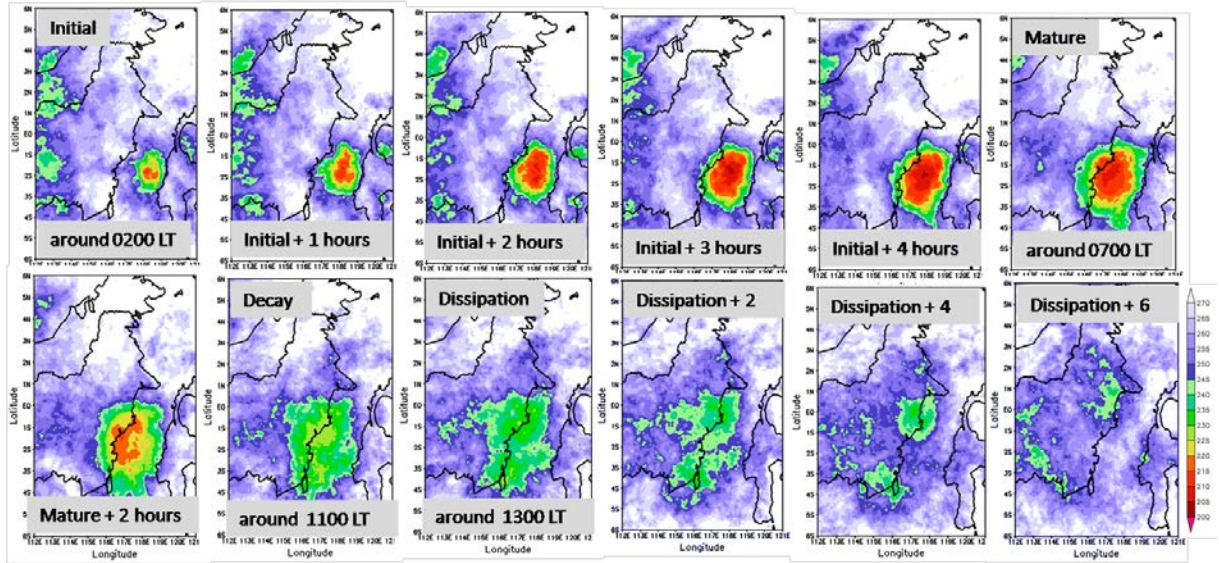


Figure 4.8. Horizontal distribution of composite of the T_{BB} for 11-case of MCC composite region 5 over the nearly same area with the case study 1. The time illustrates the average timing of the hours of initiation, mature, decay and dissipation for the 11-cases of MCC in region 5 in term of the normalized life cycle using composite analysis. Unit for T_{BB} is Kelvin.

4.1.5 MCC composite region 1, region 4 and region 6

Figure 4.9 illustrates the averaged timing of the T_{BB} in the hours of initiation, mature, decay and dissipation for the 38-case of MCC composite region 1. Figure 4.9 also shows the evolution of the development of the MCC that occur in the region 1. In general, the MCCs in this region began to develop triggered by a diurnal cycle of the cloud system over the mountains over Barisan mountains around 2300 LT in the midnight. It is similar with the schematic of the diurnal cycle by Mori et al. 2004 as described in Figure 2.16. This system grew and expanded until reaches the maximum extent of the MCC was attained at around 0700 LT. It is possible supported by the diurnal convective cloud where Mori et al. 2004 described the diurnal convective cloud reaches a maximum in the midnight at the land near the mountain and then migrate to the ocean from 0300 - 0700 LT. The MCC in this region starts decayed in the noon and dissipated in the afternoon. The MCCs that occur in region 1 will give impact to the convective activity and rainfall over the western of the Sumatra, predominantly after the MCC dissipated.

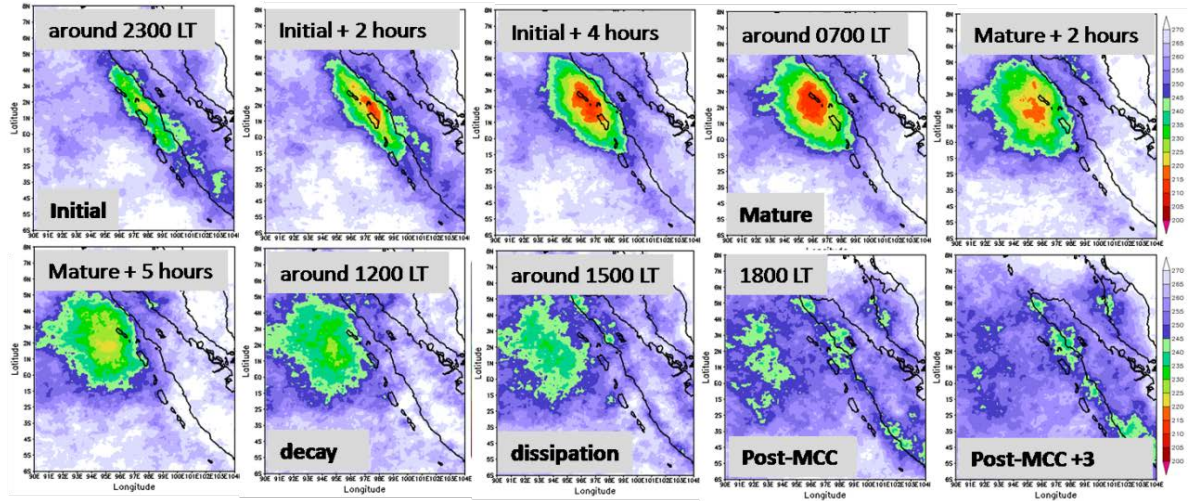


Figure 4.9. Same with Figure 4.8 but for 38-case of MCC composite region 1.

Figure 4.10 illustrates the averaged timing of the T_{BB} in the hours of initiation, mature, decay and dissipation for the 42-case of MCC composite region 4. Similar to analysis the Figure 4.9 that this figure also shows the evolution of the development of the MCC that occur in the region 4.

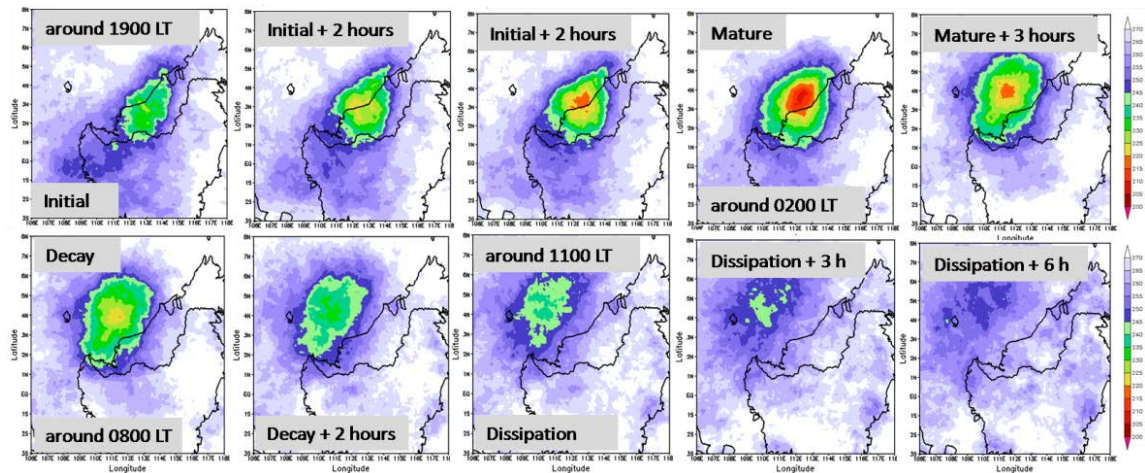


Figure 4.10. Same with Figure 4.8 but for 42-case MCC composite region 4.

The MCC developments in this region possible generated by a diurnal cycle of the cloud systems from the South China Sea as described in Figure 1.17 (Houze et al. 1981). They described that the diurnal cycle over the South China Sea dissipated in the noon and migrated to the Kalimantan Island. The systems reach maximum size in around morning. The systems start decayed and dissipated in the morning until noon, where the cloud system migrated to the South China Sea after the MCC dissipated. However, this system is possible related to the development of the diurnal cycles over the South China Sea as a triggering cloud, where

according to Houze et al. 1981, the diurnal cycles over the South China Sea began to develop in the midnight.

Figure 4.11 illustrates the averaged timing of the T_{BB} in the hours of initiation, mature, decay and dissipation for the 42-case of MCC composite region 6. Almost similar to the development of the MCC in the case study 2, where the MCC developments in this region are triggered by the orographic clouds system from the Jayawijaya mountain. The system reached maximum extent in the midnight over the continent and then decayed over the coastal around 0700 LT. The system dissipated in the noon and westward migration over the ocean.

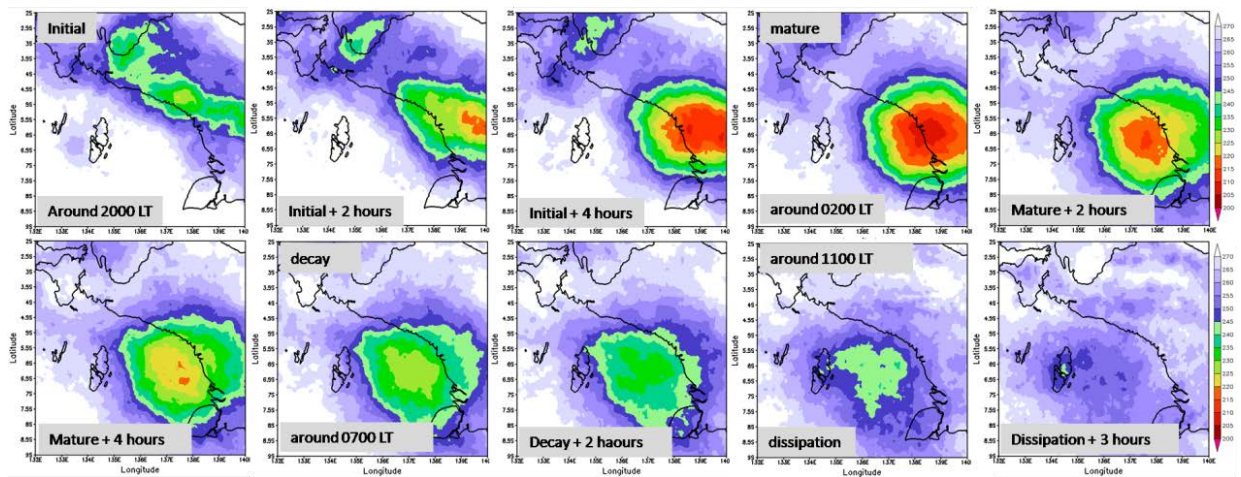


Figure 4.11. Same with Figure 4.8 but for 42-case of MCC composite region 6.

4.2 The development of new convective systems

4.2.1 The oceanic MCC

Figure 4.12 shows the horizontal distribution of C_I , wind surface vector anomaly, and surface θ during the occurrence of the MCC in the case study 1. Figure 4.12 (a) shows that some of the clouds mentioned in sub-section 4.1.1 are convective clouds indicated by high C_I values. During the initial stage, the convergent surface wind flow indicates that the land breeze triggered the development of some of the clouds on the western coast of Sumatra, whereas the westerly wind in the lower atmosphere triggered the development of some of the clouds over the nearby Indian Ocean. It is consistent with the findings of Mori et al. (2004) and Sakurai et al. (2005), who concluded that ocean convection occurs in the morning until noon, owing to the propagation of convective systems along the western coast of Sumatra, triggered by this strong land breeze. However, in this study, the convective systems discussed are defined as MCC. During the mature stage of the MCC early in the morning (0700 LT) of 28 October 2017, as shown in Figure 4.12 (b), some of the clouds over the western coast of

Sumatra and the nearby Indian Ocean merged to create the maximum extent of the MCC. The convergence of the land breeze and the westerly wind clearly supported the development of the MCC. The surface θ at the center of the MCC was relatively low (at around 297.5 K) compared with the surrounding area (299–300 K). According to Engerer et al. (2008), this area is the so-called cold pool, which is an area of downdraft air cooled by evaporation that spreads out horizontally beneath a precipitating cloud. Also, the cold pools were associated with θ decreases (Tompkins 2001) and generated by these individual convective cells in an MCS typically spread out over the surface and combine to form a large mesoscale cold pool covering a contiguous area on the scale of the entire MCS (Houze 2004).

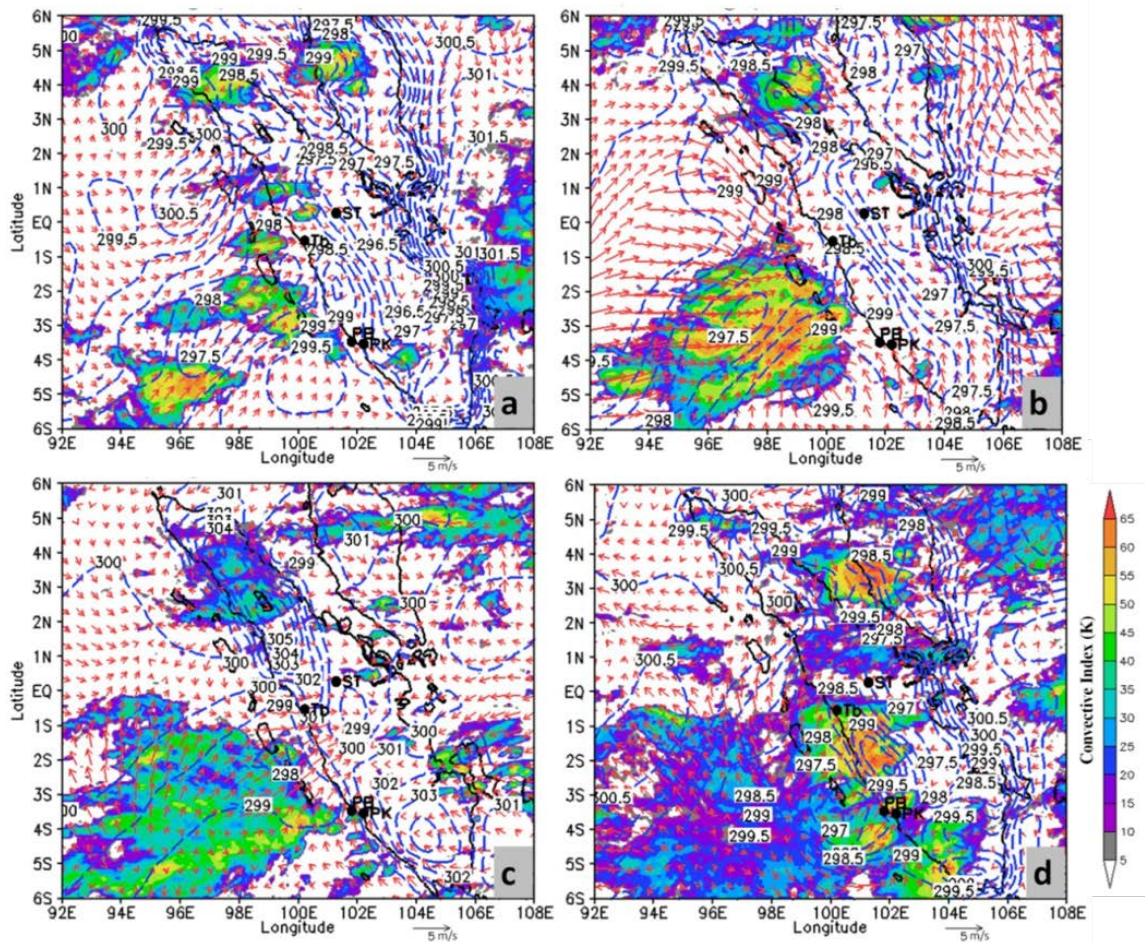


Figure 4.12. Horizontal distribution of convective index (C_1) (shaded) from infrared data of MTSAT-1R, wind surface vector anomaly (vector) from CCMP data, and surface θ (contour) from the ECMWF ERA-Interim data during the occurrence of the MCC over the Indian Ocean near Sumatra on 28 October 2007: (a) initial stage (0100 local time (LT)), showing merging of some convective clouds to create the MCC; (b) mature stage (0700 LT), showing cold pool area forming in the center of the MCC, as indicated by the low surface θ ; (c) decay stage (1300 LT), showing several new convective systems forming on the leading edge of the cold pool; (d) post-MCC stage (1900 LT), showing the new convective systems migrating from over the Indian Ocean near Sumatra toward the western coast of Sumatra. Tb, ST, PB

and PK are respectively Tabing, Simpang-Tiga, Pulau Baai and Padang Kemiling show the location of weather stations.

In this case study, the cold pool began to develop during the mature stage, and it spread increasingly until the decay stage, as shown in Figure 4.12 (c). The difference in surface θ could have acted as a trigger for the development of new convective systems to form along the leading edge of the cold pool, as in frontal theory (Figure 4.12 (c)), which is consistent with the findings of Wilson and Schreber (1986). Such new convective systems, which generated over the ocean in the daytime, eastward-propagating to the western coast of Sumatra due to of the divergent outflow of the cold pool, in conjunction with the evening sea breeze. Convective activities over Sumatra are more extensive during the evening (1900 LT) due to the new convective systems induce the land convection over the western coast of Sumatra (Figure 4.12 (d)). Therefore, this study gives a deeper insight into the mechanism of eastward-propagating convective systems, which previously have been reported to occur in the region (Mori et al. 2004).

The land-sea contrast in the timing of maximum convective activity over Sumatera Island is caused by the migration of cloud systems (Mori et al. 2004; Sakurai et al. 2005). The eastward (westward) migration of precipitation systems from the mountainous area occurs in the westerly (easterly) wind in the lower troposphere. The westward migration originating around the coast occurs in both westerly and easterly winds in the lower troposphere (Sakurai et al. 2009). The convective activity becomes intense in the western part of Sumatera Island during the daytime, and cloud systems migrate westward and eastward from this area for several hundred kilometers during the night, meaning that convection is active from the sea around Sumatera Island during the morning (Mori et al. 2004). Convection developed over and on the western side of the mountain districts of Sumatera Island in the afternoon (1500 LT). Deep cloud systems were concentrated in the evening (1800 LT) over western Sumatera Island. At night (2100, 0000, and 0300 LT) the cloud systems split and migrated both westward and eastward. In the morning (0600 and 0900 LT), the systems were off both coastlines of Sumatera Island. It was found that such diurnal cycle of cloud system migration occurred systematically over Sumatera Island (Sakurai et al. 2005). The existence of a diurnal cycle in systematic cloud generation and migration over Sumatera Island must be quite important to consider the behavior of superclusters or intraseasonal variations in this region, as suggested by Nitta et al. (1992) and Nitta and Sekine (1994). So that, comparison this result with the previous studies indicated the structure and evolution of MCCs over the Indian Ocean related to the diurnal

convective activities over Sumatra. The MCCs began to develop triggered by the diurnal variation over the western Sumatra in the evening until midnight. However, the new convective system eastward-propagating after MCCs dissipated. It triggered the development of the diurnal variation of convective activities over western Sumatra in the daytime until noon.

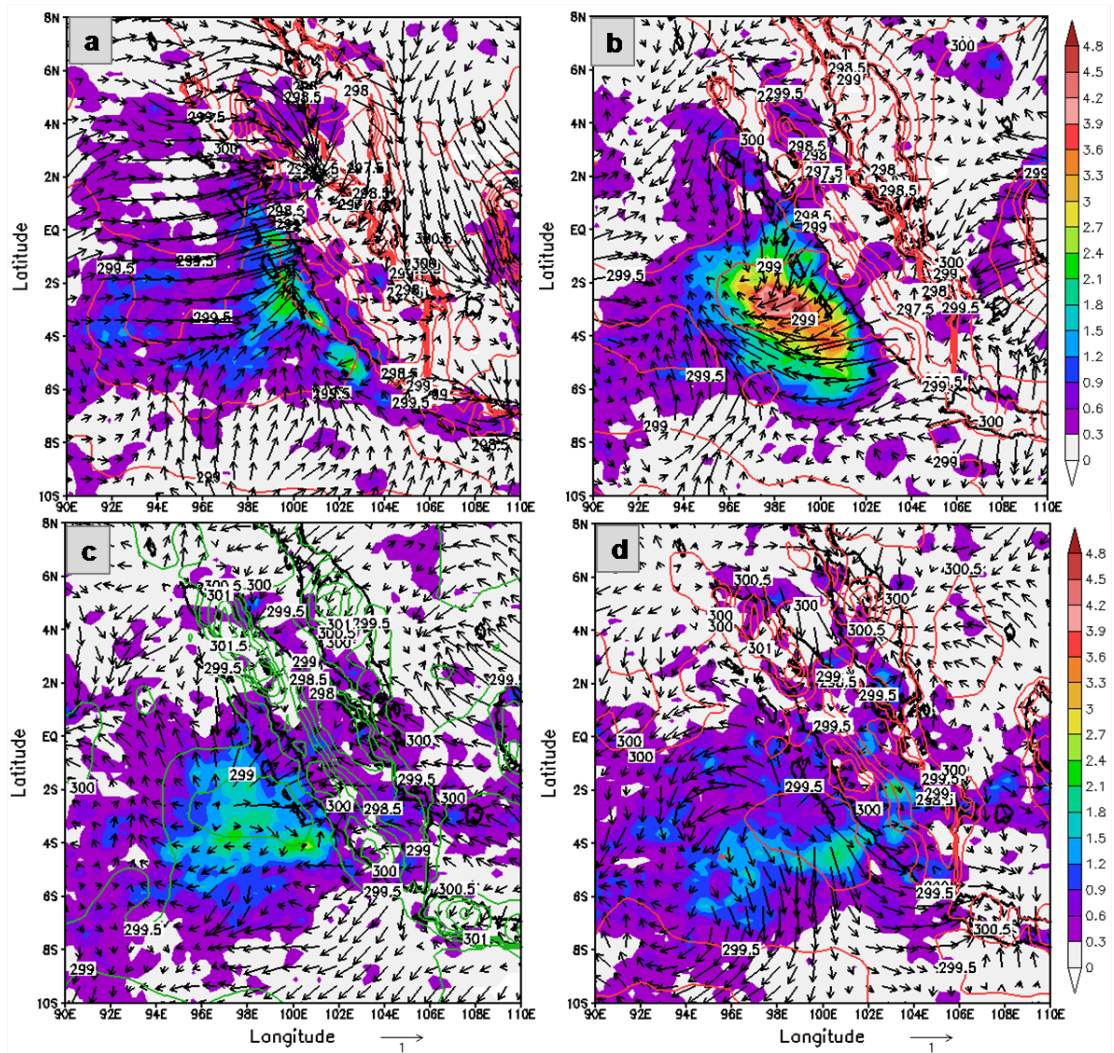


Figure 4.13. Horizontal distribution of the composite analysis of the average rainfall (shaded), wind surface vector anomaly (vector) data, and surface θ (contour) for several cases of the MCC that occur in the region 2 on the hours of initiation, mature, decay and dissipation or post-MCC. (a) Composite in initial time with the modal/dominant time are 0100 LT, (b) composite in mature time with the modal/dominant time are 0700 LT, (c) composite in decay time with the modal/dominant time are 1300 LT, and (d) composite in post-MCC time with the modal/dominant time are 1900 LT. Unit for rainfall is mmh⁻¹.

Figure 4.13 show the composite rainfall, wind vector anomaly and the surface θ for several of the MCC that occur in the region 2. Figure 4.13 (a) shows the convergent surface

wind flow as the westerly and southerly wind in the lower atmosphere which tends bring the rainfall or convective cloud. It indicates that the convergent surface wind triggered the development of some of the clouds over the Indian Ocean near the western coastal of the Sumatra during the initial stage in the midnight. Figure 4.13 (a) also show the meeting of the convergent surface wind flow with the land breeze or mountain breeze, even though the land breeze is not clearly seen. The high intensity of the rainfall also began presented at this stage. It indicates the MCC-related with the rainfall as explained in sub-section 4.4.

The pattern of composite analysis of the mature condition is consistent with the case study as shown in Figure 4.13 (b), where the convergent surface wind which interacted with land breeze became strong toward to the system area. At the same time, the peak of rainfall is presented during the mature stage in the morning. The cold pool began to appear which indicated by the value of the composite of the surface θ over the MCC system area is relatively smaller than its surrounding area. The condition of decay and post-MCC also indicated the consistency with the case study 1 as shown in Figure 4.13 (c) and (d), where the new convective systems start to appear during the decay stage that generated by the cold pool in the noon. Eastward-propagating to the western coast of Sumatra due to of the divergent outflow of the cold pool, in conjunction with the evening sea breeze during the post-MCC stage in the afternoon. Rainfall also decreased and migrated to the Sumatra after the MCC dissipated. Comparison of the MCC in the case study 1 with the composite analysis of MCC composite region 2 shows the similar pattern in the initial, mature, decay and dissipation stage as shown in Figure 4.12. It indicated that most of the MCC that occur in region 2 have similar characteristics of the development and propagation of the MCC like the MCC in the case study 1.

4.2.2 The continental MCC

Figure 4.14 shows the horizontal distribution of C_I , wind surface vector anomaly, and surface θ during the initial, mature, decay and post-MCC stage of the MCC occurrence in the case study 2. Figure 4.14 (a) shows the convergent surface wind flow as the westerly wind from Sumatra and the southerly wind from Java that triggered convection development over the Central Kalimantan during the initial stage in the evening at 1900 LT. The convergent wind also interacted with the strong sea breeze circulation and the topography lifting effect as a mountain breeze from the north. It is consistent with several previous research that stated the complex topography of the IMC leads to strong land–sea breeze circulations, with integral

convection and precipitation, over the larger islands (Yang and Slingo, 2001), such as Sumatra (Mori et al., 2004), Borneo/Kalimantan (Ichikawa and Yasunari, 2006), and New Guinea (Ichikawa and Yasunari, 2008). Figure 4.14 (a) shows the convective cloud that formed over the MCC system during initial stage was the diurnal cycle of deep convective cloud that has C_1 more than 40.

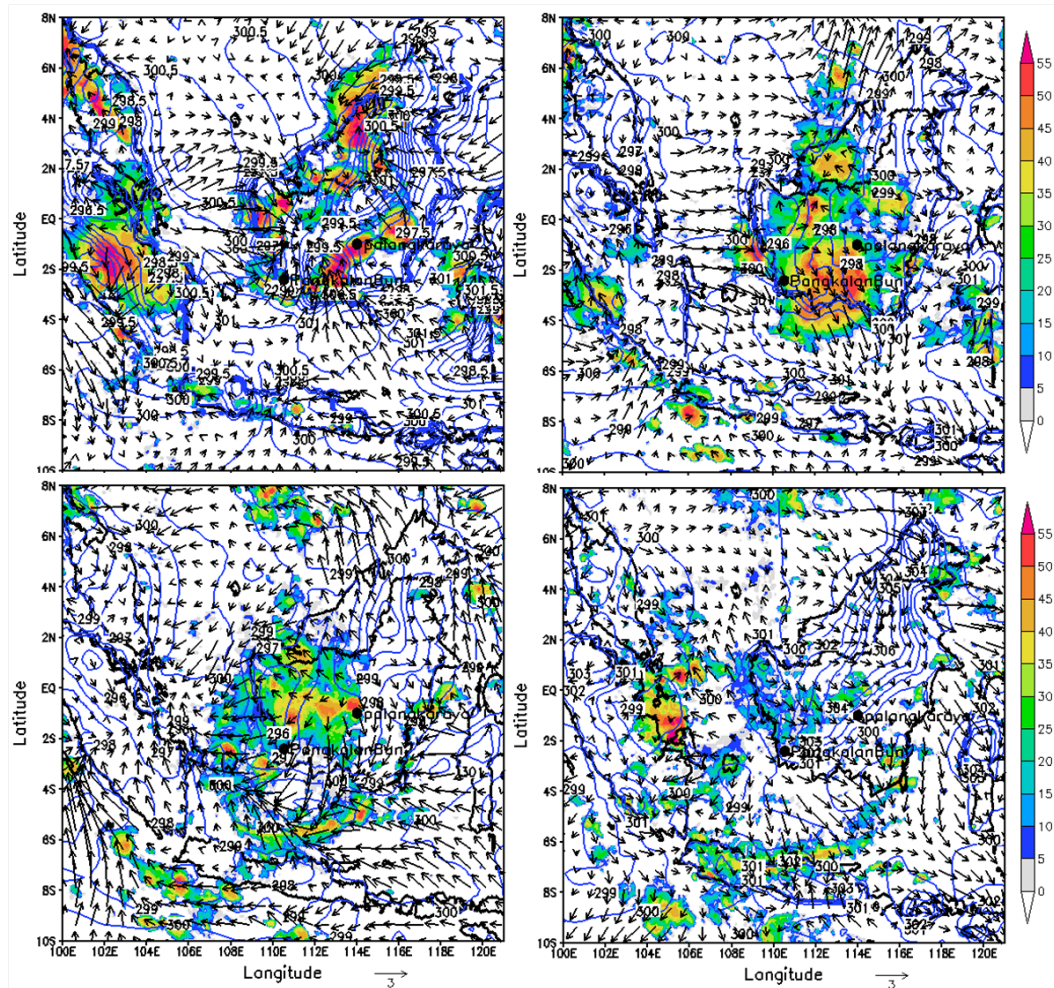


Figure 4.14. Horizontal distribution of convective index (C_1) (shaded) from infrared data of MTSAT-1R, wind surface vector anomaly (vector) from CCMP data, and surface θ (contour) from the ECMWF ERA-Interim data during the occurrence of the MCC over the Central Kalimantan as the continental MCC in the case study 2 on 14 - 15 April 2012 at time: (a) 1900 LT (initial stage), 14 April 2012; (b) 0100 LT (mature stage), 14 April 2012; (c) 0700 LT (decay stage), 15 April 2012; (d) 1300 LT (post-MCC stage + 1 hour) 15 April 2012.

Different with the oceanic MCC, the convergent surface wind in the continental MCC during a mature stage at midnight began weakened. The divergent surface wind due to land breeze circulation began to appear on the southern side of the system that propagates southward. In contrast, the convergent surface wind is still strong on the northern side of the

systems. It indicates the northern side as the leading edge of the cold pool. As noted by Tompkins (2001), the edges of cold pools contain air parcels in which falling precipitation evaporated in the sub-cloud layer and, accordingly, are colder and moister than the horizontal average. Figure 4.14 (b) shows the significant differentiation of horizontal distribution of θ in the leading edge is around 296 K and the surrounding area is around 300 K. It has been long known that the cold pools can generate the new convective systems. The forced lifting of air along the gust front or edge of a cold pool was one of the first mechanisms to be identified as responsible for convection triggering the new convective systems (Purdom 1976).

As shown in Figure 4.5 (i), most of the new convective system appear on the northern side of the system as the leading edge of the cold pool. The edge of the cold pool in the oceanic MCC is nearly presented at the all of the surrounding sides of the MCC system. During this stage, the convective activity became larger and stronger. The land breeze that indicates the divergent wind flow became stronger and widespread throughout surrounding area the systems during MCC decayed in the morning at 0700 LT (Figure 4.14 (c)). The meeting of the land breeze flow from the MCC area with the land breeze from Java Island helped the growth and movement of the new convection systems and squall line to the westward and southward migrate until Sumatra and Java Islands as shown in Figure 4.14 (d).

Figure 4.15 shows the similar pattern of the critical stage of the MCC from composite analysis with the case study. It indicated most of the MCC that occur in the region 3 which have similar characteristics in development and propagation of the MCC with the case study 2. Even though seem a little difference, among others; during the initial stage as shown in Figure 4.15 (a), the composite analysis shows that the development of the MCC is triggered by the strong surface convergent wind flow as the southerly wind and northerly wind, while the case study describes the strong southerly wind and westerly wind. The divergent surface wind flow due to land breeze circulation in the southern side of the system and the convergent surface wind at the northern side of the systems during the mature stage as illustrated in the case study, not clear in the composite analysis as describe in Figure 4.15 (b). In fact, during the mature stage, the composite analysis shows that the weak divergence appears in the surrounding area of the MCC system. However, the pattern of the divergent wind that indicates the land breeze during the MCC decayed and dissipated as shown in Figure 4.15 (c) and (d) which described the similar pattern with the case study.

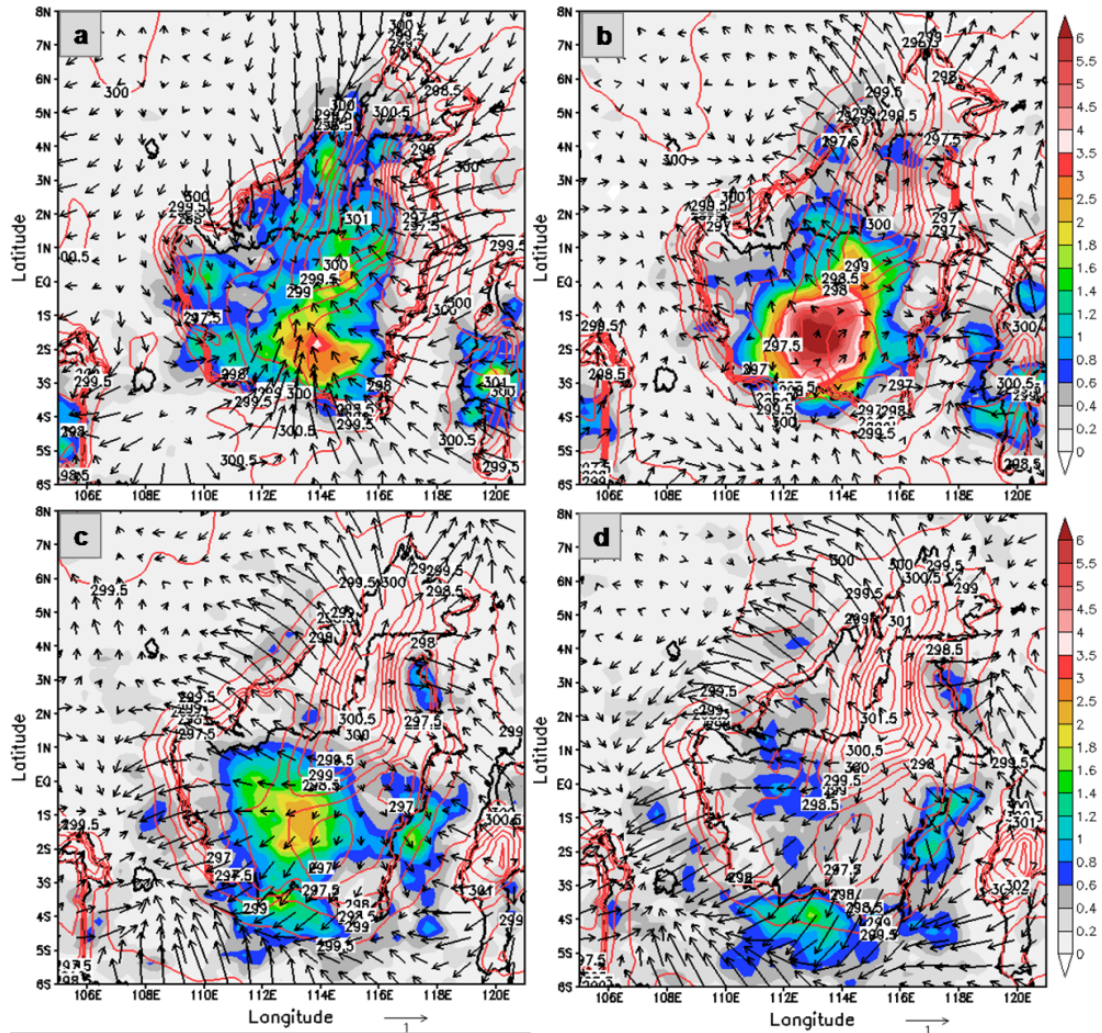


Figure 4.15. Horizontal distribution of the composite analysis of the average rainfall (shaded), wind surface vector anomaly (vector) data, and surface θ (contour) for several cases of the MCC that occur in region 3. (a). Composite in initial time with the modal/dominant time are 1800 and 1900 LT. (b). Composite in mature time with the modal/dominant time are 0100 and 0200 LT. (c). Composite in decay time with the modal/dominant time are 0700 LT. (d). Composite in post-MCC time with the modal/dominant time are 1200 and 1300 LT.

The land breeze is supported the southward migration of the new convective system that predicted influencing the rainfall over Java Island. Rainfall pattern also shows the related with convective activity and MCC, where the peak of rainfall found to the maximum extent of the MCC. Similar to the case study, the cold pool began identified during the mature stage that shown by the value of the surface θ over the MCC area is relatively smaller than the surrounding area. Overall, the composite analysis strengthens the case study analysis that concluded most of the MCC that occur in the region 3 developed and propagated like the MCC in the case study 2. Ichikawa and Yasunari (2006) investigated the time-space characteristics of diurnal rainfall over Kalimantan Island and surrounding oceans using

rainfall data from the TRMM Precipitation Radar. They showed that rainfall activity propagates to the leeward side of Kalimantan Island between midnight and morning in both the low-level easterly or westerly regimes over and around Kalimantan. It indicated that the diurnal variation of rainfall system over Kalimantan Island is associated with the MCC systems.

4.2.3 The coastal MCC

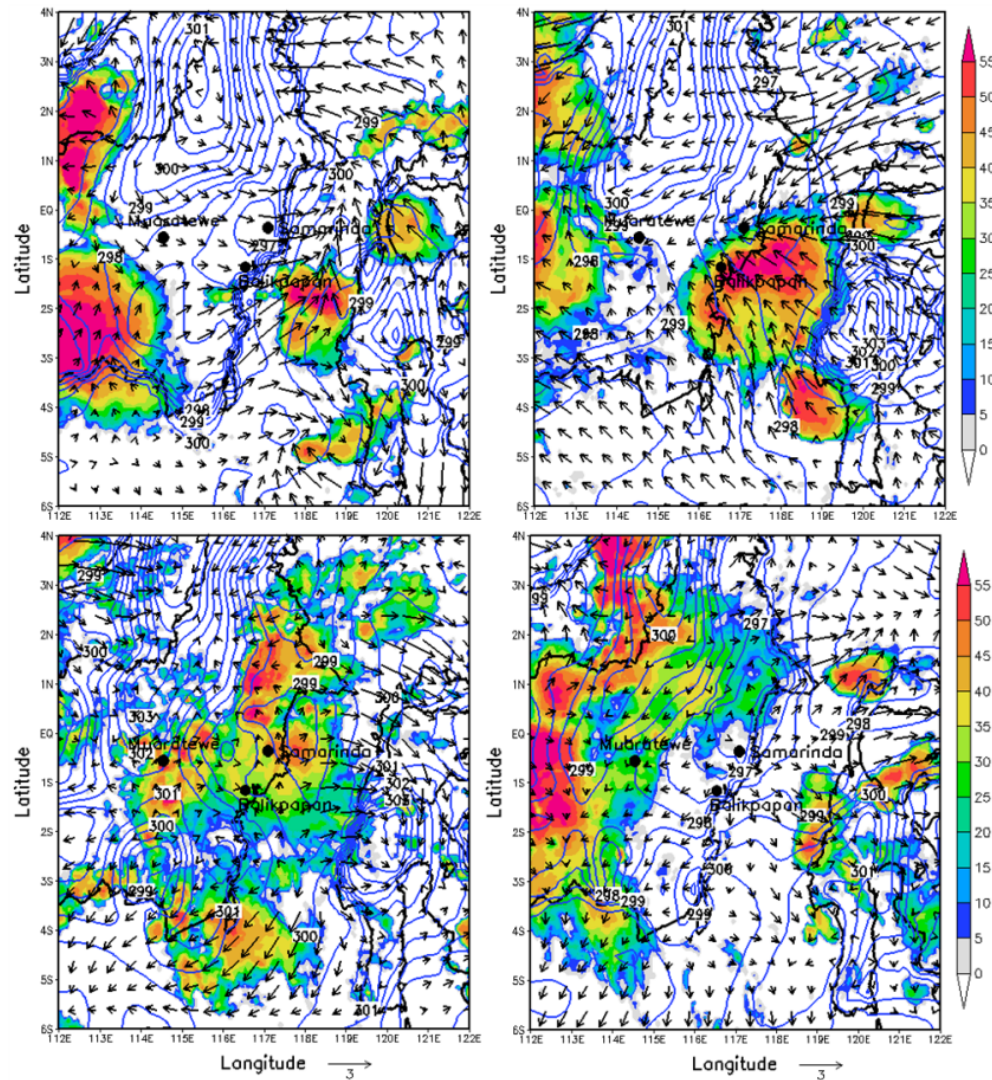


Figure 4.16. Horizontal distribution of convective index (C_1) (shaded) from infrared data of MTSAT-1R, wind surface vector anomaly (vector) from CCMP data, and surface θ (contour) from the ECMWF ERA-Interim data during the occurrence of the MCC over the western coastal of Sulawesi as the coastal MCC in the case study 3 on 23 October 2011 at time: (a) 0100 LT (initial stage); (b) 0700 LT (mature stage); (c) 1300 LT (dissipation stage); (d) 1900 LT (4 hours after post-MCC stage).

Figure 4.16 shows the horizontal distribution of C_I , wind surface vector anomaly, and surface θ during the occurrence of the coastal MCC in the case study 3. Figure 4.16 (a) shows that some of the clouds mentioned in subchapter 4.1.3 are convective clouds indicated by high C_I values. Similar to the oceanic and continental MCC, the convergent surface wind also triggered the development of the coastal MCC. The development of the coastal MCC in this case study triggered by the meeting of westward and eastward of convergent surface wind flow that indicated as the land breeze from the eastern Kalimantan and Central Sulawesi in the midnight (0100 LT) as shown in Figure 4.16 (a).

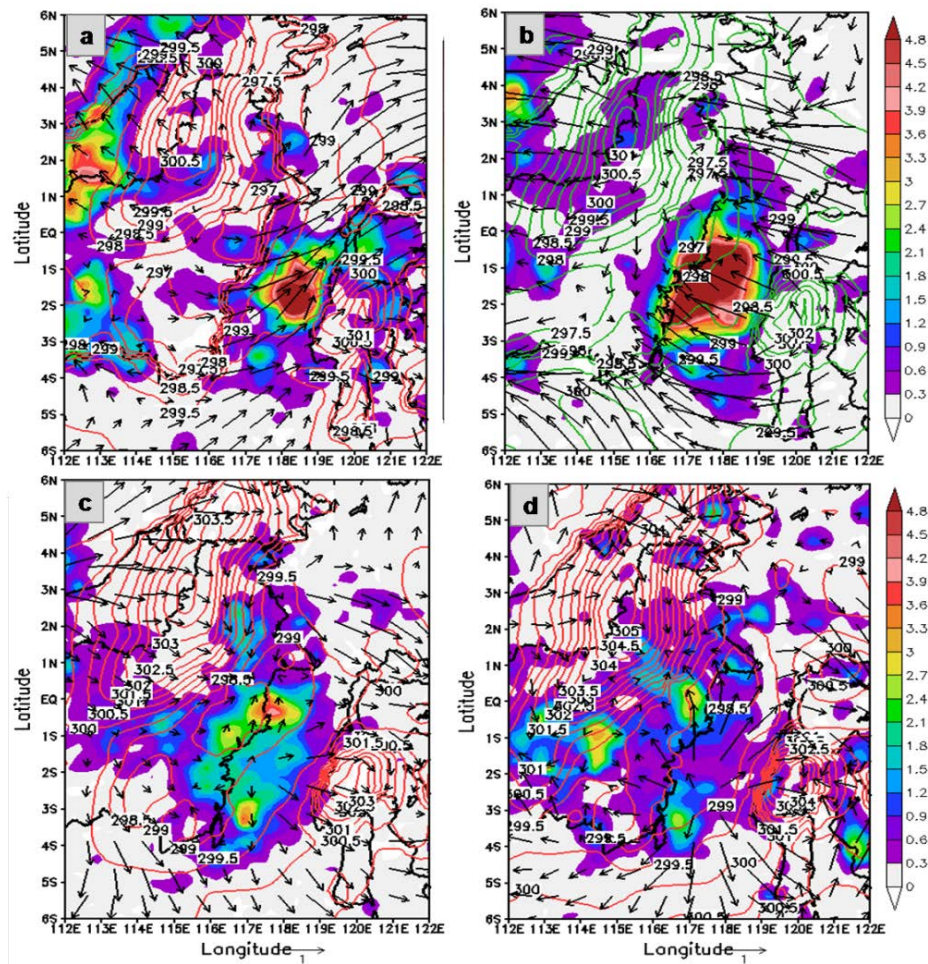


Figure 4.17. Horizontal distribution of the composite analysis of the average rainfall (shaded), wind surface vector anomaly (vector) data, and surface θ (contour) for several cases of the MCC that occur in region 5. (a). Composite in initial time with the modal/dominant time are 0000 and 0100 LT. (b). Composite in mature time with the modal/dominant time are 0600 and 0700 LT. (c). Composite in decay time with the modal/dominant time are 1200 and 1300 LT. (d). Composite in around 3 hours after post-MCC time with the modal/dominant time are 1800 and 1900 LT.

The convective system migrated westward and expanded reached maximum extent near to Samarinda and Balikpapan in the morning (0700 LT) as shown in Figure 4.16 (b). It triggered by the strong land breeze from Sulawesi and strong convergent wind flow from the southern and northern of Sulawesi. The surface θ at the center of the MCC system area was relatively low (at around 298 K) compared with the surrounding area (299–300 K). It indicated the cold pool began generated. Figure 4.16 (c) and (d) just show dissipation stage and 4 hours after the post-MCC stage, respectively, due to the data during decay stage is not available. During both of this stage, the new convective system and "bow echo like" structure is presented over Kalimantan Island that propagated westward and eastward that supported by the divergent outflow of the cold pool, in conjunction with the evening sea breeze.

The composite analysis for the MCC that occur over the region 5 already observed as shown in Figure 4.17. Figure 4.17 (a) show that in particularly the development of the MCC over the region 5 is triggered by the meeting of westward and eastward convergent surface wind flow that indicated as the land breeze from the eastern Kalimantan and Central Sulawesi in the midnight (0100 LT). It is consistent with the case study 3. The rainfall system become grew and expanded until reached a maximum size with supported by the strong convergent wind that indicated as easterly wind and the land breeze from Sulawesi as shown in Figure 4.17 (b). It indicated the consistency with the case study 3. Due to similar pattern with the case study, the composite analysis strengthen the analysis of the case study that describes during the decay and dissipation stage, the strong divergent wind is presented, and it helps the propagation of rainfall system to the Kalimantan Island as shown in Figure 4.17 (c) and (d). However, the cold pool that indicated by the surface θ is not clear by using composite analysis.

4.2.4 MCC composite region 1, region 4 and region 6

The case study that similar region with the MCC composite region 1, region 4 and region 6 is not shown in this research. However, the existence of a similar pattern and consistency between the case study and a composite analysis of three case studies have represented that a composite analysis is always consistent and strengthen the analysis of the case studies. Figure 4.18 illustrated the composite analysis for the several MCC that occur in the region 1. The process of the development of the MCC in the region 1 seen nearly similar with the MCC that occur in the case study 1. During the initial stage, the convergent surface wind flow as the westerly and southerly wind in the lower atmosphere predicted to bring the

rainfall or convective cloud from the Indian Ocean triggered the development of the MCC in the region 1. The westerly and southerly wind also interacted with the land breeze or mountain breeze from the "Barisan" mountainous in developing the MCC system as shown in Figure 4.18 (a).

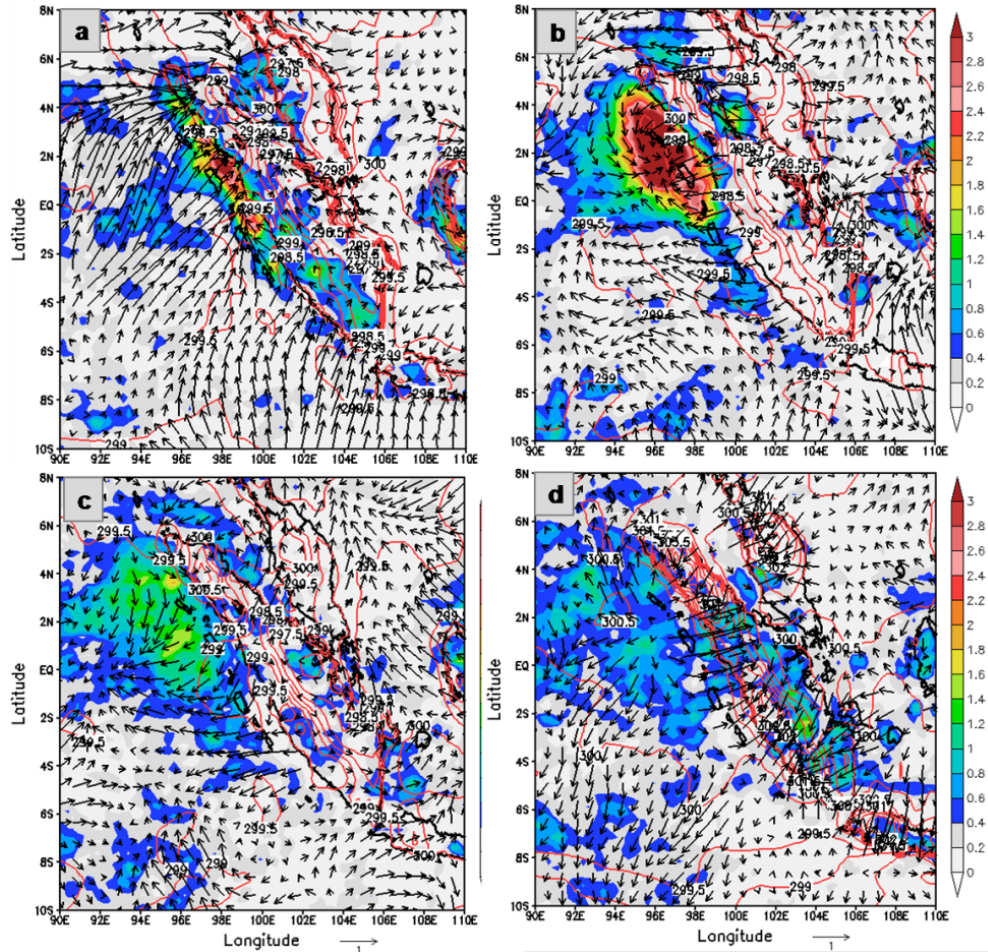


Figure 4.18. Horizontal distribution of the composite analysis of the average rainfall (shaded), wind surface vector anomaly (vector) data, and surface θ (contour) for several cases of the MCC that occur in region 1. (a). Composite in initial time with the modal/dominant time are 0200 LT. (b). Composite in mature time with the modal/dominant time are 0600 and 0700 LT. (c). Composite in decay time with the modal/dominant time are 1200 and 1300 LT. (d). Composite in post-MCC time with the modal/dominant time are 1800 and 1900 LT.

Similar to the case study 1 and MCC composite region 2, the interaction between the strong convergent surface wind and the land breeze make the clouds system rapidly grew and expand until reaches the maximum size of the rainfall system or MCC system as shown in Figure 4.18 (b). The cold pools also began indicated by the surface θ that relative smaller than the surrounding area, even though the land breeze not seen clearly. The difference in surface θ could have acted as a trigger for the development of new convective systems to formed along

the leading edge of the cold pool that began seen in decay stage of the MCC as shown in Figure 4.18 (c). The divergent outflow due to the cold pool and in conjunction with the evening sea breeze make the new convective system migrate widespread throughout in the surrounding area of the MCC system area, predominantly along the western of the Sumatra as shown in Figure 4.18 (d).

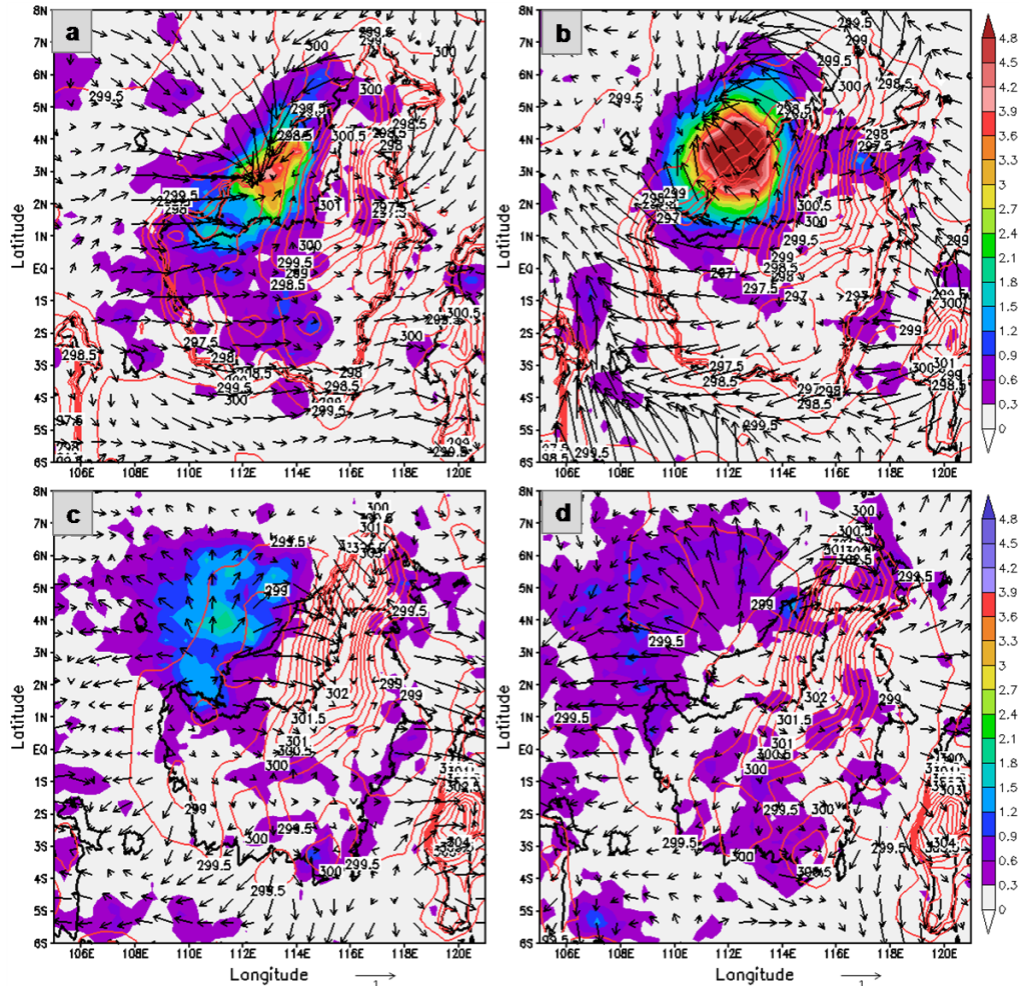


Figure 4.19. Horizontal distribution of the composite analysis of the average rainfall (shaded), wind surface vector anomaly (vector) data, and surface θ (contour) for several cases of the MCC that occur in region 4. (a). Composite in initial time with the modal/dominant time are 1900 LT. (b). Composite in mature time with the modal/dominant time are 0100 and 0200 LT. (c). Composite in decay time with the modal/dominant time are 0700 and 0800 LT. (d). Composite in dissipation time with the modal/dominant time are 1200 and 1300 LT.

Figure 4.19 illustrated the composite analysis for the several MCC that occur in the region 1. The MCC developments in this region possible generated by a diurnal cycle of the cloud systems from the South China Sea as described in Figure 1.17 (Houze et al. 1981). They described that the diurnal cycle over the South China Sea dissipated in the noon and migrated

to the Kalimantan Island. Houze et al. (1981) also presented the diurnal cycle of winds at the Borneo coast. Surface winds were onshore during the day and calm at night, in agreement with the above discussion of the relative strength of thermal sea and land breezes. A seaward component of wind was observed above the surface and strongest in the morning (0800 LT). They stated that the diurnal land–sea circulation “controlled the atmosphere’s convective response near North Borneo. Specifically, when the offshore wind component (generated diurnally) begins near midnight, there results in an immediate commencement of convection over the sea. The large-scale convergence is then locally concentrated where the diurnal land breeze meets the low-level monsoon flow.” As can be seen from the Figure 4.19 (a) that the strong convergent surface wind flow as northerly wind from the South China Sea and westerly wind triggered the development of rainfall cloud system over coastal of the northern of the Kalimantan in the late afternoon based on the dominant averaged time. The system reached maximum size in the midnight and slightly moving toward the South China Sea due to supported by the midnight land breeze as shown in Figure 4.19 (b).

The MCC composite region 6 is characterized by development the clouds system near the Jayawijaya Mountains in Merauke that triggered by the southerly wind flow and the mountain breeze as shown in Figure 4.20 (a). The clouds system continued grew and expanded due to supported by the mountain breeze as shown in Figure 4.20 (b). The process of MCC composite region 6 is similar to the case study 2 and the MCC composite region 4, where the divergent surface wind due to land breeze circulation began to appear on the southern side of the system that propagates southward. In contrast, the convergent surface wind is still strong on the northern side of the systems. It indicated the northern side as the leading edge of the cold pool. The cold pool began to appear in this stage with indicated by the lower surface θ around 297 K in the center of the system. It is smaller than the surrounding area. The clouds system westward migrated to the ocean (Arafura Sea) during the MCC decayed and dissipated as shown in Figure 4.20 (c) and Figure 4.20 (d).

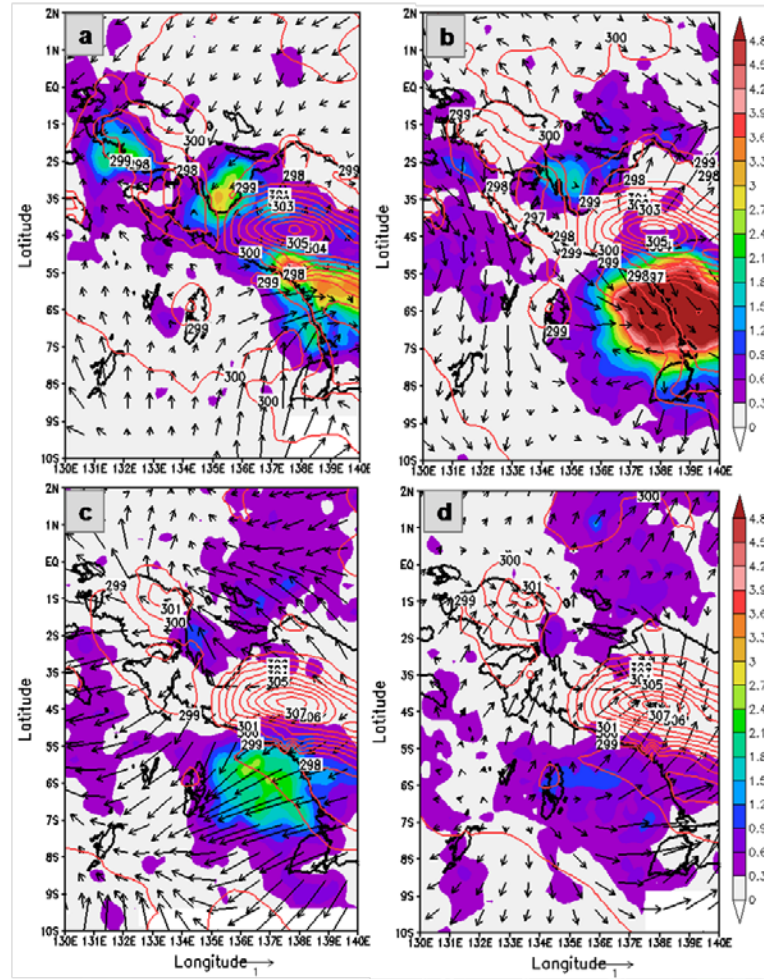


Figure 4.20. Horizontal distribution of the composite analysis of the average rainfall (shaded), wind surface vector anomaly (vector) data, and surface θ (contour) for several cases of the MCC that occur in region 6. (a). Composite in initial time with the modal/dominant time are 1800 and 1900 LT. (b). Composite in mature time with the modal/dominant time are 0100 and 0200 LT. (c). Composite in decay time with the modal/dominant time are 0700 and 0800 LT. (d). Composite in several hours after post-MCC time with the modal/dominant time are 1300 and 1400 LT.

4.3 Structure of the propagation of the MCC

Figure 4.21 depicts the time-latitude cross-section of the convective activity averaged $6^{\circ}\text{S} - 0^{\circ}\text{N}$ with determining the convective index. The convective activity is starting actively from midnight in the initial stage over the Indian Ocean (around 96°E) and became gradually more active and stronger during a mature stage in the morning over the MCC system area which followed the increased of average rainfall. The convective activity propagates eastward after the MCC dissipated by supported the westerly wind at the low level. The zonal wind direction also roughly corresponded to the migratory direction of convective activity where the zonal wind direction almost simultaneously with the generation of the eastward

propagates of convective activity. Finally, this figure describes that the characteristics of the propagation of the MCC in the case study 1 are eastward-propagating MCC.

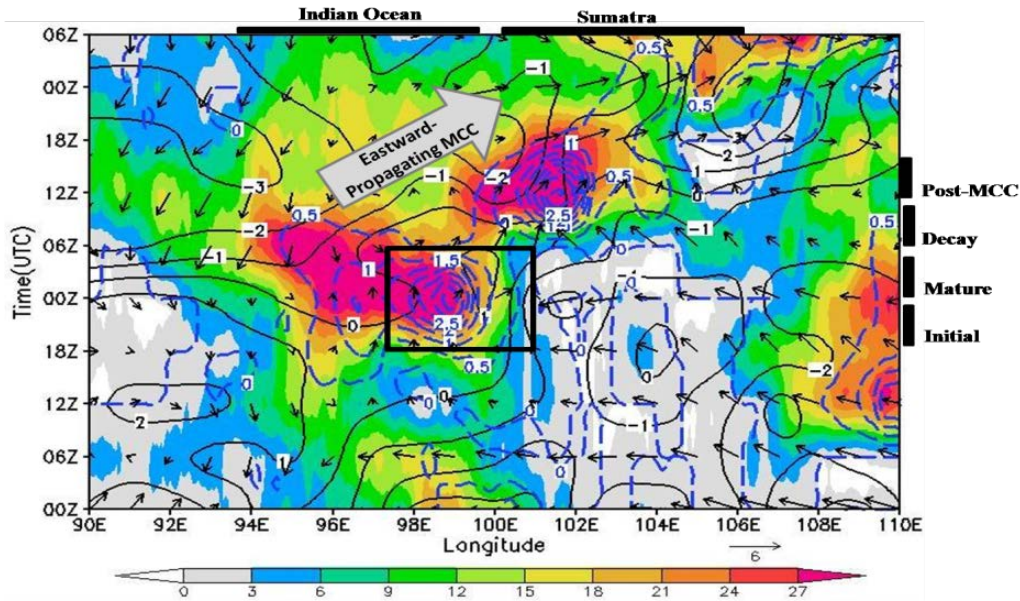


Figure 4.21. Time-longitude cross-sections (averaged for latitude 6°S - 0°N) during the oceanic MCC in case study 1, of; convective index (C_t) from infrared data of MTSAT-1R, rainfall from TRMM TMPA 3B41RT (blue dotted contour; unit mmh^{-1}), 850-hPa horizontal wind (vector arrow; upward is northward; unit ms^{-1}) and zonal wind (black contour; unit ms^{-1}) from ECMWF ERA-Interim data. The black box represents MCC area. Time in UTC, UTC = LT + 7.

The cross-section analysis in Figure 4.22 shows the propagation of the continental MCC systems. The convective activity began actively from the northern of Kalimantan as mountain region, and then the convective activity migrates southward toward to MCC area. The convective activity reached a maximum during mature which followed the increase of the average rainfall. After the MCC dissipated, the new convective activity is presented in several areas. i.e., western of Java, southern and northern of Sumatra, and northern of Kalimantan that due to southward-propagating MCC which supported by the low-level northerly wind.

Figure 4.23 show the westward-propagating characterizes the coastal MCC over the coastal of the Sulawesi. It is indicated by the migration westward of convective activity during MCC occurrences which interaction low-level northwesterly wind. The zonal wind direction also corresponds with the migration of convective activity.

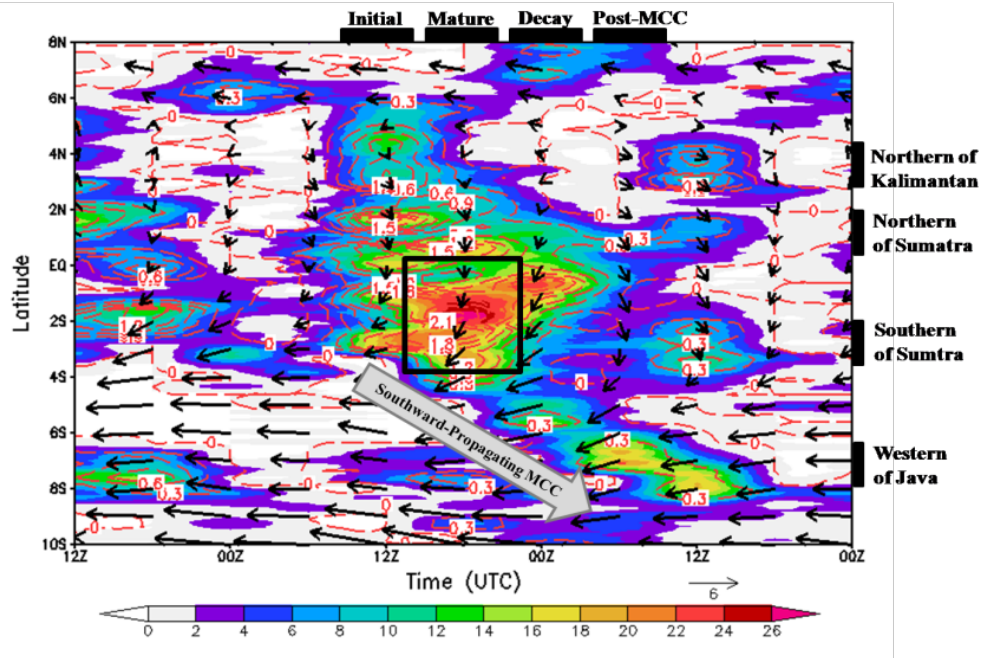


Figure 4.22. Latitude-time cross-sections (averaged for longitude 102-116°E) during the continental MCC in case study 2 of; convective index (C_i) from infrared data of MTSAT-1R, rainfall from TRMM TMPA 3B41RT (red dotted contour; unit mmh^{-1}), 850-hPa horizontal wind (vector arrow; upward is northward; unit ms^{-1}) from ECMWF ERA-Interim data. The black box represents MCC area. Time in UTC, UTC = LT + 7.

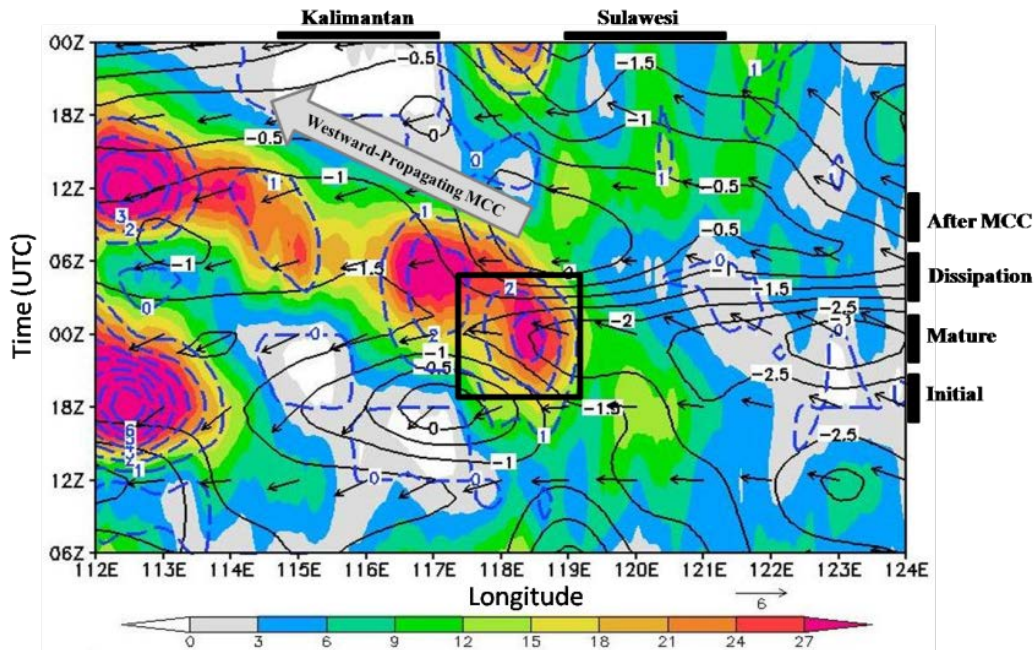


Figure 4.23. Time-longitude cross-sections (averaged for latitude 5°S - 2°N) during the coastal MCC in case study 3, of; convective index (C_i) from infrared data of MTSAT-1R, rainfall from TRMM TMPA 3B41RT (blue dotted contour; unit mmh^{-1}), 850-hPa horizontal wind (vector arrow; upward is northward; unit ms^{-1}) and zonal wind (black contour; unit ms^{-1}) from ECMWF ERA-Interim data. The black box represents MCC area. Time in UTC, UTC = LT + 7.

4.4 Rainfall system during MCC events

4.4.1 Horizontal distribution of rainfall from TRMM

Figure 4.24 shows the horizontal distribution of rainfall during the studied MCC events. During the pre-MCC and initial stage at 0100 LT (Figure 4.24 (a) and (b)), only light rainfall ($<10 \text{ mm h}^{-1}$) was observed over the Indian Ocean. However, the observed early morning (0700 LT) maximum occurred because of the increase in the number of convective clouds (Figure 4.24 (c)), rather than because of the increased in the extent of the coverage of the MCC during the mature stage (Figure 4.24 (d)). The rainfall system began to propagated slowly eastward from the Indian Ocean toward the western coast of Sumatra (Figure 4.24 (e)) during the new convective systems propagated eastward to the western coast of Sumatra at the decay stages at the daytime (1300 LT). The peak rainfall on the western coastal of Sumatra began appear in the evening at 1600 LT (Figure 4.24 (f)) until 1900 LT (Figure 4.24 (g)) due to the interaction of new convective systems with land convection which make the convective activity becomes intense on the western coast of Sumatra during the dissipation stages until post-MCC stages.

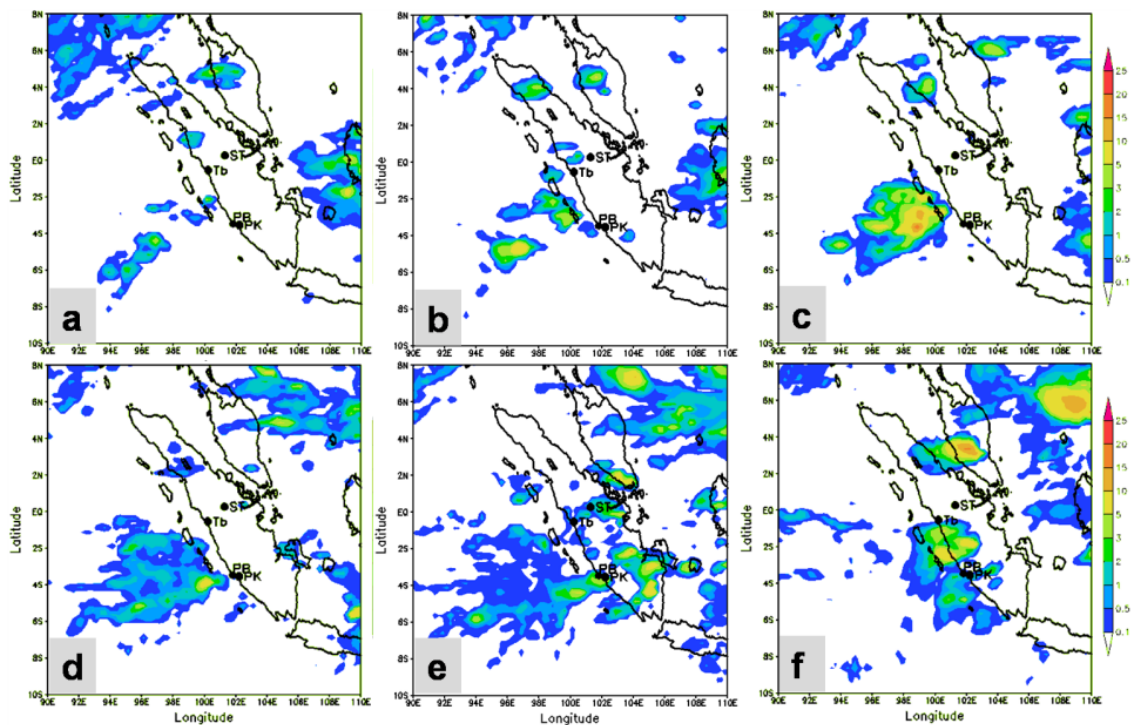


Figure. 4.24. Horizontal distribution of rainfall from TRMM TMPA 3B41RT data during the occurrence of the MCC in case study 1, 27 Oct 2007: (a) pre-MCC stage (2200 LT) and 28 Oct 2007: (b) initial stage (0100 LT); (c) mature stage (0700 LT); (d) decay stage (1300 LT); (e) dissipation stage (1600 LT); and (e) post-MCC stage (1900 LT). Tb, ST, PB and PK are respectively Tabing, Simpang-Tiga, Pulau Baai and Padang Kemiling show the location of weather stations. Unit for rainfall is mmh^{-1} .

The structure and evolution of the MCCs in the case study 2 also related to the rainfall. Figure 4.25 shows the horizontal distribution of rainfall during the continental MCC occurrence. During the MCC-12 h stage until pre-MCC stage (Figure 4.25 (a), (b) and (c)), looks the development of orographic rainfall over the Muller Mountains. The orographic rainfall become grew and merged with the other clouds that followed the rainfall increased over the MCC system area, as marked the onset of the initial stage of MCC (Figure 4.25 (d)). During the growth stage of the MCC (Figure 4.25 (e)), the sizes of the rain clouds had increased further and they began merging with each other to reaches the maximum extent of the MCC that attained at midnight (2300 LT and 0000 LT) (Figure 4.25 (f) and (g)). At this stage, the rainfall intensity reached the maximum value. Rainfall intensity significantly decreases during MCC decayed and dissipated as shown Figure 4.25 (h), (i), and (j). However, the new rainfall system appear in the surrounding area of the system due to the new convective system. In this case, squall line like structure is presented after MCC decayed. This squall line migrates to Java that causes heavy rainfall over western of Java as shown in Figure 4.25 (k) and (l).

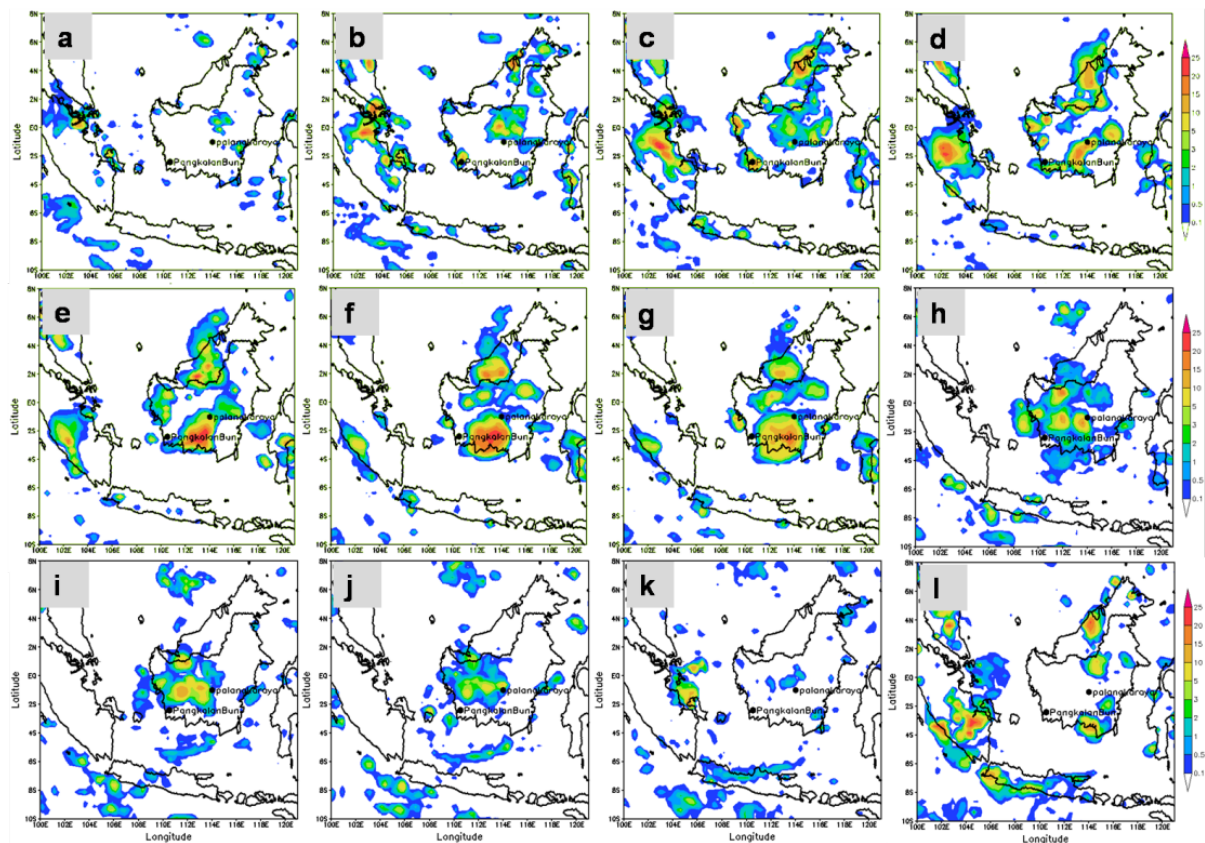


Figure 4.25. Horizontal distribution of rainfall from TRMM TMPA 3B41RT data during the occurrence of the MCC in case study 2, 14 April 2012: (a) MCC-12h stage (1300 LT); (b,c) pre-MCC stage (1500 LT to 1700 LT); (d) initial stage (1900 LT); (e) growth stage (2100 LT); ((f),(g)) mature stage (2300 LT and 0000 LT) and 15 April 2012: ((h),(i),(j)) decay stage (0300 LT, 0500 LT and 0700 LT); (k) post-MCC stage (1300 LT) and after MCC (1700 LT). Unit for rainfall is mmh^{-1} .

The rainfall pattern that similar with the evolution pattern during MCC events are also shown in coastal MCC as shown in Figure 4.26. The peak of rainfall is found during MCC reaches maximum extent in the mature stage as shown in Figure 4.26 (b). The rainfall became significantly decrease when the MCC decayed as shown in Figure 4.26 (c). However, the new rainfall system appears in the surrounding area of the system due to the new convective system as shown in Figure 4.26 (d).

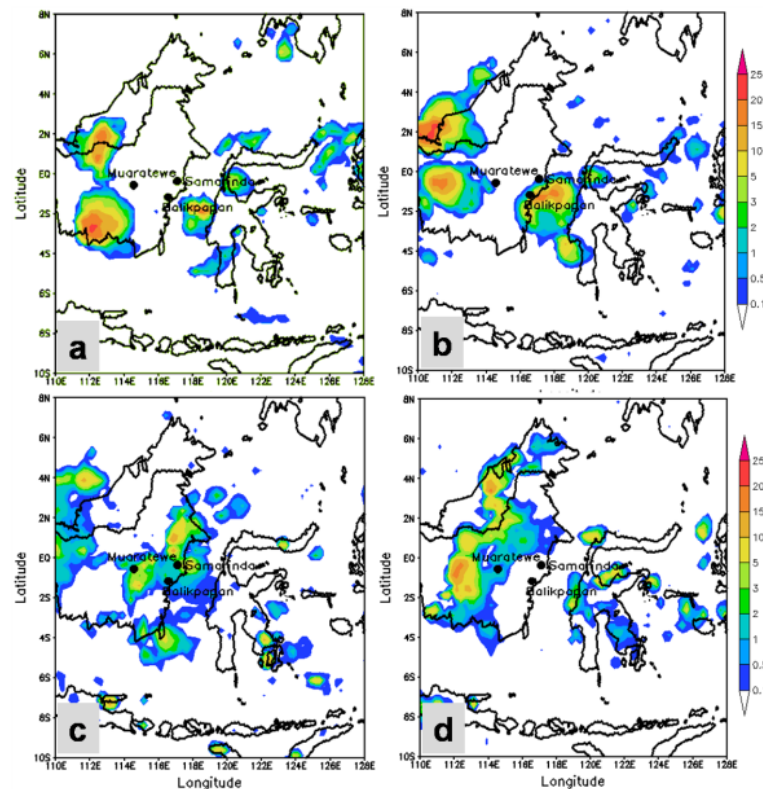


Figure 4.26. Horizontal distribution of rainfall from TRMM TMPA 3B41RT data during the occurrence of the MCC in case study 3 on 23 October 2011 at time: (a) 0100 LT (initial stage); (b) 0700 LT (mature stage); (c) 1300 LT (dissipation stage); (d) 1900 LT (4 hours after post-MCC stage). Unit for rainfall is mmh^{-1} .

Figure 4.27 shows the rainfall accumulation during the MCC events from the Pre-MCC stage until 6 hours after the post-MCC stage for all of the case study. The greatest rainfall accumulation is presented in the center of MCC system area for the oceanic,

continental and coastal MCCs. It indicated that the significant influence of MCC to the rainfall is during MCC reached maximum extent in the mature stage. However, the high rainfall accumulation also appears in several regions near the MCC system area. It indicated that the effect of MCCs are not only over the MCC system area but also influencing to the rainfall in the surrounding area of the MCC systems. In this research, the area in the surrounding of MCC systems that get affected by the MCC is mentioned as affected area by the MCC as shown in Figure 4.27 (b). The affected area by the oceanic MCC is in the western of Sumatra as shown in Figure 4.27 (a), and the affected area by the continental MCC is western of Java, southern of Sumatra, Malaysia and Brunei in the northern of Kalimantan as shown in Figure 4.27 (b). The Center Kalimantan and western of Kalimantan are the affected areas of MCC by the coastal MCC as shown in Figure 4.27 (c).

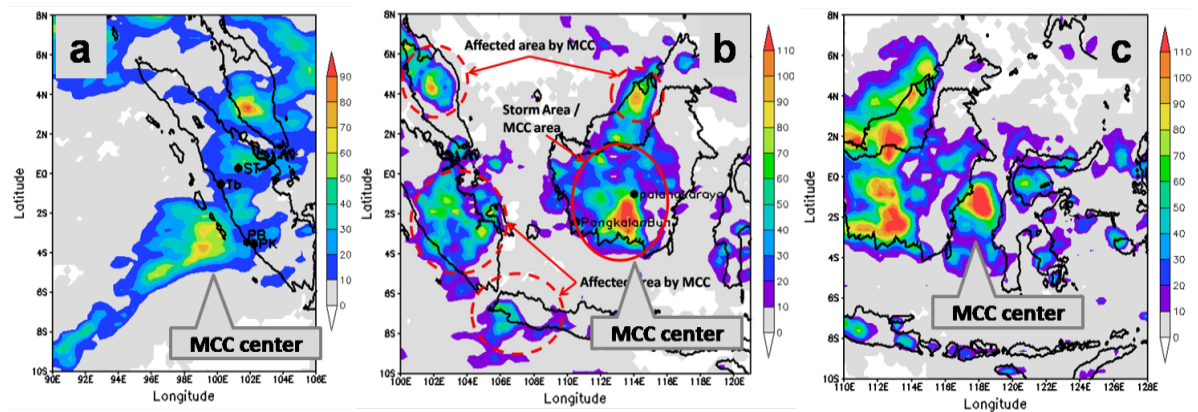


Figure 4.27. Horizontal distribution of rainfall accumulated from the Pre-MCC stage until 6 hours after the post-MCC stage. Rainfall data obtained from TRMM TMPA 3B41RT. (a) Case study 1; (b) case study 2 that shows the example of what is the meaning of the MCC rainfall in storm area or MCC area (red circle) and MCC rainfall as affected area by MCC (red dotted circle); and (c) case study 3. Unit for rainfall is mmh^{-1} .

4.4.2 Comparison with observation data from OGIMET

Comparison of the oceanic MCC in the case study 1 with the observational data as shown in Figure 4.28, the rainfall intensity increased significantly, especially during the dissipation and the post-MCC stages over some parts of western Sumatra. Heavy rainfall occurred over the southwestern coastal ocean at Pulau Baai (Bengkulu) from 1400–1900 LT, which reached a maximum intensity of around 35 mmh^{-1} at 1600–1700 LT during the dissipation stage of the MCC. During the post-MCC stage at 1900 LT, a significant increase in rainfall (up to 46 mmh^{-1}) occurred over southwestern coastal land at Padang Kemiling (Bengkulu). Rainfall also occurred over northwestern coastal land at Tabing (Padang) and over inland at Simpang-Tiga (Pekanbaru) but it was only light in intensity because of the

weaker effect of the MCC compared with the area around Bengkulu. The diurnal rainfall associated with the MCC had a similar pattern. The rainfall over the Indian Ocean occurred when the MCC started developing, and it reached a maximum when the MCC began to decay, at which time, the rain started to move toward the western coast of Sumatra. It is consistent with previous studies, which have stated that MCCs possess the potential to exert considerable impact on regional rainfall patterns.

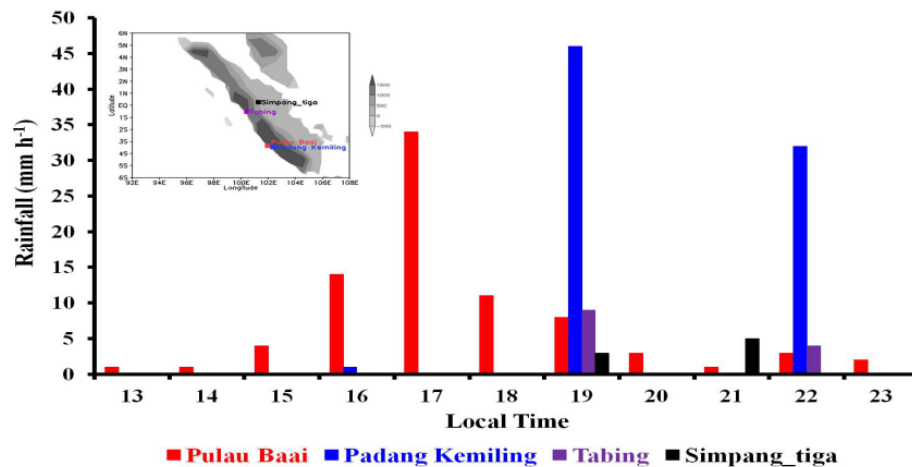


Figure 4.28. Rainfall observational data during the occurrence of oceanic MCC in the case study 1 over the Indian Ocean near Sumatra on 28 October 2007 (1300–2400 LT) at specific sites on the western coast of Sumatra: Pulau Baai weather station in Bengkulu, Tabing weather station in Padang, Simpang Tiga weather station in Pekanbaru, and Padang Kemiling weather station in Bengkulu. The figure panel shows the location of weather stations.

Figure 4.29 shows the observational data during the continental MCC occurrences. Figure 4.29 (a) shows the θ significantly decreased that followed the surface pressure increased at Palangkaraya, and Pangkalan Bun during the initial stage of MCC at 1900 LT until MCC dissipated at 0700 LT. It indicated that there is cold pool generated by MCC from initial stage until MCC dissipated. That statement reinforced by the Figure 4.29 (b) that shows there are increased significantly of relative humidity which followed the surface temperature significantly decreased during MCC events at Palangkaraya and Pangkalan Bun weather station. The rainfall intensity increased significantly, especially during the mature stage over Palngakaraya and Pangkalan Bun, as shown in Figure 4.29 (c).

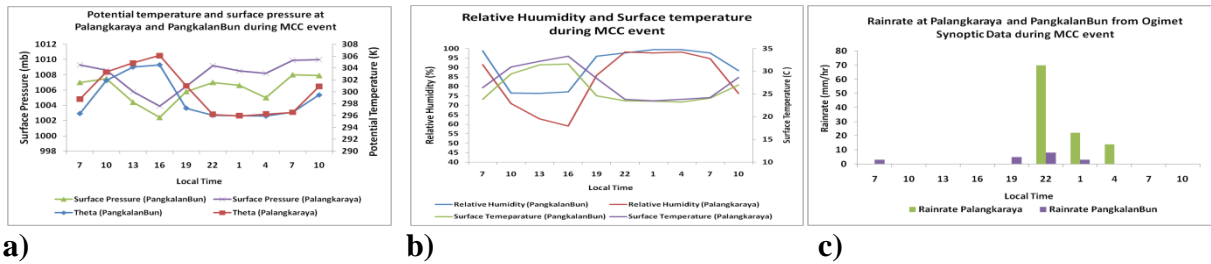


Figure 4.29. (a) Surface θ and surface pressure at Palangkaraya and Pangkalan Bun, (b) Relative humidity and surface temperature, and (c) Rainrate at Palngkaraya and Pangkalan Bun from OGIMET synoptic data during the continental MCC at 14 - 15 April 2012.

The observation data from OGIMET during the coastal MCC occurrence is shown in Figure 4.30. The cold pool seemed around at 1100 LT when the MCC migrated westward toward near Samarinda and Balikpapan during the decay stage. It indicated by the θ , and the surface temperature significantly decreased, but the surface pressure and relative humidity significantly increased at Samarinda and Balikpapan as shown in Figure 4.30 (left and middle). During the mature stage of MCC, the rainfall does not yet occur in Samarinda, but the rainfall occurs in Balikpapan. Heavy rainfall occurs during MCC dissipated due to the existence of the new convective system that migrated to Samarinda and Balikpapan. The new convective system that generated by the cold pool in MCC system migrated toward to the Kalimantan Island, and then heavy rainfall occurred in Muaratewe after MCC decayed.

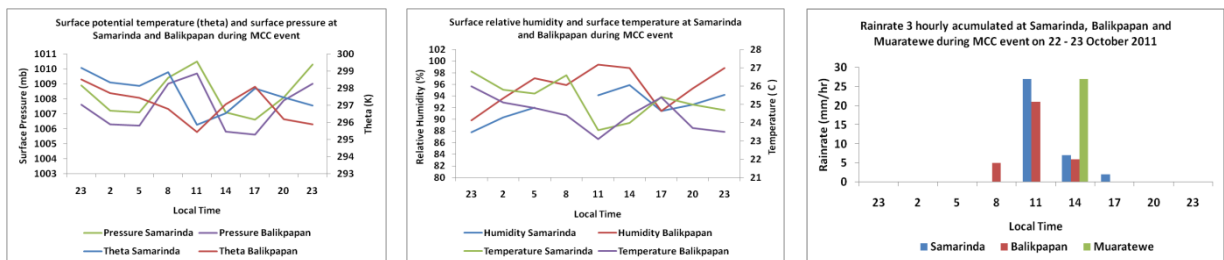


Figure 4.30. (left) Surface θ and surface pressure at Samarinda and Balikpapan, (middle) Relative humidity and surface temperature at Samarinda and Balikpapan and (right) Rainrate at Samarinda and Balikpapan from OGIMET synoptic data during the coastal MCC at 22 - 23 October 2011.

CHAPTER FIVE

THE LARGE-SCALE ENVIRONMENTAL CONDITION DURING THE CRITICAL STAGE OF MESOSCALE CONVECTIVE COMPLEXES (MCCs) OVER INDONESIAN MARITIME CONTINENT

The analyses of the environmental condition during MCC events have been described by several previous researchers in several regions in the world (e.g., Maddox 1983; Merritt 1985; Kane et al. 1987; Cotton et al. 1989; Augustine and Howard 1991; Laing 1996). In general, they found that the environmental conditions among some areas are very similar during MCC events, but several areas have different environmental conditions during MCC events. They show that certain thermodynamic patterns and dynamical features are usually present in the large-scale environments. This chapter explains the environmental conditions during critical stages of the MCC (initiation, mature, decay and dissipation or post-MCC) over IMC by using case study analysis and composite analysis. We adapt the method of Cotton et al. (1989) and Maddox (1983) for composite analysis of the environmental conditions and propagations of MCC. The ECMWF data in time resolution of 6-hourly is used for the analysis. This chapter is to strengthen the analysis in chapter 4 to give deeper insight into the mechanism of the development of the MCC-related to the environmental conditions. The result of this chapter will answer clearly the research objective about the mechanism of the development and the movement of the MCC over the IMC and the mechanism of the MCC in influencing rainfall over the IMC. However, the point of this chapter is to answer the research objective about the environmental conditions during MCC events.

The case studies that used in this chapter are the same with the case studies which have been described in chapter 4. The first case study in this research is the oceanic MCC that develops from midnight on 27 October 2007 until the early morning of 28 October 2007 over the Indian Ocean near Sumatra Island as illustrated in Figure 4.3. The second case study in this research is the continental MCC that occurred on 14 – 15 April 2012 as illustrated in Figure 4.5. The third case study in this research is the coastal MCC that occurred on 22 – 23 October 2011 as illustrated in Figure 4.7. The composite regions in this chapter were also similar to those already explained in chapter 4.

Several parameters from ECMWF data, which are available at 6-hourly intervals of $1^\circ \times 1^\circ$ horizontal resolution, were used for the analysis. The composite analysis for the environmental conditions during MCC determined by the average of environmental parameters just for the critical stages that occurred at 0000 UTC, 0600 UTC, 1200 UTC, and 1800 UTC due to the data is available in 6-hourly. However, in this study, we consider the data on time in 2300, 0000 and 0100 UTC are as the time on 0000 UTC, and the data on time in 0500, 0600 and 0700 UTC are as the time on 0600 UTC. We also considered the data on time in 1100, 1200 and 1300 UTC are as the time on 1200 UTC, and the data on time in 1700, 1800 and 1900 UTC are as the time on 1800 UTC. So that, we did a composite analysis of environmental parameters just for the critical stages that occurred at the time as mentioned above in each region. For example, from 45-cases of MCC composite region 3, but we just take 24-case during the initial stage that occurs in the time available data, 28-cases during the mature stage, 34-cases during the decay stage and 22-cases during the dissipation or post-MCC stage. So that, this composite analysis is the same as those for the surface wind which has been described in chapter 4. The detailed method has been explained in subchapter 1.4.2.3.

5.1 Condition over the initial region

The initial region of the MCCs for case study 1 was characterized by low-level convergence from the surface to 700 hPa and the strong upper-level divergence as shown in Figure 5.1 (b). In contrast, the strong upper-level divergence in case study 2 and 3 is not presented, just weak upper-level divergence is seen in Figure 5.2 (f) for case study 2 and Figure 5.3 (f) for case study 3. At 1000 hPa, the surface condition in the initial region of the MCCs shows that the depressed of surface θ in case study 1, 2 and 3 as illustrated in figure 5.1 (a), Figure 5.2 (a) and Figure 5.3 (a), respectively. However, in the case study 3, the lower θ is not clearly compared with the surrounding area. The θ is the temperature a parcel would have if it were to expand or compress adiabatically from its present pressure and temperature to a reference pressure level. In the troposphere, the θ typically increases with increasing height. Since colder air temperatures on an isobaric surface correspond to colder θ and warmer air temperatures on an isobaric surface, correspond to warmer θ , isentropic surfaces slope upward over a horizontal distance toward colder air. The colder temperatures typically associated with upper-level troughs are due to the southward transport of colder air

in the lower troposphere. Conversely, warmer temperatures linked to upper-level ridges result from the northward transport of warmer air in the lower troposphere.

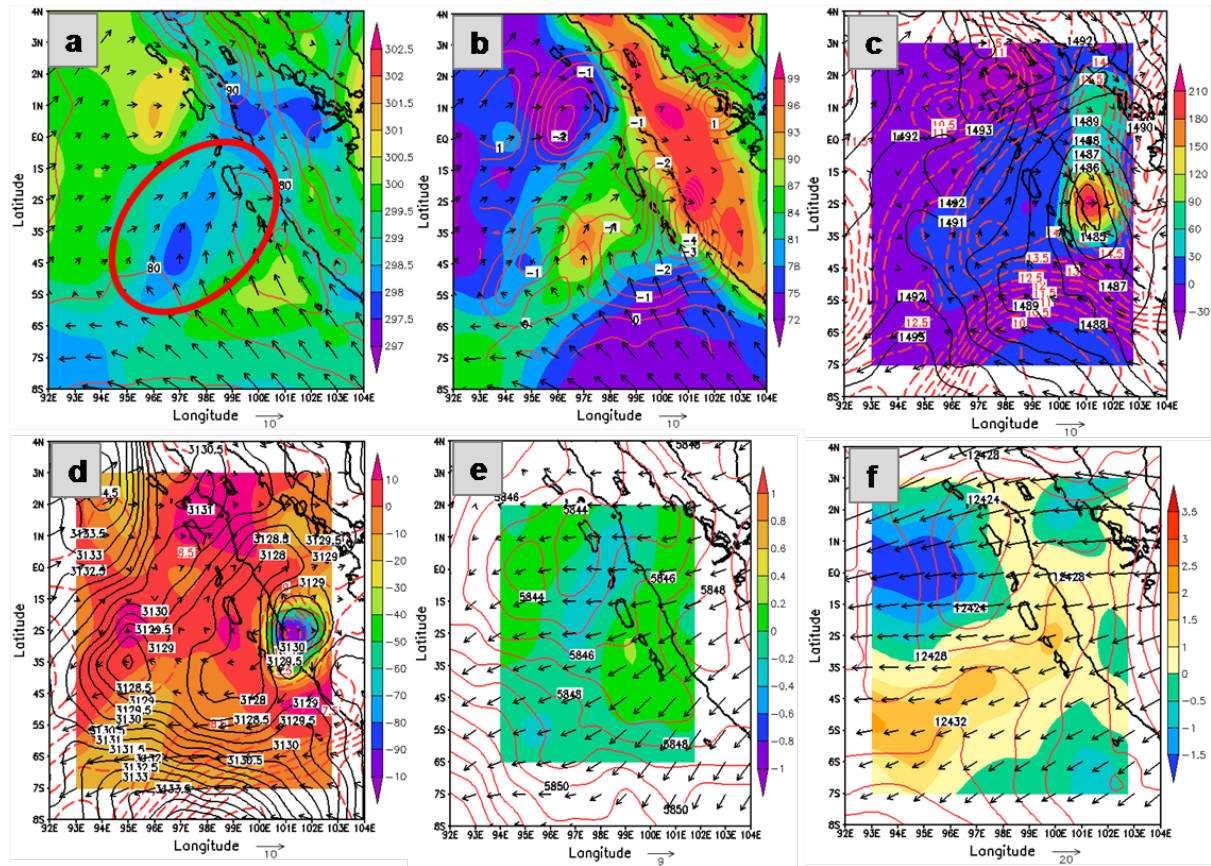


Figure 5.1. Environmental conditions during initial stage of the oceanic MCC in case study 1 using ECMWF ERA-Interim data, showing; (a). 1000-hPa θ (potential temperature in K, shaded), 1000-hPa geopotential height (m, contour) and 1000-hPa wind vector (ms^{-1} , vector). Red circle refers to the MCC location. (b). 1000-hPa divergence (10^{-5} s^{-1} , contour), 1000-hPa relative humidity (% , shaded) and 1000-hPa wind vector (ms^{-1} , vector). (c). 850-hPa geopotential height (m, black contour), 850-hPa MFC (moisture flux convergence in $10^{-3} \text{ g kg}^{-1} \text{ s}^{-1}$, shaded), 850-hPa mixing ratio (g kg^{-1} , red dotted contour) and 850-hPa wind vector (ms^{-1} , vector). (d). 700-hPa MFC (moisture flux convergence in $10^{-3} \text{ g kg}^{-1} \text{ s}^{-1}$, shaded), 700-hPa geopotential height (m, black contour), 700-hPa mixing ratio (g kg^{-1} , red dotted contour) and 700-hPa wind vector (ms^{-1} , vector). (e). 500-hPa geopotential height (m, contour) and 500-hPa vorticity advection (10^{-6} s^{-1} , shaded) and 500-hPa wind vector (ms^{-1} , vector). (f). 200-hPa divergence (10^{-5} s^{-1} , shaded), 200-hPa geopotential height (m, contour) and 200-hPa wind vector (ms^{-1} , vector).

The depressed θ with value $<298 \text{ K}$ coincided with the area of heaviest stratiform precipitation. In the case study 1 that occurred at midnight (around 0100 LT) over the sea, seen there is two regions of lower surface θ in the western coastal of the Sumatra and the Indian Ocean near Sumatra as an initial cloud of the MCC development that have been

explained in subchapter 4.1.2. In the case study 1, the initial region is not same with the mature region, but nearby the system due to the clouds system is not merged. So that, the decreased of surface θ due to the cold pool from the deep convective system and cloud system which will merger became MCC system. The cold pool has been explained in chapter 4. The cold pool also presented in the deep convective system as initial of the MCC development in case study 2 that occurred in the late afternoon (around 1900 LT). Similar to case study 1, the initial region in case study 2 is not same as the mature region, but nearby the system due to the clouds system is not merged. The cold pool of the MCC system does not yet begin during the initial stage. The cold pool also presented in the initial region of the case study 3 that occurred at midnight (around 0100 LT), but not clearly due to the decreasing of surface θ is not significantly.

The appearance of the cold pool is also supported by the high surface relative humidity. The large surface relative humidity also saw clearly in the initial region of the case study 1 (Figure 5.1(b)) which reaches more than 90%. The larger relative humidity, the moister air, which is vital for the development of clouds and precipitation. Sometimes can trigger mechanisms such as a front, outflow boundary or sea breeze moves in if the air will not have to rise much to reach saturation. A similar condition in the case study 2 as shown in Figure 5.2 (b), the surface relative humidity reached more than 90% in the initial region. In case study 3, the large surface relative humidity also found in the initial region but only around 80% as shown in Figure 5.3 (b). A local maximum in absolute humidity and a local minimum instability mark the favored region for formation of the convective systems that deep convective system is formed over there.

Figure 5.1 (a) and (b) shows the convergent surface wind flows as the land breeze triggered the development of some of the clouds on the western coast of Sumatra during initial stage in case study 1. At the same time, the westerly wind and strong southerly wind in the lower atmosphere triggered the development of some of the clouds over the nearby Indian Ocean. It also indicated by convergence pattern in the surrounding area of the initial region. Convergence means that more air is flowing into that region than flowing out. Since the air has to go somewhere, it rises, and rising air is what induces precipitation development. Heavier rainfall is often associated with regions of stronger ($>2 \times 10^{-5} \text{ s}^{-1}$) convergence. The opposite is true for areas of divergence, where more air is flowing out of the region than flowing in. To replace the net loss of air, air sinks from above and sinking air suppresses the development of clouds and precipitation. While the northerly wind flow that interaction with

the valley breeze is seen supports to the development of the MCC in the initial region of the case study 2 as shown in Figure 5.2 (a) and (b). Similar to the case study 1, this convergent wind is predicted transports the humidity. The westerly and easterly wind flows in the lower troposphere that indicated as the land breeze from Kalimantan and Sulawesi is supporting to processes grew the convection system in the case study 3. This convergent wind also transports humidity toward the system. In case study 1, convergence exceeded 10^{-5} s^{-1} over a wide area, approaching $2 \times 10^{-5} \text{ s}^{-1}$ near the convective apex at the initial region. Similar to the case study 2 that southerly convergence exceeded 10^{-5} s^{-1} over wide area toward to system. In case study 3, MCC occurred in near the convergence zone. The shortwave trough of geopotential height is presented from the south across the initial region in case study 1. However, from the west across the initial region in the case study 2 but it is absent in the case study 3 as shown in figure (a) and (b) in each Figure 5.1, 5.2 and 5.3.

The 850 hPa geopotential height, MFC field, wind field and mixing ratio, is shown in Figure 5.1 (c), Figure 5.2 (c) and Figure 5.3 (c). The geopotential height field is characterized a broad trough. In case study 2, the initial region is characterized by the longwave trough in the lower level of the troposphere. The clouds system also grew over the region between the higher MFC and less MFC that can generate the LLJ which important in MCC development. The region between higher and less MFC that hereafter mentioned as border front of MFC indicate the surface horizontal mass convergence is representative of a vertical circulation with the considerable slope. Such situations include not only warm fronts, but also subtle differences in boundary layer characteristics and depth arising from remnant outflow boundaries, differential cloud cover, or varying land surface characteristics. In these situations, localized regions of warm advection can result in sufficient lift for convective development. Furthermore, convective development may be horizontally displaced from the surface horizontal mass convergence maxima and rooted above the local boundary layer (and above a relatively cool air mass). Indeed, some forecasters look at horizontal mass convergence at levels above the surface, in search of areas where convective initiation may occur. Such scenarios may help explain the observed displacement of storms downstream of the surface MFC maxima (Hirt, 1982). Severe hail and locally heavy rainfall are the most common threats from such elevated storms, with the potential for tornadoes and damaging winds reduced owing to the stable near-surface stratification. Moisture ridge also presented over the initial region in case study 2 with the higher moisture around 14 g kg^{-1} . The moisture transported by southerly and northerly wind.

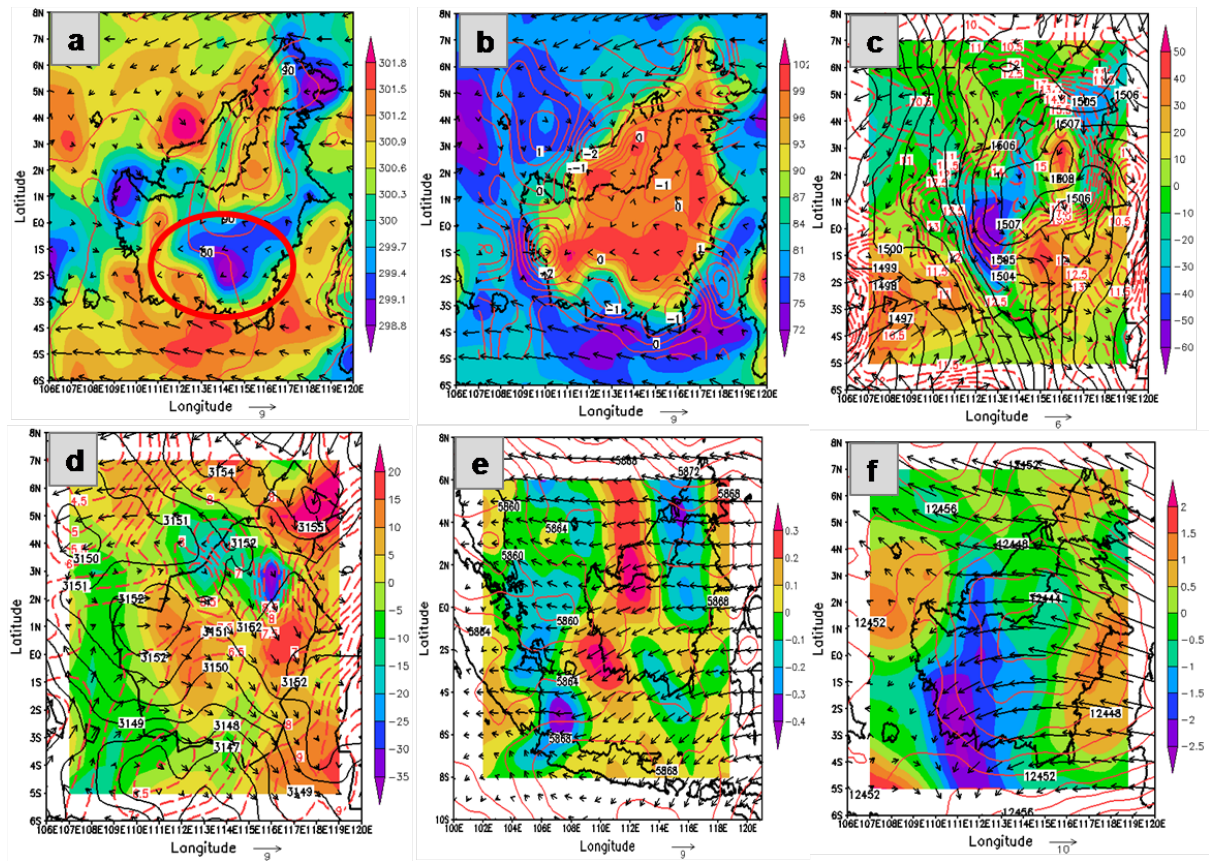


Figure 5.2. Same with Figure 5.1, but for the environmental conditions during the initial stage of the continental MCC in case study 2. The red circle in figure (a) refers to the MCC location.

In case study 1, a shortwave trough is becoming deeper at 850 hPa from the southern Sumatra and the Indian Ocean across the initial region that indicates to generate the weak LLJ as shown in Figure 5.1 (c). Thus, the LLJ stream is a current feature of the MCCs percussion environment. It is also supported by the strong warm advection, weak MFC and moisture advection that presents ahead of the trough and into the initial region with mixing ratios around 14 g kg^{-1} . It is similar with the USA MCC from the previous researcher that stated the LLJ, which is often present in the environments of MCCs from the United States (Maddox 1983; Augustine and Howard 1991; Anderson and Arritt 2001) and of long-lived MCSs over South America (Nicolini et al. 2002; Saulo et al. 2004; Salio et al. 2007). While Velasco and Fritsch (1987) show surface mixing ratios between 11 and 15 g kg^{-1} for MCC events over South America, the present analysis indicates mixing ratios at the lower end of this range for these serial MCS events. However, these lower surface mixing ratio values are typical for MCC events in the United States (Maddox 1983; Velasco and Fritsch 1987).

While the border region of the MFC is not clear seen in case study 1 at 850 hPa but it is presented at 700 hPa. A longwave trough of the geopotential height is also very clear from the north to south across the initial region that suggests a strengthening low-level flow over the initial region. Strong warm advection and moisture advection are present ahead of the trough and into the region of the initial region with mixing ratios above 14.5 g kg^{-1} as shown in Figure 5.2 (c) for case study 2 and Figure 5.3 (c) for case study 3. However, the initial region of the case study 3 is the core of the warm advection, where the mixing ratio is higher than the surrounding area. The low-level wind in this region, still northwesterly and southerly wind flow toward to system in case study 1, and westerly wind flow still support to development the system in case study 2, while the northerly wind still flows to the system in case study 3.

Figure 5.1 (d) shows that the 700 hPa geopotential field is disturbed by the existence of shortwave in the initial region of the case study 1. At the same time, the wind at level 700 hPa changes the direction became easterly flows. A 700-hPa shortwave trough is located on the southern edge of the initial region that likely generated the jet streak in the southern edge of the initial region. The atmosphere remains relatively moist, with mixing ratios above 8.5 g kg^{-1} ahead of the trough. It is also presented in the case study two but the longwave trough from the south to the north across the initial region as shown in Figure 5.2 (d). The mixing ratio is slightly less than the case study 1 around 6.5 g kg^{-1} . However, in the initial region of the case study 3 just seen the shortwave trough from the north toward to the system as shown in Figure 5.3 (d). The wind, height and moisture flux fields suggest that the long or shortwave trough is approaching the initial region. An important westerly flow and easterly flow of the case study 2 and 3, respectively is still apparent.

The 500 hPa pattern can also be used to locate where surface storms and precipitation are most likely to be occurring. Surface storms and precipitation are most often found over areas downstream of troughs (following the horizontal wind direction from a trough to a ridge). The reason for this is that rising air motion is forced in this part of the flow pattern. Rising motion means that surface air is forced to move upward toward the tropopause. In the atmosphere, clouds and precipitation develop where air rises. In case study 1, the initial region characterized by the region between two longwaves mid-level and upper-level trough or near of the center lower geopotential height. The longwave mid-level trough southward but in upper-level northward. The low geopotential height (compared to other locations at the same latitude) indicates the presence of a storm or trough at mid-troposphere levels. Positive

vorticity indicates counterclockwise rotation of the winds and lateral shear of the wind with the stronger flow to the right of the direction of flow. Negative vorticity indicates clockwise rotation of the winds and lateral shear of the wind with the stronger flow to the left of the direction of flow. Positive (or negative in the Southern Hemisphere) vorticity at 500 millibars is associated with cyclones or storms at upper levels and will tend to coincide with troughs in the geopotential height field. In case study 1, negative vorticity in 500 hPa is presented. Strong divergence is occurring in upper-level in initial region of case study 1 as shown in Figure 5.1 (f). While the wind flows dominantly westward at the level of 500 hPa and 200 hPa across the initial region of case study 1.

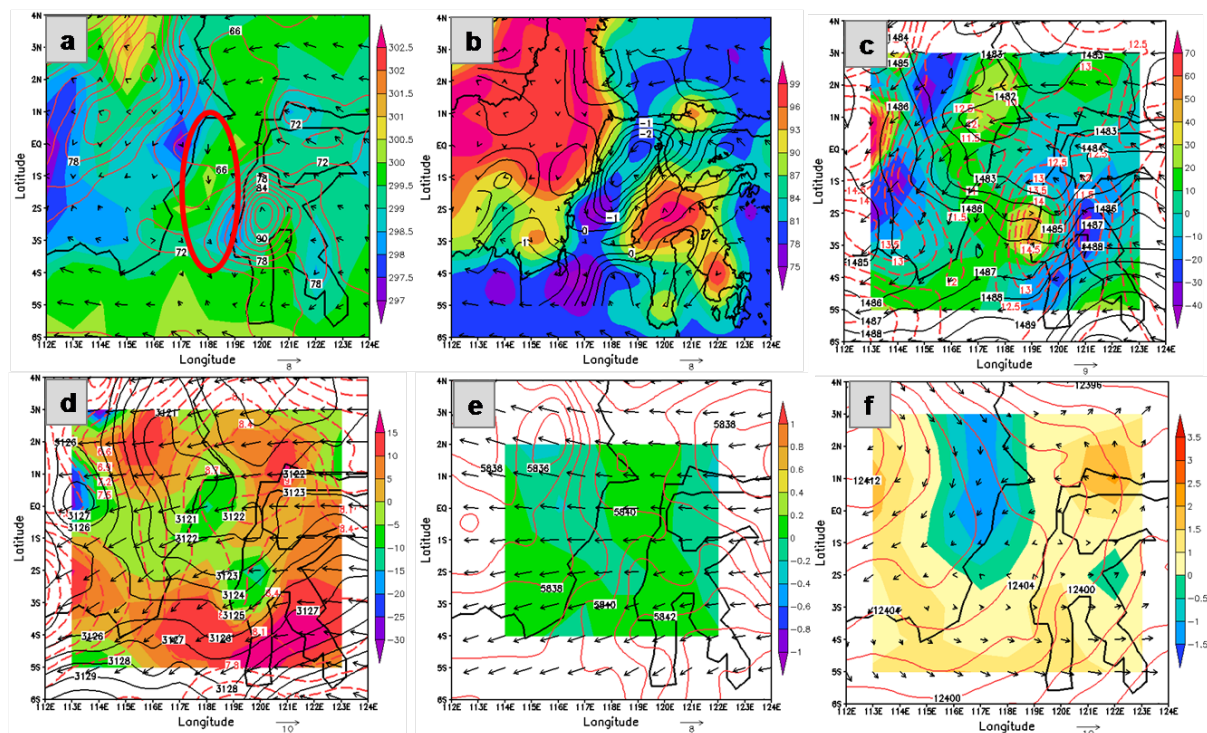


Figure 5.3. Same with Figure 5.1, but for the environmental conditions during the initial stage of the coastal MCC in case study 3. The red circle in figure (a) refers to the MCC location.

In case study 2, the initial region is characterized by a shortwave trough over the region near of the center lower geopotential height. The longwave mid-level trough eastward but in upper-level southward. Positive/negative/positive pattern of the vorticity advection in the trough area is presented in case study 2 over the initial region as shown in Figure 5.2 (e). It indicated the mid-level jet formed that support the development of the MCC. It is consistent with the several previous researchers that reported a weak mid-level shortwave is

approaching the initial area and enhances the low-level convergence associated with the LLJ (Maddox 1983, Cotton et al. 1989). The weak divergence at upper-level occurred in the initial region of the case study 2 as shown in Figure 5.2 (f). The presence of a low-level convergence and upper-level divergence couplet helps in maintaining the inflow and outflow of mass necessary for long periods of sustained deep convection. While the attendant release of latent heat further enhances the low- to mid-level convergence, thus continuously providing fuel for the MCC systems, but the latent heating is not shown in this research. Similar to case study 2, the shortwave trough in mid-level and upper-level is presented in an initial region of the case study 3 as shown in Figure 5.3 (e) and (f), but the mid-level trough is not seen clearly. The weak upper-level divergence also presented in case study 3.

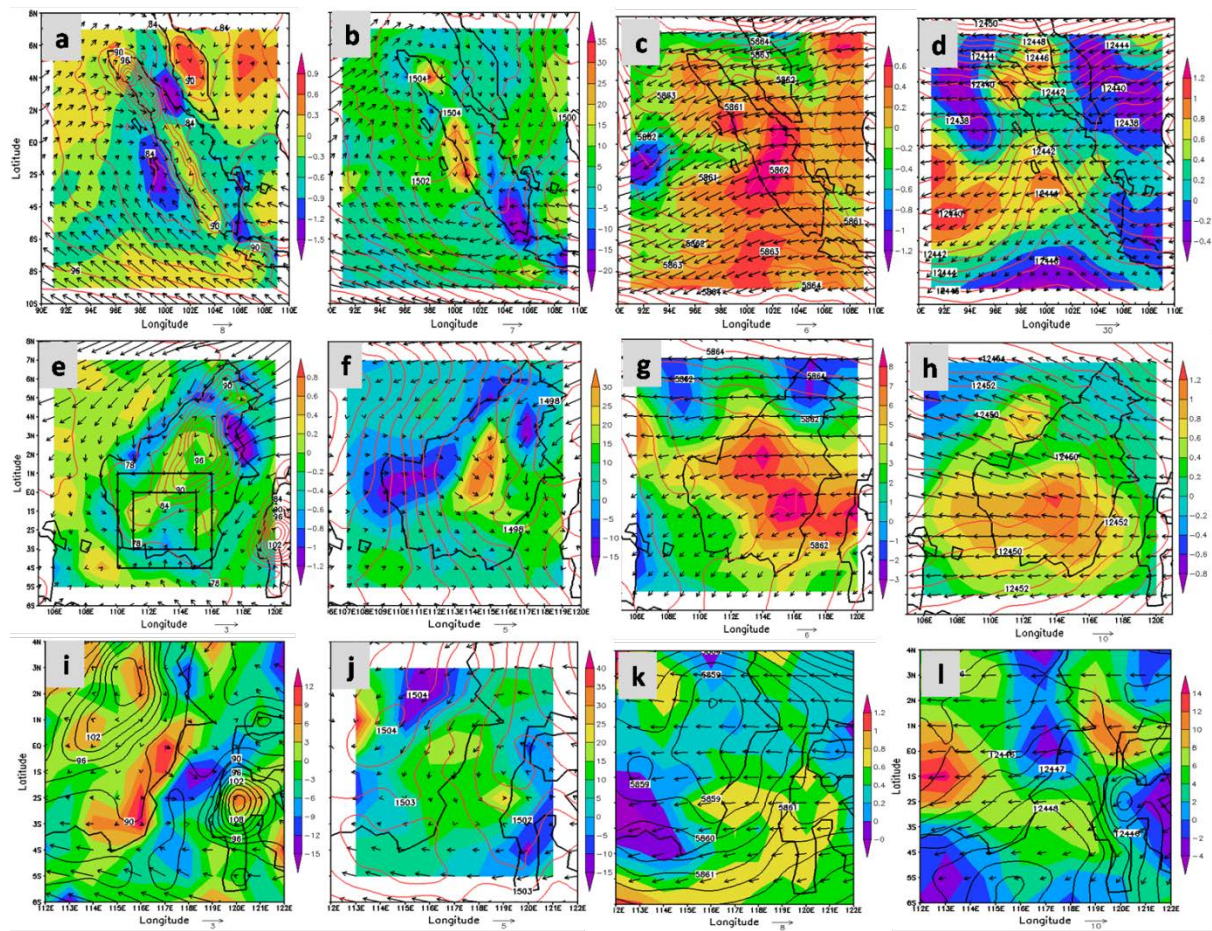


Figure 5.4. Composite analysis of the environmental conditions during initial stage using ECMWF ERA-Interim data, showing; in MCC composite region 2; (a). 1000-hPa divergence (10^{-5} s^{-1} , contour), 1000-hPa relative humidity (% , shaded) and 1000-hPa wind vector (ms^{-1} , vector); (b). 850-hPa geopotential height (m, black contour), 850-hPa MFC ($10^{-3} \text{ g kg}^{-1} \text{ s}^{-1}$, shaded) and 850-hPa wind vector (ms^{-1} , vector); (c). 500-hPa geopotential height (m, contour) and 500-hPa vorticity advection (10^{-6} s^{-1} , shaded) and 500-hPa wind vector (ms^{-1} , vector); (d). 200-hPa divergence (10^{-5} s^{-1} , shaded), 200-hPa geopotential height (m, contour)

and 200-hPa wind vector (ms^{-1} , vector). In MCC composite region 3; (e) same with (a), (f) same with (b), (g) same with (c) and (h) same with (d). In MCC composite region 5; (i) same with (a), (j) same with (b), (k) same with (c) and (l) same with (d).

Figure 5.4 shows the composite analysis for MCC composite region 2, 3 and 5. MCC composite region 2 is the similar region with the case study 1. MCC composite region 3 is the similar region with the region of the case study 2. MCC composite region 5 is the similar region with the case study 3. Comparison the case study 1 with MCC composite region 2 shows the MCCs that occurred in the region 2 have similar characteristics with the case study 1, among others; the initial region which characterized by strong low-level convergence from surface to 700 hPa and the strong upper-level divergence is also presented by the composite analysis as shown in Figure 5.4 (a) and (d). The strong convergent wind flow indicated as the southerly wind in the lower troposphere that interacted with the shortwave trough of height is presented too in the composite analysis as shown in Figure 5.4 (a) and (b). The mid-level shortwave trough and upper level longwave trough also appeared in the MCC composite region 2 as illustrated in Figure 5.4 (c) and (d). It indicated the consistency of the MCC composite region 2 with case study 1.

The weak low-level convergence as shown in Figure 5.4 (f) and the strong upper-level convergence also presented in MCC composite region 3, which strengthen the analysis of the case study 2. The convergent southerly wind flow supports the development of the MCC composite region 3 as shown in Figure 5.4 (e) that similar with the case study 3. At the same time, a significant easterly wind flow in the low-level and the westerly wind flow in the midlevel and upper-level in the initial region of the MCC composite area is consistent too with the case study 2. Similar to the case study 2, the initial region is also characterized by the mid-level and upper-level longwave trough as shown in Figure 5.4 (g) and (h) which triggered the growth of the convective system reaches the maximum extent of the MCC. The convergence in low-level as shown in Figure 5.4 (j) and upper-level divergence are also shown in MCC composite region 5 as the thorough understanding of the case study 3. However, there is slightly difference where the case study 3 presents the weak low-level convergence and upper-level divergence, but MCC composite region 5 presents the strong low-level convergence in the initial region. The initial region of MCC composite region three also characterized by the mid-level and upper-level shortwave trough as shown in Figure 5.4 (k) and (l). Similar to the case study 3, the trough is also an important role in the development of the MCC composite region. Overall, the composite analysis for all of MCC composite

regions shows the consistency with the case studies. It indicated the MCC that occurred in the region 2, 3, and 5 have the similar characteristics with the case study 1, 2, and 3, respectively.

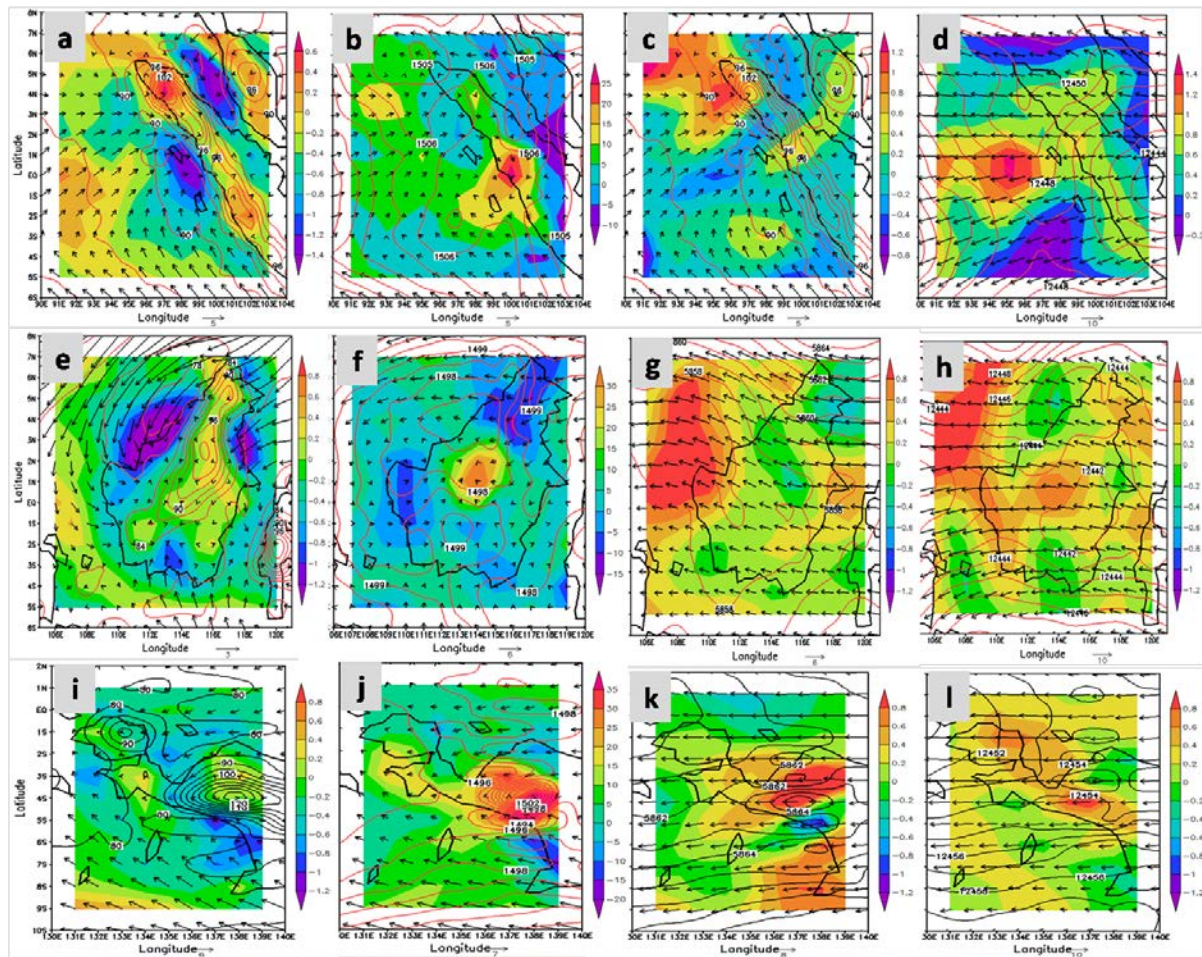


Figure 5.5. Same with Figure 5.4 but (a), (b), (c) and (d) for MCC composite region 1. (e), (f), (g), (h) for MCC composite region 4. While (i), (j), (k) and (l) for MCC composite region 6.

Figure 5.5 shows the composite analysis for MCC composite region 1, 4 and 6 during the initial stage. Almost of all the composite regions have similar characteristics for the initial regions. For example, the initial region is characterized by strong or weak low-level convergence and strong or weak upper-level divergence. The strong convergent wind flows in the lower troposphere that interacted with the shortwave trough of height is presented too in the composite analysis. The mid-level shortwave trough and upper level longwave trough also appears in the MCC composite region.

5.2 Condition over the mature region

During the mature stage, the low-level convergence is still presented in the case study one who interacted by the strong convergent wind flows indicated westerly and easterly wind as shown in Figure 5.6 (a) and (b). In contrast to case study 2, the MCC has left the region of surface convergence, and the mature stage is characterized by weak divergence in the southern edge of the system and still, exist of the weak convergence in the northern side. It is indicated by the northerly wind flow at the level of 1000 hPa as shown in Figure 5.7 (a) and (b).

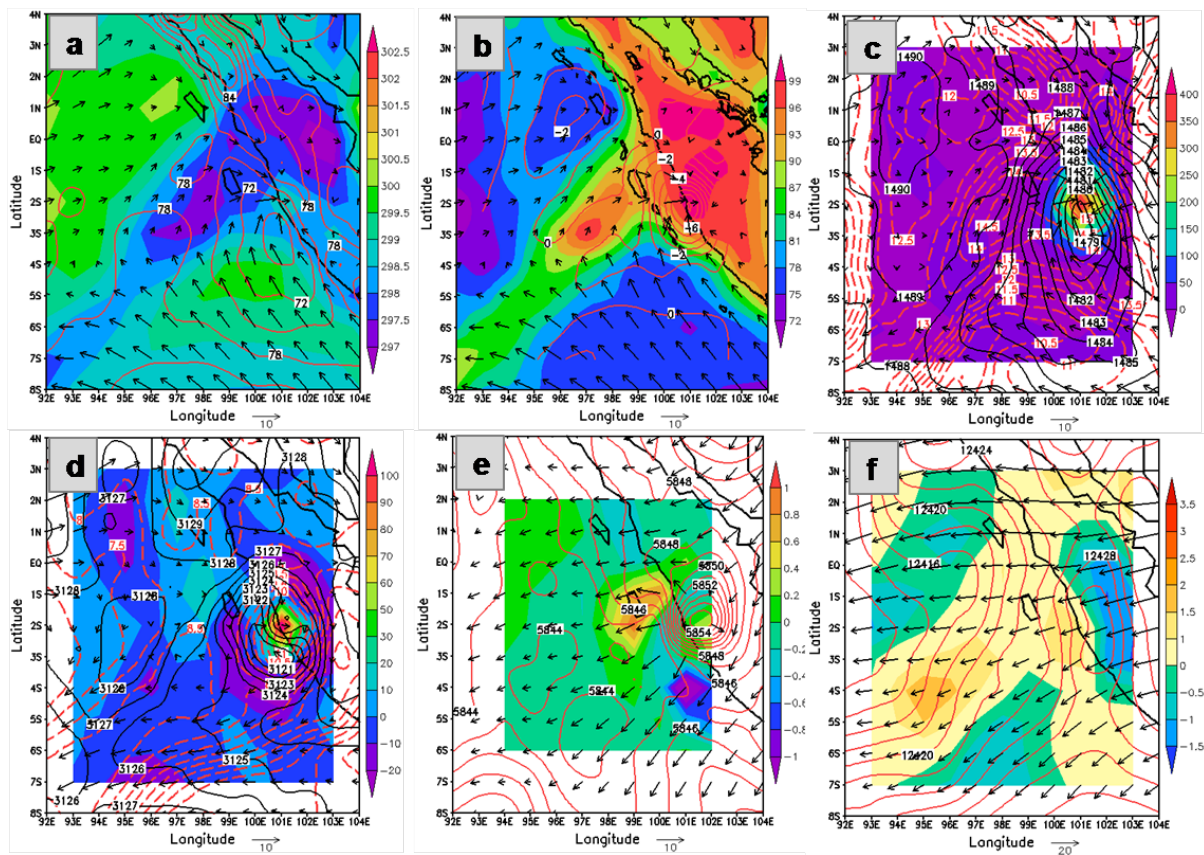


Figure 5.6. Same with Figure 5.1, but for the environmental condition during mature stage of the oceanic MCC in case study 1.

The low-level divergence at this stage reflect the dominant of precipitation-induced, tropopause cooling and rising reaches their maximum intensity at the mature stage, reflecting the contribution of mesoscale ascent and longwave radiative cooling by the upper-level cloud shield. It is consistent with Maddox 1983. Similar to the case study 2, the mature stage in the case study 3 is characterized by the weak divergence in the system and migrated westward from the MCC system that helped by the easterly wind as shown in Figure 5.8 (a) and (b).

Fritsch and Maddox (1981), Maddox et al. (1986), Wetzal et al. (1983) and Cotton et al. (1989) have observed that wind maxima are generally on the northern edges of mature MCCs and not within the interior cloud shield.

The lower surface θ is clearly presented in the initial region of the case study 1 and seen moving from the initial region. It indicated the merging of the clouds system in the initial region toward the mature region and the cold pool began in this region. However, that condition is not clearly in the case study 2 and 3 as shown in Figure 5.7 (a) and Figure 5.8 (a), where the case study 2 is nearly similar with the case study 3, the mature region is characterized by the region with significant differentiation of the θ zone. It is possible indicated the downdraft and updraft that occur in the system process between the higher and lower θ .

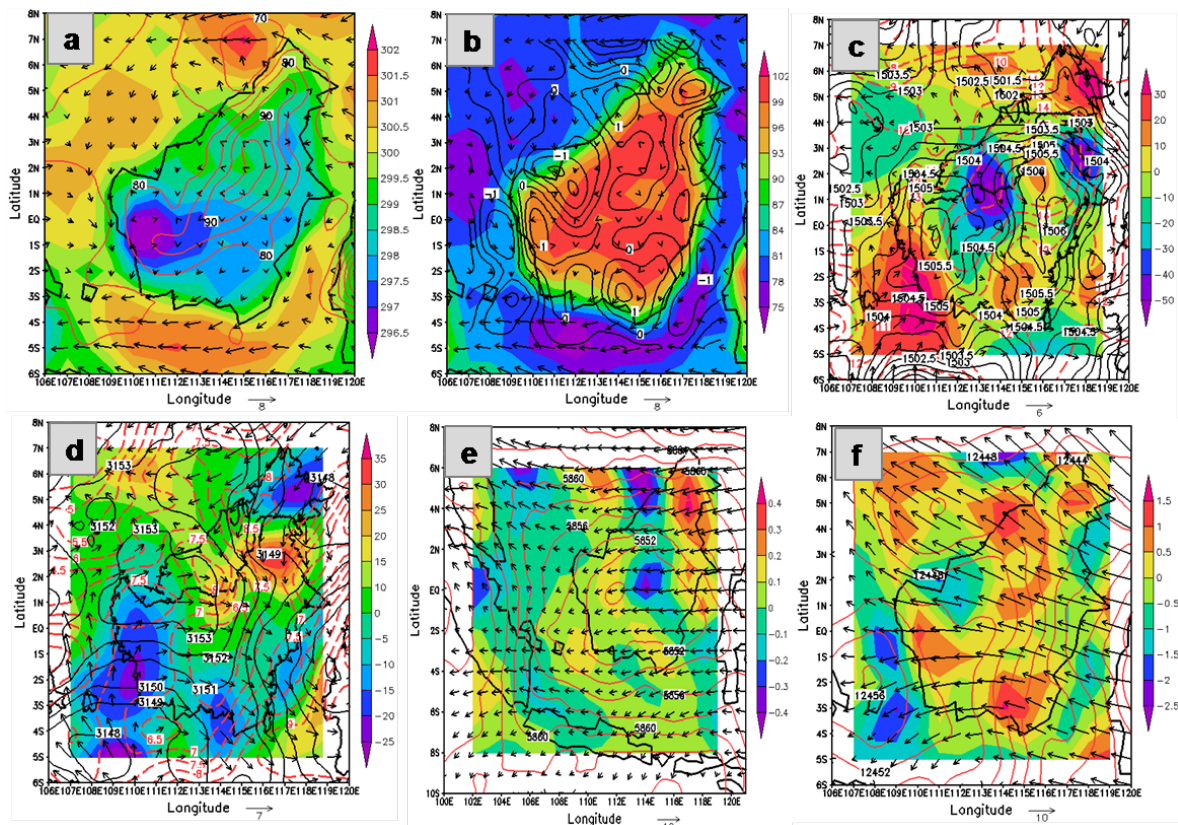


Figure 5.7. Same with Figure 5.1, but for the environmental conditions during mature stage of the continental MCC in case study 2.

The large surface relative humidity in 1000 hPa also seen clearly in the initial region of all case study, on average it is increased than the initial region as shown in Figure 5.6 (b), Figure 5.7 (b) and Figure 5.8 (b). The cold pool began to appear indicated by the lower surface θ than its surrounding areas and the relative humidity is also larger. A local maximum

in absolute humidity and a local minimum instability mark the favored region for formation of the convective systems that deep convective system is formed over there. The shortwave trough of geopotential height is still presented from the westward in initial region of the case study 1, shortwave trough southward in case study 2, while shortwave trough westward in case study 3.

The 850-hPa trough weakened at level 850 hPa that indicate generate the weak LLJ as shown in each case studies. In case study 1 as shown in Figure 5.6 (c), it is also indicated by the low-level wind convergence to the mature stage which transports moisture. Weak MFC and moisture advection that presents ahead of the trough and into the mature region then became the center of the higher mixing ratios around 14.5 g kg^{-1} , it is slightly increased from the initial region. It contrasted with Maddox 1983; Velasco and Fritsch 1987 that stated these lower surface is mixing ratio values are typical for MCC events in the United States. This condition is also found in case study 2 and 3 but the mixing ratio around 14 g kg^{-1} and 13.5 g kg^{-1} , respectively. The shortwave trough in level 850 hPa is deeper than the initial region for case study 2 and 3 as shown in Figure 5.7 (c) and 5.8 (c), respectively.

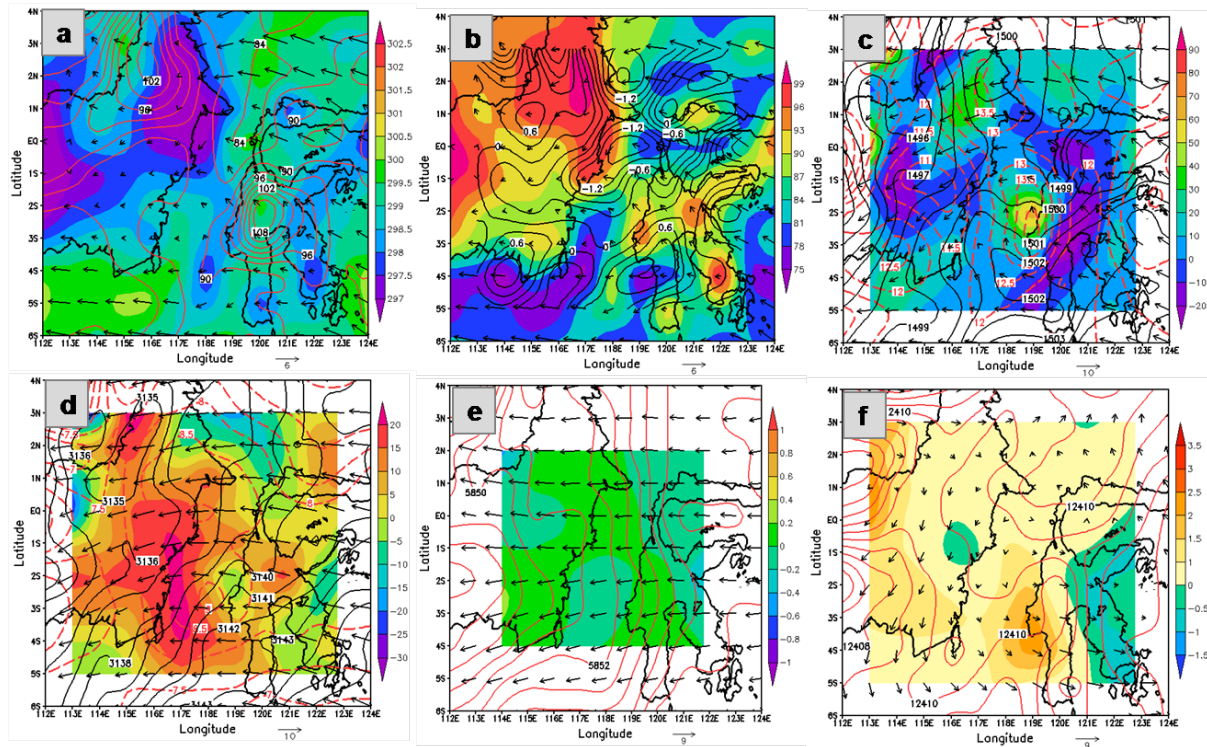


Figure 5.8. Same with Figure 5.1, but for the environmental conditions during mature stage of the coastal MCC in case study 3.

The characteristics of the front/border region between the positive of low-level MFC are still not seen in the mature region of the case study 1 as shown in Figure 5.6 (c). However, the strong low-level MFC is presented in a mature region of the case study 2 and 3 as shown in Figure 5.7 (c) and Figure 5.8 (c), respectively. This MFC is becoming stronger at the level of 700 hPa in the mature region of the case study 2 and 3. It condition shows that possible to generate the deep convection in this area still continue reaches the maximum extent of the MCC.

A 700-hPa longwave trough is located in the mature region still presented in all of the case studies as shown in Figure 5.6 (d), Figure 5.7 (d) and Figure 5.8 (d). The atmosphere remains relatively moist, with mixing ratios above 6.5 g kg^{-1} ahead of the trough for all of the case studies. A 700 hPa wind flow over the mature region also indicate significant changes. Flows over the mature region in case study 1 and case study 3 change became westerly, where flow in case study 3 has dramatically strengthened so that a distinct jet is present over the mature region. It indicates the moved westward of the system in case study 3. The flow over the mature region of the case study 2 is now easterly. The shortwave trough/ridge pattern is presented clearly over the mature region in case study 2 and case study 3, but not clear in case study 1. Bosart and Sanders (1981) noted similar characteristics with a long-lived convective system that they studied.

The longwave trough is still present in the level of 500 hPa that followed the pattern of the positive-negative of the vorticity advection that indicates there are process the development of the MCC in the initial region for all of the case studies as shown in Figure 5.6 (e), Figure 5.7 (e) and Figure 5.8 (e). However, in case study 1, the pattern does not clearly seem. The longwave trough is still presented at 500 hPa from the north across the initial region for case study 1 and 2, but not seen in case study 3 as shown in Figure 5.6 (e), Figure 5.7 (e) and Figure 5.8 (e). The initial region of case study 1 and 2 is located in the center of lower geopotential height in level 500 hPa but not for case study 3. in contrast at 200 hPa for case study 1, the longwave trough across the mature region from the south as shown in Figure 5.5 (f). The divergence on the upper-level is weak from the initial region of MCC as shown in Figure 5.6 (f) for case study 2 and in Figure 5.7 (f) for case study 3. However, the strong divergence wind is presented in case study 1 as shown in Figure 5.5 (f).

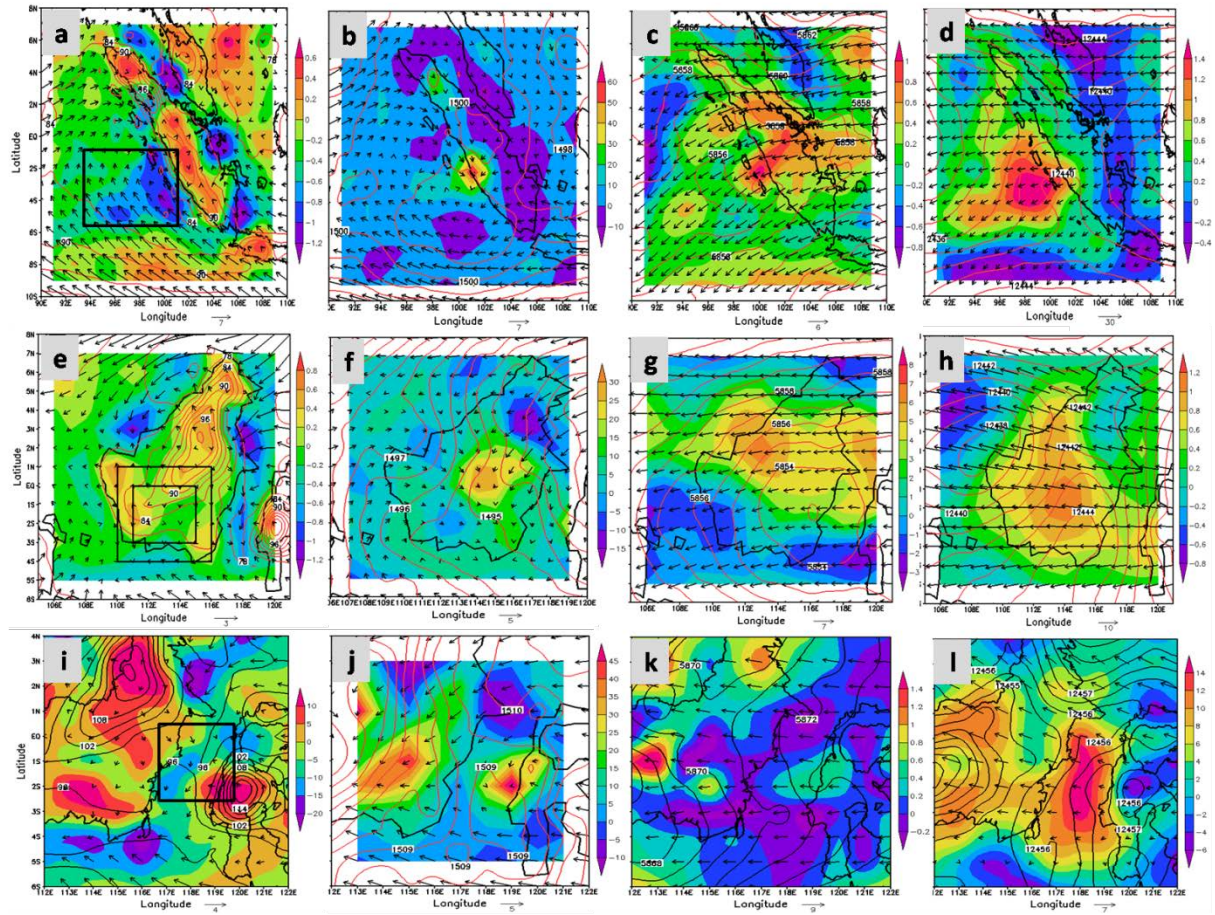


Figure 5.9. Same with Figure 5.4 but for the mature stage.

Figure 5.9 shows the composite analysis for MCC composite region 2, 3, and 5 during mature stage. MCC composite region 2 is the similar region with the case study 1. MCC composite region 3 is the similar region with the case study 2. MCC composite region 5 is the similar region with the case study 3. Comparison the case study 1 with MCC composite region 2 shows the MCCs that occurred in the region 2 have similar characteristics with the case study 1, among others; the initial region which characterized by strong low-level convergence from surface to 700 hPa and the strong upper-level divergence is also presented by the composite analysis as shown in Figure 5.9 (a) and (d). The strong convergent wind flow indicated as the southerly wind in the lower troposphere that interacted with the shortwave trough of height is presented too in the composite analysis as shown in Figure 5.4 (a) and (b). The central of lower pressure over the mature stage at the level of 500 hPa is also presented by MCC composite region 3 during mature stage. The upper-level trough over the mature seen very consistent with case study 1. The pattern of the MCC composite region 2 similar with case study 1.

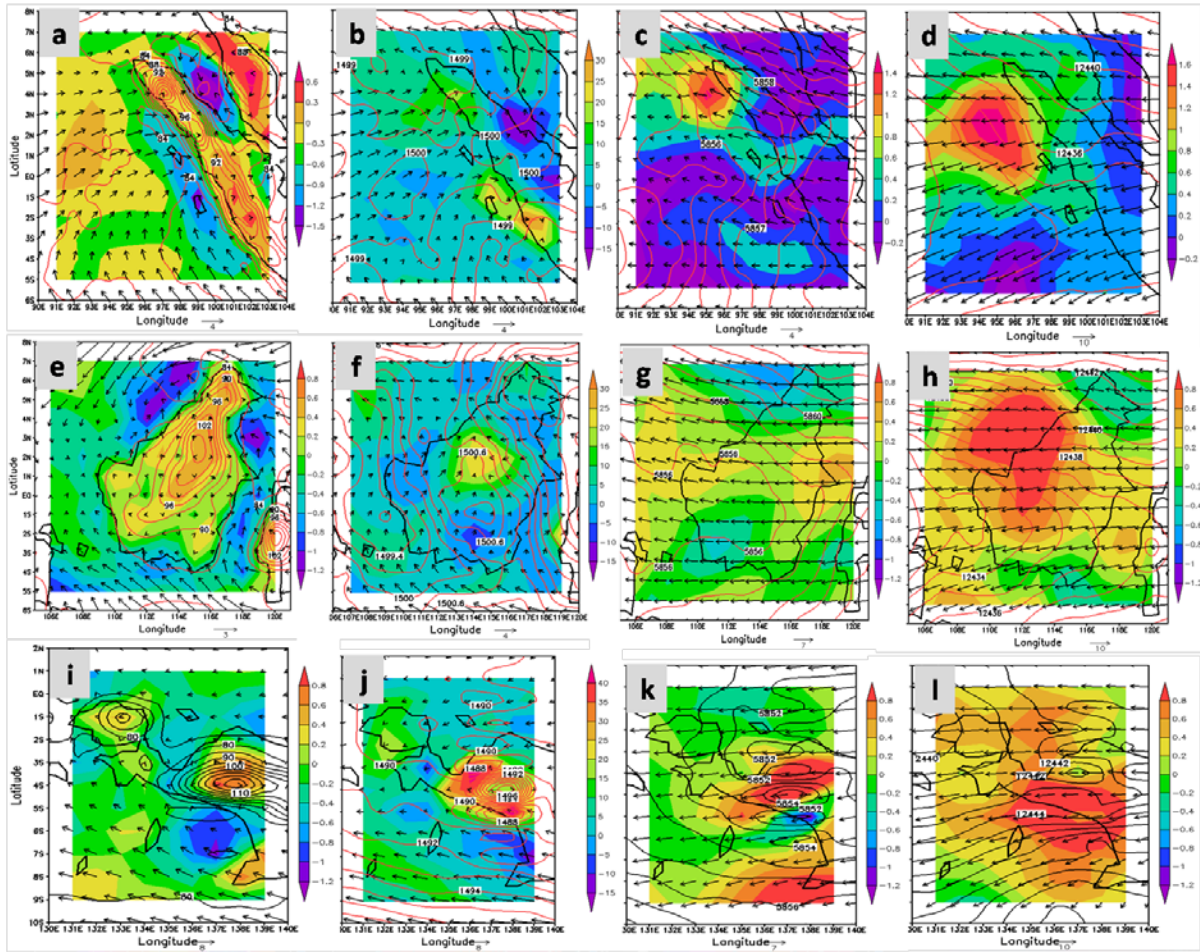


Figure 5.10. Same with Figure 5.4 but for mature stage; (a), (b), (c) and (d) for MCC composite region 1; (e), (f), (g), (h) for MCC composite region 4; and (i), (j), (k) and (l) for MCC composite region 6.

The composite 1000 hPa wind field over the mature region 3 show that the surface convergent southerly wind toward the system. However, the mature region is characterized by the weak low-level convergence and strong upper-level divergence over the mature stage of MCC composite region 3. It is slightly different with case study 2, wherein case study 2, just presents the weak upper-level divergence. Similar to the case study 2, the mature region is also characterized by the central of low pressure over the mature region of the MCC at the level of 500 hPa, and the shortwave trough over the positive/negative/positive pattern of vorticity during mature. The upper-level longwave trough is also presented across the mature region. It is consistent with case study 2. The mid-level and upper-level trough which triggered the growth of the convective system reaches the maximum extent of the MCC. Composite analysis for MCC composite region 5 shows clearly the low-level convergent and

upper-level divergent, it is slightly different with case study 3 which describe the weak low-level convergent and weak upper-level convergent. Similar to the case study 3, the trough is also an important role in the development of the MCC composite region. Overall, the composite analysis for all of MCC composite region are shows the consistency with the case study during the mature stage that indicate the MCC that occur in the region 2, 3, and 5 have the similar characteristics with case study 1, 2, and 3, respectively.

Figure 5.10 shows the composite analysis for MCC composite region 1, 4 and 6 during mature stage. Almost the composite region has similar characteristics for the mature regions, such as; the mature region characterized by strong or weak low-level convergence and strong or weak upper-level divergence. The strong convergent wind flow in the lower troposphere that interacted with the shortwave trough of height is still presented in the composite analysis. The shortwave trough is deeper than initial region, is also presented in MCC composite region. The mid-level shortwave trough and upper level longwave trough is also clearly appeared in the MCC composite region. It indicated the characteristics of the mature region of the MCC over IMC in several regions nearly similar.

5.3 Condition over the decay region

In case study 1, the decay region is still characterized by the lower surface θ as shown in Figure 5.11 (a). However, the lower θ seems separated or migrated southward, so that, the other lower center appears on the southern side of the system. It indicated the new convective system began generated by the cold pool. The center high geopotential height appears on the eastern side of the cold pool system. It indicated that the divergence field began to appear. The area that has lower θ also has the high surface relative humidity. However, the center of high relative humidity is moving to Sumatra Island as shown in Figure 5.11 (b).

The decay region in case study 1 also characterized by the weak surface divergence and convergence which still shown in Figure 5.11 (b). The weak convergence still exists in the eastern leading edge of decay region. It indicated that the weak upward motion still occurs in decay region. However, the strong convergence is start left the MCC area, is similar to Cotton et al. (1989). The central divergences are appearing over the system area, while the central convergences are moving to Sumatra Island. It indicated the propagation of the new convective system from the MCC system area toward the Sumatra Island helped by the divergences outflow from the system that interacted with the southerly wind in the lower

atmosphere. The strong surface wind flow is dominant southerly that predicted helping the propagation of the new convective system.

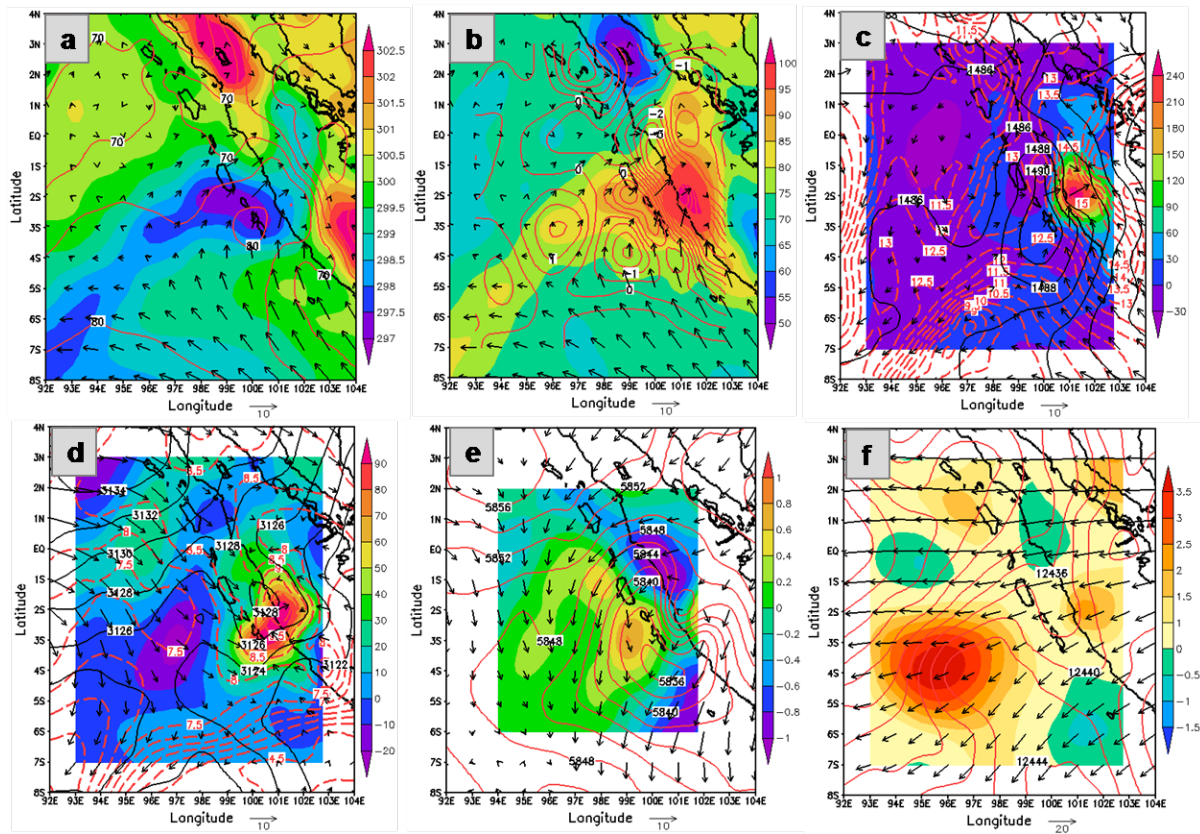


Figure 5.11. Same with Figure 5.1, but for the environmental conditions during decay stage of the oceanic MCC in case study 1.

In case study 2, the lower θ migrates westward as shown in Figure 5.12 (a). However, the higher surface relative humidity became widespread throughout to Kalimantan Island. The divergent surface wind flows due to land breeze circulation began to appear on the southern side of the system that propagates southward, but the weak convergence field still appears on the western side of the system. The decay region of the case study 3 is also characterized by the weak surface divergence as shown in Figure 5.13 (b). The region of higher surface relative humidity is also moving to the Kalimantan Island near of the system. Dominantly the surface convergent wind flows southward from the system.

At 850 hPa as shown in Figure 5.11 (c), Figure 5.12 (c) and Figure 5.13 (c). In case study 2, the MFC is begin left the MCC area to the western and eastern leading edge at 850 hPa but the high moisture flux divergence (negative value for MFC) in the south and north of leading edge of decay region. Figure 5.12 (c) shows that the MFC is strong in the north

leading edge and weak in the south leading edge. The weak MFC in the low-level and strong in the mid-level indicates that the downward motion began to occur in the south and north of leading edge, and possible from upper-level, but the MFC at upper-level is not shown in the figure. There is upward motion in the west and east of leading edge of decay region at low-level. Similar to case study 2, in case study 1 and case study 3, the higher MFC from low-level to mid-level is moving to Sumatra Island and Kalimantan Island, respectively. The trough/ridge/trough pattern is still presented, over the decay region of case study 2. However, the LLJ is seen in the southern of the system over the Java Sea, while the trough in case study 1 is not clear.

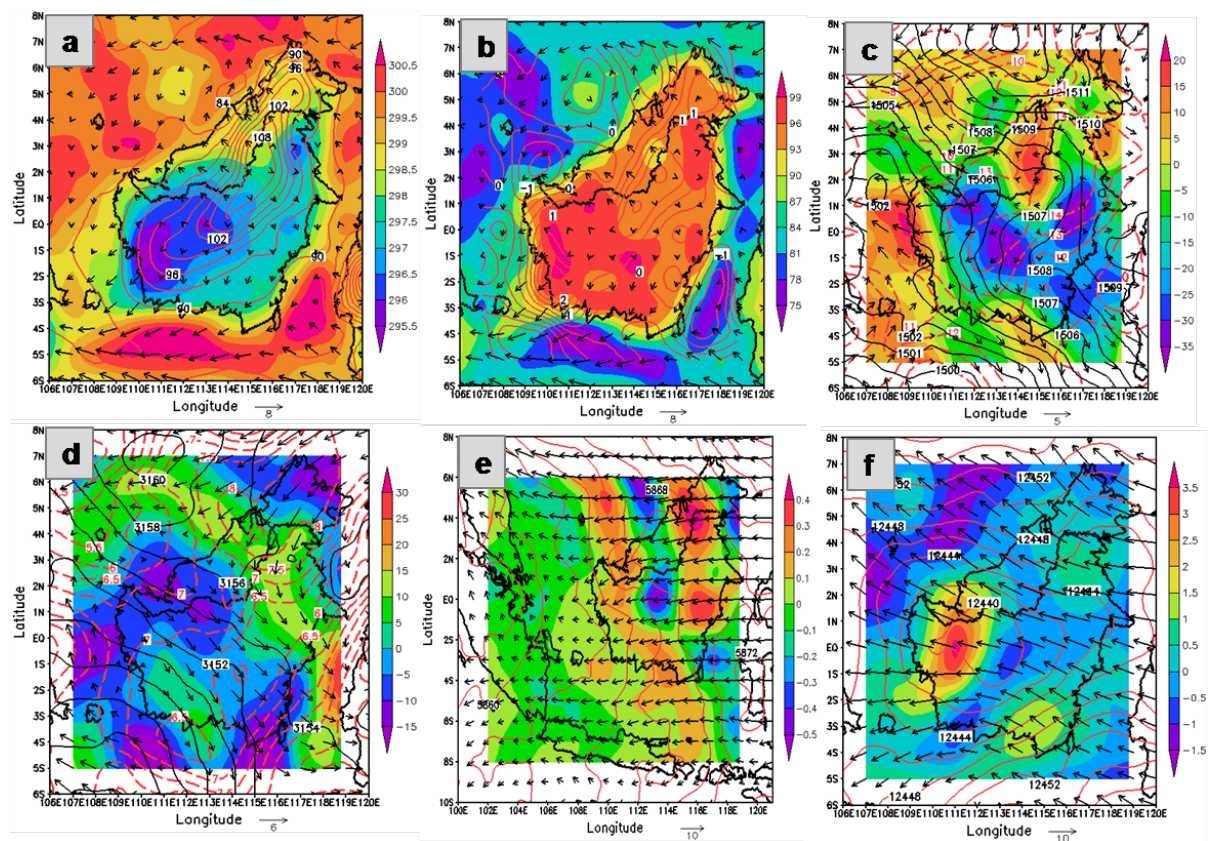


Figure 5.12. Same with Figure 5.1, but for the environmental conditions during decay stage of the continental MCC in case study 2.

At 700 hPa analysis during decay, the stage is shown in Figure 5.11 (d), Figure 5.12 (d) and Figure 5.13 (d) for case study 1, 2 and 3, respectively. A ridge of high moisture content is moving eastward with the system for case study 1 that transported by the wind flow at the level of 850 hPa and 700 hPa. While for the case study 2 and 3, is moving southward and westward, respectively. It indicated the propagation direction of the new convective

system. The mixing ratio decreased during the decay since the mature stage, where the decrease around 1 g kg^{-1} for all cases. The shortwave trough remains meridional of geopotential height still found in decay region at 850 hPa and 700 hPa, is similar with Maddox (1983) that stated the shortwave trough is very pronounced in the height and temperature field.

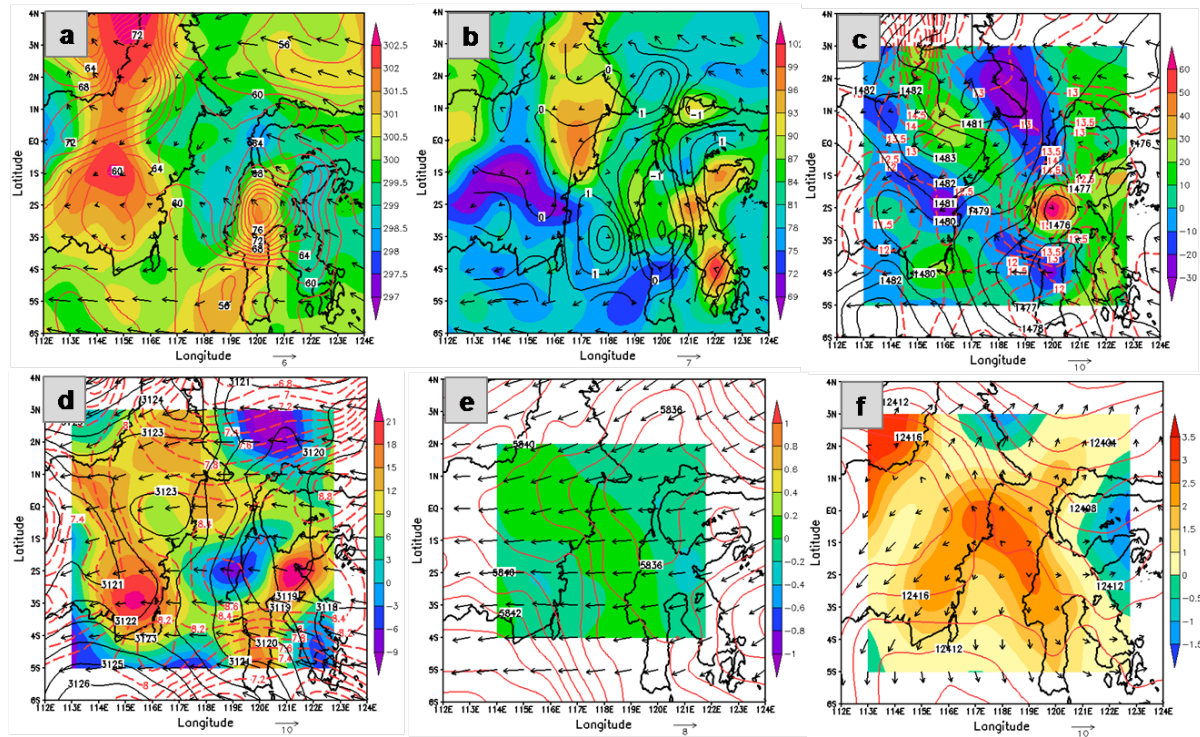


Figure 5.13. Same with Figure 5.1, but for the environmental condition during decay stage of the coastal MCC in case study 3.

At 500 hPa, the shortwave mid-level trough is very pronounced in height, and the wind fields are well balanced with the height field as shown in Figure 5.11 (e) in case study 1. While in case study 2 and 3, the wind fields are not balanced with the height field. At 200 hPa for the case study 1, the longwave trough across the decay region from as shown in Figure 5.11 (f) which followed the strong upper-level divergence. In contrast with case study 2, the upper-level divergence does not seem in decay region, but the divergence/convergence/divergence pattern is presented over the decay region. However, case study 3 is almost similar to the case study 1, where the upper-level divergence occurred over the trough of the decay region of case study 3. The upper-level wind flows dominantly westward over the decay region.

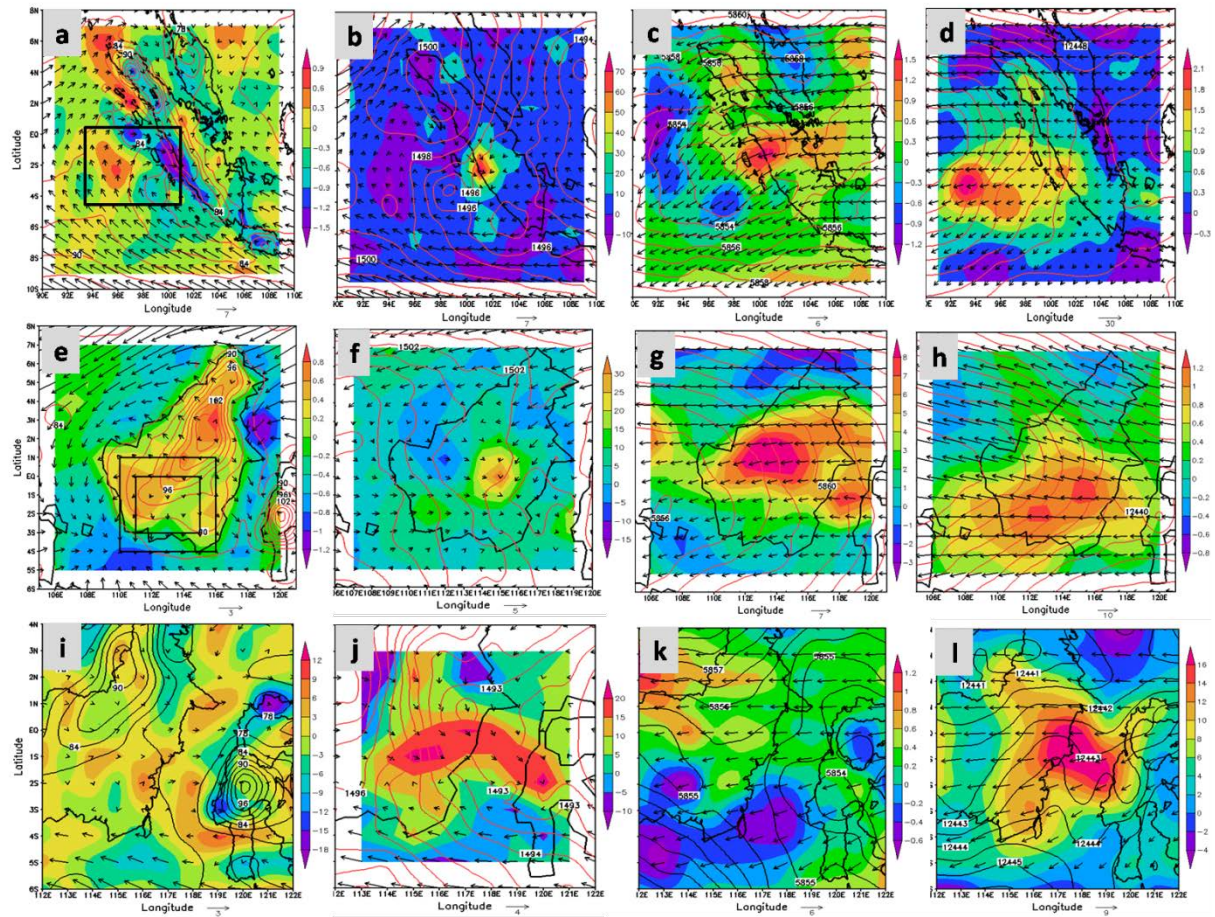


Figure 5.14. Same with Figure 5.4 but for decay stage.

Overall, from the case study, the decay region is characterized by the weak divergence and convergence. Its characteristics is also described in composite analysis. MCC composite region 2 in Figure 5.14 (a) shows that the weak divergence in the western side of the system, while the weak convergence still exists on the eastern side. It is similar to the case study 1. Surface analysis of MCC composite region 3 shows that the weak divergence has been appearing on the northern side of the system, while the weak convergence is presented on the southern side of the systems. It was also consistent with the case study 3. Consistency between composite analysis and case study also shown by the MCC composite region 5, where the weak divergence is observed in the western edge of the system, while on the eastern edge of the system still found the weak convergence. The resulting analysis from composite was also consistent with the case study about the MFC at 850 hPa which moving eastward, southward and westward for case study 1, 2, and 3, respectively. The consistency also showed by the trough pattern in each level that is nearly similar between case study and

composite analysis. The composite analysis also shows the weak or strong divergence in upper-level for each case.

Figure 5.15 shows the composite analysis for MCC composite region 1, 4 and 6 during decay stage. Comparison the case study, during decay stage, almost of all the composite region have similar characteristics for decay region, such as; the weak divergence and convergence is presented in the surface level. The weak or strong divergence is presented in upper-level. During decay, the shortwave trough still appears in the level of 850, 500 and 200 hPa.

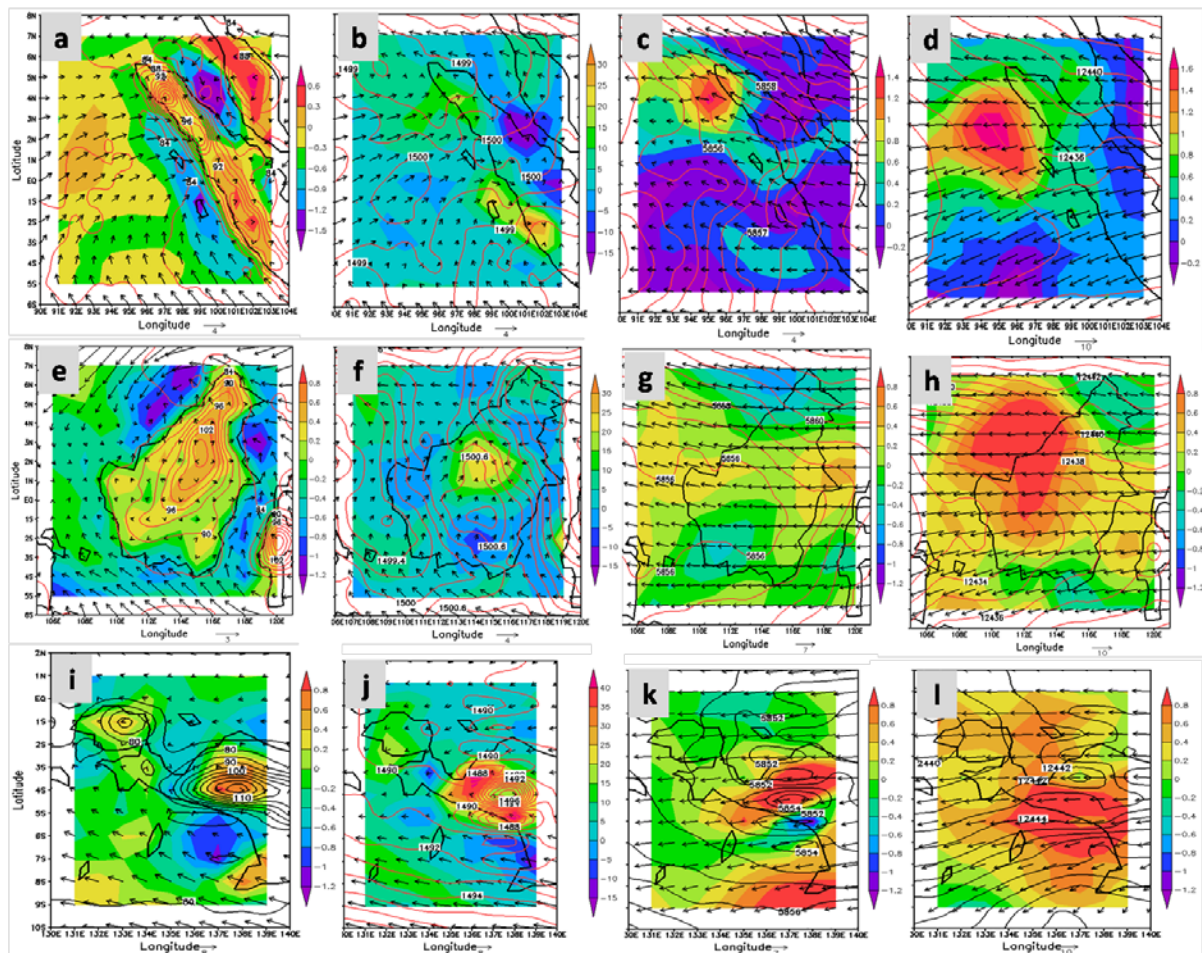


Figure 5.15. Same with Figure 5.4 but for decay stage; (a), (b), (c) and (d) for MCC composite region 1; (e), (f), (g), (h) for MCC composite region 4; and (i), (j), (k) and (l) for MCC composite region 6.

5.4 Condition over the dissipation or post-MCC region

The region of lower surface θ is already moving eastward to Sumatra for case study 1 as shown in Figure 5.16 (a) and moving southward to Sumatra and Java Islands for case study 2 as shown in Figure 5.17 (b). At the same time, the cold pool began dissipated.

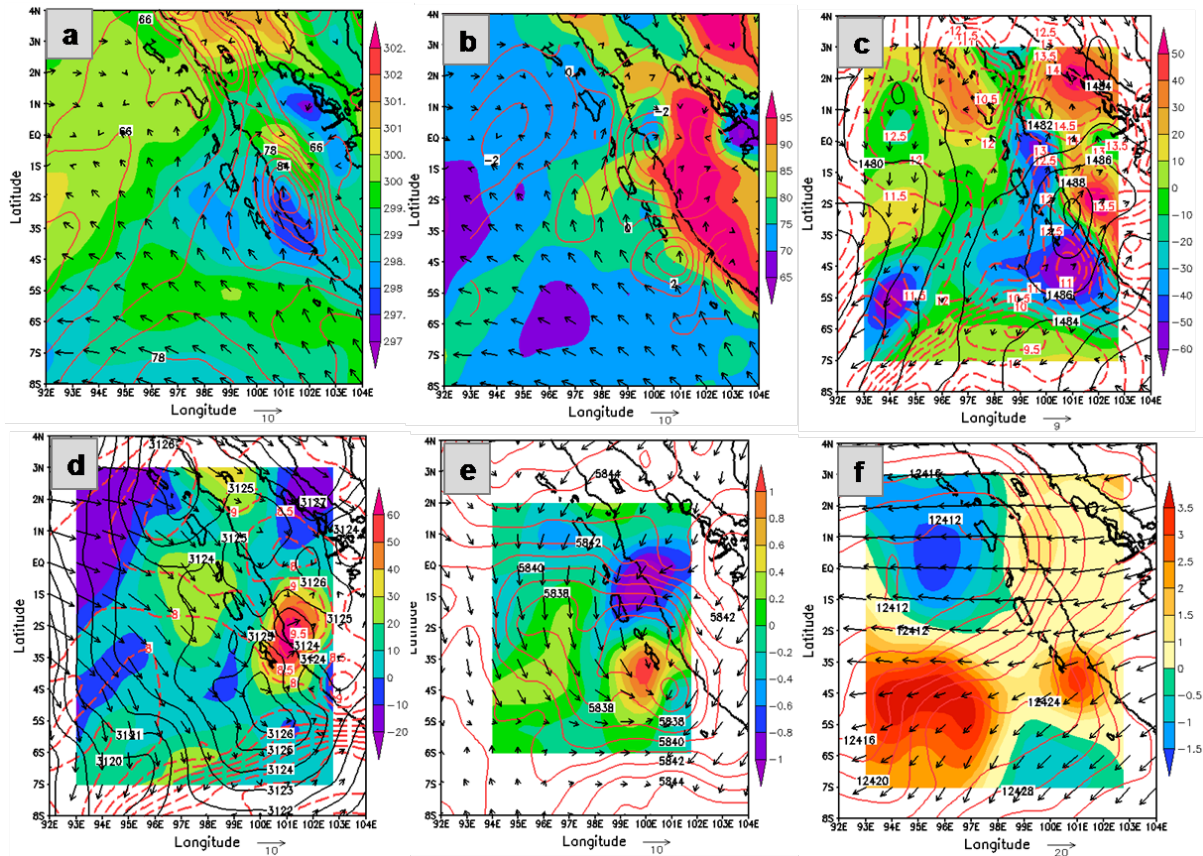


Figure 5.16. Same with Figure 5.1, but for the environmental conditions during dissipation or post-MCC stage of the oceanic MCC in case study 1.

In case study 1, the surface convergent wind flows indicated the easterly and westerly wind in the lower atmosphere which predicted helping the propagation of new convective system that generated by the cold pool. While, in case study 2, the surface convergent wind flows that indicated as land-sea breeze helping the new convective system moving southward. The center high of geopotential height is also presented over the region of the lower troposphere. The dissipation region is characterized by the strong surface divergence as shown in Figure 5.16 (b). In case study 1, the surface convergence zone is moving over the western coast of Sumatra, which also followed the region of high relative humidity. In the case study 2, the surface convergence zone is moving to the Java Sea. The relative humidity is dramatically decreased in dissipation region of the case study 2.

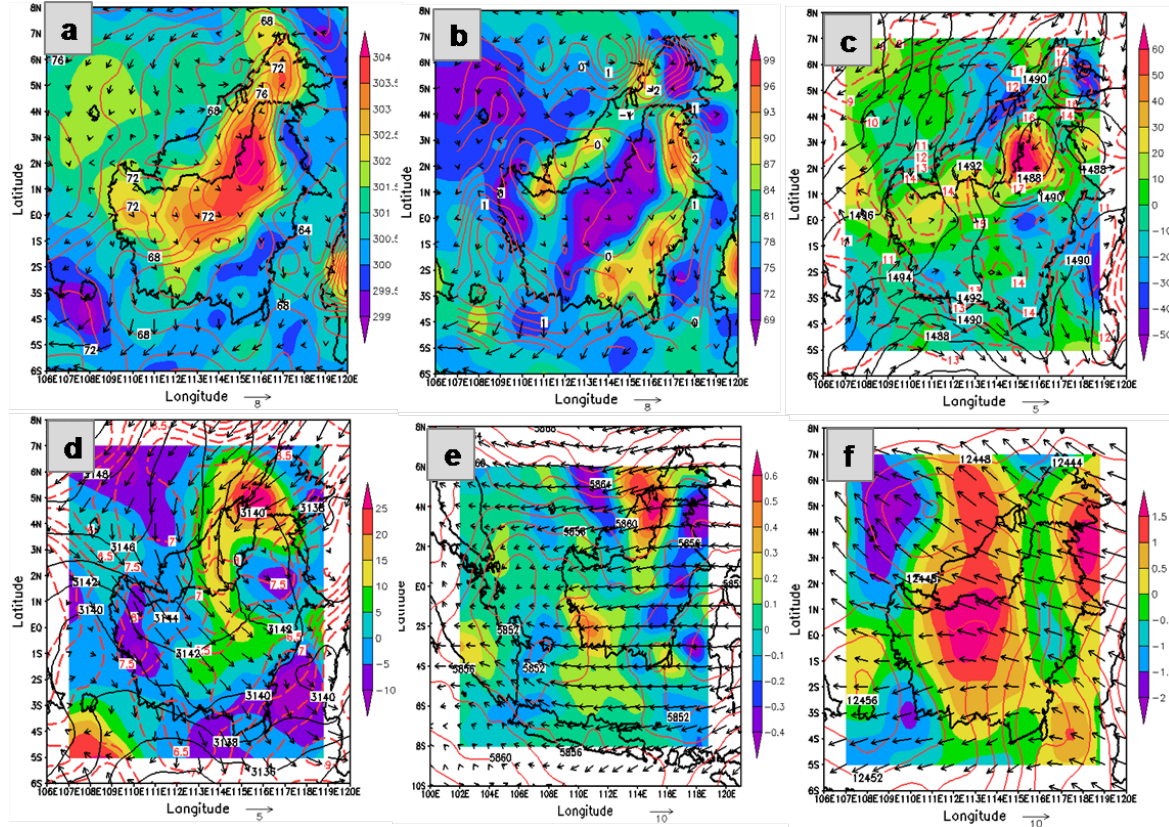


Figure 5.17. Same with Figure 5.1, but for the environmental conditions during dissipation stage or post-MCC of the continental MCC in case study 2.

At 850 hPa, in case study 1 and 2, the dissipation region is characterized by the negative MFC, and mixing ratio decreased. The shortwave trough is also moving eastward and westward for case study 1 as shown in Figure 5.16 (c) and moving southward in case study 2 as illustrated in figure 5.17 (c). The mid-level and upper-level trough are also moving from the decay region as shown in Figure 5.16 (e) and Figure 5.17 (e). The strong upper-level divergence is also moving westward and eastward for case study 1 as illustrated in figure 5.16 (f), while for case study 2, the divergence upper-level moving to the north of the system as shown in Figure 5.17 (f). Overall, the composite analysis for all of MCC composite region as illustrated in Figure 5.18 shows the consistency with the case study during dissipation or post-MCC stage. It indicated the MCC that occur in the region 2, 3, and 5 have the similar characteristics with the case study 1, 2, and 3, respectively.

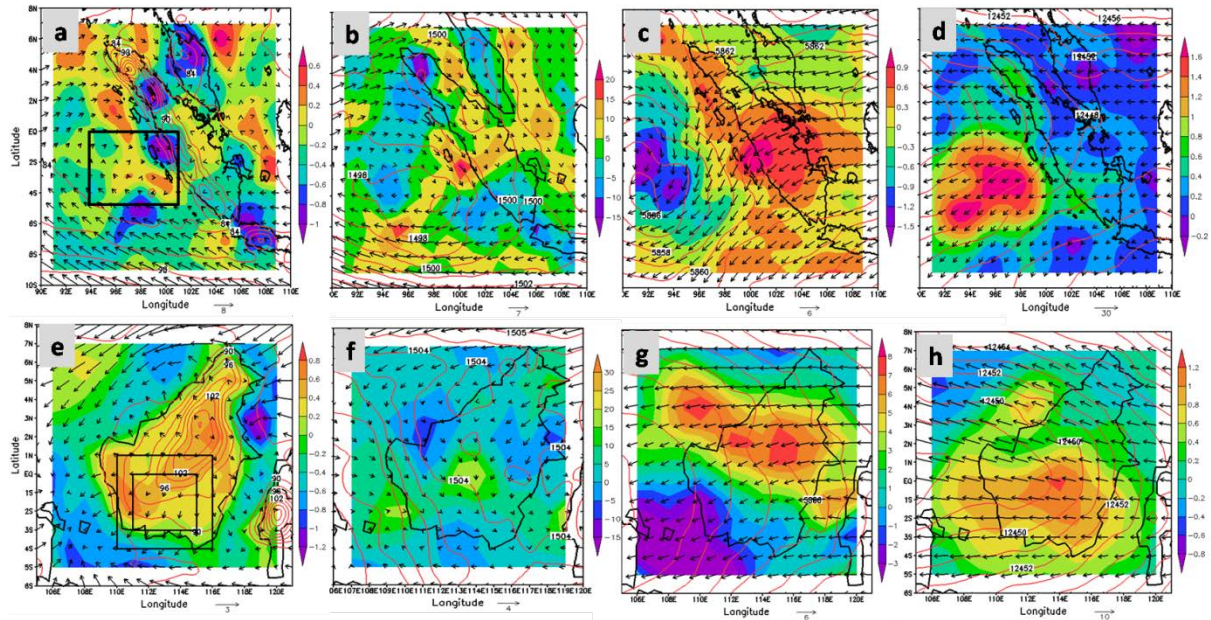


Figure 5.18. Same with Figure 5.4 but for dissipation stage.

5.5 Vertical cross section analysis

5.5.1 Divergence and vertical velocity field

Divergence is mean to denote depletion of mass, while convergence is meant to denote accumulation of mass, the forecaster is concerned with the mass divergence or mass convergence in estimating pressure or height changes. Mass divergence in the entire column of air produces pressure or height falls, while mass convergence in the entire column of air produces pressure or height rises at the base of the column. Negative divergence is sometimes called convergence. The vertical velocity at 700 hPa is shown instead of accumulated precipitation for the analysis. Negative values indicate ascending air, and positive values denote sinking air. Ascending motion is associated with cloudiness and rain. Large negative values of vertical velocity correspond to areas of heavy rainfall if moisture is available.

The vertical distribution of divergence and vertical velocity during MCC life cycle of the oceanic MCC in the case study 1 is presented in Figure 5.19. Low-level convergence at the initial stage is relative strong around $25 \times 10^{-5} \text{ s}^{-1}$. Surface convergence is confined to the lower half of the troposphere (from surface until 800 hPa), at the same time, strong divergence prevails above 800 hPa until 500 hPa around $25 \times 10^{-5} \text{ s}^{-1}$ as shown in Figure 5.19 (a). The condition is still continued until merging the clouds system from the west that helped by the westerly and easterly wind. It also helped by the land breeze or mountain breeze due to the initial stage occur in the midnight. The development of the MCC in this stage also helped by the strong southerly wind. The upward process in the growth of the cloud has been started

in this stage with averaged vertical velocity around $20 \times 10^{-2} \text{ Pa s}^{-1}$. By the mature stage, as shown in Figure 5.19 (b), convergence has strengthened through a low level (surface - 700 hPa), and strong upper-level divergence has developed a sharp maximum at 300 hPa. The convergence zone in the MCC surrounding area at the surface that shown in the initial stage is not seen in the mature stage. It indicated that the clouds system is already merging with each other to reaches maximum extent of the MCC. The updraft also becomes stronger with the averaged vertical velocity around $-40 \times 10^{-2} \text{ Pa s}^{-1}$. The surface convergent wind flows are still strong at this stage. The upward became an increase in the systems. The surface convergent wind flows as the westerly and southerly wind is still presented at this stage.

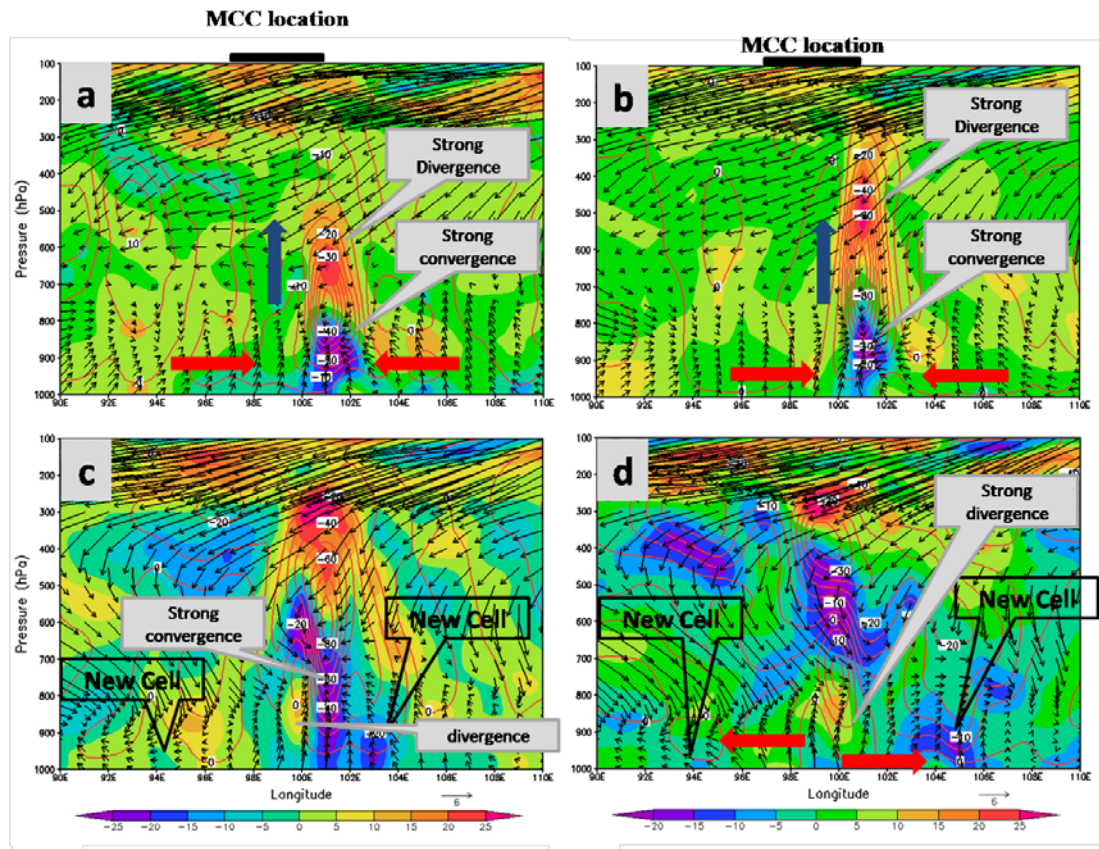


Figure 5.19. Pressure-longitude cross section (averaged for latitude $6^{\circ}\text{S} - 0^{\circ}\text{N}$) of divergence (10^{-5} s^{-1} , shaded), vertical velocity ($10^{-2} \text{ Pa s}^{-1}$, contour) and horizontal wind (vector; ms^{-1} ; upward represents northward) for MCC case study 1 using ECMWF ERA-Interim data, during (a) initiation (0100 LT), (b) mature (0700 LT), (c) decay (1300 LT) and (d) Post-MCC (1900 LT). Red arrow shaded to indicate the convergence wind and blue arrow shaded to illustrate the updraft motion.

At the decay stage, as shown in Figure 5.19 (c), the convergence become grew and expanded to the level of 500 hPa. The divergence also expands until 200 hPa. However, the weak divergence start appears on the western side of the system. The new convective system

began generated in the western and eastern side of the MCC system. At 3 hours after MCC dissipated or post-MCC stage as shown in Figure 5.19 (d), the surface convergence is no longer evident over the large averaging area. However, the convergence appears in a deep mid-tropospheric layer (800 - 400 hPa), while the strong divergence is presented in the low-level. The strong divergence also presents in the upper-level. This condition indicates that downdraft process already occurs in the system. Several new convective systems have been generated and migrated westward and southward, the new convective system shown by the propagation of the convergence zone from the system.

The vertical distribution of divergence and vertical velocity during the life cycle of the continental MCC in the case study 2 is presented in Figure 5.20. The development of the MCC in case study 2 also triggered by the strong surface and low-level convergence. The value of convergence is relative strong around $15 \times 10^{-5} \text{ s}^{-1}$ but less than case study 1. Surface convergence is confined to the lower half of the troposphere (from surface until 800 hPa), at the same time, strong divergence prevails above 700 hPa until 500 hPa around $12 \times 10^{-5} \text{ s}^{-1}$ that also less than case study one as shown in Figure 5.20 (a). By the mature stage, as illustrated in Figure 5.19 (b), the development of the MCC in this stage is triggered by the westerly and southerly wind that interacted the mountain breeze which makes merging the clouds system that shown in the initial stage. The upward process in the growth of the cloud has been started in this stage with averaged vertical velocity around $12 \times 10^{-2} \text{ Pa s}^{-1}$. In contrast with case study 1, the convergence in case study 2 during mature became weak in surface until low-level and only in the western side of the system. In fact, the strong divergence began to appear in the southeastern of the system. It is due to the effect of midnight land breeze. Upper-level strong divergence has developed a sharp maximum at 300 hPa. The updraft also becomes stronger with the averaged vertical velocity around $-12 \times 10^{-2} \text{ Pa s}^{-1}$.

At the decay stage, as shown in Figure 5.20 (c), the convergence became dissipated and changed to strong surface divergence. The divergence also expands in upper-level above 300 hPa. However, the strong divergence also appears in the midlevel. This condition indicates that the downdraft process already occurs during decay in the system. The new convective system began generated in the southern and northwestern side of the MCC system. At 3 hours after MCC dissipated or post-MCC stage as shown in Figure 5.20 (d), the strong surface convergence is presented. This convergence is widespread throughout to southward. It indicated there are propagate of the system like squall line structure as

described in subchapter 4.2.2. The downdraft process continues at this stage. Several new convective systems have been generated and migrated westward and southward, the new convective system indicated by the propagation of the convergence zone from the system.

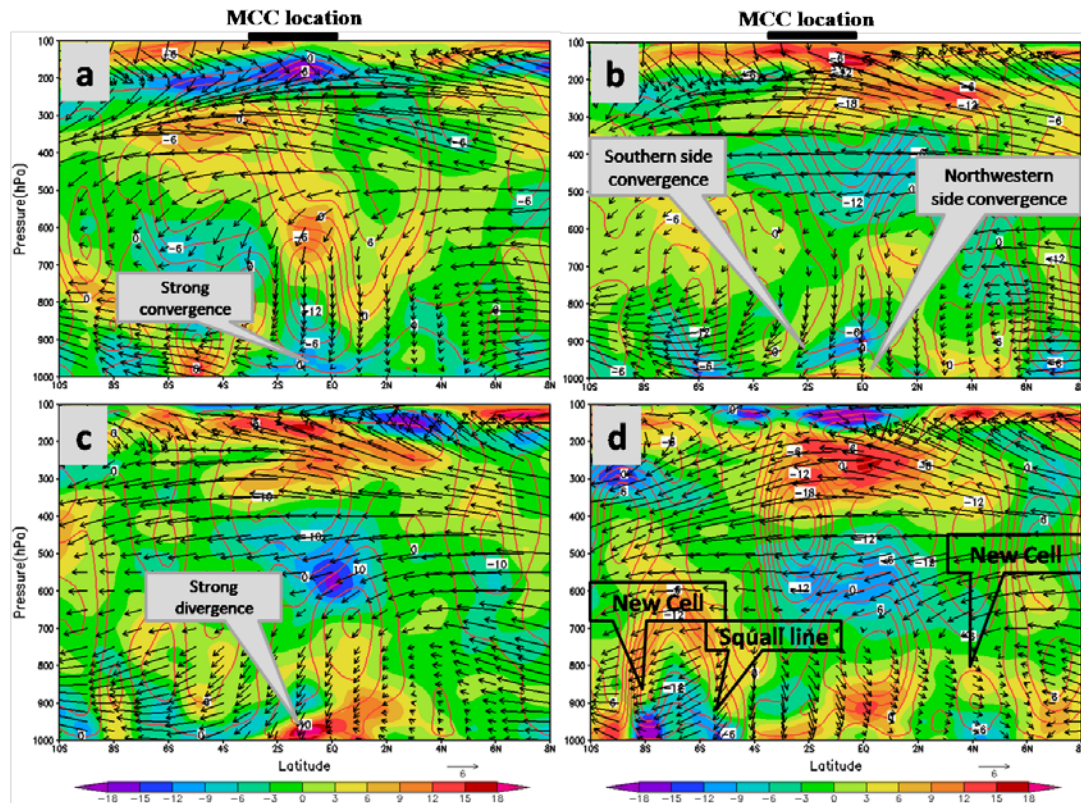


Figure 5.20. Pressure-latitude cross section (averaged for longitude 110° - 116°E) of divergence (10^{-5} s^{-1} , shaded), vertical velocity ($10^{-2} \text{ Pa s}^{-1}$, contour) and horizontal wind (vector; ms^{-1} ; upward represents northward) for MCC case study 2 using ECMWF ERA-Interim data, during (a) initiation (1900 LT), (b) mature (0100 LT), (c) decay (0700 LT) and (d) Post-MCC (1200 LT).

The vertical distribution of divergence and vertical velocity during the life cycle of the coastal MCC in the case study 3 is presented in Figure 5.21. The characteristics of MCC in case study 3 including in short-lived MCC. The development of the MCC in this case study also triggered by the strong surface and low-level convergence at the initial stage as shown in Figure 5.21 (a). The value of convergence is relative similar with case study 2. Surface convergence is confined to the lower half of the troposphere (from surface until 800 hPa), at the same time, strong divergence prevails above 700 hPa until 500 hPa around $12 \times 10^{-5} \text{ s}^{-1}$ that also similar with case study 2. The development of the MCC is triggered by the westerly and easterly wind as the land breeze from Sulawesi and Kalimantan Island. The surface convergence weakened during mature stage as shown in Figure 5.21 (b), the downdraft process began on the western side the system. At the decay stage, as shown in

Figure 5.21 (c), the convergence became dissipated and changed to strong surface divergence. The divergence also expands in upper-level above 300 hPa. The weak surface convergence is presented on the western side of the system. This convergence is widespread throughout to westward. It indicated there are propagate of the system like bow echo structure as described in subchapter 4.2.3. The downdraft process still continues at this stage. Several new convective systems have been generated and migrated westward and southward, the new convective system indicated by the propagation of the convergence zone from the system.

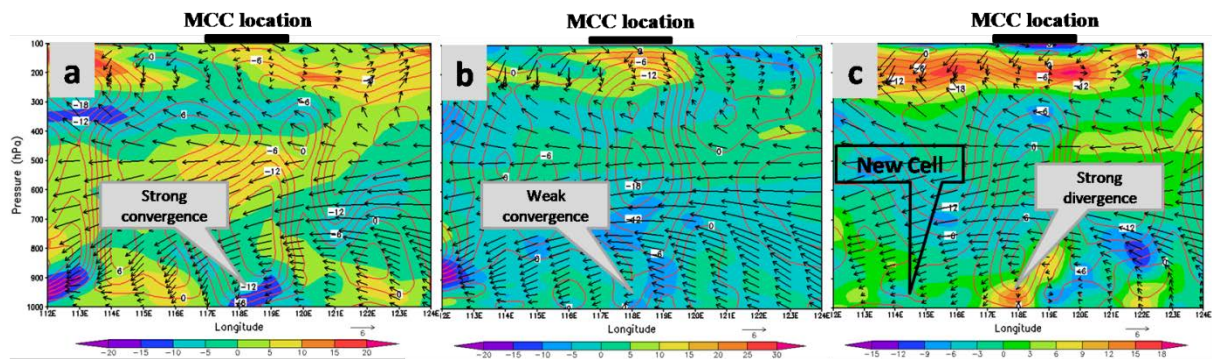


Figure 5.21. Pressure-longitude cross section (averaged for latitude $5^{\circ}\text{S} - 2^{\circ}\text{N}$) of divergence (10^{-5} s^{-1} , shaded), vertical velocity ($10^{-2} \text{ Pa s}^{-1}$, contour) and horizontal wind (vector; ms^{-1} ; upward represents northward) for MCC in case study 3 using ECMWF ERA-Interim data, during (a) initiation (0100 LT), (b) mature (0700 LT), (c) decay (1300 LT).

Comparison with the previous study, among others; Tollerud and Esbensen (1985) using composite analysis of divergence in tropical clusters have been reported that most of the convergence in the tropical clusters was below 800 hPa until the dissipation stage. It is different with the study result where the convergence during mature reaches the level of 700 hPa, in fact, reaches until midlevel (500 hPa) during the MCC decayed. This result also different with Maddox (1983) and Cotton et al. (1989) that stated deep layer of convergence at the mature stage and persisting thereafter. This difference possible due to the location of the MCC system where this MCC develop over the Indian Ocean which is one of heat sources that are interpreted as the driving force for the global circulation in the tropics (Ramage, 1968). This area is also one of the regions where deep cumulus convection and heavy rainfall occurs most frequently in the tropics (Yamanaka et al. 2008). In general, the evolution of these divergence profiles is similar to that found for tropical convective systems by Reed and Recker (1971), Riehl et al. (1974), Frank (1978) and Leary (1979). However, the

divergence profile at the time of the system is a little bit similar to the presented by Williams and Gray (1973).

Comparison with the composite analysis in MCC composite region two as shown in Figure 5.22 shows that in general there is consistency for all case in the region with the case study 1. The strong convergence is presented in surface level during initial stage and the weak divergence in the level of 800 hPa - 400 hPa as shown in Figure 5.22 (a). The ascending air began to appear in the initial region. During mature stage as shown in Figure 5.22 (b), similar to the case study, the surface convergence still appears in the mature region and strong divergence is presented on the upper level. The convergence reaches until low-level during decay stage, and the strong divergence still appears on the upper level as shown in Figure 5.22 (c). The convergence region is moving eastward and westward after MCC dissipated and the mid-level convergence appears over the dissipation region as shown in Figure 5.22 (d). The wind flow in each stage is relatively similar between case study and composite analysis. This consistency indicated that the MCC which occurred in region 2 around the Indian Ocean near of Sumatra Island have characteristics like the oceanic MCC in case study 1.

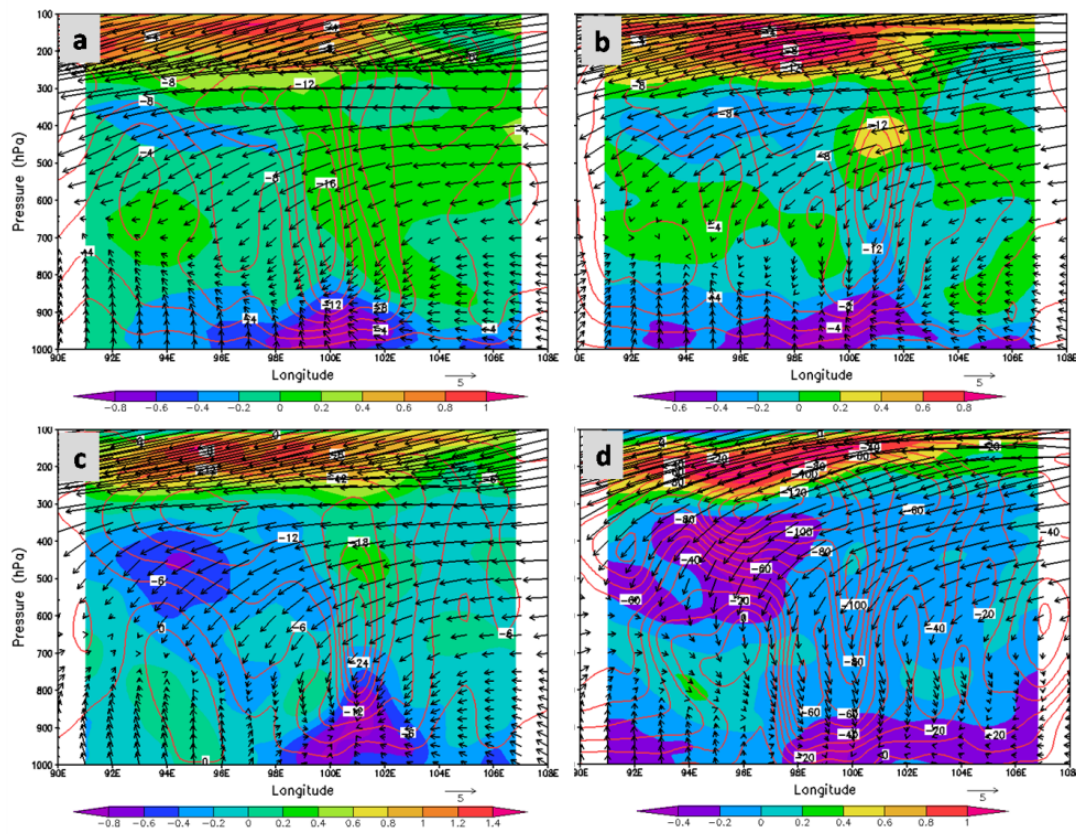


Figure 5.22. Same with Figure 5.19 but for MCC composite region 2.

Comparison with the composite analysis in MCC composite region 3 as shown in Figure 5.23 shows that in general there is consistency for MCC composite region 3 with the case study 2. The strong convergence is presented in surface level during initial stage and the weak divergence in the level of 800 hPa - 400 hPa as shown in Figure 5.23 (a). The ascending air began to appear in the initial region. Similar to the case study, the surface convergence still appears in the mature region, but the strong divergence also appears on the southern side of the system as shown in Figure 5.23 (b). However, a little different with the case study, during decay stage of MCC composite region 3, the divergence became to grew and expanded until midlevel, but the strong divergence still presented in surface level as shown in Figure 5.23 (c). The strong surface divergence becomes stronger and surface convergence dissipated during decay stage. At the same time, the new convective systems are appearing. The wind flow in each stage is relatively similar between case study and composite analysis. This consistency indicated that the continental MCC which occur in region 3 around the Central Kalimantan have characteristics like the continental MCC in case study 2.

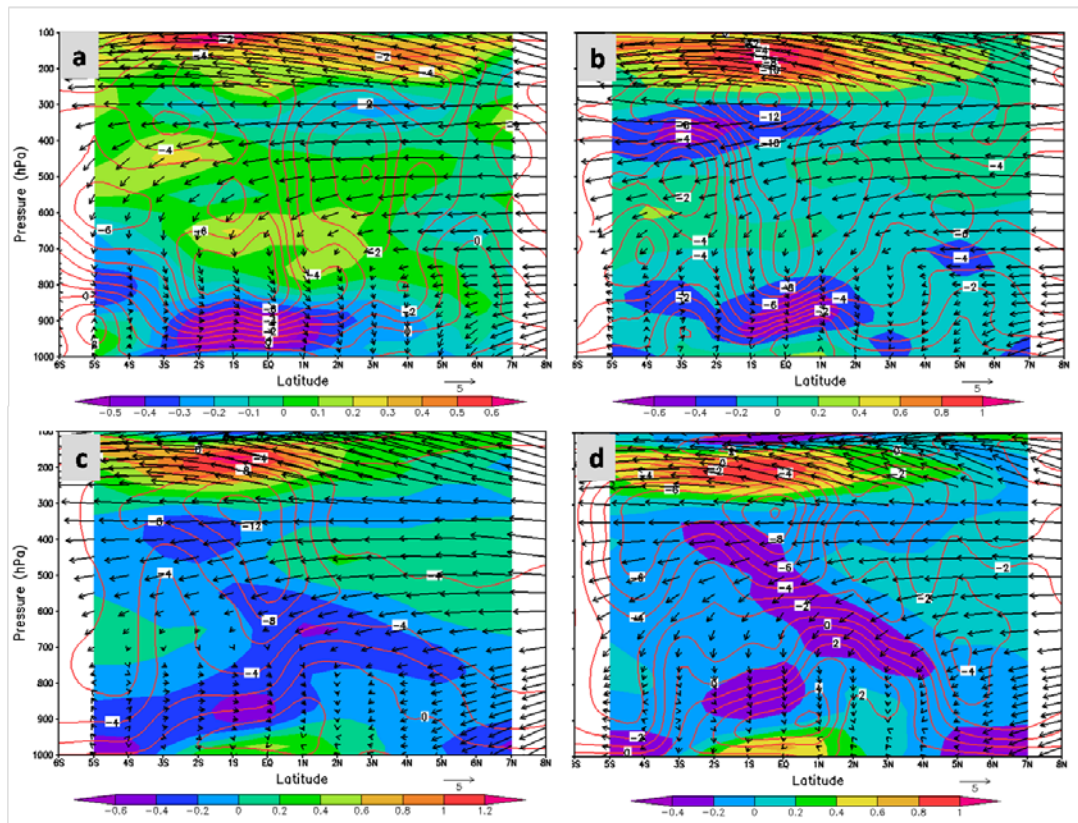


Figure 5.23. Same with Figure 5.20 but for MCC composite region 3.

In general, the consistency for MCC composite region 5 with the case study 3 is also presented. The MCC composite region 5 is also triggered by the strong surface and low-level convergence at the initial stage as shown in Figure 5.24 (a). At the same time, strong divergence prevails above 700 hPa until 500 hPa that also similar with case study 3. The development of the MCC in this region is triggered by the westerly and easterly wind as the land breeze from Sulawesi and Kalimantan. The surface convergence weakened during mature stage as shown in Figure 5.24 (b), and the convergence is became dissipated and changed to strong surface divergence during decay stage as shown in Figure 5.24 (c). The divergence also expands in upper-level above 300 hPa. The downdraft process still continues at this stage, and several new convective systems have been generated and migrated westward and southward also presented by composite analysis for MCC composite region 5. It indicated similar characteristics with case study 3. The wind flow in each stage is relatively similar between case study and composite analysis. This consistency indicated that the coastal MCC which occur in region 5 around the coastal near the Sulawesi Island have characteristics like the coastal MCC in case study 3.

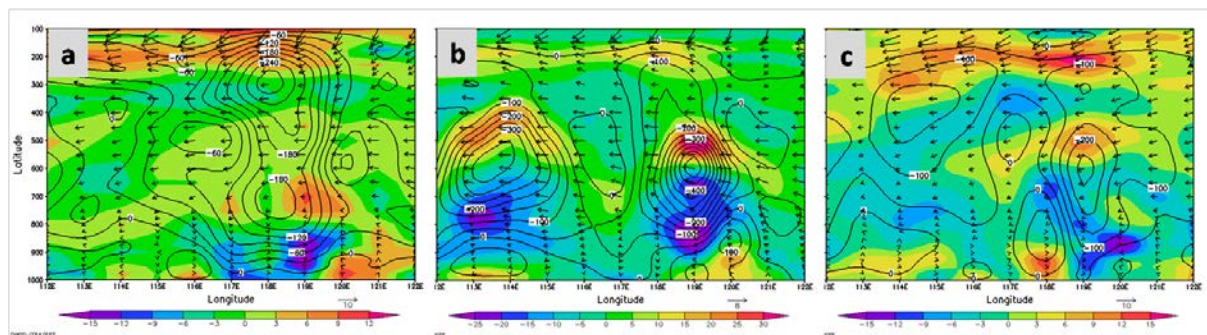


Figure 5.24. Same with Figure 5.21 but for MCC composite region 5.

5.5.2 Temperature advection and vorticity advection field

Cold advection is the process in which the wind blows from a region of cold air to a region of warmer air. Winds are blowing from a region of cold air to a region of warmer air, which results in cooling of the warmer region. As the cold advection persists, temperatures in the warmer region will begin to decrease as the colder air moves into the region of warmer air. Warm advection is the process in which the wind blows from a region of warm air to a region of cooler air. Winds are blowing from a region of warm air to a region of colder air, which results in a warming of the colder region. As the warm advection persists, temperatures in the colder region will begin to increase as the warmer air moves into the region of colder air. Vorticity is the localized rotation of the air. Air that rotates counterclockwise, such as in

cyclones and troughs, is said to have positive vorticity. Clockwise rotating air, such as in high-pressure systems and ridges, has negative vorticity. The advection of vorticity at high levels will result in response at the surface which will attempt to offset the effects of the advection. More specifically, vorticity advection is indicative of rising motion/falling pressures at the surface.

The vertical distribution of temperature advection and vorticity advection during the life cycle of the MCC in the case study 1 is presented in Figure 5.25. Several previous researchers have been reported that the initial region of the MCCs is characterized by organized upward motion, among others; Maddox (1983) and Cotton et al. (1989) have been described that surface of the initial region just presented of warm advection. The other paper like Moteki et al. (2008) and Nachamkin et al. (1994) reported that the surface cold advection characterizes initial stage of MCC. It is different with this study result, where the initial region of the case study one characterized by the warm-cold advection in the surface of the initial region. This condition which followed the positive/negative/positive pattern of vorticity advection in midlevel as shown in Figure 5.25 (a), the possibility can trigger the LLJ that related to the development of the MCC. The upward motion also occurs in the initial region by the strong warm advection. Large-scale warm advection is focused on the MCC at the initial stage and becomes concentrated on the MCCs eastern side by the mature stage as shown in Figure 5.25 (b). Maddox and Doswell (1982) and others have shown how this warm advection is primarily responsible for the environmental upward vertical motion (as opposed to differential vorticity advection) that helps trigger and organize the MCC. The vorticity is indeed weak in the lower troposphere. However, although the warm advection pattern is much more pronounced, the initial region is characterized by positive vorticity advection.

During mature stage, the warm surface advection and cool advection is decreased. However, the strong warm advection is appeared in the midlevel make the midlevel as the warm core. A similar structure has been documented for both tropical and midlatitude convective systems, e.g., Riehl et al. (1973), Ninomiya (1971), Frank (1978) and Bosart and Sanders (1981). It indicated the existence of the process of updraft and downdraft motion. The regions of positive and negative vorticity advection are indicated over the mature region that possible to generate the low-level jet which important in the development of the MCC. The warm surface advection dissipated at decay stage and cold advection is widespread throughout the surrounding area of the MCC system as shown in Figure 5.25 (c) and (d). The cold advection migrates eastward and westward by helped the westerly wind and sea breeze.

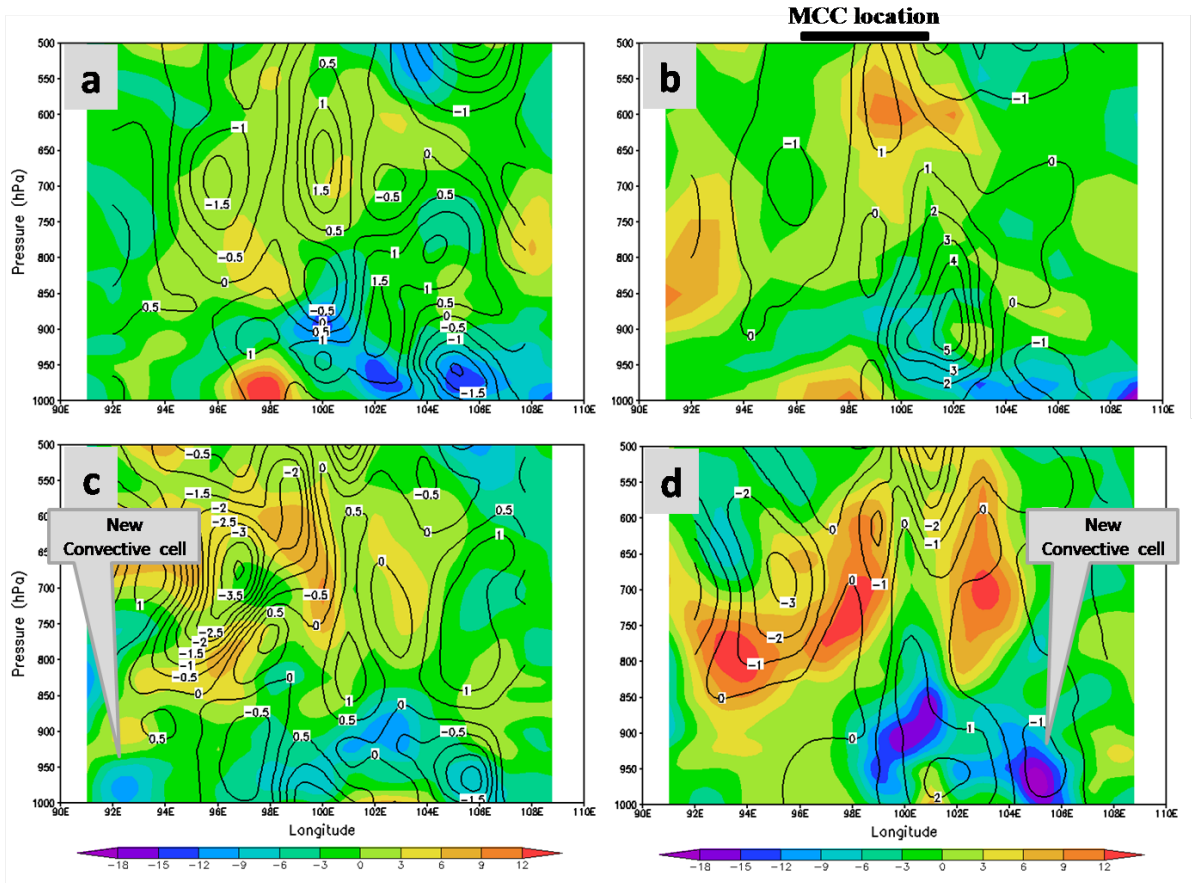


Figure 5.25. Pressure-longitude cross section (averaged for latitude 6°S - 0°N) of vorticity advection (contour; 10^{-8} s^{-1}) and temperature advection (shaded; 10^{-5} Ks^{-1}) for MCC case study 1 using ECMWF ERA-Interim data, during (a) initiation (0100 LT), (b) mature (0700 LT), (c) decay (1300 LT) and (d) Post-MCC (1900 LT).

The composite analysis for MCC composite region 2 indicate characteristics of temperature advection and vorticity advection that relatively similar with the oceanic MCC in the case study 1. The development of MCC in this region triggered by the surface warm-cold advection during initial stage as shown in Figure 5.26 (a). The mature region of MCC composite region also indicate the positive/negative/positive pattern of vorticity advection over the system, at the same time the warm advection appear in the upper-level and cold advection appears on the surface as shown in Figure 5.26 (b). The surface cold advection seems separated and migrated westward and eastward during MCC decayed and dissipated which indicate as the new convective system as shown in Figure 5.26 (c) and (d).

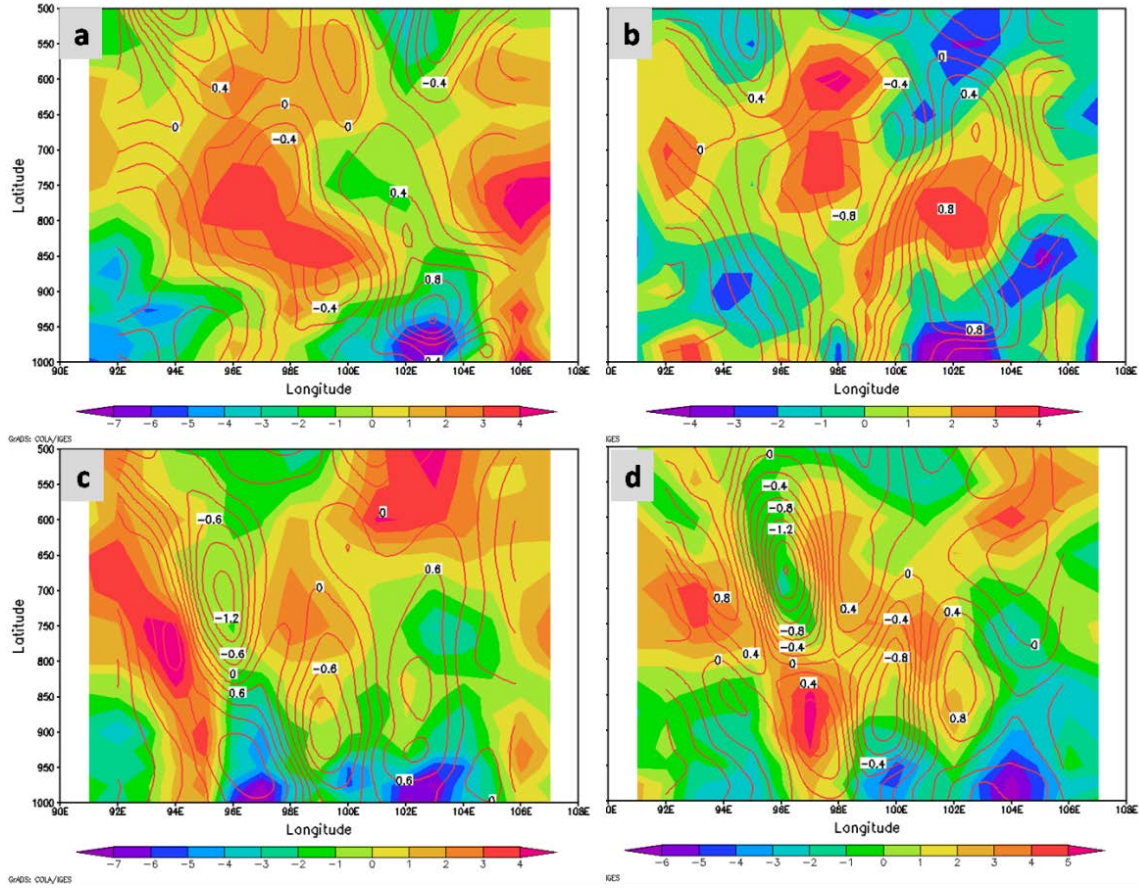


Figure 5.26. Same with Figure 5.25 but for composite analysis of MCC composite region 2.

The vertical distribution of temperature advection and vorticity advection during the life cycle of MCC in the case study 2 is presented in Figure 5.27. In contrast with case study 1, the initial region of the case study 2 characterized by the weak warm advection in the surface of the initial region. This condition just followed the positive of vorticity advection in midlevel as shown in Figure 5.27 (a). The upward motion also occurs in the initial region by the strong warm advection. The vorticity is indeed weak in the lower troposphere. During mature stage as shown in Figure 5.27 (b), cool advection is dominant on the southern edge of the system, possible due to the land breeze. However, the strong warm advection still appears on the northwestern edge of the system. It indicates the existence of the process of updraft and downdraft motion. The warm surface advection dissipated at decay stage and cold advection is widespread throughout the surrounding area of the MCC system as shown in Figure 5.27 (c) and (d). The cold advection migrates eastward and westward by helped the westerly wind and sea breeze.

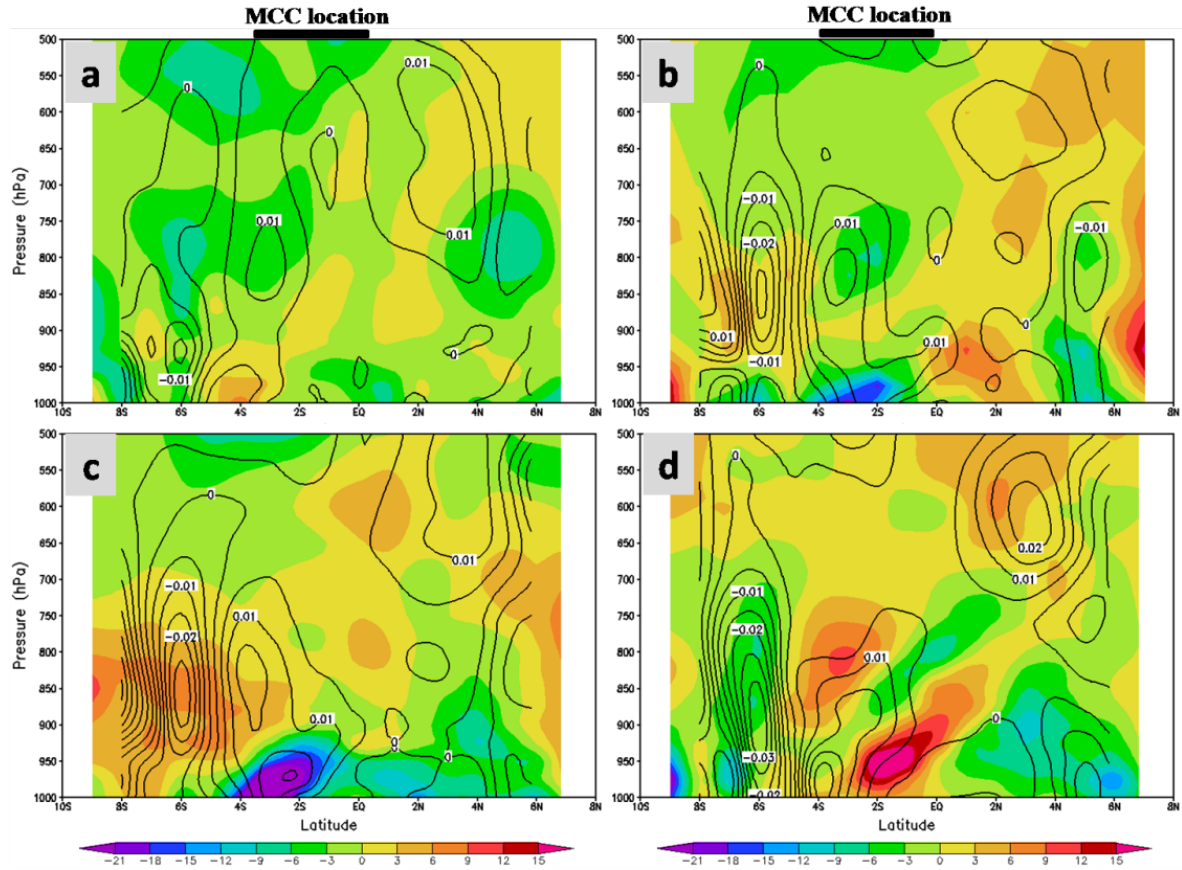


Figure 5.27. Pressure-latitude cross section (averaged for longitude 110° - 116° E) of vorticity advection (contour; 10^{-6} s^{-1}) and temperature advection (shaded; 10^{-5} K s^{-1}) for MCC case study 2 ECMWF ERA-Interim data, during (a) initiation (1900 LT), (b) mature (0100 LT), (c) decay (0700 LT) and (d) Post-MCC (1200 LT).

The composite analysis for MCC composite region 3 indicate characteristics of temperature advection and vorticity advection that relatively similar with the continental MCC in the case study 2. However, by composite analysis, the development of MCC triggered by the surface strong cold advection during initial stage as shown in Figure 5.28 (a). During mature as shown in Figure 5.28 (b), MCC composite region 3 is also presented the weak warm advection on the surface. The surface cold advection seems clearly separated and migrated northwestward and southward during MCC decayed and dissipated as shown in Figure 5.28 (c) and (d).

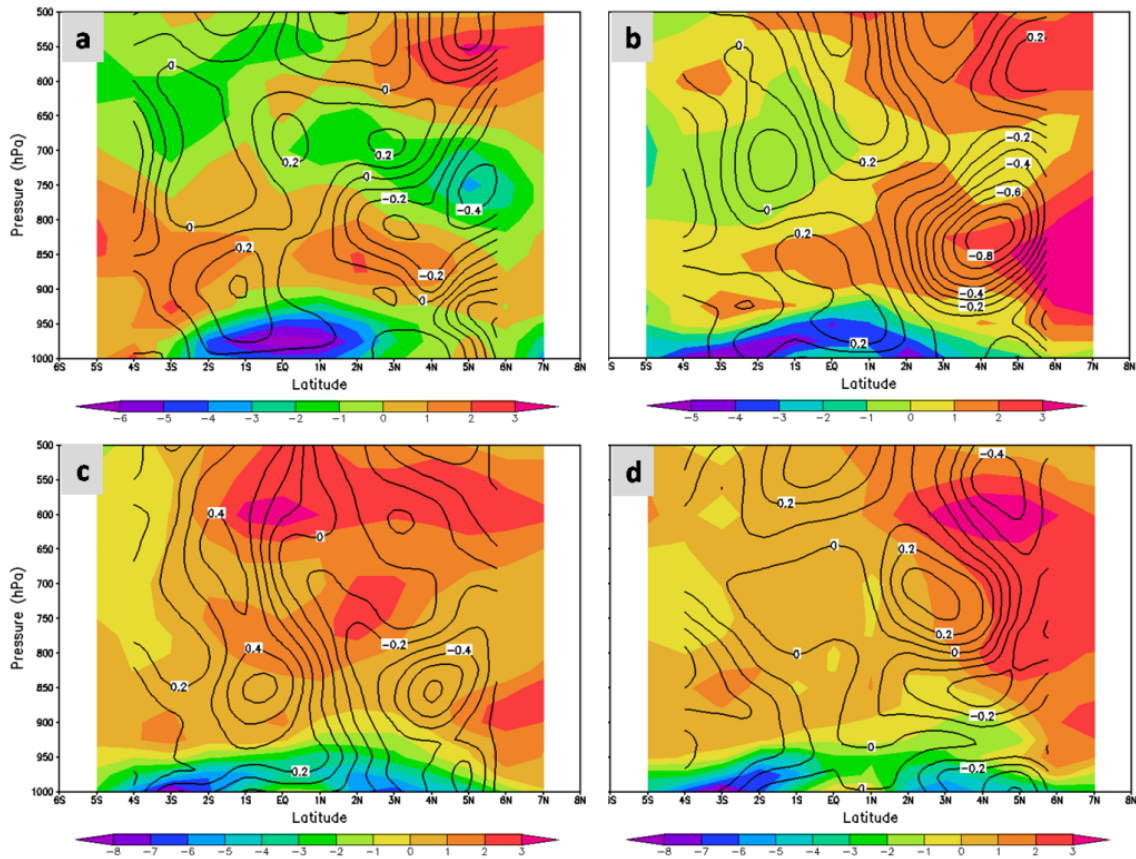


Figure 5.28. Same with Figure 5.27 but for composite analysis of MCC composite region 3.

The vertical distribution of temperature advection and vorticity advection during the life cycle of MCC in the case study 3 is presented in Figure 5.29. Almost similar with case study 2, the initial region of the case study 3 is characterized by the weak warm advection in the surface of the initial region. This condition just followed the positive of vorticity advection in midlevel as shown in Figure 5.29 (a). The upward motion also occurs in the initial region by the strong warm advection. The vorticity is indeed weak in the lower troposphere. During mature stage as shown in Figure 5.29 (b), cool advection is expanded until upper-level, at the same time the strong warm advection also expanded until upper-level. So that, the development of the MCC occurred in front between cold advection and warm advection. It indicates the process updraft and downdraft of the MCC development. It also indicated the existence of the jet streak. Maddox and Doswell (1982) and others have shown how this warm advection is primarily responsible for the environmental upward vertical motion (as opposed to differential vorticity advection) that helps trigger and organize the MCC. The surface cold advection seems clearly separated and migrated westward and

eastward during MCC decayed and dissipated which indicated the new convective system as shown in Figure 5.29 (c).

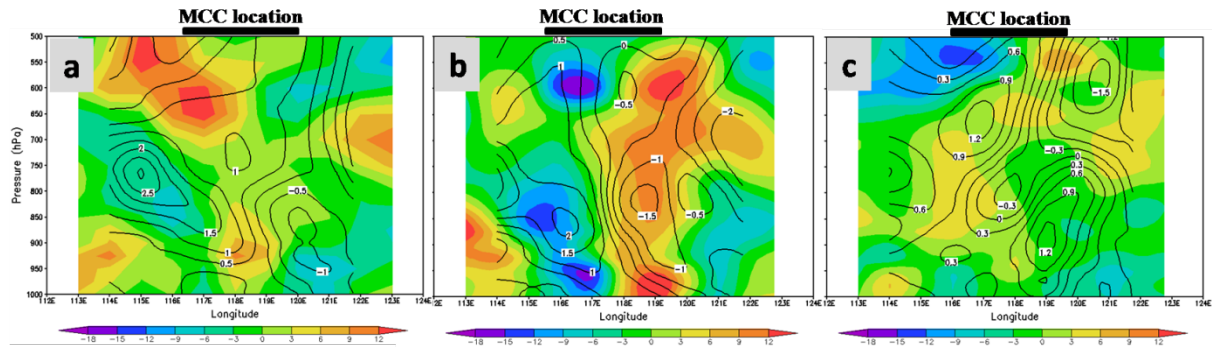


Figure 5.29. Pressure-longitude cross section (averaged for latitude 5°S - 2°N) of vorticity advection (contour; 10^{-8} s^{-1}) and temperature advection (shaded; 10^{-5} Ks^{-1}) for MCC case study 3 using ECMWF ERA-Interim data, during (a) initiation (0100 LT), (b) mature (0700 LT), (c) decay (1300 LT).

By composite analysis of MCC composite region 5 as shown in Figure 5.30. The condition of the initial region from the composite analysis is not representative of the case study, where the MCC composite region show the cold advection in surface level as shown in Figure 5.30 (a). However, the mature region is characterized by the strong cold and warm advection in surface level until upper-level, even though the surface warm is not very strong as shown in Figure 5.30 (b). It is relatively consistent with the case study 3. During decay, similar to a case study, the cold advection seems clearly separated that possibly indicate the new convective system as shown in Figure 5.30 (c).

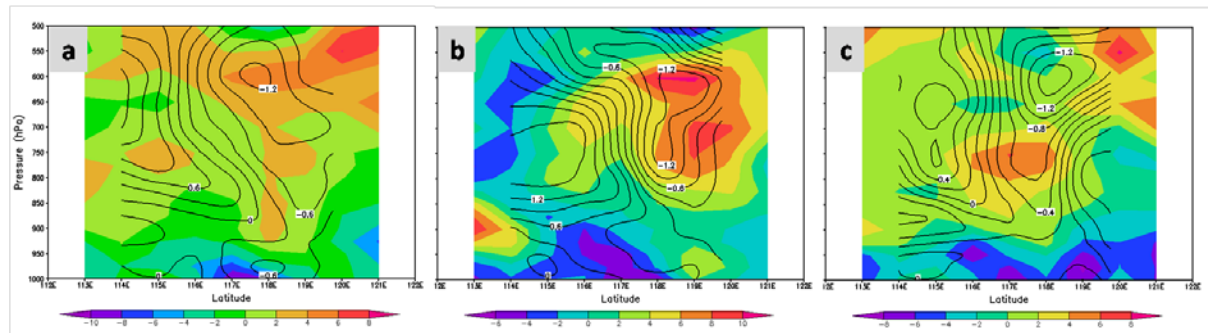


Figure 5.30. Same with Figure 5.28 but for MCC composite region 5.

5.5.3 Equivalent potential temperature and relative humidity field

Equivalent potential temperature, θ_E , is the temperature that results after all latent heat is released in a parcel of air and the then brought adiabatically to the 1000 hPa level. The θ_E increases as dewpoint and temperature increases. A region with a relatively high θ_E is often

the region with the most instability. Warmer low-level temperatures and higher low-level dewpoints increase instability. The LLJ from a moisture source will often bring in higher θ_E values and thus increased instability. θ_E ridge is regions with higher θ_E . They are often the bursting point for convective activity.

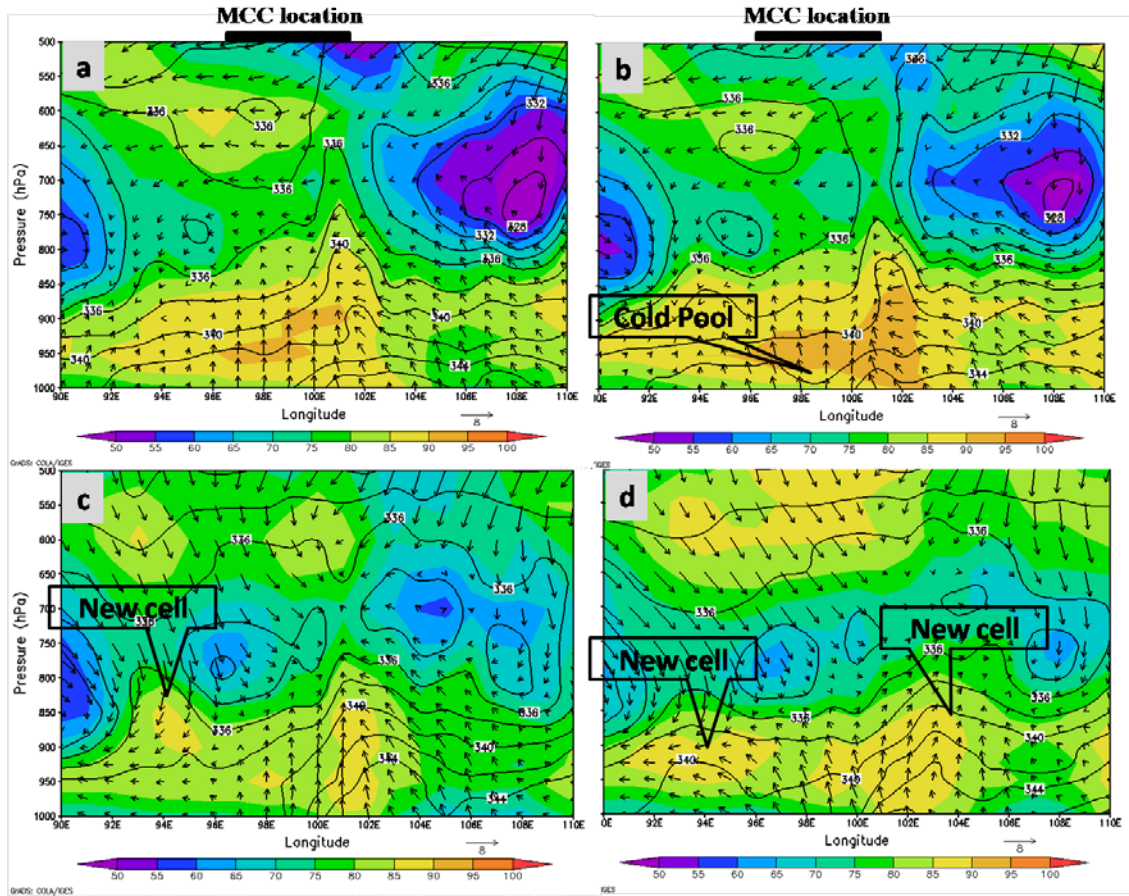


Figure 5.31. Pressure-longitude cross section (averaged for latitude 6°S - 0°N) of θ_E (contour; K) and relative humidity (shaded; %) and horizontal wind (vector; ms^{-1} ; upward represents northward) for MCC in case study 1 using ECMWF ERA-Interim data, during (a) initiation (0100 LT), (b) mature (0700 LT), (c) decay (1300 LT) and (d) Post-MCC (1900 LT).

The vertical distribution of θ_E and relative humidity during the life cycle of MCC in the case study 1 is presented in Figure 5.31. θ_E exceeded 344 K in the lower troposphere in the eastern side of the system during initial stage as shown in Figure 5.31 (a), denoting a major source of energy driving the MCC. One can see an influx of air with high θ_E at 850 hPa, one indicator of high flood potential. A cross-section through the layer of high θ_E air reveals other ingredients for the MCC and heavy rainfall. A deep layer of high specific humidity and rising motion. This maximum θ_E extends upward through midlevel, and with the southwesterly winds over the region, provides low to mid-level warm advection to the MCC region. The high θ_E during initial stage reaches level 650 hPa. It indicates the jet streak

or LLJ generate in this system. The location of a low-level moisture source and associated inflow in the MCC is consistent with the composite analysis of Maddox (1983) and Cotton et al. (1989).

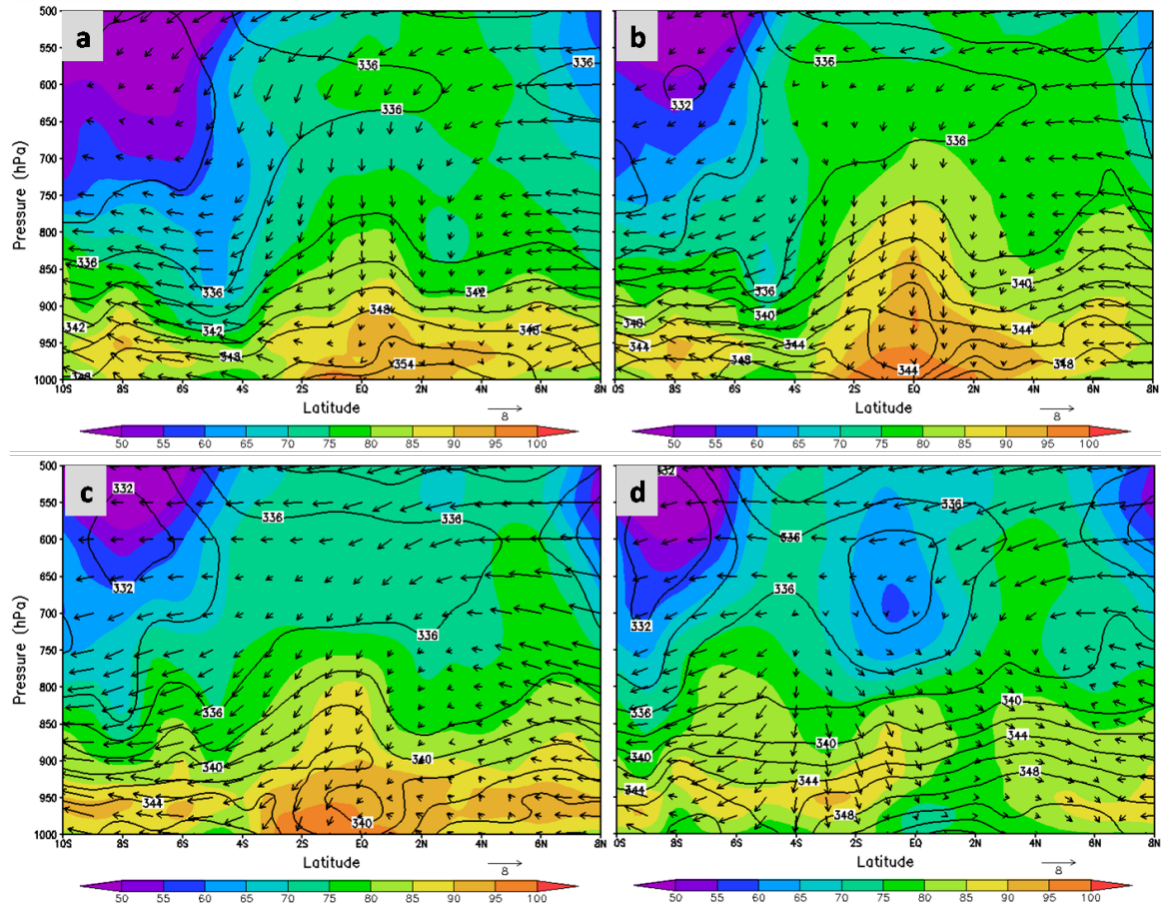


Figure 5.32. Pressure-latitude cross section (averaged for longitude 110° - 116°E) of θ_E (contour; K) and relative humidity (shaded; %) and horizontal wind (vector; ms^{-1} ; upward represents northward) for MCC in case study 2 using ECMWF ERA-Interim data, during (a) initiation (1900 LT), (b) mature (0100 LT), (c) decay (0700 LT) and (d) Post-MCC (1200 LT).

The θ_E of an air parcel increases with increasing temperature and increasing moisture content. Therefore, in a region with adequate instability, θ_E ridges) are often the burst points for thermodynamically induced thunderstorms and MCS. θ_E ridges can often be found in those areas experiencing the greatest warm air advection and moisture advection as shown in the Figure 5.31. The relative humidity also increases in region θ_E ridge. During mature stage as shown in Figure 5.31 (b), the θ_E ridges weakened just until low level but the relative humidity widespread throughout to all the system, the depressed θ_E values coincided with the area of heaviest stratiform precipitation. During the decay and dissipation as shown in Figure

5.31 (c) and (d), the θ_E decreased, and the θ_E ridges propagate that followed by the high relative humidity. It indicated the new convective system would be generated. This condition in case study 1, relatively similar to the case study 2 and 3 as shown in Figure 5.32 and Figure 5.33, respectively, but the θ_E ridges is not very strong. However, the θ_E in the case study 2 shows the condition instability that related with the development of the convective. The θ_E decreased, and the θ_E ridges propagate that followed by the high relative humidity. It indicates the new convective cell will also be generated shown in case study 2 and 3. It expected the high θ_E causes a low-level wind association with the MCC, through a thermal contrast between the system and its surrounding area.

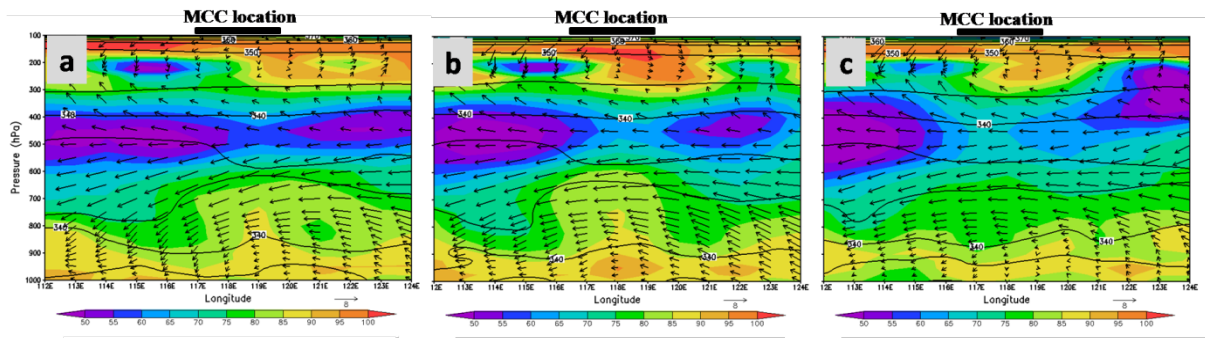


Figure 5.33. Pressure-longitude cross section (averaged for latitude 5°S - 2°N) of θ_E (contour; K) and relative humidity (shaded; %) and horizontal wind (vector; ms^{-1} ; upward represents northward) for MCC in case study 3 using ECMWF ERA-Interim data, during (a) initiation (0100 LT), (b) mature (0700 LT), (c) decay (1300 LT).

CHAPTER SIX

THE CONTRIBUTION OF MESOSCALE CONVECTIVE COMPLEXES (MCCs) TO TOTAL RAINFALL AND EXTREME RAINFALL OVER INDONESIAN MARITIME CONTINENT

This chapter has determined the contribution of MCC to total rainfall over IMC in the global, seasonal and monthly analysis. The result of this chapter will answer clearly the research objective about the contribution of MCCs to total rainfall in IMC and the relationships of MCC to extreme rainfall over the IMC. The detailed method has been explained in subchapter 1.4.2.4.

6.1 The contribution of MCC to total rainfall

6.1.1 Global analysis

The contribution of MCC to total rainfall over IMC already observed in this research. Figure 6.1 shows the frequency of the contribution of MCC to the total rainfall during the 15-year in a period of 2001 to 2015 over the IMC. The pattern of the MCC contribution is nearly similar to the geographic distribution of MCC over IMC during 15-years as described in Figure 3.1 (chapter 3), where the greatest contribution of MCC most frequently occurs in the MCC concentrated region. It proved that the MCC occurrences are associated with the rainfall. One can see that maximum contribution of MCCs globally which around 18-20% are mostly frequent occur in five regions as shown in Figure 6.1, i.e., 1) along the coastal of the western of the Sumatra, 2) the the South China Sea near Sarawak or the northern part of the Kalimantan Island, 3) the Central Kalimantan around 3°S-1°N; 111° -115°E, 4) the central Sulawesi around 4° - 2°S; 120° - 123°E, and 5) Merauke over Papua Island in location around of 8° - 5°S and 135.5° - 140°E. The greatest contribution from of them found in the central Kalimantan that reached 20%. The amount of MCC is happening in this area, one of which caused by the Kalimantan vortex that also related with mesoscale convective rainfall as described by Koseki et al. (2014).

The greater contribution of the oceanic MCC just found in the Indian Ocean was reached 14-18%. Chapter 4 have been described that most of the oceanic MCCs that occurred in the Indian Ocean will be migrated to the western coast of Sumatra Island during MCC dissipated. It indicated that the greater contribution of MCC in the western coast of Sumatra Island was the possibility due to the MCC which occurred over the Indian Ocean. The oceanic

MCCs also gave the great contribution over the South China Sea in around 13-17%. In detail, MCCs contribute to the total rainfall over Papua Island reached 14 - 18% in two locations, i.e., located in around 8° - 5°S and 135.5° - 140°E and located over around 132.5° - 136.5°E and 4° - 1°S. The existence of MCC is related with the orographic from Jayawijaya mountainous. The great contribution around 13-17% also occurred off the coast of West Kalimantan and on two locations over Sulawesi, i.e., in South Sulawesi and South East Sulawesi. MCC contributed very small in along the Java Island until East Nusa Tenggara because MCC was rarely found in this location.

Overall, the contribution of MCCs to the total rainfall over IMC just up to 20% due to the rainfall over IMC was contributed from various weather systems occurring on a range of temporal and spatial scales, from individual cumulus clouds, through cloud superclusters and tropical storms, right up to planetary scale interannual variations which constitute the ENSO. Comparison of this result with the result by Nesbitt et al. 2006 shown the MCSs that produced more than 50% of the rainfall during 5-years over IMC is also possible including MCCs. Comparison of this result with MCC in the other country show that the contribution value in this result is relatively similar to several regions, for example, Durkee et al. (2009) found the contribution of MCCs to South America rainfall just up to 21% for 10-years. Laing et al. (1999) have also reported that MCCs in the West Africa region contribute up to 22%. The regions which a significant contribution of MCCs have a similar pattern with regions that a lot of the large volumetric rainfall (Hirose et al. 2009) and have a similar pattern with geographical distributions of annual rainfall amounts of 3-year TRMM-PR rainfall data over IMC (Mori et al. 2004). It indicated that MCC contribute to the rainfall over IMC. The distribution of MCCs was found in this study have almost similar pattern with the distribution of MCSs for 4-years in IMC (Virtz and Houze 2015). The greatest contribution of MCC in this research is mostly concentrated in the continent and coastal than in the ocean. It is possible related to the paper of Qian (2008) that stated most of the rainfall over IMC is concentrated in the land. The previous researcher of Mori et al. (2004) and Ogino et al. (2016) reported the high intensity of rainfall frequently occurs in the coastal region over the IMC. It also described in this research that some of the coastal regions have the large contribution of MCC. It indicated the coastal MCCs also contribute the coastal rainfall. Nesbitt et al. (2006) have indicated that MCSs produce as much as 90% of rainfall in the land areas that nearly similar with this result where the continental MCCs contributed most of the greater contribution of MCCs.

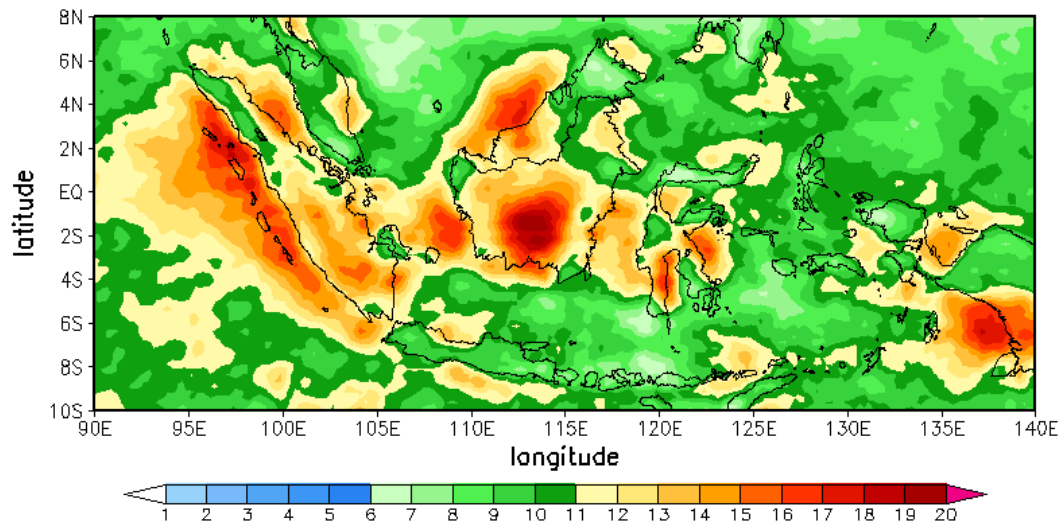


Figure 6.1. The frequency distribution of MCC contribution to total rainfall during 2001-2015. The legend is representing the percentage of MCC contribution.

6.1.2 Seasonal analysis

In the seasonal analysis, the greatest contribution of MCC to total rainfall during DJF concentrated in the coastal area near the northern part of Sumatra, which reached 18-22% as shown in Figure 6.2 (a). However, a considerable contribution ranges from 14-20% also found in several locations such as the Central Kalimantan, the South China Sea near Sarawak, South Sulawesi, the coast of Central Sulawesi and Merauke on the Papua Island. During DJF, the MCC also contributed significantly to the several regions over the Pacific Ocean and the Indian Ocean up to 18%. Several of previous work has reported that the characteristics of rainfall over Java Island are heavy rainfall during DJF season, but the few systems of MCC that occur in near the Java Island is just contributing up to 6 - 8%. The contribution of MCC over East Nusa Tenggara is less than 6 %.

The impact of MCC to rainfall is more clearly found during MAM as shown in Figure 6.2 (b) where the great percentage value of MCC contribution found in many areas over the IMC. The region that has great contribution during MAM is almost similar to DJF seasons, but, the value of the contribution in that region increased, and the contribution area also expanded. In detail, the greatest contribution more than 24% found in two locations are in the South China Sea near the Brunei Darussalam and the Central Kalimantan. The contributions of MCC in surrounding of both locations are also quite large ranges 16-20% is possible also because of the influence of MCC that occurs in both locations. The great contribution that occurs on the continent also found over Southern Sumatra and Sulawesi in several locations

over which reaches 16-20%. The contributions of MCC in some coastal areas were also high around 16-20% is in the area near the coast of North Sumatra and Malaysia, in the coastal area near West Kalimantan, in the Java Sea near the coastal areas of Java Island and the coastal area near Merauke on Papua island. The great contribution also scattered in several locations in the Indian Ocean and the Pacific Ocean. MCC also influencing the rainfall along from the Java Island until East Nusa Tenggara to remain weak in the MAM season, its contribution is slight along the land in this area, but the large contribution seen in some coastal regions along this area.

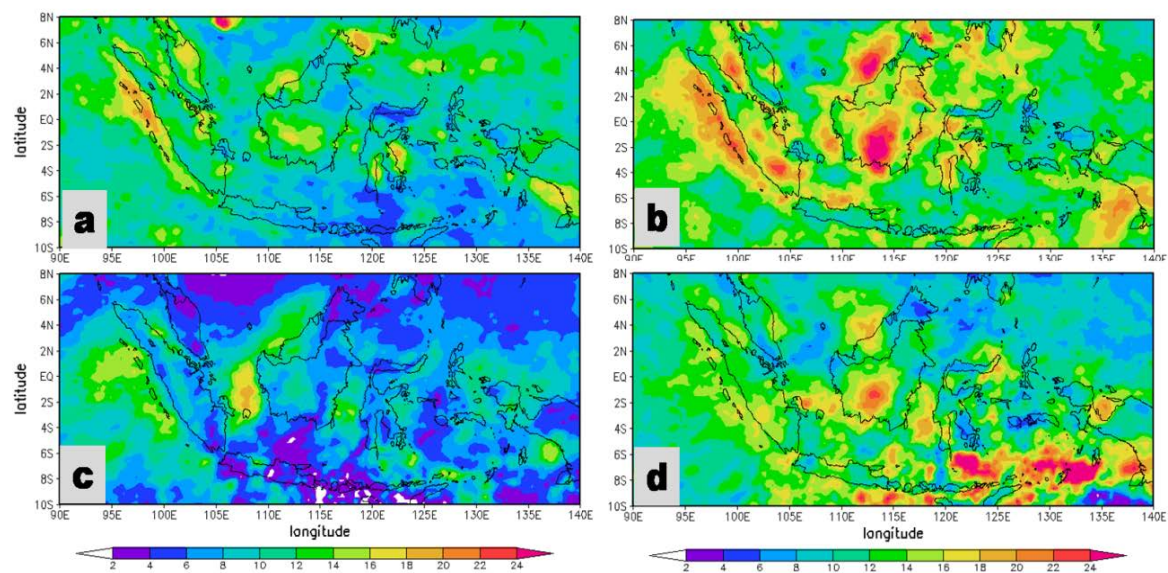


Figure 6.2. Spatial distribution of percentage for the MCC contribution to total rainfall during 2001-2015 in each season; (a) DJF, (b) MAM, (c) JJA, and (d) SON. The legend is representing the percent of MCC contribution.

During JJA, the impact of MCC to total rainfall is slightly less over continent where the MCC contribution just found up to 10% (Figure 6.2 (c)). The MCC has a strong influence only at a few locations in the Indian Ocean, in coastal areas near West Kalimantan and coastal areas near Merauke on Papua Island. The contribution showed it is quite large compared with other regions are about 16-22%. Figure 6.2 (c) also shows that the greatest contribution is just given by the oceanic MCC. The continental MCC is not too influencing to the rainfall during JJA.

Figure 6.2 (d) shows the greatest contribution of MCC during SON that around of more than 24% is concentrated on the Arafura Sea, the Banda Sea, and the Flores Sea. However, comparison with Figure 3.5 (d) about the seasonal distribution of MCC occurrences

show that just a few of MCC found in the Arafura Sea, the Banda Sea and the Flores Sea. It is possible because of there are an effect from MCC that occur over Merauke, Papua Island which is moving toward that three sea areas after MCC dissipated. In the conclude of chapter 4 stated that the MCC is not only influencing the rainfall in the MCC area but also influencing the rainfall in the surrounding area by inducing of the new convective cell that generated of the cold pool. The great contribution of the continental MCC to total rainfall during SON is mostly located in the Central Kalimantan and southern Sumatra, while the contribution of the coastal MCC almost exists along the western coast of Sumatra, the South China Sea near Brunei Darussalam, Makassar Street, and Cendrawasih Bay.

Overall, the great contribution of MCC over the Central Kalimantan and the South China Sea near of the Kalimantan were found in each season. It is consistent with the frequency distribution of MCC that found in each season as described in Figure 3.5 (chapter 3). It is also possibly related with the cold surges and the Kalimantan vortex. The cold surge also induces heavy rainfalls along the western coast of the South China Sea (Vietnam and Malay) near of the IMC, in particular, when synoptic-scale cyclonic disturbances are formed near Kalimantan and southern Philippines (Wu et al. 2011). The greatest contribution of MCC is more existence over continent than the ocean, where found almost in each season in several areas over the continent, except in July. The greatest contribution of the oceanic MCC just concentrated in the Indian Ocean near Sumatra in each season. The contribution of MCCs over Java Island almost small in each season, but the contribution a slightly increased during JJA, it is due to there is the contribution of MCCs from Kalimantan like the explanation in chapter 4. It is also suggested that existence of vortex over the South China Sea close to Kalimantan probably contributed to extreme rainfall during JJA due to the onset of Asian Summer Monsoon Season (Yihui and Yanju 2001).

6.1.3 Monthly analysis

Figure 6.3 shows the contribution of MCC against the monthly total rainfall for the month of January to June. During January, the maximum contribution of MCCs to January total rainfall was mostly concentrated on the western near the northern Sumatra up to 30%. The MCC contributed 22-28% of the rainfall to the same area during February until May, while in June the contribution in this area less than 10%. The greatest contribution of MCCs was also found on the Central Kalimantan for each month except June, even the contribution in this area reached more than 30% during March and April. The great contribution in the

South China Sea near Brunei Darussalam occurs in March and April. The great contribution of MCC over Sulawesi is just found in April. The contributions of MCC is also high over the Pacific Ocean near Maluku that occurred in January and May. The great contribution of MCC is also found in several locations in the Indian Ocean almost on every month from January to June. The great contributions of the coastal MCC mostly occur on Merauke of the Papua Island. The MCC contributed is very small on the Java Island.

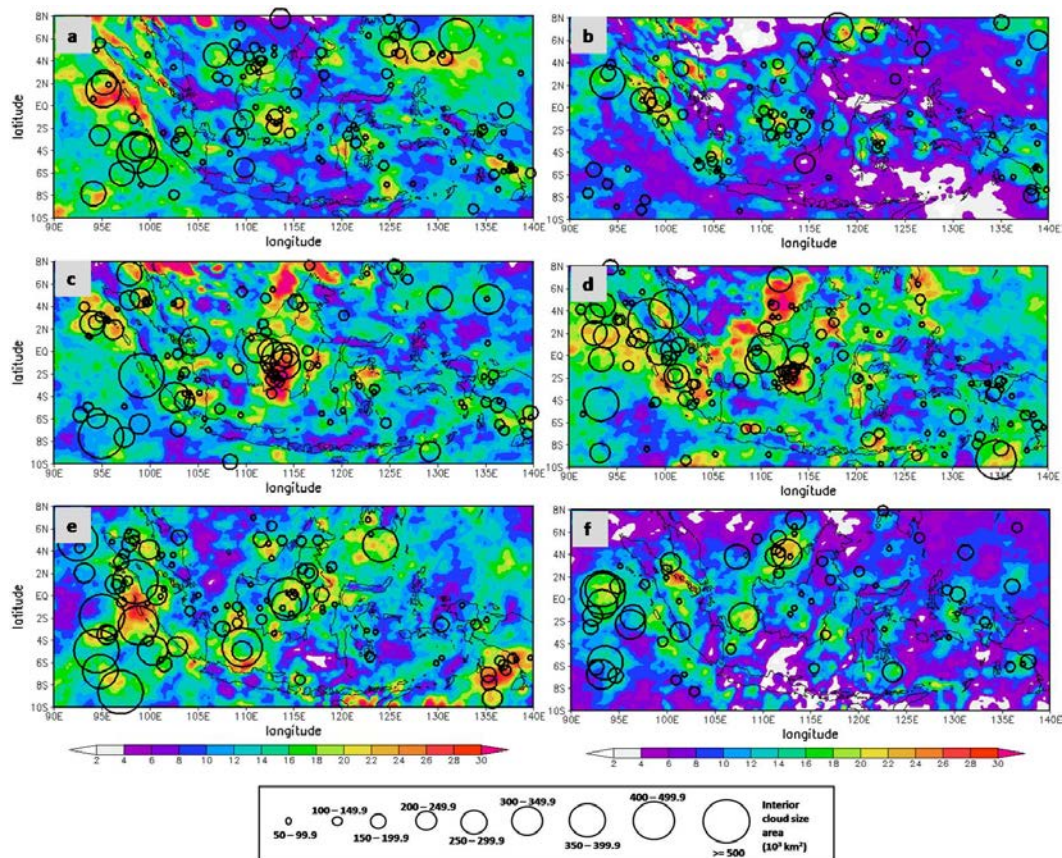


Figure 6.3. Frequency distribution of percentage for the MCC contribution to monthly rainfall during 2001-2015 (shaded), the legend representing the percentage of MCC contribution. The circles representing the interior cloud size area (10^3 km^2) for the MCC at the time of maximum extent of the interior cloud size area when the mature stage.

Figure 6.4 shows the contribution of MCC against the monthly total rainfall for the month of July to December. The greatest contribution found in November in several areas that even reach more than 30% in the Arafura Sea, Banda Sea and the Flores Sea, this is possible because of there is an effect from MCC that occur over Merauke, Papua Island which is moving toward that three sea areas after MCC dissipated. The great contribution of MCCs to November rainfall also found in some area. i.e., on the Indian Ocean near Sumatra, on the

South China Sea near Kalimantan Island, on the Central Kalimantan, on the coast of Merauke Papua Island and over Cendrawasih Bay.

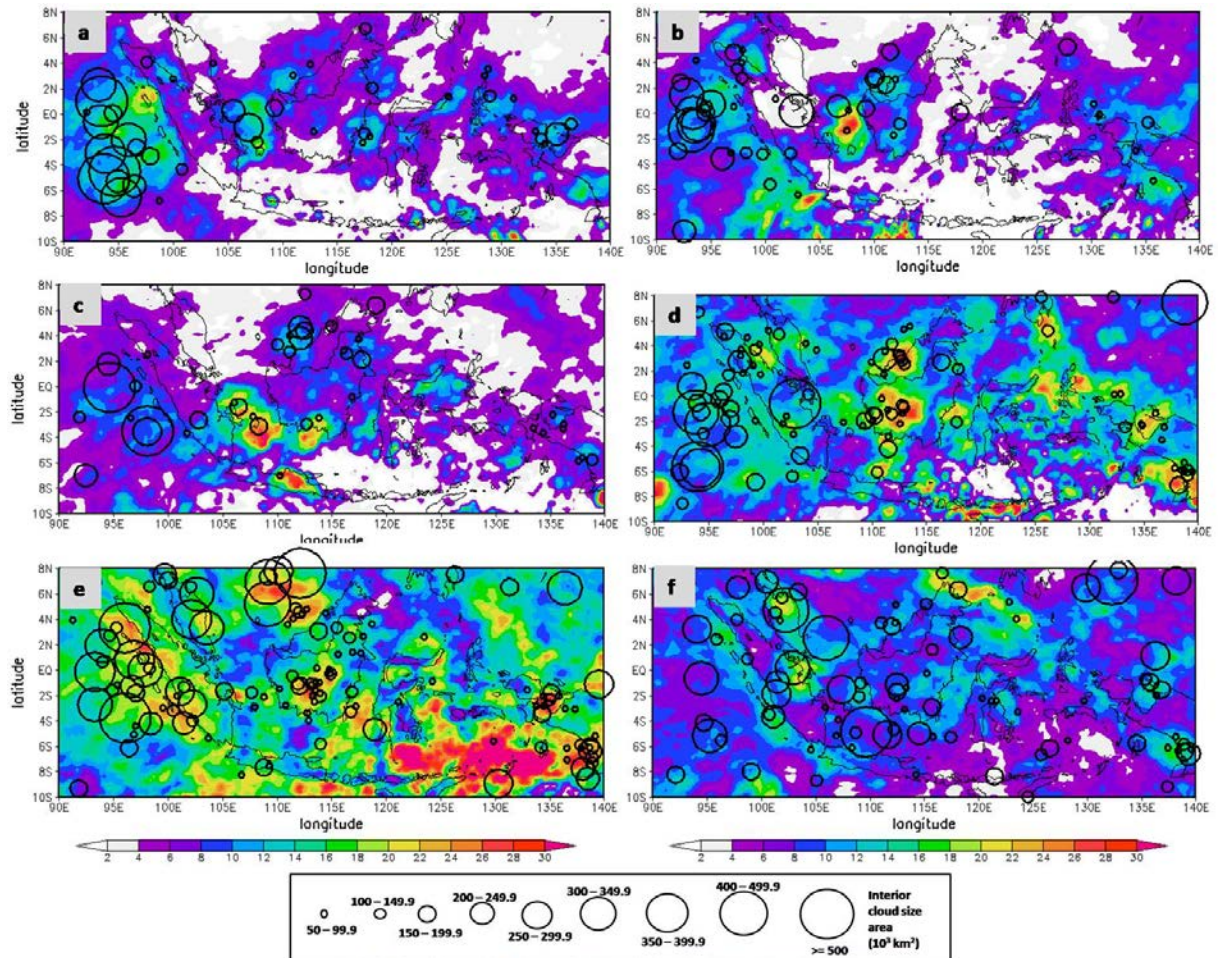


Figure 6.4. Same with Figure 6.3 but for July, August, September, October, November, and December

The almost same condition with November also found in October but with the contribution less than November. During July until September and December, the contribution of MCCs to total rainfall has considerably weak, where the maximum contribution just found in one and two location, like in July, the maximum contribution just found in the Indian Ocean and the coastal of West Kalimantan up to 18%. Even the contribution of MCCs along Java Island until East Nusa Tenggara is less than 4%, the same condition with August, but the contribution in the coastal of West Kalimantan in August has the percentage value more than July up to 28%. Slightly different to September, the maximum contribution up to 28% found in the three location. i.e., the coastal east on Southern Sumatra, on the Java Sea near the Central Kalimantan and Eastern Java. MCC is not too influencing the

monthly total rainfall in December, where one can see that on average the contribution is less than 8%.

6.2 The contribution of MCC to extreme rainfall

6.2.1 Spatial analysis of MRV and STD

Figure 6.5 showed the climatology of maximum rainfall during 15-years on the period of 2001-2015 for each season. During DJF as shown in Figure 6.5 (a), the greatest value of the climatology of maximum rainfall almost found in several regions in Java Island with value is around 4 - 5 mmhr^{-1} . The maximum rainfall that has great value also frequent occurred over Cendrawasih Bay, in the coastal region of West Irian Jaya and the valley area of Jayawijaya Mountain in Papua Island. The four other region that found maximum rainfall frequently is in the Southern of Sumatra (Lampung and South Sumatra), Central Kalimantan, over the South China Sea near Kalimantan Island and the border area of Central Sulawesi and South Sulawesi. During MAM as shown in Figure 6.5 (b), the maximum rainfall more frequently occurs over continent than the ocean. Figure 6.5 (b) also shows that the great maximum rainfall is nearly found on the major islands such as Sumatra, Kalimantan, Java, Papua and only slightly in the Central Sulawesi. It supports the result by Qian (2008) who stated the precipitation over the maritime continent is mostly concentrated over the continent. The greatest maximum rainfall was frequently found over Cendrawasih Bay. Maximum rainfall was rarely found along the small islands of Bali to East Nusa Tenggara during MAM.

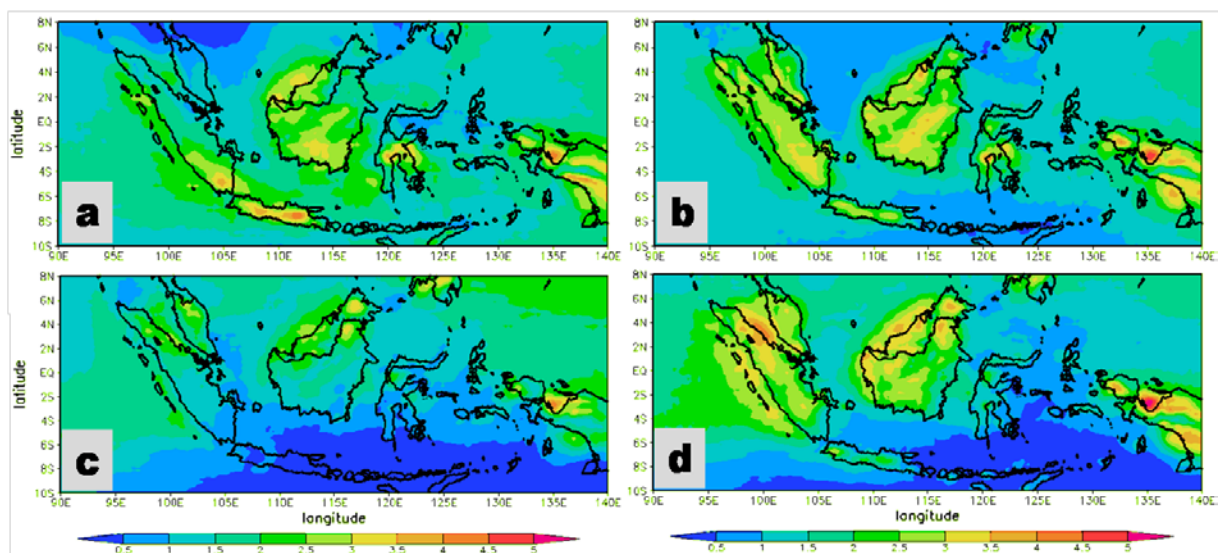


Figure 6.5. Horizontal distribution of climatology of the maximum rainfall during 15-years on the 2001-2015 period for each season; a) DJF, b) MAM, c) JJA, d) SON. Unit of rainfall is in mmhr^{-1} .

During JJA, the maximum rainfall found in North Sumatra, East Kalimantan and Cenderawasih Bay, but the value is less than the other seasons (Figure 6.5 (c)). The maximum rainfall is mostly concentrated over the ocean. It is similar with Kikuchi and Wang (2008). The maximum rainfall was frequently found in the Indian Ocean with a value around 2 - 3 mmhr⁻¹, while the maximum rainfall in small intensity was found in the region along Java Island until East Nusa Tenggara. During SON as shown in Figure 6.5 (d), the maximum rainfall was found over the ocean, in the Indian Ocean near Sumatra and the South China Sea near Kalimantan, but also found over land such as, along of Sumatra, Kalimantan, and Papua. Sometimes also occur over Java Island, but very rare occur along of Bali until East Nusa Tenggara.

Overall, the maximum rainfall is mostly concentrated over the continent than the ocean in each season. The greatest maximum rainfall was found over the Cenderawasih Bay, in the coastal region of West Irian Jaya. In contrast, the maximum rainfall was rarely found along Bali until East Nusa Tenggara in each season. It is consistent with Qian (2008) that stated the precipitation over IMC is mostly concentrated over the continent. Most of the extreme rainfall was found over the southern of IMC on DJF, and in the northern of IMC on JJA. The extreme rainfall is frequently occurring over IMC due to the IMC is located in the warm pool region where convective activities are most intense all over the world (Ramage 1968). The convection over the IMC represent a dominant heat source for atmospheric circulation and play an important role in the variability of the tropical climate and global circulation.

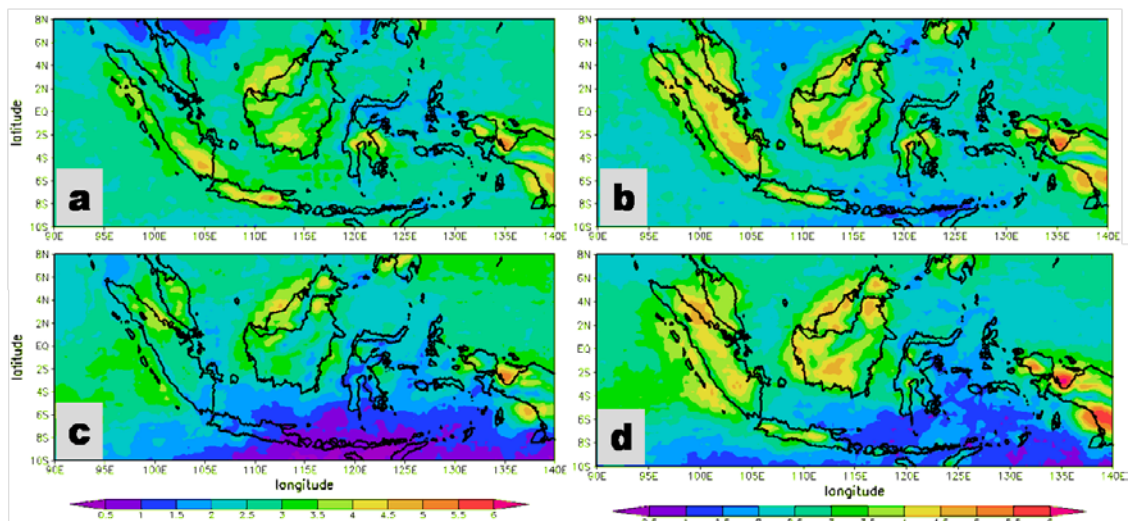


Figure 6.6. Horizontal distribution of standard deviation from the mean of maximum rainfall during 15-years on the 2001-2015 period for every season; a) DJF, b) MAM, c) JJA, d) SON. Unit of rainfall is in mmhr^{-1} .

Figure 6.6 shows the horizontal distribution of STD from mean of maximum rainfall during 15-years on the period of 2001-2015 for each season. During DJF (Figure 6.6 (a)), the greatest values of STD was found in the region that has maximum rainfall as described in Figure 6.5 (a). The value is slightly larger around $1\text{-}2 \text{ mmhr}^{-1}$ above the mean of maximum rainfall. The STD indicates that the data points tend to be very close to the mean. Almost the same with DJF, on MAM (Figure 6.6 (b)), the greatest values of STD was found in the region that has maximum rainfall, but in Java Island, the difference value between STD and MRV is quite large. The difference between STD and MRV is also considerable on JJA that occurred in the Indian Ocean (Figure 6.6 (c)). The greatest values of STD was found in the region that is often the appearance of maximum rainfall during SON (Figure 6.6 (d)).

6.2.2 Extreme threshold analysis

On DJF as shown in Figure 6.7, the greatest value of extreme threshold on EET-1 is around $6\text{--}10 \text{ mmhr}^{-1}$ (Figure 6.7 (a)). While, on EET-2 is around $12\text{--}16 \text{ mmhr}^{-1}$ (Figure 6.7 (b)) and on EET-3 is around $16\text{--}22 \text{ mmhr}^{-1}$ (Figure 6.7 (c)). It found in region which have high MRV and STD, i.e. over Cendrawasih Bay, in the coastal region of West Irian Jaya and also often occur in the valley area of Jayawijaya Mountain in Papua Island, in the Southern of Sumatra (Lampung and South Sumatra), Central Kalimantan, over South China Sea near Kalimantan Island and on the border area of Central Sulawesi and South Sulawesi. It is also noted that over Java Island, extreme rainfall always occurs in all types of EET during DJF. That threshold value is almost the same as the threshold from Indonesian Meteorological Agency (BMKG).

Figure 6.7 (b) shows that the great value of extreme threshold in each type is most frequent found over continent than the ocean. It indicated that rainfall is more prevalent on the continent when the MAM season. The greatest value for EET-1 is around $6\text{--}8 \text{ mmhr}^{-1}$ (Figure 6.7 (a)), for EET-2 is around $12\text{--}16 \text{ mmhr}^{-1}$ (Figure 6.7 (b)) and for EET-2 is around $16\text{--}20 \text{ mmhr}^{-1}$ (Figure 6.7 (c)). Spatial features of EETs in MAM are same like DJF, which showed that maximum rainfall of all EET types is active and intensive in almost all region, except southeastern of IMC.

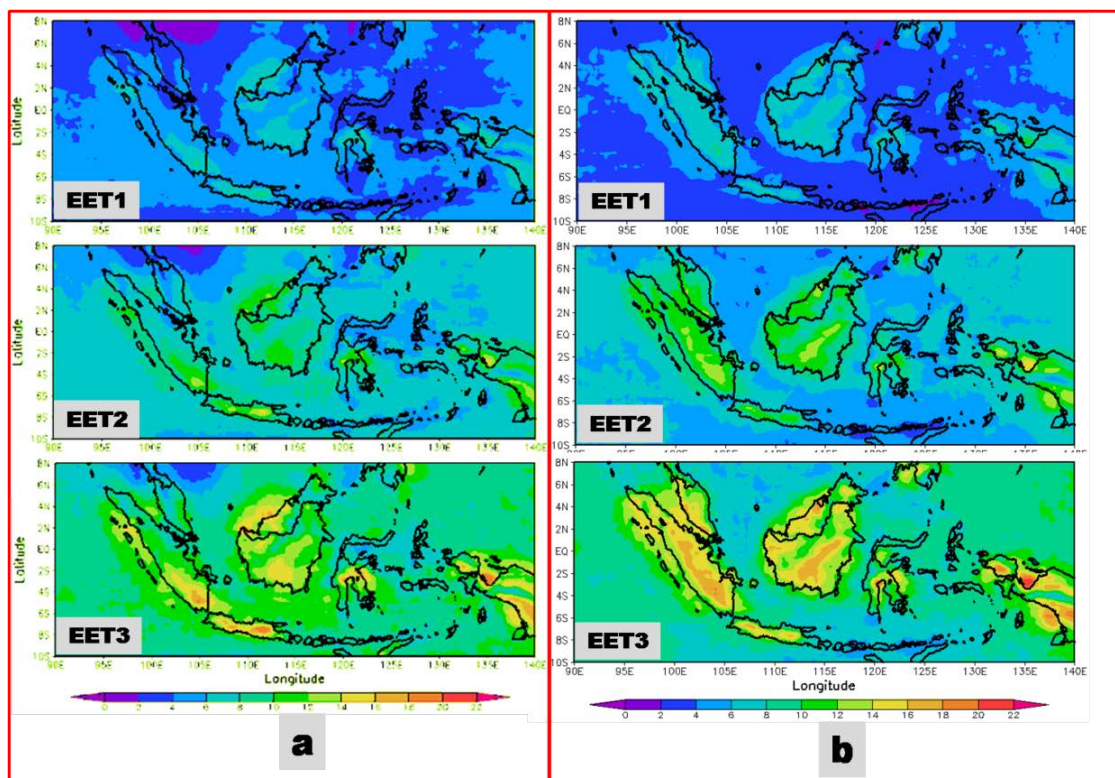


Figure 6.7. Extreme threshold (a) DJF (left) and (b) MAM (right) during 15-years on the 2001-2015 period for all type. Unit of rainfall is in mmhr^{-1} .

The greatest value of extreme rainfall was related to the amount of maximum rainfall that occurred in some area. In JJA (Figure 6.8 (a)), the highest value of extreme threshold only exists in some areas such as North Sumatra, East Kalimantan, Cenderawasih Bay, and some of over the Indian Ocean. The greatest value of extreme threshold for EET-1 around $8\text{--}10 \text{ mmhr}^{-1}$, for EET-2 around $12\text{--}14 \text{ mmhr}^{-1}$ and for EET-3 around $16\text{--}20 \text{ mmhr}^{-1}$. The area along Java until East Nusa Tenggara have a small value of the extreme threshold.

During SON (Figure 6.8 (b)), the greatest value of extreme rainfall is mostly found over the ocean, in the Indian Ocean near Sumatra and the South China Sea near Kalimantan Island, but was also found over land such as, along of Sumatra, Kalimantan, and Papua. Sometimes was also occurred over Java Island, but the very small value in along of Bali until East Nusa Tenggara. The greatest value of the extreme threshold for EET-1 is around $8\text{--}10 \text{ mm hr}^{-1}$, for EET-2 is around $12\text{--}16 \text{ mmhr}^{-1}$ and for EET-3 is around $18\text{--}22 \text{ mmhr}^{-1}$. Overall, the greatest value of the extreme threshold is mostly concentrated over continent than the ocean in each season. The extreme threshold is always high over Cenderawasih Bay, in the coastal region of West Irian Jaya in every season and every type of extreme rainfall. In contrast, the small value of the extreme threshold is always found along Bali until East Nusa

Tenggara in each season. It indicates that the magnitude of extreme threshold over the region depends on the amount of maximum rainfall that occur in that region.

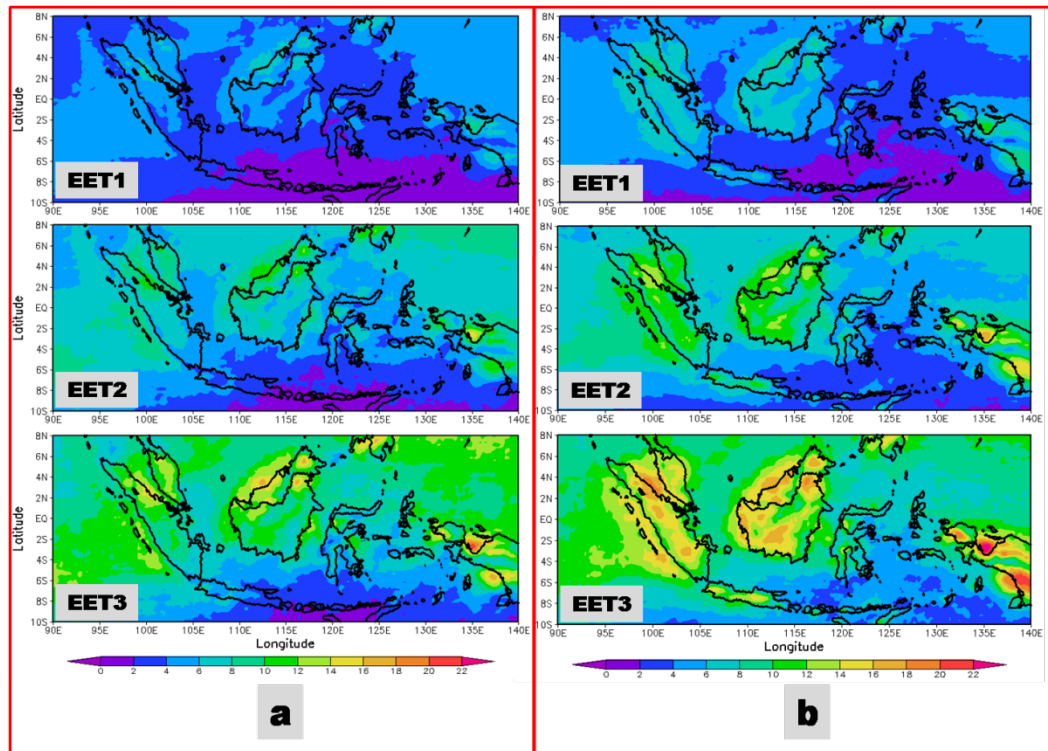


Figure 6.8. Same with Figure 6.7 but for (a) JJA and (b) SON.

6.2.3 Accumulated rainfall produced by extreme rainfall

The greatest values of mean accumulated rainfall that produced by EET-1 on DJF is mostly concentrated in the South China Sea near Kalimantan Island with value is around 1000 - 1200 mm/month as shown in Figure 6.9 (a). The great value with around 800 - 1000 mm/month was found in the Indian Ocean near Sumatra, on all of Java land, on Cendrawasih Bay, in the coastal region of West Irian Jaya and the valley area of Jayawijaya Mountain in Papua Island.

The four other region that has the great value of rainfall produced by EET-1 are in the Southern of Sumatra (Lampung and South Sumatra), Central Kalimantan, over the South China Sea near Kalimantan Island and the border area of central Sulawesi and South Sulawesi. The smallest values were found along Bali Island until East Nusa Tenggara. EET-2 produces the same EET-1 but a smaller total quantity of rainfall over IMC on DJF. The greatest values were observed in still around in the Southern of Sumatra (Lampung and South Sumatra), in the South China Sea near West Kalimantan, over Cendrawasih Bay, and several regions of Java Island. The greatest value is around 350-500 mm/month. The amount of

rainfall produced by EET-3 in DJF will be smaller and only covers the same area as that produced by the EET-2 but with a smaller amount of approximately 160-200 mm/month.

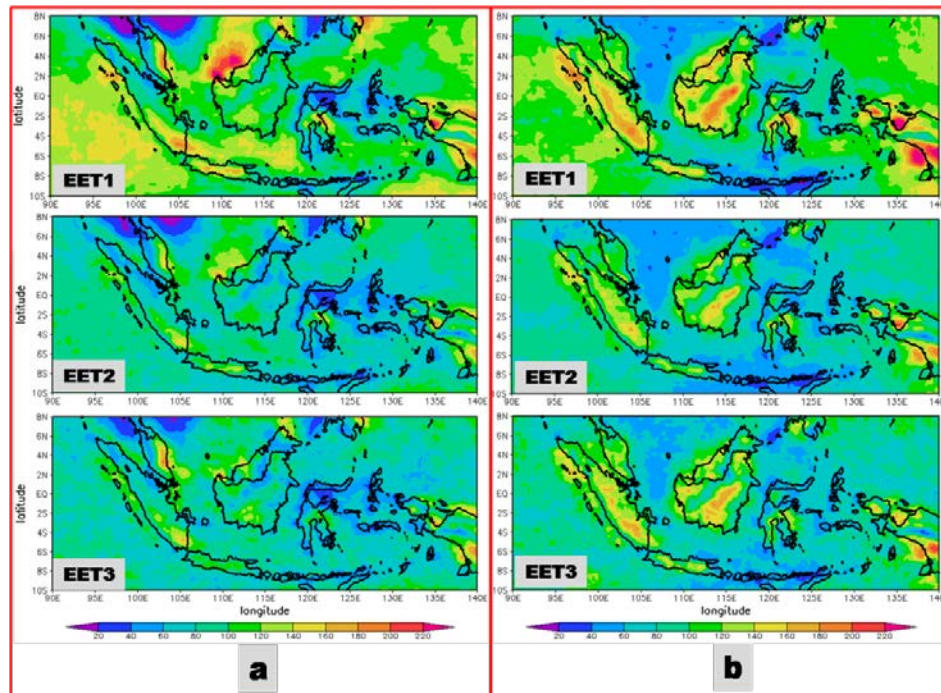


Figure 6.9. The climatology of accumulated rainfall of (a) DJF (left) and (b) MAM (right) during 15-years on the 2001-2015 period for all type. Unit of rainfall is in mm/month.

During MAM (Figure 6.9 (b)), the great values of mean rainfall accumulated produced by EET-1 are mostly frequent occur over continent than the ocean, where the highest value is around 1000 - 1200 mm/month that found on Cendrawasih Bay and the leeward valley of Jayawijaya Mountain near Merauke. The great value nearly 800 - 1000 mm/month also occurs throughout the mainland of Sumatra, Central Kalimantan, and Java. The smallest value was found along the small islands of Bali to East Nusa Tenggara. Along the mainland of Sumatra, Central Kalimantan, Java and over Cendrawasih Bay and the leeward valley of Jayawijaya Mountain near Merauke, the rainfall produced by EET-2 and EET-3 are also high is around 350 - 500 mm/month and 160 - 200 mm/month, respectively.

The mean of accumulated rainfall produced by EET-1 during JJA (Figure 6.10 (a)) over the Indian Ocean is very high around 800 - 1200 mm/month, especially around 90° - 92°E and 8° - 4°S. The other region which has high value produced by EET-1 was found in the valley of Jayawijaya Mountain and Cendrawasih Bay. The rainfall accumulated in the same area with EET-1 still have the greatest value produced by EET-2 and EET-3 is around 400 - 500 mm/month and 180 - 200 mm/month, respectively. During JJA, the rainfall

accumulations produced by each type of extreme rainfall with a high value is not found on the mainland.

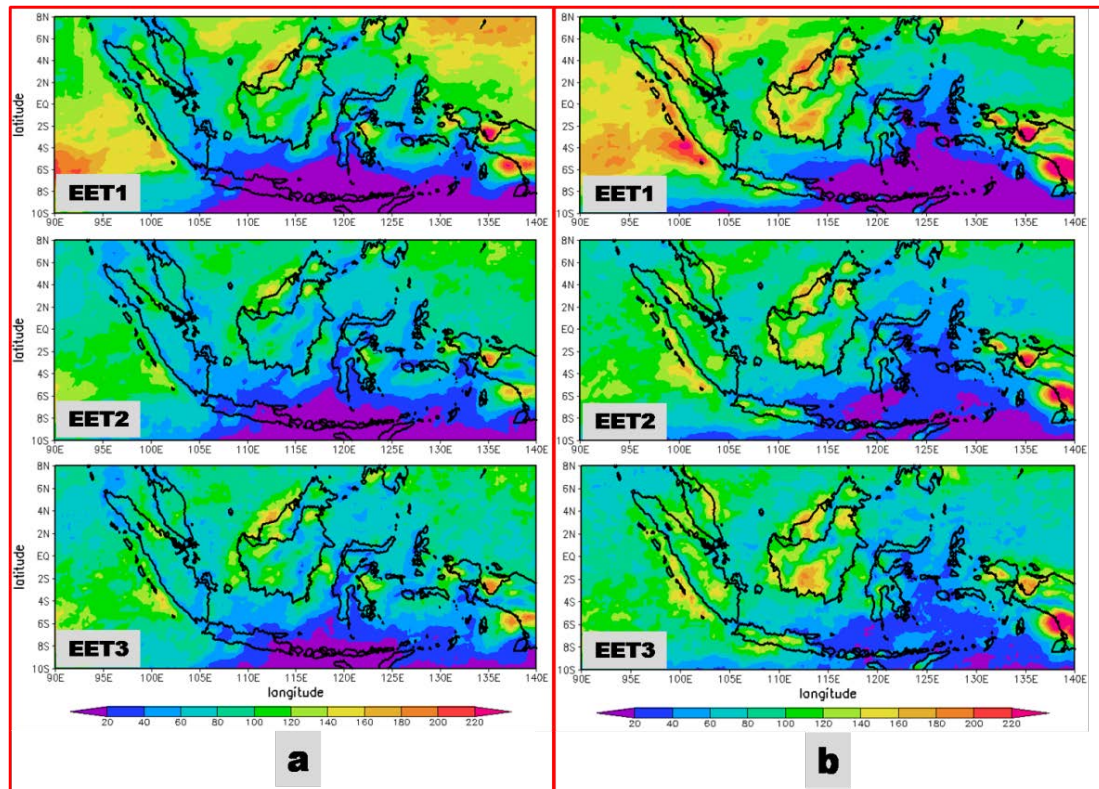


Figure 6.10. Same with Figure 6.9 but for (a) JJA and (b) SON.

The mean of accumulated rainfall produced by EET-1 during SON (Figure 6.10 (b)) was found in the Indian Ocean. The other region which has high value produced by EET-1 was found in the valley of Jayawijaya Mountain, Cendrawasih Bay, nearly of all over Kalimantan Island, along with mainland of Sumatra Island and some area over Java Island. The rainfall accumulated in the same area with EET-1 still have the greatest value produced by EET-2 and EET-3 around 400 - 500 mm/month and 180 - 200 mm/month, respectively.

6.2.4 Seasonal contribution of MCCs to extreme rainfall

Figure 6.11 shows the contribution of MCC to extreme rainfall season during DJF and MAM on 15-years (2001-2015) for all extreme type. On DJF as shown in Figure 6.11 (a), the greatest contribution that around 18-24 % of MCCs on EET-1 were found in three location over IMC, i.e. at the Central Kalimantan, the coastal region of Sumatra Island near of North Sumatra and the valley of Jayawijaya Island near of Merauke. The contributions of MCC to EET-2 at three locations above increased around 24-36%, and not only increased its value, but

the area of contribution is also widespread, for example, the contribution of MCCs in the coastal areas of Sumatra which was just near North Sumatra in EET-1 becomes widespread along the coast of the Sumatra Island, found new region with great contribution of MCC to EET-2. The region which has a great contribution on EET-3 nearly the same with the area which has a high contribution on EET-2, but found the new area which has a great contribution. Its value also nearly the same is around 24-36%, but there is few region with the greatest value reached 36-45% that indicated by red color in the Figure 6.11 (a).

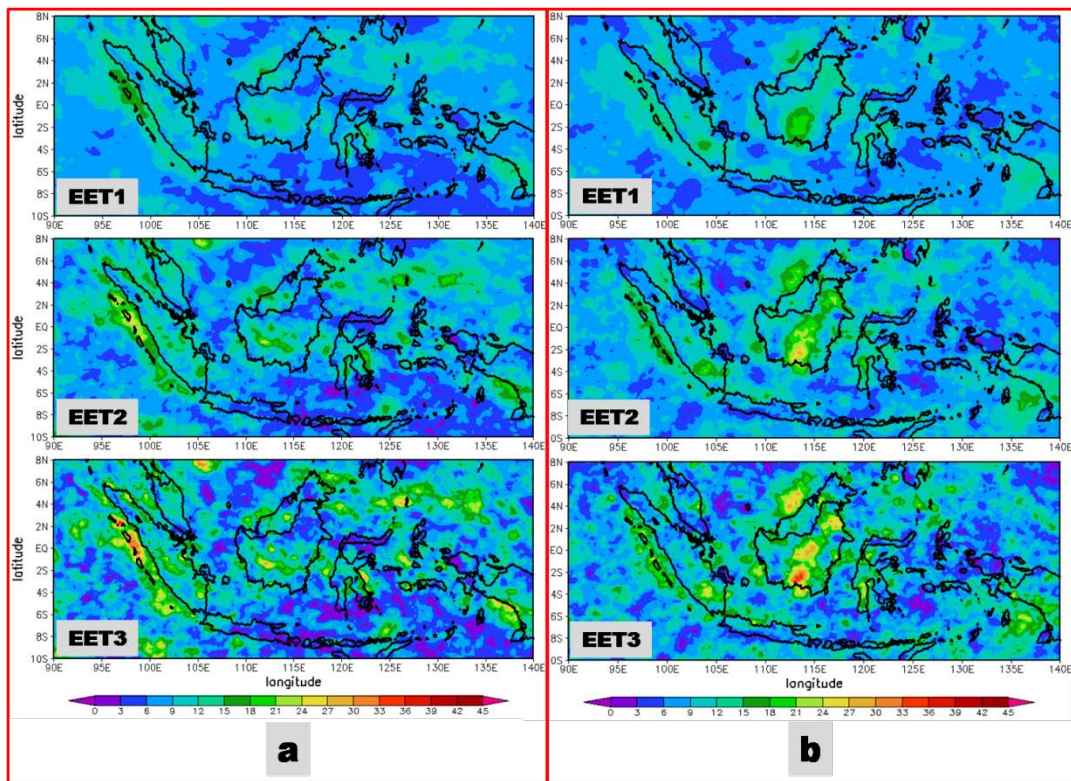


Figure 6.11. The contribution of MCC for extreme rainfall at (a) DJF and (b) MAM during 15-years (2001-2015) for all extreme type EET-1, EET-2, EET-3. Units are in percentage.

The spatial distribution of the mean contribution of MCCs to IMC total rainfall is a very similar pattern to that of the frequency distribution of MCC systems where the greatest contribution is found in the area of the frequent occurrence of MCC and otherwise. The MCC does not only contribute to rainfall, but the MCC give a contribution to its surrounding area by the results already explained in chapter 4. So that, it is certain that high percentage values in the coastal areas of Sumatra due to there is the contribution of MCC that occurred in the Indian Ocean and on mainland Sumatra. The contribution of MCC in the South China Sea near Kalimantan is small while there are many MCC concentrated in that area, it's due the high value of maximum rainfall and accumulated rainfall that produced by extreme rainfall is

mostly concentrated in that area, So, it indicated that MCC does not contribute the extreme rainfall over that area but maybe due to the other factor like Borneo vortex.

Figure 6.12 shows that the greatest contribution of MCC on EET-1 is just found in the central Kalimantan region around 18-24%. The contributions of MCC on central Kalimantan on EET-2 increased become around 24-30%, and the area of contribution is also extended along East Kalimantan. There are other regions which have a high contribution, i.e. South Sumatra, East Kalimantan, and the South China Sea near Brunei. The great contribution of MCC that around 18 - 24% is mostly concentrated over the coastal region of Sumatra, South Sumatra, the South China Sea near Brunei, Arafura Sea near Merauke, this is support by the result Ogino et al. (2016). The other region is some region on Sulawesi and in along of Central Kalimantan to East Kalimantan, even the contribution of MCC to EET-3 for some areas in the Central Kalimantan (indicated by red color in Figure 6.12) is great reached around 40%.

The contribution of MCC on EET-1, EET-2 and EET-3 quite large over the Indian Ocean at JJA about 18-24%, 21-27% and 27-36%, respectively. The other ocean regions also have a high contribution rate for all types of extreme rainfall, i.e. the coastal ocean near of West Kalimantan, South China Sea, the Pacific Ocean near Papua Island, Makassar Strait and the Arafura Sea near the coast of Papua. Only a small proportion of high contribution of MCC in Central Kalimantan. During JJA, the regions with a high percentage do occur in areas that are often the occurrence of MCC. It is also suggested that existence of vortex over the South China Sea close to Kalimantan probably contributed to extreme rainfall during JJA due to the onset of Asian Summer Monsoon Season (Yihui and Yanju, 2001).

At SON as shown in Figure 6.12 (b), the greatest contribution around 18 - 24 % of MCCs on EET-1 was found in four regions over IMC, i.e. at the Central Kalimantan, the Cendrawasih Bay in the coastal region of West Irian Jaya, the valley of Jayawijaya Island near of Merauke and the Banda Sea. The contributions of MCC on EET-2 at that four regions above increased around 24 - 33%. The region that has a great contribution on EET-3 nearly the same with the region on EET-2, but the new area which has great contribution was found. Its value is also nearly the same around 24 - 33%, but there is one region with the greatest value reached 36 - 45%, i.e. in Cendrawasih Bay. Overall, on SON, the contribution of MCCs to extreme rainfall over IMC is higher on the continent than Ocean.

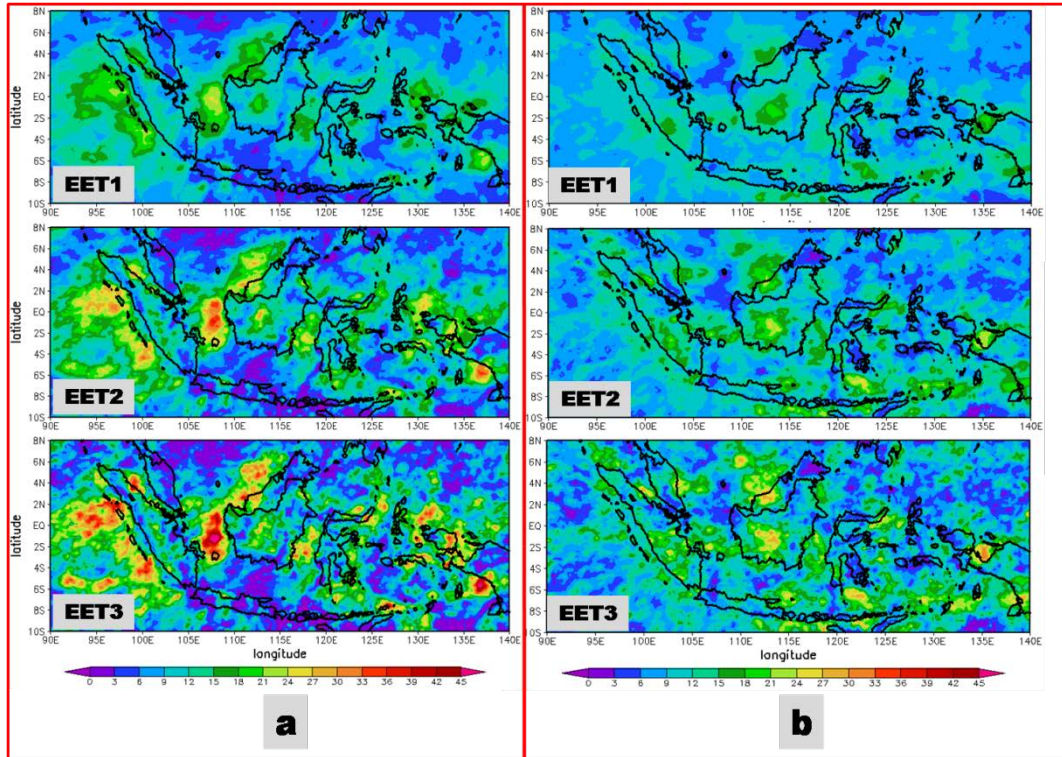


Figure 6.12. Same with Fig. 6.11 but for (a) JJA and (b) SON.

Overall, the contribution of MCCs on EET-3 is higher than the other types of extreme rainfall. The greatest contribution of MCC on average on each season for EET-1, EET-2 and EET-3 is around 18 - 24%, 21 - 33%, and 24 - 36%, respectively, while the contribution of MCC to EET3 in several areas reached 36 - 45%. The regions with a high percentage do occur in areas that are often the occurrence of MCC. It is consistent with Fritsch et al. (1986), and McAnelly and Cotton (1989) were able to determine that these MCC's produced most of the summer rainfall over the great US central plains, and MCSs contribute greater than 70% of the rainfall in the Tropics but make up a much smaller fraction of the cloud cover (Mohr et al. 1999), MCCs also play a major role in the rainfall regimes of the tropics include Indonesia Maritime Continent (Houze 1977; Chang et al. 1987) and many previous studies of MCC examined that the passage of an MCC are capable of producing tornadoes, severe hail, and damaging winds, heavy precipitation produced by MCCs (Maddox 1980, 1981; McAnelly and Cotton 1989).

MCC is more contribution to extreme rainfall over continent than over the oceans in every season except JJA season is most of the high contribution in the Indian Ocean. The greatest contribution was always found on Central Kalimantan and along the valley of Jayawijaya mountain. It is consistent with Maddox (1980), and Laing and Fritsch (1997) in

their study of MCC find a few things, among others; (1) most of MCC tend to occur on the continent, (2) tend to be formed in the zone of the gradient between Outgoing Longwave Radiation (OLR) maximum and (3) tends to occur in the Lee (relative to the flow the main intermediate level) of elevation areas like a mountain and the convection over Kalimantan (Kalimantan Island) related to sea breeze convergence is able to aggregate into MCCs later in the day, which move off land to give the greatest precipitation during the local morning time over the oceans (Williams and Houze 1987).

CHAPTER SEVEN

CONCLUSION AND FUTURE WORK

7.1 Conclusion

A climatological study of MCCs during 2001 - 2015 over the IMC has been identified using IR satellite imagery with creating an algorithm that combines criteria of cloud coverage, eccentricity, and cloud lifetime. A total of 1028 MCCs were identified and tracked during the 15-year period from 2001 to 2015. Most of these MCCs were over the continental area, mainly near the mountains and the high elevation areas. This characteristic is similar to the global population of MCCs by Ashley et al. (2003) and Laing and Fritsch (2000) that found the mean location for MCC genesis and initiation are located on the lee side of major mountain ranges. The results of this study suggest that large-scale topography is a critical factor in the spatial and diurnal patterns of MCC in IMC. The interaction of topographic effects and regional circulation may play some role in the MCC occurrences. A mountain breeze and a valley breeze are two related, localized winds that occur one after the other on a daily cycle which also give a contribution to convective activity over the IMC due to IMC is a unique geographical region that composed of a complex system of mountainous islands. The interaction between the topography with the westerly wave propagation is assisted in the development of convective storm or MCC in Africa (Garstang et al. 1987). Of great importance, is the study of Morel et al. (2002). They studied a large number of MCS (including MCC) over a large part of Europe using satellite infrared imagery, and among other conclusions, they found that these systems are mainly continental, strongly related with orography and in their majority are in phase with the diurnal radiative heating. Their results strengthen the analysis of this results study.

The greatest frequency of distribution of the MCC over the IMC is the continental MCC that reached 42.32% from all events. While the oceanic and coastal MCC around 31.23% and 26.46%, respectively. This result is similar to the global MCCs by Laing and Fritsch (1997). The favored region for development of the continental MCC is in the Central Kalimantan. The Indian Ocean is the favored region for the oceanic MCCs due to this area is one of heat sources that interpreted as the driving force for the global circulation in the tropics (Ramage 1968). The Indian Ocean is also one of the regions where deep cumulus convection

and heavy rainfall occurs most frequently in the tropics (Yamanaka et al. 2008). This result also supported by previous research, among other; Trismidianto (2012) that stated there are many MCC occurrences over the Indian Ocean near Sumatra and Ismanto (2011) stated that one of concentration area for oceanic MCC is the Indian Ocean. There are several favored region for the coastal MCCs. i.e., the coastal of western of Sumatra, the South China Sea near the northern of Kalimantan, and the coastal of Merauke. MCCs that occurred in favored region is usually found in each season and month. However, MCCs rarely found along the Java Island to the East Nusa Tenggara because of the low-lying region. The peak of MCC occurrence over the IMC is during MAM with around 33.56% due to likely linked to the synoptic-scale environment, which is more baroclinic in nature compared to the late summer months. Around of 26,26% and 25,29%, MCC occurrences are found in DJF and SON, respectively. The season with fewer events is JJA, around of 14.79%.

The average of cloud shield area size of MCCs is around 315,000 km². It is slightly less than with global MCC by Laing and Fritsch (1997) that stated the mean cloud-top area for the global population is 354,000 km². However, the MCCs in the IMC is more than from MCC in the western Pacific region that has the greatest frequency of MCC between 2×10^5 km² until 3×10^5 km² as reported by Miller and Fritsch (1991). The MCCs in the IMC is also more than with MCC over subtropical South America that has cloud size area 256,500 km² (Durkee and Mote 2009). Although some MCCs produce cold cloud shields that extend over a million km², the size, and duration of MCSs and MCCs are positively correlated, i.e., larger systems tend to last longer (Tollerud et al. 1992, Laurent 1996, Laing and Fritsch 1997). The MCC with small size most frequently occurred in the continent, in contrast, the MCC with the medium and large size are most concentrated over the ocean. The MCC systems are longer lasting in the western Indonesian than in the central Indonesian and eastern Indonesian. Most of the oceanic MCC concentrated over the Indian Ocean. Most of them have large interior cloud size over 300,000 km² even much going MCC which has a scale of 500,000 km². The majority of MCCs over the IMC are more circular due to the average of eccentricity for all of the MCCs over the IMC are 0.85. It indicated that majority of MCCs over the IMC are more circular which similar to MCCs over the USA (Augustine et al. 1989).

The average duration of the MCCs over IMC was approximate ~9 .5 hours, and the maximum duration was 10 hours that very similar to the distribution and average for MCCs in the southern Africa (~9.5 h; Blamey and Reason, 2012), but it is slightly shorter than the

global average (~10 h; Laing and Fritsch, 1997) and much less than those found in subtropical South America (14 h; Durkee and Mote, 2009). The long-lived MCCs with duration more than 20 hours occurred in March, May, July, September, and November and most of the short-lived MCCs with duration 6 - 7 hours occurred in March - May, July, September, and December. The oceanic MCCs are slightly larger and last longer than the continental and coastal MCCs. A distinguishing factor in the longevity and size distributions of MCSs appears to be the strength of the early growth. The critical importance of the early growth was quantified by Tollerud et al. (1992) in their analysis of the relationship between early growth rates and cold cloud shield size. They found that the growth rate of the cold cloud shield in the first three hours of the life cycle of an MCS was a strong predictor of the eventual size and duration of the system. Similarly, McAnelly and Cotton (1986, 1989) identified a meso- α -scale convective cycle that occurs early in the growth phase and argues that it distinguishes between the early stage evolution of an MCC and other shorter-lived MCSs. The duration of the MCCs is related with a maximum area of MCCs but not related with the MCC location. The MCCs over the MCC are nocturnal that similar with previously reported that one of the more intriguing aspects of MCCs is that all populations are predominantly nocturnal (Maddox 1980, Velasco and Fritsch 1987, Miller and Fritsch 1991, Laing and Fritsch 1993).

In general, the greatest frequency of occurrences for initiation occurred between 1900 – 2200 LT. The systems reached the maximum size extent after midnight or early morning in predominantly between 0100 - 0500 LT and then MCC start to decayed in the morning a few hours after sunrise, predominantly around 0700 - 0900 LT. The systems dissipated from the daytime until the afternoon, around 1000 - 1500 LT. It indicated that the majority of MCCs over IMC exhibit a nocturnal life cycle that begins in the mid-to-late afternoon, peaks after midnight and ends shortly after daybreak. Nocturnal growth in convective storms has been hypothetically related to the differential radiative heating between the MCC and the environment, which leads to peripheral environmental subsidence and low-level convergence into the system (Gray and Jacobson 1977). The coastal and continental MCCs are relatively similar than the general MCC population over the IMC. In contrast, the life cycle of oceanic MCCs was found to be slightly different from the general MCC population over the IMC. The oceanic MCCs dominantly develops in midnight, and reach maximum size in the morning and then MCCs decayed and dissipated from noon until afternoon. Morning development of oceanic systems has been noted by Machado et al. (1993), Mapes and Houze (1995) and

Devlin (1995). This difference in life cycles for oceanic systems suggests that the life cycles are not totally dictated by the diurnal radiation cycle, but may also be affected by such factors as surface properties, regional physiography and/or secondary dynamical processes driven by the relatively stronger over diurnal land circulation.

The evolution and propagation of the MCC over the IMC have been observed using the case study and composite analyses. Results found that the majority of MCCs over the IMC developed when several small clouds or orographic clouds merged and grew larger because of interactions between the convergent surface wind flows and the land-sea breeze. Those observed in this study were usually nocturnal and reached a maximum at midnight. Convergent wind flows allowed the clouds to grow to a maximum size, and land-sea breezes became stronger during the mature stage. The MCCs decayed and dissipated because of divergent outflows from the cold pool, in conjunction with the land-sea breezes that generated and propagated new convective systems. These new convective systems migrated to areas surrounding the MCCs, helped by land-sea breezes and interactions between the cold pool outflow and the westerly/southerly/easterly/northerly winds. During propagation, the new convective systems induced convective clouds in the areas surrounding them, which also followed the propagation of advection and convergence fields. It triggered new growth of either convective systems or continuous heavy rainfall systems induced by the new convective systems.

For detail the conclusion of the evolution and propagation of MCCs over the IMC, we create the schematic representations of the evolution and propagation of the MCCs based on the case study and composite analysis. The MCC over the western coastal of the Sumatra as described in region 1 began to develop from several convective clouds from the south and west that helped by southerly wind flow and westerly wind flow which interacted with the land breeze and mountain breeze in midnight as shown in Figure 7.1 (initial stage). The cloud system grew and expanded reached the maximum extent due to the meeting of the strong land breeze and westerly flow, at the same time the rainfall increasing, and cold pool began to developed in around morning as shown in Figure 7.1 (mature stage). The MCCs began to dissipated, and new convective systems were generated owing to the development of the cold pool, during MCC decayed and dissipated in the noon until afternoon. The new convective system generated over the western coastal of the Sumatra during the noon propagated to the along of the western of Sumatra that produced the heavy rainfall because of the divergent

outflow of the cold pool, in conjunction with the evening sea breeze. So that, the propagation characteristics of the MCCs over the western coastal of the Sumatra is dominantly eastward-propagating.

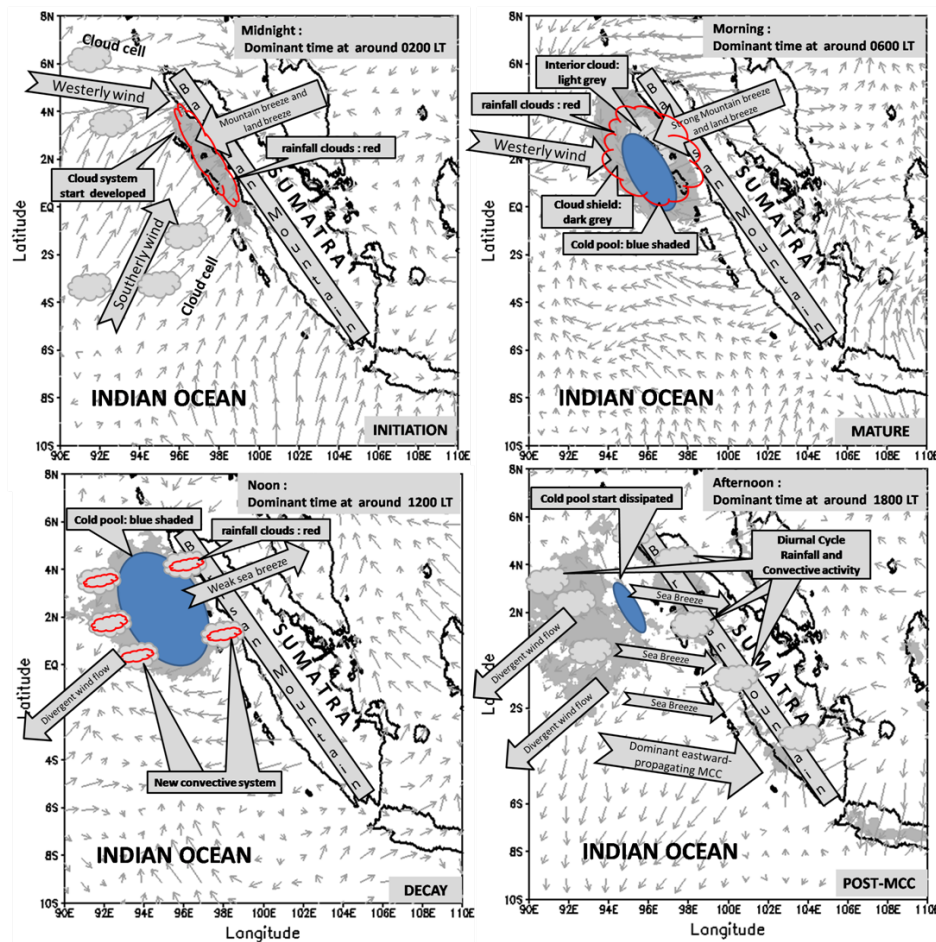


Figure 7.1. Schematic representations of the evolution and propagation of the MCC over region 1 related to the diurnal rainfall variation along the western coast of Sumatra. Light and dark gray areas illustrated the MCC cloud shield and convective clouds, respectively.

The development process of the MCCs over the Indian Ocean near Sumatra which described in region 2 and case study 1 as illustrated in Figure 7.1. The MCCs development in this region is nearly similar with the MCC which occurred in the western coastal of Sumatra. However, the MCC in this region is usually generated by deep convective cloud, and the strong convergent flow is presented during mature stage. The MCCs in this region also related to the diurnal rainfall variation over the western coastal of the Sumatra due to the new convective system dominantly eastward-propagating. The result of the MCC in region 1 and

region 3 give a deeper insight into the mechanism of eastward-propagating convective systems, which previously have been reported to occur in the region (e.g., Mori et al. 2004).

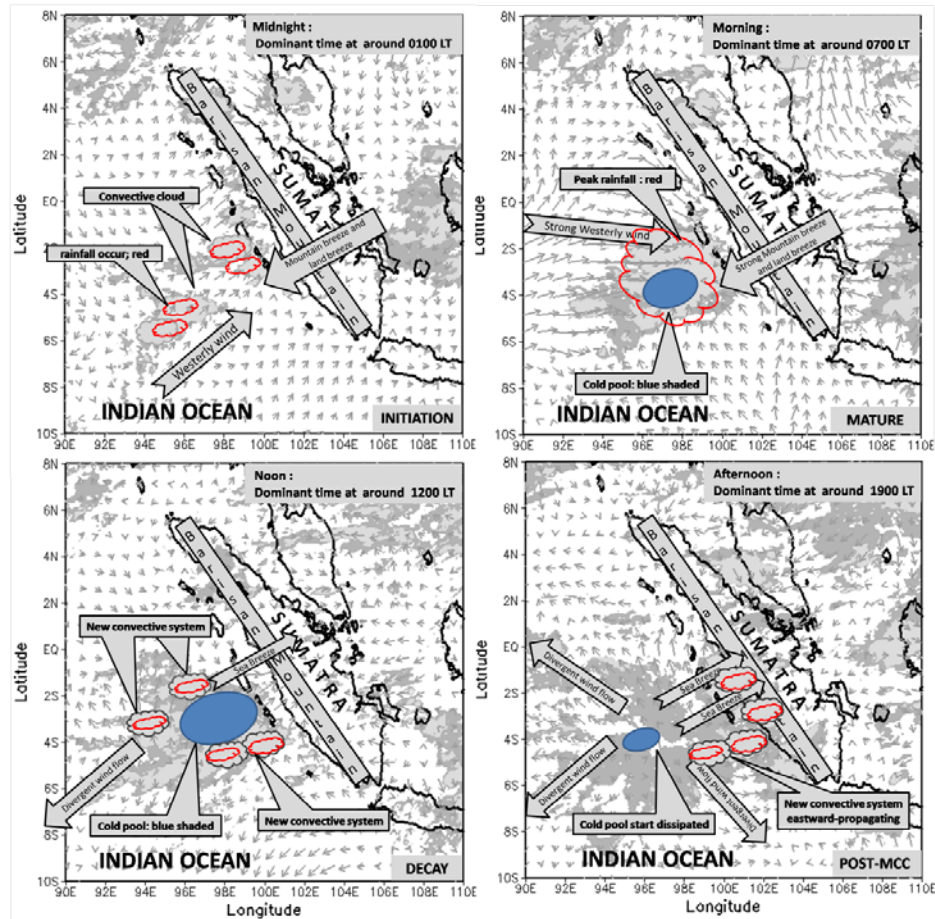


Figure 7.2. Schematic representations of the evolution and propagation of the MCC over region 2 related to the diurnal rainfall variation over the western coast of Sumatra. Light and dark gray areas illustrated the MCC cloud shield and convective clouds, respectively.

Results found that MCCs of which develops over the Indian Ocean and western coastal of Sumatra as shown in Figure 7.1 and Figure 7.2 are related to the diurnal convective activity over the western Sumatra. It is indicated by several previous studies, for example, Renggono et al. (2001) showed that diurnal variations of convective activities are prominent in the mountainous area in Sumatera. They showed that convective clouds tend to develop from 1300 LT to 2100 LT and that after the decay of convective clouds, stratiform clouds develop until early morning (0600 LT). From observations by GPS-derived precipitable water, radiosondes, and surface weather station, Wu et al. (2003) showed that a rainfall event often occurs as intensive showers during a short period in the late afternoon and early evening

at the mountainous area of Sumatra, and suggested that the evaporation of water from the surface by the strong solar heating and horizontal transport of water vapor by thermally induced local circulation play an important role in diurnal variations of convective activities. Recently, Mori et al. (2004) showed time and spatial variations of rainfall around the west coast of Sumatra by using data observed by TRMM. They showed that the peak of rainfall and convective activity over Sumatra in the daytime until afternoon, at the same time, this results study show that the MCCs started migrated to the Sumatra Island.

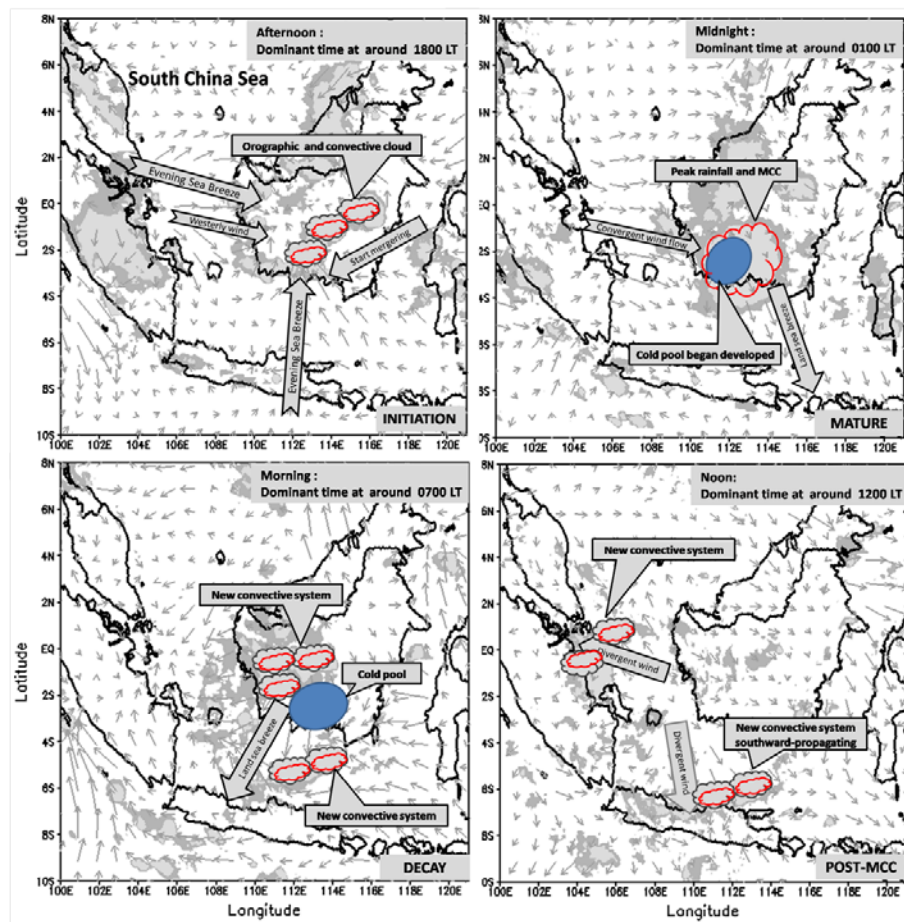


Figure 7.3. Schematic representations of the evolution and propagation of the MCC over region 3 related to the diurnal rainfall variation over the southern of Sumatra and Java Islands. Light and dark gray areas illustrated the MCC cloud shield and convective clouds, respectively.

Figure 7.3 illustrated the evolution and propagation of the MCC that occurred over the Central Kalimantan was described as region 3 and case study 2. In general, the MCCs in this region is usually develops triggered by the orographic clouds from the north that interacted with the convergent wind flow as the evening sea breeze from Java and eastern of Sumatra.

The convergent wind became weak during mature due to the impact of the land breeze in the midnight. The new convective system start appears during MCC decayed in surrounding edge of the cold pool. Sometimes the MCC in this area generates the squall line on the southern side of the system. The new convective system migrates westward to Sumatra and migrates southward to Java Island after the MCC dissipated. So that, the MCCs in this region in influencing the diurnal variation over Sumatra and Java. This result strengthens the analysis of the result from Shibagaki et al. 2006 that reported the westward-propagating meso- β -scale cloud clusters developed in eastern Sumatra, and an orographic cloud system formed over a mountain range in western Sumatra during case study on active phase of ISO that already described in Figure 1.10.

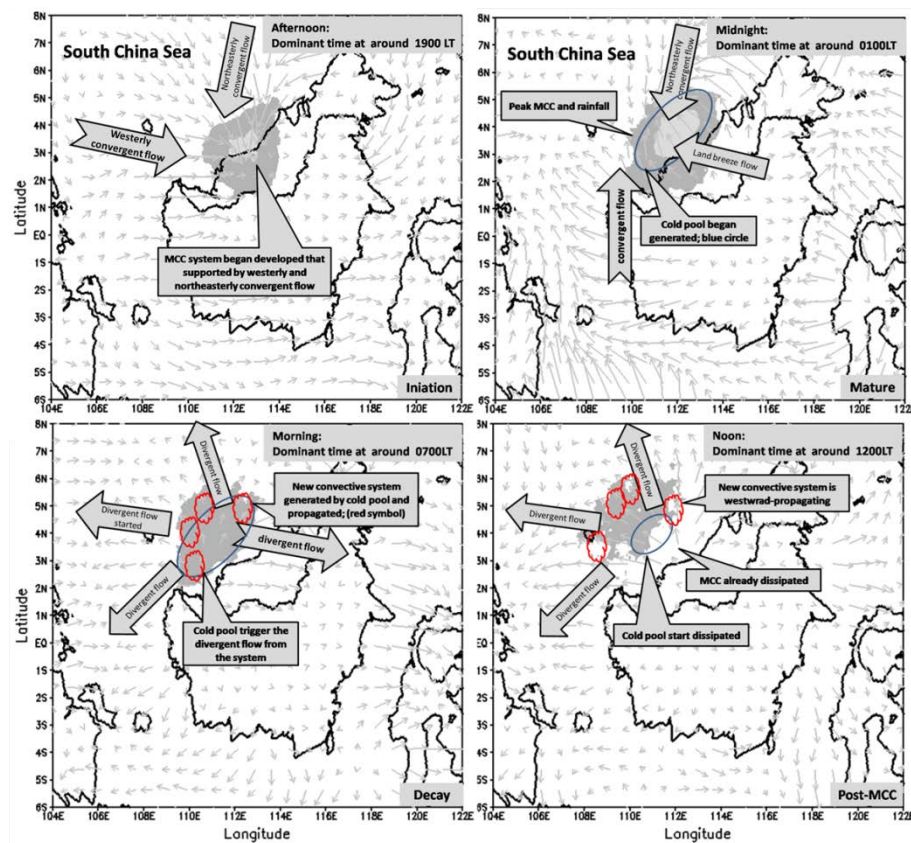


Figure 7.4. Schematic representations of the evolution and propagation of the MCC over region 4 related to the development of the convective system over the South China Sea. Light and dark gray areas illustrated the MCC cloud shield and convective clouds, respectively.

MCCs that occurred over the South China Selatan near of northern of Kalimantan Island is usually beginning develops triggered by the convergent wind flow that indicated as the westerly and northerly wind from the South China Sea as illustrated in Figure 7.4. The

system reaches maximum extent due to interaction with the midnight land breeze that followed the rainfall also reached the maximum, and cold pool started develops. The new convective system began to appear during MCC decayed, and migrate westward after the MCC dissipated. So that, this MCC is not giving significant impact to the continent due to migrating to the South China Sea. However, the MCCs in this region is possible as one of the triggers to the development of the other convective system over the South China Sea, which previously has been reported about the mechanism of the development of the convective system over the South China Sea by Houze (1981) as described Figure 1.7. Houze et al. (1981) showed that morning precipitation over the sea near north-west Kalimantan Island was caused by the convergence of the land breeze and monsoon wind (Johnson and Kriete, 1982).

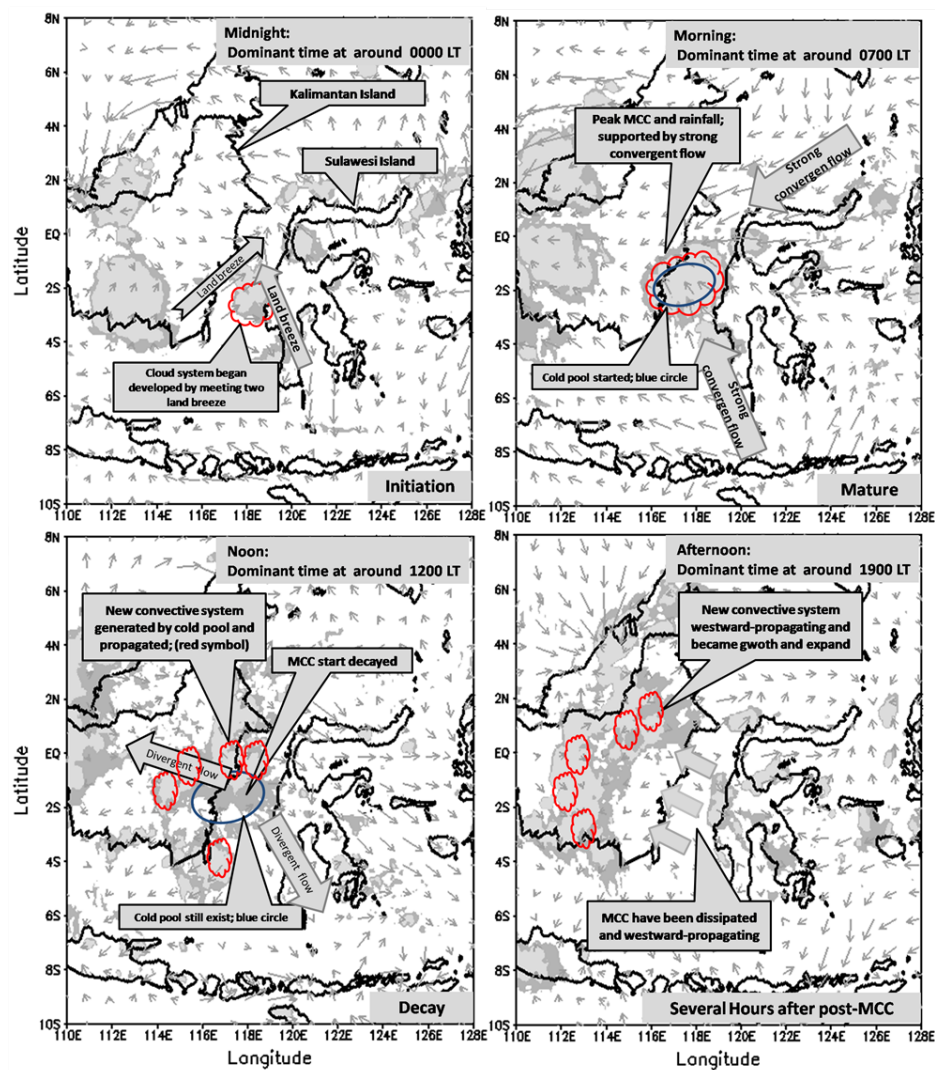


Figure 7.5. Schematic representations of the evolution and propagation of the MCC over region 5 related to the diurnal rainfall variation over the Kalimantan Island. Light and dark gray areas illustrated the MCC cloud shield and convective clouds, respectively.

The existence of the meeting of land breeze from Kalimantan and the land breeze from Sulawesi is usually as a trigger to the development of the MCC in the coastal of the Sulawesi or Kalimantan or in between of them as illustrated in Figure 7.5. The system reached maximum due to supported by the strong convergent wind flow from northern side and southern side of the Sulawesi Island that toward to the system area. Similar with the MCC in the other area, the rainfall reaches maximum extent, and cold pool began to developed during mature stage. The new convective system began to appear during MCC decayed and after several hours MCC dissipated, the new convective system has been migrated and influencing the convective activity over the Kalimantan Island. Sometimes the MCC in this region generates the other type of MCS like a bow echo structure.

Figure 7.6 shows that MCCs in this region began to developed triggered by the southerly wind flow and valley breeze from Jayawijaya mountain. Similar to the other region, MCC with maximum size will generate the maximum rainfall. MCC in this region reached maximum extent in the continent, but this system decayed and dissipated in the ocean (Arafura Sea) due to the system migrate westward during maximum to decay.

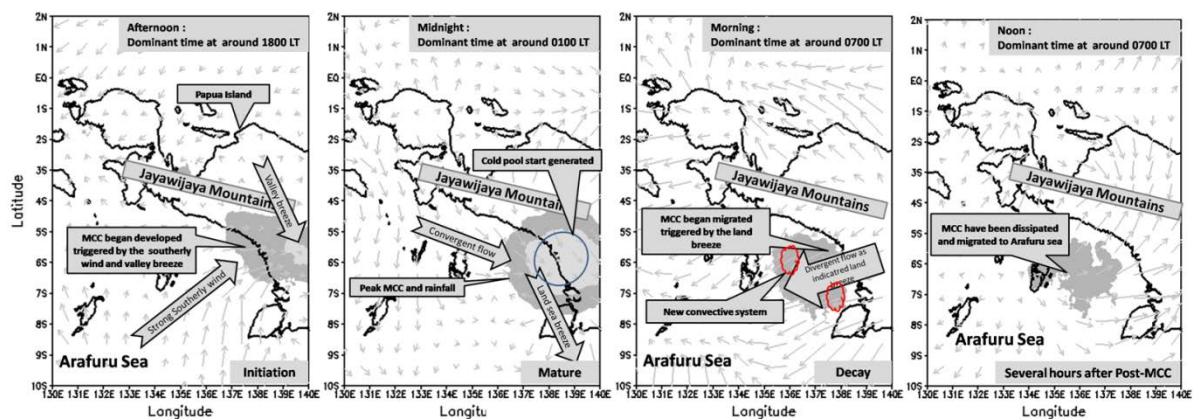


Figure 7.6. Schematic representations of the evolution and propagation of the MCC over region 6 related to the development of the convective system over the Arafura Sea. Light and dark gray areas illustrated the MCC cloud shield and convective clouds, respectively.

The evolution pattern during MCC events indicated similar pattern with the rainfall system. It indicated the MCCs are associated with the rainfall. The peak of rainfall is found

during MCC reaches maximum extent in the mature stage. The rainfall became significantly decrease when the MCC decayed. However, the new rainfall system appears in the surrounding area of the system due to the new convective system. The greatest rainfall accumulation is presented in the center of MCC system area for the oceanic, continental and coastal MCCs. It indicated that the significant influence of MCC to the rainfall is during MCC reached maximum extent in the mature stage. However, the high rainfall accumulation also appears in several regions near the MCC system area. It indicated that the effect of MCCs are not only over the MCC system area but also influencing to the rainfall in the surrounding area of the MCC systems.

The results from this study showed that, in general, the initial stage of the MCC was characterized by strong low-level convergence and vertical convection and was largely driven by the convergence of the moisture flux in the lower troposphere. The mature stage of the MCC was characterized by weak surface convergence, strong upper-level divergence, and a shortwave ridge in the mid- and upper-levels. Where there was strong surface divergence, the decay and dissipation stages were very similar, and surface convergence left the system. Movement of most MCCs resulted from the combined contributions of advection and the propagation of surface convergence. Results from this research show that these large convective systems tended to form in the vicinity of the terminus of a low-level jet that transported moist and warm air to the originating regions of the MCCs. Shortwave troughs and baroclinic zones were associated with MCC development. Results from the composite analysis were consistent with the case study, which indicates that MCCs in the same area as the case study shared the characteristics of the case study. The MCCs that occurred over the western coastal of Sumatra influenced the convective activity over the island of Sumatra; those that occurred over the northern coastal area of Kalimantan triggered a diurnal cycle over the South China Sea, and those that occurred in the coastal region of Papua near Merauke were related to cloud development over the Arafura Sea.

The MCC first develops when instability is at its greatest due to latent heating. The greatest severe weather that occurs with an MCC tends to occur in the developing stages since each storm has more energy and instability. As the cluster of storms becomes more numerous the severity of the storms will often decrease but the areal coverage of precipitation and storms increases during mature. They can remain organized and travel great distances before the storm complex dissipates. It is often after midnight before MCCs will dissipate. They can

dissipate by moving into an environment where the moisture, wind shear, lift, and instability is no longer able to sustain the system. The movement of most MCCs is the result of the combined contributions of advection and propagation. It is especially true of the intense convective rain areas responsible for the bulk of the severe weather and flooding. The advective component correlates strongly with the mean flow in the cloud layer. The departure from the mean cloud layer flow is strongly influenced by the speed and direction of the low-level inflow of high θ_E air feeding the deep convective overturning. New growth favors this inflow area and the systems, therefore, tend to propagate toward the source of the high θ_E air, i.e., in a direction opposite the low-level inflow. It has been shown that a reasonable estimate of the speed and direction of MCCs can be obtained from the vector difference between the mean flow in the cloud layer and the low-level jet.

More studies have shown that the tendency for MCCs to propagate toward the source of the high θ_E air feeding the convection is augmented or possibly even dominated by the interaction of the MCC-generated cold pool. This leads to enhanced convergence and deeper lifting along the right (left) flank of northern (southern) hemisphere convective lines. Additional convection as a result of the enhanced forcing re-enforced the cold outflow thereby promoting a further rightward (leftward) advancement of a northern (southern) hemisphere line. This condition is also shown in this research. There are several of evidence that shows that MCCs substantially alter their large scale environment. The most commonly observed changes show that the systems generate a positive\negative\positive pattern of vorticity advection and moisture flux convergence which possible generated mid level jet and LLJ. They are also typically manifested as a mid-level mesovortex, a high-level anticyclone, and a surface-based cold pool and mesohigh. The presence of the strong warm advection characteristic of MCC environments, in general, suggests that, in addition to the interaction of the convectively-generated cold pool with the ambient shear, the large-scale environment itself can contribute significantly to the ascent air that comprises MCC region. Specifically, the warm advection implies, and observations confirm (eg., Maddox 1983, Augustine and Howard 1991, Smull and Augustine 1993, Trier and Parsons 1993, Augustine and Caracena 1994), that there is a sloping isentropic lift as an inherent part of the MCC environment.

MCCs can contain squall lines and/or multicell and/or bow echo. MCCs in IMC is frequently located in the upper short-wave trough. An upper short-wave trough tends to be associated with MCC development. The low-level wind accelerations that they produce

provide a significant enhancement to the low-level warm advection and convergence that would normally be present as a result of an approaching short wave and/or a synoptic scale circulation. This research reveals that these large convective systems form in the vicinity of the terminus of an LLJ that is supplying high- θ_E air to the MCC genesis region. So that if the weak mid-level short wave is approaching the genesis area and enhances the low-level convergence associated with the LLJ. Results also found the oceanic MCCs are slightly larger and last longer than the continental and coastal MCCs due to the convergent wind flows become stronger during the mature stage, while the convergent wind flows become weakened during mature stage of the continental and coastal MCCs. The convergent wind flows of the coastal and continental MCCs are weakening due to the effect of the land breeze where the majority of the continental and coastal MCCs reached maximum extent in the midnight.

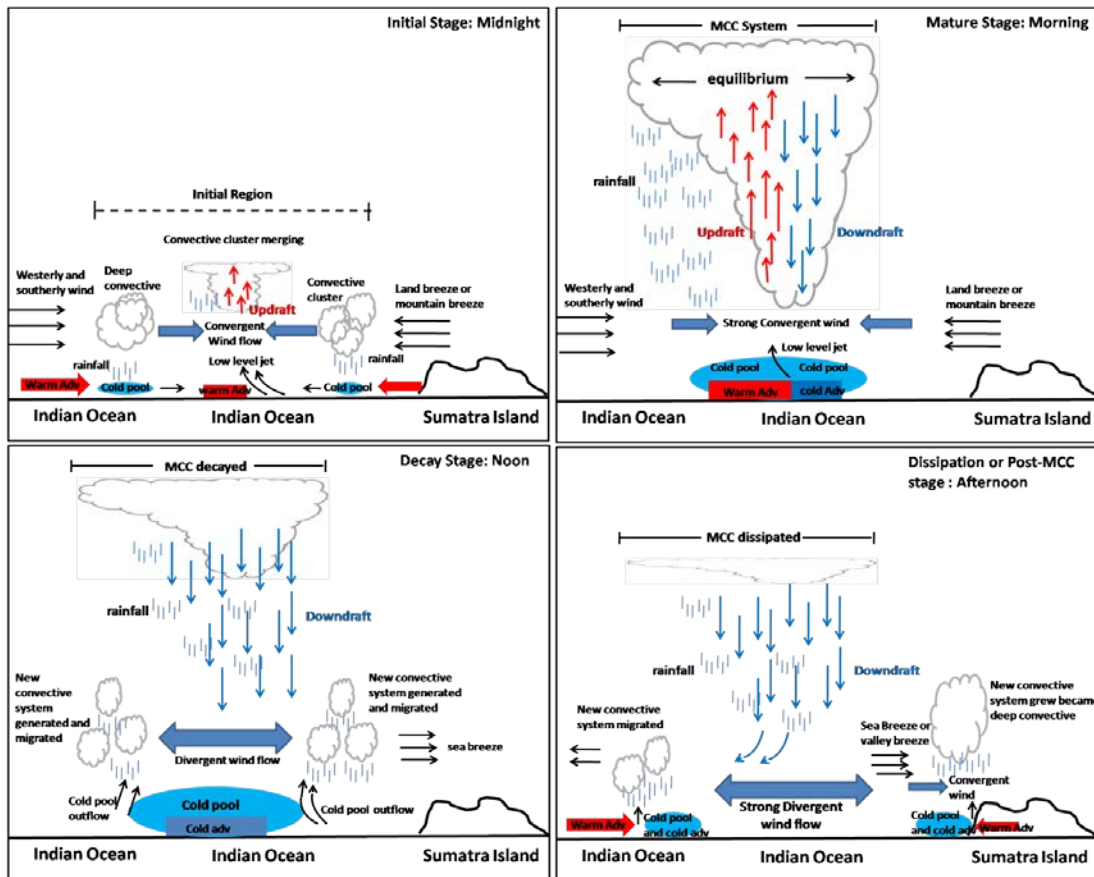


Figure 7.7. Vertical schematic representations of the development of the MCC over region 2 related in the Indian Ocean.

Warm advection dominates the lower troposphere while diffluence is the rule at high levels. The presence of the strong warm advection characteristic of MCC environments, in

general, suggests that, in addition to the interaction of the convectively-generated cold pool, the large-scale environment itself can contribute significantly to propagate of the MCC. An upper short-wave trough tends to be associated with MCC development. The low-level wind accelerations that they produce provide a significant enhancement to the low-level warm advection and convergence that would normally be present as a result of an approaching short wave. The surface convergence wind flows in the lower atmosphere is also important in this process. The example simple vertical schematic processes for the development of the MCC is shown in the below figure. The main point of Figure 7.7 show that the clouds develop triggered by the LLJ, in the warm advection area, and the clouds reached maximum size due to the strong convergent wind flow and the LLJ. The new convective system began to appear during MCC dissipated due to the cold pool outflow, and the new convective system migrated helped by the land-sea breeze circulation, at the same time, the cold advection and convergence field moving that support the new convective system inducing the other convective cloud while they are propagated. Overall, the development of the continental, coastal and oceanic MCCs is relatively similar but just different in the time occurrences, the strong or weak of the divergence field, temperature advection field, θ_E ridge, the short wave trough and the direction of the convergent wind flows. However, the main point of the mechanism of the development of the continental and coastal MCCs are relatively similar with the oceanic MCCs.

Based on a case study and composite analysis, the initial region of the MCC system over IMC is characterized as follows in Table 7.1:

Table 7.1. The comparison of the environmental condition of the continental, coastal and oceanic MCC during the initial stage.

	The oceanic MCC	The continental MCC	The coastal MCC
Surface and Low	Maximum surface convergence and strong low-level convergence		
	Surface Potential temperature clearly was seen	Surface Potential temperature is not clearly seen	
	Occur in midnight	Occur in late afternoon	Occur in midnight
	Helped by interaction of westerly wind, strong southerly wind, and land breeze	Helped by interaction of northwesterly wind, strong southerly wind, and mountain breeze	Helped by interaction of the meeting of two land breeze from Kalimantan and Sulawesi
	High relative humidity more than 90%		High relative humidity around 80%

	Shortwave trough	Shortwave trough/ridge/trough pattern	Shortwave trough
	Weak moisture flux convergence	Positive/negative border of moisture flux convergence	High moisture flux convergence
	Higher mixing ratio		Center of higher mixing ratio
Middle	Possibility generated the storm	Positive/negative/positive pattern of the vorticity advection (Possibility generated the storm and mid level jet)	Possibility generated the storm
	Strong short-wave trough that is moving over the leading edge		
	Strong acceleration of wind		
Upper	Shortwave trough northward	Shortwave trough southward	Shortwave trough eastward
	Strong upper-level divergence	Weak upper-level divergence	

While the mature region of the MCC system over IMC is characterized as follows in Table 7.2:

Table 7.2. The comparison of the environmental condition of the continental, coastal and oceanic MCC during the mature stage.

	Ocean	Continental	Coastal
Surface and Low	Surface convergence stronger than initial	Weak convergence in northern edge and weak divergence in southern edge	Weak convergence
	Relative humidity increase		
	High moisture content		
	Shortwave trough deeper		
	Weak moisture flux convergence	Strong moisture flux convergence	
Middle	Weak positive vorticity	Positive/negative/positive pattern of the vorticity advection (strong mid level jet)	Weak positive vorticity
	Center low geopotential height	Short-wave ridge	Shortwave trough
Upper	Longwave trough		
	Strong divergence	Weak divergence	

The decay and dissipation region of the MCC system over IMC is characterized as follows in Table 7.3:

Table 7.3. The comparison of the environmental condition of the continental, coastal and oceanic MCC during the decay and dissipation stage.

	Ocean	Continental	Coastal
Surface and Low	Lower potential temperature and higher relative humidity zone migrate eastward	Lower potential temperature and higher relative humidity zone migrate westward and southward	Lower potential temperature and higher relative humidity zone migrate westward
	Weak surface divergence		
	Moisture content decrease		
	Moisture flux convergence left the system		
Middle	the short-wave mid level trough is very pronounced		
	Weak positive vorticity		
Upper	long-wave trough across still presented		
	upper-level divergence moving westward and eastward	upper-level divergence also moving northward	upper-level divergence also moving westward

The contribution of the MCC to the total rainfall and extreme rainfall over the IMC has been determined in this study. One of the result shows that the MCC not only contribute to rainfall in the MCC area but the MCC give a contribution to its surrounding area. A large number of MCCs over IMC in this study found at mainly continental, strongly related with orography. The greatest contribution of the MCC to the total rainfall and extreme rainfall is most frequently occurs in the concentrated area of the MCC occurrences. The greatest contribution of the oceanic MCC is in the Indian Ocean that always gave the great contribution in this area in each season and the peak of the contribution in MAM and SON. While the greatest contribution of the continental MCC is in central Kalimantan and Merauke, which almost occur in each season, except in JJA with a few percentage. The coastal region that always contributed by the coastal MCC is in western coastal of the Sumatra, Cendrawasih Bay and the South China Sea near the northern coastal of the Kalimantan Island.

The result also shows that the greatest contribution MCC to total rainfall for DJF season are in the coastal area near the northern part of Sumatra, which reached 18-22%. But a considerable contribution ranges from 14-20% also occurred in several locations such as Central Kalimantan, the South China Sea near Sarawak, South Sulawesi, on the coast of

Central Sulawesi and over Merauke on the Papua Island. The greatest contribution during MAM is relative similar with DJF, but the percentage value is a slightly increase around of more than 24% found in two locations i.e., on the South China Sea near the Brunei Darussalam and Central Kalimantan. During JJA, the impact of MCC to JJA rainfall is slightly less over continent where the MCC contribution just found up to 10%. MCC has a strong influence only at a few locations in the Indian Ocean, in coastal areas near West Kalimantan and coastal areas near Merauke Papua Island. The large contribution from continental MCC to total rainfall during SON is located in the Central Kalimantan and Southern Sumatra, while the contribution of coastal MCC almost exists along the western coast of Sumatra, the South China Sea near Brunei Darussalam, Makassar Street, and Cendrawasih Bay. The greatest contribution is more existence over continent than the ocean, where found almost in every season in some area over the continent, except in July. The greatest contribution of MCC oceanic just concentrated in the Indian Ocean near Sumatra in every season.

In the monthly analysis, the result shows the contribution of MCCs to monthly total rainfall up to 30% in several areas. During January, the maximum contribution of MCCs to total rainfall monthly was found on the west coast near the northern Sumatra up to 30%. The largest contribution of the continental MCCs also found on the Central Kalimantan for each month except June, even a percentage value in this area reached more than 30% during the month of March and April. The largest contribution of the coastal MCCs in the South China Sea near Brunei Darussalam that most frequently occurred in March and April. The greatest contribution of the oceanic MCCs in the Indian Ocean that most frequently occurs in November. The great contribution of the MCCs to November rainfall also found in some area. i.e., on the Indian Ocean near Sumatra, on the South China Sea near Borneo (Kalimantan) Island, on Central Kalimantan, on the coast of Merauke Papua Island and over Cendrawasih Bay. The contribution of MCCs along Java Island until East Nusa Tenggara is less than 4% in each month.

The maximum rainfall is mostly concentrated over continent than the ocean on each season. The maximum rainfall was always found over Cenderawasih Bay, in the coastal region of western Papua with the highest value. In contrast, the maximum rainfall is very rare found along Bali until East Nusa Tenggara in each season. Most of the extreme rainfall was found over the southern of IMC on DJF and the northern of IMC on JJA. Almost the same

with DJF, in MAM, the greatest values of STD occurred in areas that are often the appearance of maximum rainfall, but in Java Island, the difference value between STD and MRV is quite large. The considerable difference between STD and MRV on JJA occurred in the Indian Ocean. The greatest values of STD also occurred in areas that are often the appearance of maximum rainfall during SON. The distribution of EET-1 around 1 to 10 mmhr⁻¹, EET-2 around 2 - 15 mmhr⁻¹, and EET-3 around 4 - 22 mmhr⁻¹. The highest extreme threshold is more frequently occur over continent than over the sea in every season. The extreme threshold always high over Cenderawasih Bay, in the coastal region of West Irian Jaya in very season and every type of extreme rainfall. In contrast, the small value of extreme threshold exists along Bali until East Nusa Tenggara in every season. It indicates that the magnitude of extreme threshold over some area depends on the amount of maximum rainfall that occurs in this areas.

The highest values of mean accumulated rainfall produced by EET-1, EET-2 and EET-3 in each season around 1000 - 1200 mm/month, 350-500 mm/month and 160-200 mm/month, respectively. The contribution of MCC coastal found in the coastal region of Sumatra, in the South China Sea near West Kalimantan, over Cendrawasih Bay, in the valley of Jayawijaya Mountain and the Central Kalimantan. The contribution of MCC on EET-3 over IMC on each season is higher than the other types of extreme rainfall. The greatest contribution of MCC on average on each season to EET-1, EET-2 and EET-3 is around 18-24%, 24-36%, and 27-39%, respectively, but several regions have a contribution on EET3 reached 36 - 45%. The contribution of MCC to extreme rainfall is mostly concentrated over continent than the oceans on each season except JJA, where mostly concentrated over the Indian Ocean. The greatest contribution was always found on the Central Kalimantan and along the valley of Jayawijaya mountain. Results found that majority of the MCCs over the IMC produced extreme rainfall because the contributions from the MCCs were up to 45% greater for type 3 extreme events than for the other types.

This research found that the greatest contribution of the MCC is during MCC reached maximum extent. It is different with the previous work that stated the early growth period also appears to be the most crucial time for the development of severe weather (high wind, tornadoes, and hail). For example, in an analysis of 12 nocturnal MCCs, Maddox et al. (1986) found that over 80% of the severe weather occurred during the initiation period. Likewise, in a comprehensive analysis of Oklahoma mesoscale convective precipitation systems, Houze et

al. (1990) found that tornado and hail reports were biased toward the early stages of the systems' development. Similarly, Tollerud and Collander (1993) investigated 350 MCCs that occurred in the U.S. during the ten-year period 1978-87 and found that an overwhelming fraction of the severe weather occurs in the initiation phase. On the other hand, nearly half of the severe wind reports occur during the developing and mature stages. Although it is not known what fraction of the global population of MCSs produces severe weather, about half of the systems that occur in the central U.S. exhibit some type of severe activity (Houze et al. 1990). Of this number, about twice as many severe events occur in linearly-organized systems compared to the more circular MCCs (Tollerud and Bartels 1988). Nevertheless, U.S. MCCs are prolific producers of severe events. Moreover, Maddox (1980) points out that one in every five MCCs produces injuries or death.

7.2 Future work

One of the conclusions of this research is the majority of MCCs over the IMC contributed to total rainfall and extreme rainfall over the IMC. The combination of the land-sea breeze and cold pool outflows from the decaying MCC was a significant factor in the formation of the new convective systems that induces strong rainfall in its surrounding areas. For example, the majority of the new convective system generated by the decaying MCC over the western coastal of the Sumatra as region 1 propagates to the along of the western of Sumatra that produced the heavy rainfall. In future studies, this information about the development and movement of MCCs should be integrated into regional weather models to allow precise prediction of MCCs. It can become one of the early warning systems for the climate hazards over Indonesia.

Figure 2.6 in Chapter 2 shows that the variability which influencing the climate of the IMC occurs on timescales ranging from intra-diurnal (e.g. sea-breezes) to interannual (e.g. the El Niño Southern Oscillation) and on spatial scales ranging from a few kilometres (e.g. individual cloud cells), to thousands of kilometres (e.g. the Madden-Julian Oscillation), to planetary scale ENSO oscillations. The important result of this research is that MCCs contribute to extreme rainfall locally, which possible organized by the Madden-Julian Oscillation, which is in turn connected to ENSO. The process that couples the land, ocean, and atmosphere take place in association with multiple interacting space and timescales. So that, for further long-term predictions, however, the effects of large-scale environments, i.e.

the Madden-Julian Oscillation (MJO), El Niño-Southern Oscillation (ENSO), and Indian Ocean Dipole (IOD), on MCCs in the IMC need to be considered.

Kalimantan Island is one of the places that most frequently found of MCC occurrences, especially in the Central Kalimantan and northern Kalimantan Island. Our hypothesis, one of the factors that cause of many MCCs occurrences over Kalimantan Island is the cold surge from the south china sea and the Borneo vortex. At the time of the Asian winter monsoon takes place, often a cold air mass propagation of high-pressure center in the mainland of Asia toward the South and to the East. The propagation of this cold air mass is then known as cold surge which is one of the synoptic scale weather phenomena that have a significant influence during Asian winter monsoon. Cheang (1987), defines cold surge as a cold air mass carried by the wind north-south circulation (meridional) due to the interference of high pressure in the region of Siberia. Although the active period is only of the order of the day but cold weather impact the surge has destroyed part of East Asia and also affect the rainfall in the Southeast Asia region (Chang et al. 2005). According to Hattori et al. (2010), the cold surge activities could increase rainfall in the Java Sea, Kalimantan Island, and the Philippines. There is a strong correlation between the activity of cold surge with increased convection in Indonesia Southern Region (Compo et al. 1999). Borneo vortex are strong storms that form in the South China Sea and bring strong winds and heavy rainfall to West Borneo/Kalimantan. A Borneo vortex generally has a shallow vertical structure, but in the extreme case, it could intensify into a tropical storm, and in one instance, even a typhoon with a deep vortex tube and a well-formed eyewall despite its proximity to the Equator. Interesting to explain the modulation of the cold surge and Borneo vortex in influencing the MCC occurrence over the Kalimantan Island.

REFERENCE

- Adler, R. F., and A. J. Negri, 1988: A satellite infrared technique to estimate tropical convective and stratiform rainfall. *J. Appl. Meteor.*, **27**, 30-51.
- Ahrens, C. D., 2001: Cloud Development and Precipitation. *Essentials of Meteorology – An Invitation to the Atmosphere*, 504 pp.
- Anderson, C. J. and Arritt, R. W., 1998: Mesoscale convective complexes and persistent elongated convective systems over the United States during 1992 and 1993. *Mon. weather Rev.*, **126**, 578 - 599.
- Arnaud, Y., Desbois, M., and Maizi, J., 1992: Automatic tracking and characterization of African convective systems on Meteosat pictures, *Journal of Applied Meteorology*, **31**: pp.443-453.
- Asai, T., S. Ke, and Y. Kodama, 1998: Diurnal variability of cloudiness over East Asia and the western Pacific Ocean as revealed by GMS during the warm season. *J. Meteor. Soc. Japan*, **76**, 675–684.
- Ashley, W. S. 2003: A distribution of mesoscale convective complex rainfall in the United State. *American Meteorology Society*, **131**, 3003 – 301
- Atlas, R., R. N. Hoffman, J. Ardizzone, S. M. Leidner, J. C. Jusem, D. K. Smith, and D. Gombos, 2011: A cross-calibrated, multiplatform ocean surface wind velocity product for meteorological and oceanographic applications. *Bull. Amer. Meteor. Soc.*, **92**, 157-174.
- Augustine, J. A., and K. W. Howard, 1991: Mesoscale convective complexes over the United States during 1986 and 1987. *Mon. Wea. Rev.*, **119**, 1575–1589.
- Augustine, J. A., and K. W. Howard, 1989: Mesoscale convective complexes over the United States during 1985. *Mon. Wea. Rev.*, **116**, 685–701.
- Augustine, J. A., and F. Caracena, 1994: Lower-tropospheric precursors to nocturnal MCS development over the Central United States. *Wea. Forecasting*, **9**, 116–135.
- Bjerknes, J., 1969: Atmospheric teleconnections from the equatorial pacific. *Mon. Wea. Rev.* **97**. 163-172.
- Blamey, R. C., and Reason, C. J. C. 2012: The role of mesoscale convective complexes in southern Africa Summer Rainfall. *J. Clim* **26**.
- Brito, A.L., Veiga, J.A.P. and Yoshida, M.C, 2014: Extreme Rainfall Events over the Amazon Basin Produce SignificantQuantities of Rain Relative to the Rainfall Climatology. *Atmospheric and Climate Sciences*, **4**, 179-191.
- Bosart, L. F., and F. Sanders. 1981: The Johnstown flood of July 1977: A long-lived convective system. *J. Atmos. Sci.*, **38**, 1616-1642.
- Carbone, R. E., J. D. Tuttle, D. A. Ahijevych, and S. B. Trier, 2002: Inferences of predictability associated with warm season precipitation episodes, *J. Atmos. Sci.* **59**, 2033–2056.
- Carvalho, L. M. V. dan Jones, C. 2001: A Satellite method to identify structural properties of mesoscale convective systems based on the Maximum Spatial Correlation Tracking Technique (MASCOTTE). *J. of Applied Meteorology. American Meteorology Society*, **40**, 1683-1701.
- Chang, C.P., Z. Wang., J. Ju., and T. Li., 2004: On the relationship between western maritime continent monsoon rainfall and ENSO during Northern Winter. *J. Climate.*, **17**. 665-672.

- Chang, C.P., Harr, P.A., dan Chen, H.J., 2005: Synoptic disturbance over the equatorial South China Sea and western maritime continent during boreal winter. *Monthly Weather Review*. Vol. **133**. 489-503.
- Chen, S. S., R. A. Houze Jr., and B. E. Mapes 1996: Multiscale variability of deep convection in relation to large-scale circulation in TOGA COARE. *J. Atmos. Sci.*, **53**, 1380–1409.
- Chen, S. S., and R. A. Houze, Jr., 1997: Diurnal variation and life-cycle of deep convective systems over the tropical Pacific warm pool. *Q. J. R. Met. Soc.*, **123**, 357-388.
- Cheang, B. K., 1987: Short and Long Range Monsoon Prediction in Southeast Asia. *Journal of Earth System Science*, Vol.102. 219-239.
- Cheng, C.-P., and R. A. Houze, Jr., 1979: The distribution of convective and mesoscale precipitation in GATE radar echo patterns. *Mon. Wea. Rev.*, **107**, 1370-1381.
- Chong, M., P. Amayenc, G. Scialom, and J. Testud. 1987: A tropical squall line observed during the COPT 81 experiment in West Africa. Part I: Kinematic structure inferred from dual-Doppler radar data. *Mon. Weather Rev.*, **115**, 670–694.
- Collier, J. C., K. P. Bowman, and G. R. North, 2004: A comparison of tropical precipitation simulated by the community climate model with that measured by the Tropical Rainfall Measuring Mission satellite. *J. Climate*, **17**, 3319–3333.
- Compo, G. P., G. N. Kiladis, and P. J. Webster, 1999: The horizontal and vertical structure of east Asian winter monsoon pressure surges. *Quart. J. Roy. Meteor. Soc.*, **125**, 29–54.
- Cotton, W. R., R. L. George, P. J. Wetzel, and R. L. McAnelly. 1983: A long-lived mesoscale convective complex. Part I: The mountain-generated component. *Mon. Wea. Rev.*, **111**, 1983-1918.
- Cotton, W. R., Lin, M. S., McAnelly, R. L. dan Tremback, C. J. 1989: A Composite Model of Mesoscale Convective Complexes. *Mon. Wea. Rev.* **116**, 939 - 949.
- Curtis, S., 2008: The El Niño–Southern Oscillation and global precipitation. *Geogr. Compass*, **2**, 600–619.
- D'Amato, N., & Lebel, T. 1998: On The Characteristics of the Rainfall Events in the Sahel with a View to the Analysis of Climatic Variability. *International Journal of Climatology*, **18**, 955-974.
- Dee, D. P., S. M. Uppala, A. J. Simmons, P. Berrisford, P. Poli, S. Kobayashi, U. Andrae, M. A. Balmaseda, G. Balsamo, P. Bauer, P. Bechtold, A. C. M. Beljaars, L. van de Berg, J. Bidlot, N. Bormann, C. Delsol, R. Dragani, M. Fuentes, A. J. Geer, L. Haimberger, S. B. Healy, H. Hersbach, E. V. Holm, L. Isaksen, P. Kallberg, M. Kohler, M. Matricardi, A. P. McNally, B. M. Monge-Sanz, J. J. Morcrette, B. K. Park, C. Peubey, P. de Rosnay, C. Tavalato, J. N. Thepaut, and F. Vitart. 2011: The ERA-Interim reanalysis: configuration and performance of the data assimilation system. *Quart. J. Roy. Meteor. Soc.*, **137**, 553-597, doi: 10.1002/qj.828.
- Desbois, M., Kayiranga, T., Gnamien, B., Guessous, S., and Picon, L., 1988: Characterization of some elements of the Sahelian climate and their annual variations for July 1983, 1984, and 1985 from the analysis of METEOSAT ISCCP data. *Journal of Climate*, **1**: pp. 867-904.
- Devlin, K. I., 1995: Application of the 85Ghz ice scattering signature to a global study of mesoscale convective systems. M.S. thesis, Texas A&M University, 99 pp.
- Durkee, J. D. dan Mote, T. L. 2009: A Climatology of Warm Season Mesoscale Convective Complexes in Subtropical South America. *Int J. Clim.*, **12** pp.
- Durkee, J. D., Mote, T. L. dan Shepherd, M. J. 2009: The Contribution of Mesoscale Convective Complexes to Rainfall across, Subtropical South America. *Int J. Clim.*, vol **22**.
- Engerer, N. A., Stensrud, D. J., dan Coniglio, M. C. 2008: Surface Characteristics of Observed Cold Pools, *Monthly Weather Review*, **136**, 4839 – 4849.

- Frank, N. L., 1970: Atlantic tropical systems of 1969. *Mon. Wea. Rev.*, **98**, 307-314.
- Frank, W. M., 1978: The life cycles of GATE convective systems. *J. Atmos. Sci.*, **35**, 1256–1264.
- Fritsch, J. M., and R. A. Maddox, 1981: Convectively-driven mesoscale systems aloft. Part I: Observations. Part II: Numerical simulations. *J. Appl. Meteor.*, **20**, 9-26.
- Fritsch, J. M., Kane, R. J. dan Chelius, C. R. 1986 : The Contribution of Mesoscale Convective Weather System to the Warm Season Precipitation in the United States. *J. Climate Appl. Meteor.*, **25**, 1333 - 1345.
- Fritsch, J. M., J. D. Murphy, and J. S. Kain. 1994: Warm core vortex amplification over land, J. Atmos. Sci., 51, 1781–1806.
- Frich, C., Alexander, L.V., Della-Marta, P., Gleason, B., Haylock, M., Klein Tank, A.M.G. and Peterson, T. 2002: Observed Coherent Changes in Climatic Extreme during the Second Half of the Twentieth Century. *Climate Research*. **19**, 193-212. <http://dx.doi.org/10.3354/cr019193>.
- Garstang, M., Kelbe, B. E., Emmitt, G. D., and London, W. B. 1987: Generation of convective storms over the escarpment of northeastern south africa. *Monthly weather review*, **115**, 429–443.
- Gao, X., Pal, J.S. and Giorgi, F. 2006: Projected Changes in Mean and Extreme Precipitation over the Mediterranean Region from a High Resolution Double Nested RCM simulation. *Geophysical Research Letters*. **33**.
- Gray, W. .M. dan Jacobson, R. W. 1977: Diurnal Variation of Deep Convective System in The Tropics. *Mon, Weather Rev.*, **105**, 1171 - 1188.
- Grimm, V. R. Barros, and M. E. Doyle, 2000: Climate variability in southern South America associated with El Niño and La Niña events. *J. Climate*, **13**, 35–58.
- Hadi, T.W., T. Horinouchi, T. Tsuda, H. Hashiguchi, and S. Fukao, 2002: Sea-breeze circulation over Jakarta, Indonesia: A climatology based on boundary layer radar observations. *Mon. Wea. Rev.*, **130**, 2153–2166.
- Hamada, J.-I., Yamanaka, M.D., Matsumoto, J., Fukao, S., Winarso, P.A., Sribimawati, T., 2002: Spatial and temporal variations of the rainy season over Indonesia and their link to ENSO. *J. Meteorol. Soc. Jpn.* **80**, 285–310.
- Hamada, J.-I., Yamanaka, M.D., Mori, S., Tauhid, Y.I., Sribimawati, T., 2008: Differences of rainfall characteristics between coastal and interior areas of central western Sumatera, Indonesia. *J. Meteorol. Soc. Jpn.* **86**, 593–611.
- Hartmann, D. L., H. H. Hendon, and R. A. Houze Jr. 1984: Some implications of the mesoscale circulations in tropical cloud clusters for large-scale dynamics and climate. *J. Atmos. Sci.*, **41**, 113–121, doi:10.1175/1520-0469(1984)041,0113:SIOTMC.2.0.CO;2.
- Haylock, M., and J. McBride, 2001: Spatial coherence and predictability of Indonesian wet season rainfall. *J. Climate*, **14**, 3882–3887.
- Hendon, H. H., 2003: Indonesian rainfall variability: Impacts of ENSO and local air–sea interaction. *J. Climate*, **16**, 1775–1790.
- Hirt, W. D., 1982: Short-term prediction of convective development using dew-point convergence. Preprints, *Ninth Conf. on Weather Forecasting and Analysis*, Seattle, WA, *Amer. Meteor. Soc.*, 201–205.
- Hirose, M., R. Oki, A. D. Short, and K. Nakamura, 2009: Regional characteristics of scale-based precipitation systems from ten years of TRMM PR data. *J. Meteor. Soc. Japan.*, **87A**, pp. 353-368, doi: [10.2151/jmsj.87A.353](https://doi.org/10.2151/jmsj.87A.353).
- Hodges, K. I. and Thorncroft, C. D 1997: Distribution and statistics of African convective systems based on the ISCCP meteosat imagery. *Mon. Weather. Rev.* **125**. 2821-2837.

- Houze, R. A. Jr. 1977: Structure and Dynamics of a Tropical Squall Line System. *Mon. Wea. Rev.*, **105**, 1540 - 1567.
- Houze, R. A., Jr., S. G. Geotis, F. D. Marks, Jr., and A. K. West, 1981: Winter monsoon convection in the vicinity of north Borneo. Part I: Structure and time variation of the clouds and precipitation. *Mon. Wea. Rev.*, **109**, 1595-1614.
- Houze, R. A. Jr., and C. -P. Cheng, 1977: Radar characteristics of tropical convection observed during GATE: Mean properties and trends over the summer season. *Mon. Wea. Rev.*, **105**, 964-980.
- Houze, R. A., Jr. 1982: Cloud clusters and large-scale vertical motions in the tropics, *J. Meteorol. Soc. Jpn.*, **60**, 396-410.
- Houze, R. A., Jr., S. A. Rutledge, M. I. Biggerstaff, and B. F. Smull. 1989: Interpretation of Doppler weather-radar displays in midlatitude mesoscale convective systems, *Bull. Am. Meteorol. Soc.*, **70**, 608-619.
- Houze, R. A. Jr. 2004: Mesoscale Convective System, *Review of Geophysics, American Geophysical Union*, 43 pp.
- Houze, R. A., Jr., B. F. Smull, and P. Dodge. 1990: Mesoscale organization of springtime rainstorms in Oklahoma, *Mon. Weather Rev.*, **118**, 613-654.
- Houze Jr., R. A. 1993: Cloud Dynamics. Waltham, MA: *Academic Press*.
- Houze, R. A., Jr., S. S. Chen, D. E. Kingsmill, Y. Serra, and S. E. Yuter. 2000: Convection over the Pacific warm pool in relation to the atmospheric Kelvin-Rossby wave, *J. Atmos. Sci.*, **57**, 3058-3089.
- Houze, R. A., Jr., and A. K. Betts. 1981: Convection in GATE, *Rev. Geophys.*, **19**, 541-576.
- Hoxit, L. R., C. F. Chappel, and J. M. Fritsch, 1976: Formation of mesolows or pressure troughs in advance of cumulonimbus clouds. *Mon. Wea. Rev.*, **104**, 1419-1428.
- Huffman, G.J., Bolvin, D.T. 2013: TRMM and other data precipitation data set documentation. Available online ftp://meso-a.gsfc.nasa.gov/pub/trmmdocs/3B42_3B43_doc.pdf (accessed on 30 December 2015).
- Ichikawa, H., and T. Yasunari, 2006: Time-space characteristics of diurnal rainfall over Borneo and surrounding oceans as observed by TRMM-PR. *J. Climate*, **19**, 1238-1260.
- Ichikawa, H., and T. Yasunari, 2008: Intraseasonal variability in diurnal rainfall over New Guinea and the surrounding oceans during Austral summer. *J. Climate*, **21**, 2852-2868.
- Ismanto, H. 2011: Characteristics of Mesoscale Convective Complexes over Maritime Continent. *Tesis Magister*, FITB, ITB.
- James, J. 1992: A preliminary study of mesoscale convective complexes over the mid-latitudes of eastern Australia. *Tech. Report 66, Bureau of Meteorology*, Australia, 30 pp.
- Janowiak, J.E., P.A. Arkin, and M. Morrissey, 1994: An examination of the diurnal cycle in oceanic tropical rainfall using satellite and in situ data. *Mon. Wea. Rev.*, **122**, 2296-2311.
- Johnson, R.H. and D.C. Kriete, 1982: Thermodynamic and circulation characteristics of winter monsoon tropical mesoscale convection. *Mon. Wea. Rev.*, **110**, 1898-1911.
- Jorgensen, D. P., and M. A. LeMone, 1989: Vertical velocity characteristics of oceanic convection. *J. Atmos. Sci.*, **46**, 621-640.
- Kane, R. J., C. R. Chelius, and J. M. Fritsch, 1987: Precipitation characteristics of mesoscale convective weather systems. *J. Climate Appl. Meteor.*, **26**, 1345-1357.
- Kawashima, M., Fujiyoshi, Y., Ohi, M., Honda, T., Mori, S., Sakurai, N., Abe, Y., Harjupa, W., Syamsudin, F., Yamanaka, M.D., 2011: Case study of an intense wind event

- associated with a mesoscale convective system in west Sumatera during the HARIMAU2006 campaign. *J. Meteorol. Soc. Jpn.* 89A, 239–257.
- Kikuchi, K., and B. Wang, 2008: Diurnal precipitation regimes in the global tropics. *J. Climate*, **21**, 2680–2696.
- Kingsmill, D. E., and R. A. Houze Jr. 1999: Kinematic characteristics of air flowing into and out of precipitating convection over the west Pacific warm pool: An airborne Doppler radar survey, *Q. J. R. Meteorol. Soc.*, **125**, 1165–1207.
- Koseki, S., T. Y. Koh, and C. K. Teo., 2014: Borneo vortex and mesoscale convective rainfall. *Atmos. Chem. Phys.* **14**, 4539–4562
- Laing, A. G. dan Fritsch, J. M. 1993 : Mesoscale Convective Complexes Over the Indian Monsoon Region. *American Meteorology Society*, **121**, 2254 – 2263.
- Laing, A. G., & Fritsch, J. M. (1993). Mesoscale Convective Complexes in Africa. *Monthly Weather Review*, **121**, 2254-2263.
- Laing, A. G. 1993 : Mesoscale Convective Complexes in Africa. *American Meteorology Society*, **6**, 911 – 919.
- Laing, A. G., 1996: A global climatology of mesoscale convective complexes. Doctoral dissertation, The Pennsylvania State University, 158 pp.
- Laing, A. G. dan Fritsch, J. M. 1997: The Global Population of Mesoscale Convective Complexes. *Q. J. R. Meteorol. Soc.* , **123**, 389-405.
- Laing, A. G. (1999) : Contribution of Mesoscale Convective Complexes to Rainfall in Sahelian Africa :estimates from Geostationary Infrared and Passive Microwave Data. *Journal of Applied Meteorology*. **38**, 957 – 964.
- Laing, A. G. dan Fritsch, J. M. 2000: The Large Scale environment of the Global Population of Mesoscale Convective Complexes. *Monthly Weather Review*, **128**, 2756 - 2776.
- Laing, A. G. 2003 : *Mesoscale Convective System*. Ensyclopedia Of Atmospheric Science. Elseiver Science Ltd., 1251 - 1261.
- Lau, K. M., and J. Zhou, 2003: Anomalies of the South American summer monsoon associated with the 1997-99 El Niño- Southern Oscillation. *Int. J. Climatol.*, **23**, 529–539.
- Laurent, H., 1996: Tracking of convective cloud clusters from Meteosat data. *Tenth Meteosat Scientific Users' Conference*.
- Lauwaet, D., van Lipzig, N.P.M., De Ridder, K., (2009). The effect of vegetation changes on precipitation and mesoscale convective systems in the Sahel. *Climate Dynamics*, in press
- Leary, C. A., 1979: Behavior of the wind field in the vicinity of a cloud cluster in the intertropical convergence zone. *J. Atmos. Sci.*, **36**, 631-639.
- LeMone, M. A., and E. J. Zipser, 1980: Cumulonimbus vertical velocity events in GATE. Part I: Diameter, intensity, and mass flux. *J. Atmos. Sci.*, **37**, 2444-2457.
- Lindzen, R. S., A. Y. Hou., 1988: Hadley circulations for zonally averaged heating centered off the equator. *J. Atmos. Sci.* **45**. 2416-2427.
- Lopez, R. E. 1977: The log-normal distribution and cumulus cloud populations. *Mon. Weather. Rev.*, **105**, 865 - 872.
- Love, B. S., A. J. Matthews, G. M. S. Lister, 2011: The diurnal cycle of precipitation over the Maritime Continent in a high-resolution atmospheric model. *Quart. J. Roy. Meteor. Soc.*, **137**, 934-947, doi: 10.1002/qj.809.
- Lucas, C., M. A. LeMone, and E. J. Zipser, 1994: Vertical velocity in oceanic convection off tropical Australia. *J. Atmos. Sci.*, **51**, 3183–3193
- Machado, L., Desbois, M., and Duvel, J-P., 1992: Structural characteristics of deep convective systems over Tropical Africa and the Atlantic Ocean, *Monthly Weather Review*, **120**, pp. 392-406.

- Madden, R.A., Julian, P.R., 1971. Detection of a 40–50 day oscillation in the zonal wind in the tropical Pacific. *J. Atmos. Sci.* 28, 702–708.
- Madden, R. A., and P. R. Julian, 1972: Description of global-scale circulation cells in the tropics with a 40–50 day period. *J. Atmos. Sci.*, 29, 1109–1123.
- Madden, R. A., and P. R. Julian. 1994: Observations of the 40–50 day tropical oscillation: A review, *Mon. Weather Rev.*, **112**, 814–837.
- Maddox, R. A. 1980: Mesoscale Convective Complexes, *Bull. Amer. Meteor. Soc.* **61**, 1374 - 1387.
- Maddox, R. A. 1981: Satellite Depiction of the Life Cycle of a Mesoscale Convective Complexes. *Mon. Wea. Rev.*, **109**, 1583 - 1586.
- Maddox, R. A., and C. A. Doswell, III, 1982: An examination of jet stream configurations, 500 mb vorticity advection and low-level thermal advection patterns during extended periods of intense convection. *Mon. Wea. Rev.*, **110**, 184–197.
- Maddox, R. A., D. M. Rodgers, and K. W. Howard, 1982: Mesoscale convective complexes over the United States during 1981 – An annual summary. *Mon. Wea. Rev.*, **110**, 1501–1514.
- Maddox, R. A. 1983: Large Scale Meteorological Conditions Associated with Midlatitude Mesoscale Convective Complexes. *Mon. Wea. Rev.*, **111**, 1475 - 1493.
- Maddox, R. A. dan Heckman, B. E. 1982: The Impact of Mesoscale Convective Weather System upon MOS Temperature Guidance. *Preprint, Ninth Conf. On Weather Analysis and Forecasting, Seattle, Amer. Meteor. Soc.*, 214 -218.
- Maddox, R. A., Howard, K. W., Bartels, D. L. and Rogers, D. M., 1986: Mesoscale convective complexes in the middle latitudes. In: *Mesoscale Meteorology and Forecasting* (ed. P.S. Ray). *American Meteorology Society*, 390–413.
- Mathon, V., and Laurent, H., 2001: Life cycle of Sahelian mesoscale convective cloud systems. *Quarterly Journal of the Royal Meteorological Society*, 127: pp. 377–406.
- Mathon, V., Laurent, H., and Lebel, T., 2002: Mesoscale convective system rainfall in the Sahel. *Journal of Applied Meteorology*, 41: pp. 1081–1092.
- Mapes, B. E., T. T. Warner, and M. Xu. 2003: Diurnal patterns of rainfall in northwestern South America, Part III: Diurnal gravit waves and nocturnal convection offshore, *Mon. Weather Rev.*, 131, 830–844.
- Mapes, B. E., and R. A. Houze Jr. 1995: Diabatic divergence profiles in western Pacific mesoscale convective systems, *J. Atmos. Sci.*, 52, 1807–1828.
- Mapes, B. E., and R. A. Houze, Jr., 1993: Cloud clusters and superclusters over the oceanic warm pool. *Mon. Wea. Rev.*, **121**, 1398–1415.
- Mason, S. J., and M. R. Jury, 1997: Climate variability and change over southern Africa: A reflection on underlying processes. *Prog. Phys. Geogr.*, **21**, 23–50.
- Matsumoto, J., 1992. The seasonal changes in Asian and Australian monsoon regions *J. Meteorol. Soc. Jpn.* 70, 257–273.
- McAnelly, R. L. and Cotton, W. R. 1986: Meso- β -scale characteristics of an episode of meso- α -scale convective complexes. *Mon Wea Rev.* 114 1740–1770
- McAnelly, R. L. and Cotton, W. R. 1989: The precipitation life cycle of mesoscale convective complexes over the central United States. *Mon. Wea. Rev.* **117** 784 - 808
- McAnelly, R. L. dan Cotton, W. R. 1989: The Precipitation life cycle of Mesoscale Convective Complexes over the Central United States. *Mon. Wea. Rev.*, **117**, 784 - 808.
- McBride, J., 1998. Indonesia, Papua New Guinea, and tropical Australia: the southern hemisphere monsoon. *Meteorol. Monogr.* 27, 89–100.

- McBride, J. L., 1999: Indonesia, Papua New Guinea, and Tropical Australia: The Southern Hemisphere summer monsoon. *Meteorology of the Southern Hemisphere*, Meteor. Monogr., No. 49, *Amer. Meteor. Soc.*, 89–99
- Merrit, J. 1985: The synoptic environment and movement of mesoscale convective complexes over the United States, M.S. Thesis. 129 pp. Penn. State Univ.
- Merrit, J. H., and J. M. Fritsch. 1984: On the movement of the heavy precipitation areas of midlatitude mesoscale convective complexes. *Amer. Meteor. Soc.*, 529–536.
- Miller, R. A., & Frank, W. M. (1993). Radiative forcing of simulated tropical cloud clusters. *Monthly Weather Review*, **121**, 482–498.
- Miller, D. dan Fritsch, J. M. 1991: Mesoscale Convective Complexes in Western Pacific Region. *Amer. Meteor. Soc.*, **119**, 2978 – 2992.
- Mohr K., Famiglietti J. and Zipser E. 1999: The contribution to tropical rainfall with respect to convective systems type, size, and intensity estimated from the 85-GHz ice-scattering signature. *Journal of Applied Meteorology*, 38: pp. 596–606.
- Mohr, K. I., and E. J. Zipser, 1996: Mesoscale convective systems defined by their 85-GHz ice scattering signature: Size and intensity comparison over tropical oceans and continents. *Mon. Wea. Rev.*, **124**, 2417–2437.
- Mohr, K. I., J. S. Famiglietti, and E. J. Zipser, 1999: The contribution to tropical rainfall with respect to convective system type, size, and intensity estimated from the 85-GHz ice-scattering signature. *J. Appl. Meteor.*, **38**, 596–606.
- Moncrieff, M. W. 1992: Organized convective systems: Archetypal dynamical models, mass and momentum flux theory, and parameterization, *Q. J. R. Meteorol. Soc.*, 118, 819–850.
- Moncrieff, M. W., and E. Klinker (1997), Organized convective systems in the tropical western Pacific as a process in general circulation models: A TOGA COARE case-study, *Q. J. R. Meteorol. Soc.*, **123**, 805 – 827.
- Mori, S., Jun-Ichi, H., Tauhid, Y. I., Yamanaka, M. D., Okamoto, N., Murata, F. Sakurai, N., Hashiguchi, H. dan Sribimawati, T. 2004: Diurnal Land-Sea Rainfall Peak Migration over Sumatera Island, Indonesian Maritime Continent, Observed by TRMM Satellite and Intensive Rawinsonde Soundings. *American Meteorology Society*, **132**, 2021 – 2039.
- Mori, S., Hamada, J.-I., Sakurai, N., Fudeyasu, H., Kawashima, M., Hashiguchi, H., Syamsudin, F., Arbain, A.A., Sulistyowati, R., Matsumoto, J., Yamanaka, M.D., 2011. Convective systems developed along the coastline of Sumatera Island, Indonesia observed with an X-band Doppler radar during the HARIMAU2006 campaign. *J. Meteorol. Soc. Jpn.* 89A, 61–81.
- Morel, C. and Senesi, S. 2002: A climatology of mesoscale convective systems over Europe using satellite infrared imagery II: Characteristics of European mesoscale convective systems. *Q. J. R. Meteorol. Soc.*, **128**. 1973–1995.
- Moteki, Q., R. Shirooka, H. Kubota, T. Ushiyama, K. K. Reddy, K. Yoneyama, M. Katsumata, N. Sato, K. Yasunaga, H. Yamada, B. Geng, M. Fujita, M. Yoshizaki, H. Uyeda, and T. Chuda, 2008: Mechanism of the northward propagation of mesoscale convective systems observed on 15 June 2005 during PALAU2005. *J. Geophys. Res.*, **113**, D14126, doi:10.1029/2008JD009793.
- Murakami, M., 1983: Analysis of the deep convective activity over the western Pacific and Southeast Asia. Part I: Diurnal variation. *J. Meteor. Soc. Japan*, **61**, 60–75.
- Murakami, T., Matsumoto, J., 1994: Summer monsoon over the Asian Continent and western North Pacific. *J. Meteorol. Soc. Jpn.* 72, 719–745.
- Nachamkin, J. E., R. L. McAnelly, and W. R. Cotton, 1994: An observational analysis of a developing mesoscale convective complex. *Mon. Wea. Rev.*, **122**, 1168–1188.

- Nakazawa, T., 1988: Tropical super clusters within intraseasonal variations over the western Pacific. *J. Meteor. Soc. Japan.*, **66**, 823-839.
- Nesbitt, S. W., E. J. Zipser, and D. J. Cecil, 2000: A census of precipitation features in the tropics using TRMM: Radar, ice scattering, and lightning observations. *J. Climate*, **13**, 4087–4106, doi:10.1175/1520-0442(2000)013<4087:ACOPFI.2.0.CO;2.
- Nesbitt SW, Zipser EJ. 2003. The diurnal cycle of rainfall and convective intensity according to three years of TRMM measurements. *Journal of Climate* **16**: 1456–1475.
- Nesbitt, S. W., Cifelli, R., & Rutledge, S. A. 2006: Storm Morphology and Rainfall Characteristics of TRMM Precipitation Features. *Monthly Weather Review*, **134**, 2902-2721.
- Newell, R. A., J. W. Kidson, D. G. Vincent and G. J. Boer, 1974: The general circulation of the tropical atmosphere, Vol. 2, The MIT Press, Chapter 6 and 7, p. 1-54.
- Nicolini, M., C. Saulo, J. C. Torres, and P. Salio, 2002: Strong South American low-level jet events characterization during warm season and implications for enhanced precipitation, *Meteorologica* (Special Issue on South American Moonsoon System) **27**, 59–69.
- Ninomiya, K., 1971: Mesoscale modification of synoptic situations from thunderstorm development as revealed by ATS III and aerological data. *J. Appl. Meteor.*, **9**, 197-203
- Nitta, T., and S. Sekine., 1994: Diurnal variation of convective activity over tropical western Pacific. *J. Meteor. Soc. Japan.*, **72**, 627-641.
- Nitta, Ts, Mizuno, T., Takahashi, K., 1992: Multiscale convective systems during the initial phase of the 1986/87 El Niño. *J. Meteorol. Soc. Jpn.* **70**, 447–466.
- Ogino, S.-Y., Yamanaka, M.D., Mori, S., Matsumoto, J., 2016: How much is the precipitation amount over the tropical coastal region?. *J. Clim.* **29**, 1231–1236.
- Ohsawa, T., Ueda, H., Hayashi, T., Watanabe, A., Matsumoto, J., 2001: Diurnal variations of convective activity and rainfall in tropical Asia. *J. Meteorol. Soc. Jpn.* **79**, 333–352.
- Oki, T., and K. Musiake, 1994: Seasonal change of the diurnal cycle of precipitation over Japan and Malaysia. *J. Appl. Meteor.*, **33**, 1445–1463.
- Pandya, R., and D. Durran 1996: The influence of convectively generated thermal forcing on the mesoscale circulation around squall lines, *J. Atmos. Sci.*, **53**, 2924–2951.
- Payne, S. W., and M. M. McGarry. 1977: The relationship of satellite inferred convective activity to easterly waves over West Africa and the adjacent ocean during phase III of GATE, *Mon. Weather Rev.*, **105**, 413–420.
- Peatman, S.C., Matthews, A.J., Stevens, D.P., 2014. Propagation of the Madden–Julian oscillation through the Maritime Continent and scale interaction with the diurnal cycle of precipitation. *Q. J. R. Meteorol. Soc.* **140**, 814–825.
- Purdom, J. F. W., 1976: Some uses of high-resolution GOES imagery in the mesoscale forecasting of convection and its behavior. *Mon. Wea. Rev.*, **104**, 1474–1483.
- Qian, J.-H., 2008: Why precipitation is mostly concentrated over islands in the Maritime Continent. *J. Atmos. Sci.* **65**, 1428–1441.
- Ramage, C.S., 1968: Role of a tropical “maritime continent” in the atmospheric circulation. *Mon. Weather Rev.* **96**, 365–369.
- Rasmussen, K. L., and R. A. Houze Jr., 2011: Orographic convection in South America as seen by the TRMM satellite. *Mon. Wea. Rev.*, **139**, 2399–2420.
- Rasmussen, K. L., M. D. Zuluaga, and R. A. Houze Jr., 2014: Severe convection and lightning in subtropical South America. *Geophys. Res. Lett.*, **41**, 7359–7366, doi:10.1002/2014GL061767.
- Reed, R. J., and E. E. Recker, 1971: Structure and properties of synoptic scale wave disturbances in the equatorial western Pacific. *J. Atmos. Sci.*, **28**, 117-1133.

- Renggono, F., Hashiguchi, H., Fukao, S., Yamanaka, M.D., Ogino, S.-Y., Okamoto, N., Murata, F., Harijono, S.W.B., Kudsy, M., Kartasasmita, M., Ibrahim, G., 2001. Precipitating clouds observed by 1.3-GHz L-band boundary layer radars in equatorial Indonesia. *Ann. Geophys.* 19, 889–897.
- Reynold, H. 1990: Mesoscale Convective Complexes an Overview. *A Report Degree of Master of Science, University of Toronto*, 25 pp.
- Rickenbach, T. M., and S. A. Rutledge. 1998: Convection in TOGA COARE: Horizontal scale, morphology, and rainfall production, *J. Atmos. Sci.*, 55, 2715–2729.
- Riehl, H., L. Cruz, M. Mata and C. Muster, 1973: Precipitation characteristics during the Venezuela rainy season. *Quart. J. Roy. Meteor. Soc.*, **99**, 746-757.
- Riehl, H., D. Rossignol and W. Luckefedt, 1974: on the structure and maintenance of west African squall lines. *ASECNA B.P. 3144*. 29 pp
- Rodgers, D. M., K. W. Howard, and E. C. Johnston, 1983: Mesoscale convective complexes over the United States during 1982. *Mon. Wea. Rev.*, **111**, 2363-2369.
- Rodgers, D. M., M. J. Magnano, and J. H. Arns, 1985: Mesoscale convective complexes over the United States during 1983. *Mon. Wea. Rev.*, **113**, 888-901.
- Romatschke, U., and R. A. Houze, Jr., 2013: Characteristics of precipitating convective systems accounting for the summer rainfall of tropical and subtropical South America. *J. Hydrometeorol.*, **14**, 25-46.
- Salio P, Nicolini M, Zipser EJ. 2007. Mesoscale convective systems over southeastern South America and their relationship with the South American low-level jet. *Monthly Weather Review* **135**: 1290–1309.
- Sakurai, N., Murata, F., Yamanaka, M.D., Hashiguchi, H., Mori, S., Hamada, J.-I., Tauhid, Y.-I., Sribimawati, T., Suhardi, B., 2005. Diurnal cycle of migration of convective cloud systems over Sumatera Island. *J. Meteorol. Soc. Jpn.* 83, 835–850.
- Sakurai, N., Kawashima, M., Fujiyoshi, Y., Hashiguchi, H., Shimomai, T., Mori, S., Hamada, J.-I., Murata, F., Yamanaka, M.D., Tauhid, Y.I., Sribimawati, T., Suhardi, B., 2009: Internal structures of migratory cloud systems with diurnal cycle over Sumatera Island during CPEA-I campaign. *J. Meteorol. Soc. Jpn.* 87, 157–170.
- Saulo, A. c., L. J. Ferreira, J. Mejia, and M. Seluchi, 2004: Description of the thermal low characteristics using SALLJEX special observations. CLIVAR Exchanges, Vol. 9, No. 1, International CLIVAR Project Office, 9–11.
- Schröder, M., König, M., & Schmetz, J. (2009). Deep convection observed by the Spinning Enhanced Visible and Infrared Imager on board Meteosat 8: Spatial distribution and temporal evolution over Africa in summer and winter 2006. *Journal of Geophysical Research Atmospheres*, **114**. doi:10.1029/2008JD010653
- Schumacher, C., and R. A. Houze Jr., 2004: Stratiform rain in the tropics as seen by the TRMM precipitation radar. *J. Climate*, 16, 1739–1756, doi:10.1175/1520-0442(2003)016,1739:SRITTA.2.0.CO;2.
- Schumacher, C., R. A. Houze Jr., and I. Kraucunas. 2004: The tropical dynamical response to latent heating estimates derived from the TRMM Precipitation Radar, *J. Atmos. Sci.*, 61, 1341–1358.
- Shibagaki, Y., Shimomai, T., Kozu, T., Mori, S., Fujiyoshi, Y., Hashiguchi, H., Yamamoto, M. K., Fukao, S., Yamanaka, M. N. 2006 : Multiscale aspect of Convective Systems Associated with an Intraseasonal Oscillation over the Indonesian Maritime Continent. *American Meteorology Society*, **134**, 1682 – 1696.

- Silva, V. B. S., and T. Ambrizzi, 2006: Inter-El Niño variability and its impact on the South American low-level jet east of the Andes during austral summer—Two case studies. *Adv. Geosci.*, **6**, 283–287.
- Slingo, J., P. Inness, R. Neale, S. Woolnough, and G. Y. Yang, 2003: Scale interactions on diurnal to seasonal timescales and their relevance to model systematic errors. *Ann. Geophys.*, **46**, 139–155.
- Smull, B. F., and J. A. Augustine, 1993: Multiscale analysis of a mature mesoscale convective complex. *Mon. Wea. Rev.*, **121**, 103–132.
- Steiner, M., R. A. Houze Jr., and S. E. Yuter, 1995: Climatological characterization of three-dimensional storm structure from operational radar and rain gauge data, *J. Appl. Meteorol.*, **34**, 1978–2007.
- Sturman, A. P., Tapper, N. J. 1996: The weather and climate of Australia and New Zealand Oxford University Press, Melbourne 476 pp.
- Strachan, J., 2007: Understanding and Modelling the Climate of the Maritime Continent. Doctoral Thesis. University of Reading. 227 pp.
- Sui, C. H., X. Li, and K.-M. Lau, 1998: Radiativeconvective processes in simulated diurnal variations of tropical oceanic convection. *J. Atmos. Sci.*, **55**, 2345–2357.
- Sui, C. H., K. M. Lau, Y. N. Takayabu, and D. A. Short, 1997: Diurnal variations in tropical oceanic cumulus convection during TOGA COARE. *J. Atmos. Sci.*, **54**, 639–655.
- Supari., 2012: Spatiotemporal characteristics of extreme rainfall events over Java island, Indonesia. *Tesis Magister*. UGM.
- Takayabu, Y. N., 2002: Spectral representation of rain profiles and diurnal variations observed with TRMM PR data over the equatorial area. *Geophys. Res. Lett.*, **29**, 10.1029/2001GL014113.
- Tan, J. Jakob, C. Rossow, W.B. and Tselioudis G. 2015: Increases in tropical rainfall driven by changes in frequency of organized deep convection. *Nature*. vol. 519. doi:10.1038/nature14339
- Tao, W, K., S. Lang, J. Simpson, C. H. Sui, B. Ferrier and M.-D. Chou. 1996: Mechanisms of cloud-radiation interaction in the tropics and midlatitude. *J. Atmos. Sci.*, **53**, 2624–2651.
- Tollerud, E. I., Augustine, J. A. and Jamison, B. D. 1992 ‘Cloud top characteristics of mesoscale convective systems in 1986’. Pp. J3–J7 in preprint volume of the 6th conference on satellite meteorology and oceanography, *Am. Meteorol. Soc.*, Atlanta, USA
- Tollerud, E. I., and S. K. Esbensen, 1985: A composite life cycle of nonsquall mesoscale convective systems over the tropical ocean. Part I: Kinematic fields. *J. Atmos. Sci.*, **42**, 823–837.
- Tollerud EI, Rodgers DM, Brown K. 1987: Seasonal, diurnal, and geographic variations in the characteristics of heavy-rain-producing mesoscale convective complexes: a synthesis of eight years of MCC summaries. Preprints, *11th Conference Weather Modification*. Edmonton, 143–146.
- Tollerud, E. I., and R. S. Collander, 1993: A ten year summary of severe weather in mesoscale convective complexes. Proc. 17th Conf. on Severe Local Storms, St. Louis, MO, *Amer. Meteor. Soc.*, 533–537.
- Tollerud, E. I., and D. M. Rodgers, 1991: The seasonal and diurnal cycle of mesoscale convection and precipitation in the central United States: Interpreting a 10-year satellite-based climatology of mesoscale convective complexes. Preprints, Seventh Conf. on Applied Climatology, Salt Lake City, UT, *Amer. Meteor. Soc.*, 63–70.
- Tompkins, A, M. 2001: Organization of tropical convection in low vertical wind shears: the role of cold pools *J. Atmos. Sci.* **58** 1650–1672.

- Toracinta, E. R., and E. J. Zipser., 2001: Lightning and SSM/I-Ice-Scattering Mesoscale Convective Systems in the Global Tropics. *Amer. Meteo. Soc.* **40**, 983 - 1002.
- Trier, S. B., and D. B. Parsons, 1993: Evolution of environmental conditions preceding the development of a nocturnal mesoscale convective complex. *Mon. Wea. Rev.*, **121**, 1078–1098.
- Trismidianto, 2012: a study of mesoscale convective complexes (MCCs) activities in the western Indian Ocean and their effects on convection over Sumatra Island. *Tesis Magister*, FITB, ITB.
- Tyson, P. D., and R. A. Preston-Whyte, 2000: The Atmosphere and Weather of Southern Africa. *Oxford University Press*, 396 pp
- Valor G.B., and D. J. M. G. López, 2014: OGIMET – professional information about meteorological conditions in the world. <http://www.ogimet.com>, (accessed 30 December 2015).
- Velasco, I. dan Fritsch, J. M. 1987: Mesoscale Convective Complexes in the America. *J. Geophysic. Res.*, **92**, 9591-9613.
- Vera C, Baez J, Douglas M, Manuel CB, Marengo J, Meitin J, Nicolini M, Nogues-Paegle J, Paegle J, Penalba O, Salio P, Silva Dias MA, Silva Dias P, Zipser EJ. 2006. The South American low level jet experiment. *Bulletin of the American Meteorological Society* **87**: 63–77.
- Virts, K. S., and R. A. Houze, Jr., 2015: Variation of lightning and convective rain fraction in mesoscale convective systems of the MJO. *J. Atmos. Sci.*, **72**, 1932-1944, doi: [10.1175/JAS-D-14-0201.1](https://doi.org/10.1175/JAS-D-14-0201.1).
- Wallace, J.M., and Hobbs, P.V., 2006: Atmospheric Science: An introduction survey (second edition). *Academic Press, University of Washington*, 1977. 467 p.
- Webster, P. J., & Stephens, G. L. (1980). Tropical upper-tropospheric extended clouds: Inferences from Winter MONEX. *Journal of Atmospheric Sciences*, **37**, 1521-1541.
- Wetzel, P. J., W. R. Cotton, and R. L. McAnelly, 1983: A long-lived mesoscale convective complex. Part II: Evolution and structure of the mature complex. *Mon. Wea. Rev.*, **111**, 1919-1937.
- Wheeler, M. C., and H. H. Hendon, 2004: An all-season real-time multivariate MJO index: Development of an index for monitoring and prediction. *Mon. Wea. Rev.*, **132**, 1917-1932.
- Whitehall, K., 2014: Investigating an Automated Method to Explore Mesoscale Convective Complexes in West Africa. Doctoral Thesis. Howard University. 140 pp.
- Williams, M., and R. A. Houze Jr., 1987: Satellite-observed characteristics of winter monsoon cloud clusters. *Mon. Wea. Rev.*, **115**, 505-519, doi: [10.1175/1520-0493\(1987\)115<0505:SOCOWM>2.0.CO;2](https://doi.org/10.1175/1520-0493(1987)115<0505:SOCOWM>2.0.CO;2).
- Williams, K. T., and W. M. Gray, 1973: Statistical analysis of satellite observed trade wind cloud clusters in the western North Pacific. *Tellus*. **25**, 313-336.
- Wilson J W and Schreiber W E. 1986: Initiation of convective storms at radar-observed boundary-layer convergence lines *Mon. Wea. Rev* **114** 2516-2536 doi: [10.1175/1520-0493\(1986\)114<2516:IOCSAR>2.0.CO;2](https://doi.org/10.1175/1520-0493(1986)114<2516:IOCSAR>2.0.CO;2)
- Wu, P.-M., Hamada, J.-I., Mori, S., Tauhid, Y.I., Yamanaka, M.D., Kimura, F., 2003: Diurnal variation of precipitable water over a mountaneous area in Sumatera Island. *J. Appl. Meteorol.* **42**, 1107–1115.
- Wu, P.-M., Fukutomi, Y., Matsumoto, J., 2011: An observational study of the extremely heavy rain event in northern Vietnam during 30 October–1 November 2008. *J. Meteorol. Soc. Jpn.* **89A**, 331–344.
- Yamanaka, M. D., H. Hashiguchi, S. Mori, P. Wu, F. Syamsudin, T. Manik, Hamada J.-I., M. K. Yamamoto, M. Kawashima, Y. Fujiyoshi, N. Sakurai, M. Ohi, R. Shirooma, M.

- Katsumata, Y. Shibagaki, T. Shimomai, Erlansyah, W. Setiawan, B. Tejasukmana, Y. S. Djajadihardja, and J. T. Anggadiredja, 2008: HARIMAU radar-profiler network over Indonesian maritime continent: A GEOSS early achievement for hydrological cycle and disaster prevention. *J. Disaster. Res.*, **3**, 78-88.
- Yamanaka, M. D. 2016: Physical climatology of Indonesian maritime continent: An outline to comprehend observational studies. *Atmospherics research elsevier*. <http://dx.doi.org/10.1016/j.atmosres.2016.03.017>
- Yang, G.-Y., Slingo, J., 2001: The diurnal cycle in the tropics. *Mon. Weather Rev.* **129**, 784– 801.
- Yasunari, T., 1981: Temporal and spatial variations of monthly rainfall in Java, Indonesia. *Southeast Asian Stud.* **19**, 170–186.
- Yihui, D., and L. Yanju., 2001: Onset and the evolution of the summer monsoon over the south china sea during SCSMEX field experiment in 1998. *J. of the Met. Soc. of Japan*, **79**, 255-276.
- Yuan, J., and R. A. Houze Jr., 2010: Global variability of mesoscale convective system anvil structure from A-Train satellite data. *J. Climate*, **23**, 5864-5888, doi: [10.1175/2010JCLI3671.1](https://doi.org/10.1175/2010JCLI3671.1)
- Zhang, D.-L., and J. M. Fritsch. 1988: A numerical investigation of a convectively generated, inertially stable, extratropical warmcore mesovortex over land. Part I: Structure and evolution, *Mon. Weather Rev.*, **116**, 2660–2687.
- Zhang, C. D., 2005: Madden-Julian oscillation. *Rev. Geophys.*, **43**, 1–36.
- Zhou, L., and Y. Wang, 2006: Tropical Rainfall Measuring Mission observation and regional model study of precipitation diurnal cycle in the New Guinean region. *J. Geophys. Res.*, **111**, D17104, doi:10.1029/2006JD007243.
- Zipser, E. J., and M. A. LeMone, 1980: Cumulonimbus vertical velocity events in GATE. Part II: Synthesis and model core structure. *J. Atmos. Sci.*, **37**, 2458-2469.
- Zolman, J. L., E. J. Zipser, and K. I. Mohr, 2000: A comparison of tropical mesoscale convective systems in El Niño and La Niña. *J. Climate*, **13**, 3314–3326.